



Development and characterization of nano- microfibers for the encapsulation and release of bioactive phenolic compounds

Shekarforoush, Elhamalsadat

Publication date:
2018

Document Version
Publisher's PDF, also known as Version of record

[Link back to DTU Orbit](#)

Citation (APA):
Shekarforoush, E. (2018). Development and characterization of nano- microfibers for the encapsulation and release of bioactive phenolic compounds. Kgs. Lyngby, Denmark: Technical University of Denmark.

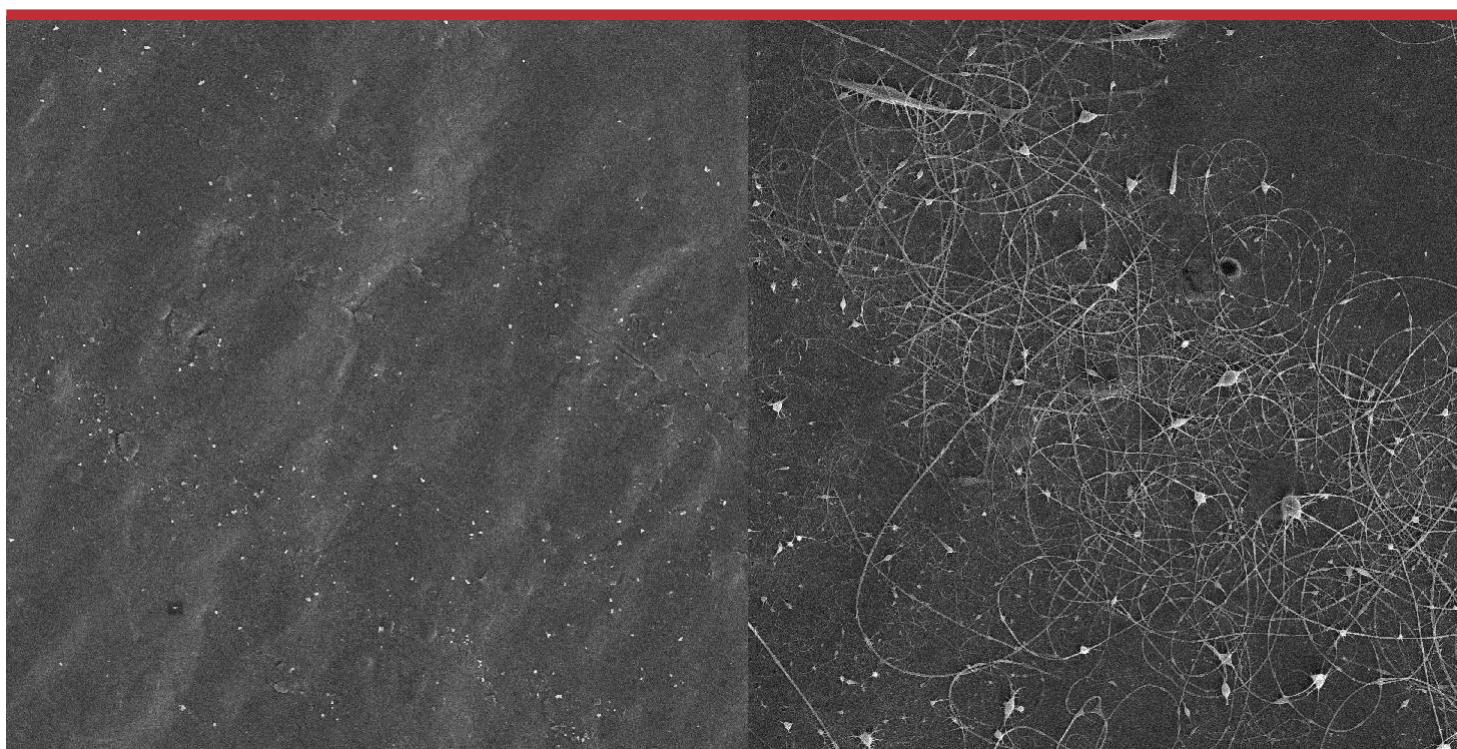
General rights

Copyright and moral rights for the publications made accessible in the public portal are retained by the authors and/or other copyright owners and it is a condition of accessing publications that users recognise and abide by the legal requirements associated with these rights.

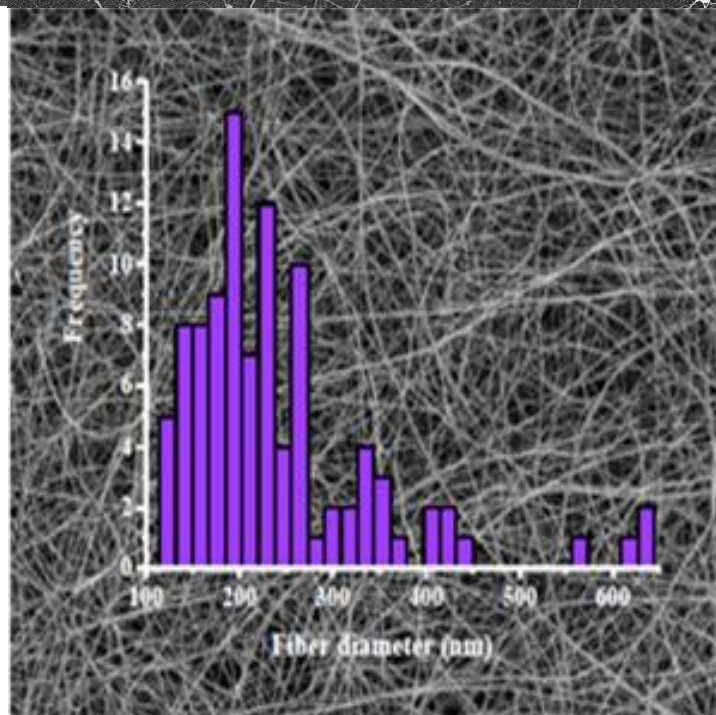
- Users may download and print one copy of any publication from the public portal for the purpose of private study or research.
- You may not further distribute the material or use it for any profit-making activity or commercial gain
- You may freely distribute the URL identifying the publication in the public portal

If you believe that this document breaches copyright please contact us providing details, and we will remove access to the work immediately and investigate your claim.

Development and characterization of nano-microfibers for the encapsulation and release of bioactive phenolic compounds



Elhamalsadat Shekarforoush
 PhD Thesis
 2018



Development and characterization of nano-microfibers for the encapsulation and release of bioactive phenolic compounds



PhD Thesis

by

Elhamalsadat Shekarforoush

Submitted: 30.04.2018

National Food Institute

Technical University of Denmark

Kemitorvet 202, 2800 Kongens Lyngby, Denmark

Preface

This thesis presents the results of my work as a PhD student and is submitted to meet the requirements for obtaining the PhD degree at the National Food Institute, Technical University of Denmark. The PhD scholarship was co-funded by a third of a PhD stipend from the Technical University of Denmark. The project was also supported by the European Union FP7 project “Nano3Bio” (grant agreement no 613931). The work was conducted in the Research group of Nano-Bio Science at the National Food Institute, Technical University of Denmark, from 1st of February 2015 to 30th of April 2018 under the principle supervision of Professor Ioannis S. Chronakis and co-supervision of Dr. Ana Carina Loureiro Mendes.

Acknowledgment

Numerous people have been engaged in this thesis in different ways to which I would like to say thanks! First of all, I would like to thank my supervisors; Professor Ioannis S. Chronakis and Dr. Ana Carina Loureiro Mendes for all patience and great expertise, for always having their door open for discussions, help and guidance.

Also I would like to thank Professor Thomas Andresen for access to cell laboratory facilities and also Dr. Adele Faralli and Dr. Fatemeh Ajalloueiian for good collaboration and for presenting me to cell culturing for Permeability and Cytotoxicity tests of electrospun fibers.

Also I would like Dr. Hamed Safafar for collaborating and supporting me thorough antioxidants methods.

Also I would like to acknowledge Assistant Professor Sophie Beeren, Senior Researcher Sokol Ndoni and Guanghong Zeng for great discussions related to the ^1H NMR, Size-exclusion chromatography (SEC) and Atomic force microscopy (AFM), respectively.

Also thank you to the people in buildings 227 and 201 for good social activities and for contributing to a good research environment.

Last but not least, I wish to thank my loved ones for inspiring me to pursue my dreams, for encouraging me during the difficult times and for being patient with me throughout my undergraduate and graduate journey. My family specially my father and mother; you have sacrificed so much for me to achieve this lifelong goal. This work is entirely dedicated to you. I am forever grateful towards you for being my constant source of inspiration and strength and for showing me the proper perspective for life and living.

Elhamalsadat Shekarforoush 2018

Abstract

In this PhD project, electrospun nano-microfibers of polysaccharides xanthan gum, and chitosan, as well as phospholipids were investigated as encapsulating matrices of phenolic bioactives, that are the most abundant bioactives in our diet.

The processing of electrospun xanthan gum nanofibers using formic acid as a solvent was reported for the first time (*Paper I*). Morphological studies by scanning electron microscopy show that uniform fibers with average diameters ranging from 128 ± 36.7 to 240 ± 80.7 nm are formed depending on the polysaccharide concentration (0.5 to 2.5 wt/vol%) (Paper I). At the polysaccharide concentrations where nanofiber formation was observed, an increase of the elastic modulus and first normal stress differences is observed. Fourier transform infrared spectroscopy and circular dichroism measurements indicated that an esterification reaction took place, where formic acid reacted with the pyruvic acid groups of xanthan. Therefore, formate groups neutralized the pyruvic charges, which in turn stabilized the helical conformation of xanthan.

The potential to utilize electrospun xanthan nanofibers as a delivery carrier system of bioactive phenolic compounds was investigated (*Paper II*). Gallic acid (GA) and (–)-epigallocatechin gallate (EGCG) were encapsulated within xanthan nanofibers, and their release was studied in relevant media at pH 6.5 and 7.4. A sustained release of the bioactives up to 60-80% was observed over 8h. Furthermore, the xanthan-GA and xanthan-EGCG nanofibers were incubated with Caco-2 cells, and the cell viability, transepithelial transport and permeability properties across cell monolayers were investigated. An increase of permeability of Ga and EGCG was observed when the polyphenols were loaded into xanthan nanofibers, comparatively to the non-

encapsulated bioactives. These results suggested that xanthan nanofibers have the ability to enhance the transepithelial permeation of phenolic compounds *in vitro* by inhibiting efflux transporters and opening the tight junctions.

Novel electrospun xanthan-chitosan (X-Ch) nanofibers were developed as a carrier for the delivery of curcumin (Cu), a model hydrophobic phenolic bioactive (*Paper III and IV*). Nanofibers stable in aqueous media were produced by the electrospinning of X-Ch viscoelastic gels with average diameter of 750 nm. The addition of curcumin led to the increase in average fiber diameters to 910 nm. A sustained release of curcumin of 8-10% from X-Ch nanofibers was observed over a period of 12 h for the different pH media (2.2, 6.5, and 7.4) at 37°C. However, after 120 h, 20% of Cu was released from X-Ch nanofibers in pH 2, while nearly 50% of Cu was released in neutral media, through a non-Fickian mechanism. The data support that X-Ch nanofibers could be used as a carrier for the encapsulation of hydrophobic bioactive compounds with long-term pH-stimulated release properties.

Furthermore, the potential to utilize X-Ch nanofibers to enhance the transepithelial transport and permeability of curcumin across Caco-2 cell monolayer was investigated (*Paper IV*). After 24 h of incubation, the exposure of Caco-2 cell monolayers to X-Ch-Cu nanofibers resulted in a cell viability of ~80%. A 3-fold increase of curcumin permeability was observed when the polyphenol was loaded into X-Ch nanofibers, compared to the free curcumin. This increased transepithelial permeation of curcumin was induced by interactions between the nanofibers and the Caco-2 cells that led to the opening of the tight junctions.

In the last study of the thesis (*Paper V*), electrospun phospholipid (asolectin) microfibers were investigated as an antioxidant and encapsulation matrix for curcumin and vanillin. Release

studies in aqueous media revealed that the phenolic bioactives were released mainly due to swelling of the phospholipid fiber matrix over time. Asolectin fibers were observed to have antioxidant properties, which were improved after the encapsulation of the phenolic compounds, as observed from total antioxidant capacity (TAC) and the total phenolic content (TPC) assays. Furthermore, the antioxidant capacity of curcumin/phospholipid and vanillin/phospholipid microfibers was observed to remain stable over time at different temperatures (refrigerated, ambient) and pressures (vacuum, ambient), while the non-encapsulated phenolic compounds decreased their TAC and TPC values. Therefore, this study confirms the efficacy of electrospun phospholipid microfibers as encapsulation and antioxidant systems.

Resumé (Danish)

I dette ph.d.-projekt blev elektrospundne nano-mikrofibre af polysakkariders xanthangummi og chitosan samt fosfolipider som indkapslingsmatricer af fenoliske bioaktiver, der er de mest hyppige bioaktive stoffer i vores kost, undersøgt.

Behandlingen af nanofibre af elektrospunden xanthangummi under anvendelse af myresyre som opløsningsmiddel blev rapporteret for første gang (*Paper I*). Morfologiske undersøgelser ved at scanne med elektronmikroskop viser, at ensartede fibre med gennemsnitlige diametre fra 128 ± 36.7 til 240 ± 80.7 nm dannes afhængigt af polysakkaridkoncentrationen (0.5 til 2.5 vægt/volumen %) (*Paper I*). Ved polysakkaridkoncentrationerne, hvor nanofiberdannelse blev observeret, observeres en stigning i elastisk modulus samt de første normale spændingsforskelle. Fourier transform infrared spectroscopy (FTIR)- og cirkulære dikroisme-målinger viste, at en esterificeringsreaktion fandt sted, hvor myresyre reagerede med xanthans pyrodruesyregrupper. Formatgrupper neutraliserede derfor de pyruviske ladninger, der igen stabiliserede den spiralformede konformation af xanthan.

Potentialet for at anvende elektrospundne xanthannanofibre som et leverancebærende system af bioaktive fenolforbindelser blev undersøgt (*Paper II*). Gallussyre (GA) og θ -epigallocatechin gallat (EGCG) blev indkapslet i xanthannanofibre, og deres frigivelse blev undersøgt i relevante medier ved en pH på 6.5 og 7.4. Der blev observeret en vedvarende frigivelse af bioaktiverne op til 60-80 % over 8 timer. Endvidere blev xanthan-GA- og xanthan-EGCG-nanofibre inkuberet med Caco-2-celler, og cellelevedygtighed, transepithelial transport- og permeabilitetsegenskaberne på tværs af cellemonolagene blev undersøgt. Der blev observeret en stigning i permeabiliteten af Ga og EGCG, når polyfenolerne blev anbragt i xanthannanofibre,

sammenlignet med de ikke-indkapslede bioaktive stoffer. Disse resultater tydede på, at xanthannanofibre har evnen til at forøge transepithelial permeationen af fenolforbindelser in vitro ved at inhibere effluxtransportører og åbne cellemellemrummene.

Nye elektrospundne xanthan-chitosan (X-Ch)-nanofibre blev dannet som bærer til levering af curcumin (Cu), hydrofobe fenoliske bioaktiver (*Paper III og IV*). Nanofibre, stabile i vandige medier, blev fremstillet ved elektrospinding af X-Ch-viskoelastiske geler med en gennemsnitlig diameter på 750 nm. Tilsætningen af curcumin førte til stigningen i gennemsnitlige fiberdiametre til 910 nm. Der blev observeret en vedvarende frigivelse af curcumin på 8-10 % fra X-Ch-nanofibre over en periode på 12 timer for de forskellige pH-medier (2.2, 6.5 og 7.4) ved 37 °C. Efter 120 timer blev imidlertid 20 % af Cu frigivet fra X-Ch-nanofibre i pH 2, medens næsten 50 % af Cu blev frigivet i neutrale medier gennem en ikke-Fick'sk mekanisme. Dataene understøtter, at X-Ch-nanofibre kan anvendes som bærer til indkapsling af hydrofobe bioaktive forbindelser med langvarige pH-stimulerede frigivelsesegenskaber.

Endvidere blev potentialet for at udnytte X-Ch-nanofibre til at forbedre transepithelial transport og permeabilitet af curcumin over Caco-2-cellemonolag undersøgt (*Paper IV*). Efter 24 timers inkubation resulterede eksponeringen af Caco-2-cellemonolag på X-Ch-Cu-nanofibre i en cellelevedygtighed på ~ 80 %. Der blev observeret en trefoldig stigning i curcuminpermeabilitet, når polyfenolen blev fyldt i X-Ch-nanofibre, sammenlignet med den frie curcumin. Denne øgede transepithelial permeation af curcumin blev induceret af interaktioner mellem nanofibre og Caco-2-cellerne, der førte til åbningen af cellemellemrummene.

I afhandlingens sidste undersøgelse (*Paper V*) blev elektrospundne fosfolipide (asolectin) mikrofibere undersøgt som en antioxidant- og indkapslingsmatrix for curcumin og vanillin.

Frigivelsesundersøgelser i vandige medier afslørede, at de fenoliske bioaktiver blev frigivet hovedsagelig på grund af hævelse af fosfolipidfibermatrixen over tid. Det blev observeret, at solectinfibre havde antioxidantegenskaber, som blev forbedret efter indkapslingen af fenolforbindelserne, målt ud fra total antioxidantkapacitet (TAC) og totalt fenolindhold (TPC). Desuden blev det observeret, at antioxidantkapaciteten af curcumin/fosfolipid og vanillin/fosfolipidmikrofibre forblev stabil over tid ved forskellige temperaturer (nedkølede omgivelser) og tryk (vakuum omgivelser), mens de ikke-indkapslede fenolforbindelser reducerede deres TAC- og TPC-værdier. Derfor bekræfter denne undersøgelse virkningen af elektrospundne fosfolipidmikrofibre som indkapslings- og antioxidantssystemer.

Table of contents	Page
Preface	i
Acknowledgment	ii
Abstract	iii
Resumé (Danish)	vi
List of abbreviations	x
List of publications	xii
International conference contributions	xiv
CHAPTER	
1 Introduction	1
2 Literature review	4
2.1. Principles of electrospinning	4
2.2. Materials used in electrospinning technology	7
2.2.1. Biopolymers and biomolecules	8
2.2.1.1. Xanthan Gum	9
2.2.1.2. Chitosan	10
2.2.1.3. Phospholipids	12
2.3. Applications of Electrospinning	14
2.3.1. Encapsulation of bioactives within electrospun fibers	15
2.3.1.1. Vanillin	16
2.3.1.2. Curcumin	17
2.3.1.3. Epigallocatechin gallate (ECGC)	19
2.3.1.4. Gallic acid (GA)	20
2.3.2. Caco-2 cell model – the oral delivery system	21
3 Results and discussion	24
3.1. Part A – electrospinning	24
3.1.1. Development of xanthan nanofibers- Paper I	24
3.1.2. Application of xanthan nanofibers- Paper II	36
3.1.3. Development of xanthan-chitosan nanofibers- Paper III	69
3.1.4. Application of xanthan-chitosan nanofibers- Paper IV	75
3.1.5. Application of Asolection phospholipid microfiber- Paper V	115
3.2. Part B – Hydrogel (Supporting paper)	132
3.2.1. Nanostructures as hydrogels made from co-assembly of chitosan and phospholipids- Paper VI	132
4 Conclusions	145
5 References	146

List of abbreviations

AA Aq	Acetic acid aqueous	GA	Gallic acid
AB	Apical-to-basolateral	GI tract	Gastrointestinal tract
AcrA Aq	Acrylic acid aqueous	GlcN	Glucosamine
AFM	Atomic force microscopy	GlcNAc	N-acetyl glucosamine
ANOVA	Analysis of variance	GT	Gum tragacanth
BA	Basolateral-to-apical	HA	Hyaluronic acid
BSA	Bovine serum albumin	HBSS	Hanks' balanced salt solution
CA	Cellulose acetate	HDACS	Hexamethylene-1,6-diaminocarboxysulphonate
CA Aq	Citric acid aqueous	HEPES	4-(2-hydroxyethyl)-1-piperazineethanesulfonic acid solution,
CD	Cyclodextrin	HFP	1,1,1,3,3,3 hexafluoro-2-propanol.
CD	Circular Dichroism	HPMC	Hydroxypropyl methylcellulose
CD-IC	Cyclodextrin inclusion complex	ICF	Intensity correlation function
Ch	Chitosan	LY	Lucifer yellow dilithium salt
CHCl ₃	Chloroform	MES	Methanesulfonic acid
CNFs	Cellulose nanofibers	MTS	3-(4,5-dimethylthiazol-2-yl)-5-(3-carboxymethoxyphenyl)-2-(4-sulfophenyl)-2H-tetrazolium
CSS	Cholesteryl-succinyl silane	MW	Molecular weight
Cu	Curcumin	N1	First normal stress difference
D	Diameter	NLCs	Nanostructured lipid carriers
DAPI	4,6-diamidino-2-phenylindole	P	Phospholipids
DCM	Dichloromethane	P _{app}	Apparent permeability coefficient
DDA	Degree of deacetylation	PBS	Phosphate-buffered saline solution
DMEM	Dulbecco's modified Eagle's medium	PCL	Poly(caprolactone)
DMF	Dimethylformamide	PEG	Poly(ethyleneglycol)
DMSO	Dimethyl sulfoxide	PEG400	polyethylene glycol 400
DP	Degree of polymerization	PEO	Poly ethylene oxide;
DPBS	Dulbecco's Phosphate Buffered Saline	PGA	Poly glycolic acids
ECH	Epi- chlorohydrin	PLA	Poly lactic acids
EE	Encapsulation efficiency	PLGA	Lactic-co-glycolic acid
EGCG	(-)-Epigallocatechin gallate	PLLA	Poly (L-lactic acid)
ESEM	Environmental Scanning Electron Micrograph	PMS	Phenazine methosulfate
FA	Formic acid	PU	Poly(urethane)
FBS	Fetal bovine serum	PVA	Poly(vinyl alcohol)
Fig.	Figure	PVP	polyvinyl pyrrolidone
FLUO	Fluorescein sodium salt	RH	Relative humidity
FSP	Fish sarcoplasmic proteins	SEC	Size-Exclusion Chromatography
FTIR	Fourier transform infrared spectroscopy	SEM	Scanning Electron Micrograph

TAC	Total antioxidant capacity
TBS	Tris-buffered saline solution
TEER	Transepithelial electrical resistance
TFA	Trifluoroacetic acid
TPC	Total phenolic content
X	Xanthan gum
X-Ch	Xanthan gum-Chitosan
X-Ch+Cu	Xanthan-chitosan nanofibers
X-Ch-Cu	Curcumin-loaded xanthan-chitosan nanofibers
3-D networks	Three-dimensional networks
e.g.	Example Gratia (for example)
et al.	Et cetera
G'	Elastic Modulus
G''	Viscous Modulus
i.e	Id Est (that is)
tan δ	Interfacial loss factor
wt/vol%	Weight/Volume%
ω	Frequency

List of publications

Paper I

Electrospinning of Xanthan Polysaccharide

Elhamalsadat Shekarforoush, Adele Faralli, Sokol Ndoni, Ana C. Mendes, Ioannis S. Chronakis

Macromolecular Materials and Engineering 302, no. 8 (2017)

Paper II

Enhanced transepithelial permeation of gallic acid and (-)-epigallocatechin gallate across human intestinal Caco-2 cells using electrospun xanthan nanofibers

Adele Faralli, Elhamalsadat Shekarforoush, Ana C. Mendes, Ioannis S. Chronakis

Colloids and Surfaces B (submitted)

Paper III

Electrospun polysaccharide nanofibers as delivery carrier of hydrophobic bioactives

Elhamalsadat Shekarforoush, Fatemeh Ajalloueian, Guanghong Zeng, Ana C. Mendes, Ioannis

S. Chronakis

Materials Letters 228 (2018): 322-326

Paper IV

In vitro permeability enhancement of curcumin across Caco-2 cells monolayers using electrospun xanthan-chitosan nanofibers

Adele Faralli, Elhamalsadat Shekarforoush, Fatemeh Ajalloueian, Ana C. Mendes, Ioannis S.

Chronakis

Carbohydrate Polymers Journal (submitted)

Paper V

Electrospun Phospholipid Fibers as Micro-Encapsulation and Antioxidant Matrices

Elhamalsadat Shekarforoush, Ana C. Mendes, Vanessa Baj, Sophie R. Beeren, Ioannis S.

Chronakis

Molecules 22, no. 10 (2017): 1708

Paper VI

Co-assembly of chitosan and phospholipids into hybrid hydrogels

Ana C. Mendes, Elhamalsadat Shekarforoush, Christoph Engwer, Sophie Beeren, Christian

Gorzelanny, Francisco M. Goycoolea, Ioannis S. Chronakis

Pure and Applied Chemistry 88, no. 9 (2016): 905-916

International conference contributions

Shekarforoush, E., Mendes, A. C., Engwer, C. et al. (2017). The electrospinning of xanthan gum: from solution to nanofiber formation, Applied Nanotechnology and Nanoscience International Conference, October 18-20, Rome, Italy. Oral presentation.

Shekarforoush, E., Mendes, A. C., Engwer, C. et al. (2017). Hybrid Hydrogels by the co-assembly of Chitosan with Phospholipids, European Rheology Conference, April 3-6, Copenhagen, Denmark. Poster presentation.

Shekarforoush, E., Mendes, A. C., Chronakis, I. S. (2016). Electrospinning of Chitosan-Xanthan Nanofibers, Sustain-ATV Conference, November 30, Lyngby, Denmark. Poster presentation.

Shekarforoush, E., Mendes, A. C., Chronakis, I. S. (2016). Development and Characterization of Electrospun Curcumin Loaded Chitosan-Xanthan Nanofibers, International Society for Biomedical Polymers and Polymeric Biomaterials (ISBPPB) Conference, August 11-12, New Jersey, United States. Poster presentation.

Mendes, A. C., Shekarforoush, E., Chronakis, I. S. et. al. (2016). Chitosan/Phospholipids Hybrid Nanofibers and Hydrogels for Life Sciences Applications, Sustain-ATV Conference, November 30, Lyngby, Denmark. Poster presentation.

Mendes, A. C., Shekarforoush, E., Stephansen, K. B. et. al. (2016). Electrospinning of Functional Phospholipid Fibers, Electrospin 2016 Conference, June 28th– July 1, 2016, Otranto, Italy. Oral presentation.

1. Introduction

Studies associated with the nano-microstructures of biopolymers (polysaccharides and proteins) and phospholipids have been receiving particular attention within the last years, in food and pharmaceutical research. Reasons for that rely on to their favorable properties such as biocompatibility, biodegradability and sustainable supply, among other.^{1,2} One of the major applications of those nano-microstructures is encapsulation of bioactive compounds. The encapsulation can protect the bioactive compounds from the environmental and gastro-intestinal tract conditions against degradation, mask odors and tastes of the bioactive components and prevent them from interactions with other food components.^{3,4} There are a broad range of bioactive compounds that are widely used in food and pharmaceutical industries. Among them, phenolic compounds, are the most abundant bioactives in our diet.^{5,6} They are classified as water-soluble (phenolicacids, phenyl propanoids, flavonoids, and quinones) and water-insoluble compounds (condensed tannins, lignins, and certain hydroxycinnamic acids). These compounds have diverse biological properties including antioxidant, anti-cancer, anti-microbial.⁷⁻¹⁰ However, the health benefits of pristine phenolics are limited due to their low solubility, low permeation, low bioavailability, and damage against environmental stresses. Therefore, designing adequate carriers by using nano-microstructures of biopolymers and phospholipids are necessary to overcome these limitations.

This PhD project aimed to investigate:

- i) the processing of polysaccharides such as xanthan gum, chitosan and phospholipids using electrospinning technology for the development of novel nano-microstructures (particularly nano-microfibers);

- ii) the potential of these nano-microstructures to encapsulate and release phenolic bioactive compounds;
- iii) the potential of these nano-microstructures to improve the bioavailability of the phenolic compounds;
- iv) the potential of these nano-microstructures to preserve chemically and stabilize the phenolic compounds.

The main results obtained during this PhD project are presented in five papers.

Paper I described the electrospinning of xanthan gum. The correlation between the concentration and the rheological properties of xanthan solutions, with the morphology of the nanofibers is investigated. Circular dichroism, Fourier transform infrared spectroscopy, size-exclusion chromatography were used to characterize the physicochemical properties of xanthan solutions in formic acid and electrospun xanthan nanofibers. The use of electrospun xanthan nanofibers as a delivery carrier of phenolic compounds Gallic acid (GA) and (-)-epigallocatechin gallate (EGCG) was further studied in Paper II. The release behavior of phenolic compounds from xanthan fibers in bio-relevant buffers in different pH was studied. Also the effect of the xanthan nanofibers on the transepithelial permeation of phenolic compounds was studied *in vitro* using human intestinal Caco-2 cells. Paper III focus on the development of a novel electrospun fiber matrix, made from viscoelastic gels of xanthan and chitosan. On Paper III, the morphology, rheological and adhesion properties, as well as the encapsulation and release of a phenolic compound (curcumin) were investigated. Paper IV explored the *in vitro* potential of electrospun xanthan gum-chitosan nanofibers to enhance the permeability of curcumin across Caco-2 cells monolayers. Paper V, electrospun phospholipid fibers were produced as micro-encapsulation and

antioxidant matrices for the preservation and release of phenolic compounds (vanillin and curcumin).

2. Literature review

2.1. Principles of electrospinning

Electrospinning, a term derivative from ‘electrostatic spinning’, is a simple and effective top-down fabrication process for producing non-woven fibrillary structures made of (bio)polymers and long-chain molecules whose diameters can be controlled from the nano to the micro scale.^{11,13–16} Electrospinning consists of charging the surface of (bio) polymer solution droplets, through the applications of high-voltage electrostatic fields, thereby inducing the ejection of a liquid jet through a spinneret (typically a metallic syringe needle).

A typical electrospinning set-up (**Figure 1**) involves infusion pump to carry a polymer solution in a syringe mounted to a spinneret. The spinneret is typically connected to the positive conductor, plugged to the high voltage power supply, whereas the counter conductor (usually grounded) is connected to the collector. The applied high voltage applied to the polymers solution in the spinneret induces the ejection of a liquid jet through the spinneret.

The curved form of pendant droplet at the end of capillary tip changes into a conical form with increasing voltage, which is known as the Taylor cone. By applying a significant voltage to the spinneret, the charge gathered within the polymer droplet overcomes its surface tension and causes the polymer solution to eject from the spinneret tip to the collector. The solvent evaporates and therefore the jet solidifies as the polymer jet moves in the air towards the collector, leading to a fibrous mat on the collector.^{17–20}

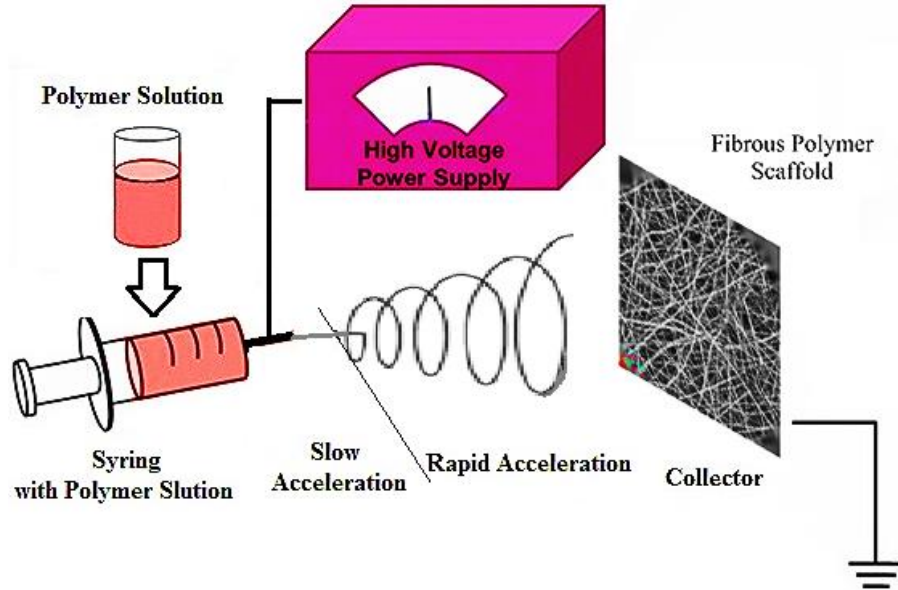


Figure 1. Typical electrospinning set-up was presented at Sustain-ATV Conference 2016.

Several parameters in the electrospinning process can control the production and the morphology of the fibers. Electrospinning process parameters include the distance between the spinneret and collector, the flow rate and the applied voltage. Furthermore, the properties of the electrospun solution such as concentration, viscosity, conductivity, surface tension, dielectric constant and the environmental variables such as humidity and temperature where the process is conducted, also affect substantially the fiber processing.

Common effects of the electrospinning processing parameters on the fiber morphology are summarized in **Figure 2**. As an example an increase in the flow rate or a decrease in the syringe tip to the collector plate distance sometimes ends up in the formation of fibers with larger diameters.²¹

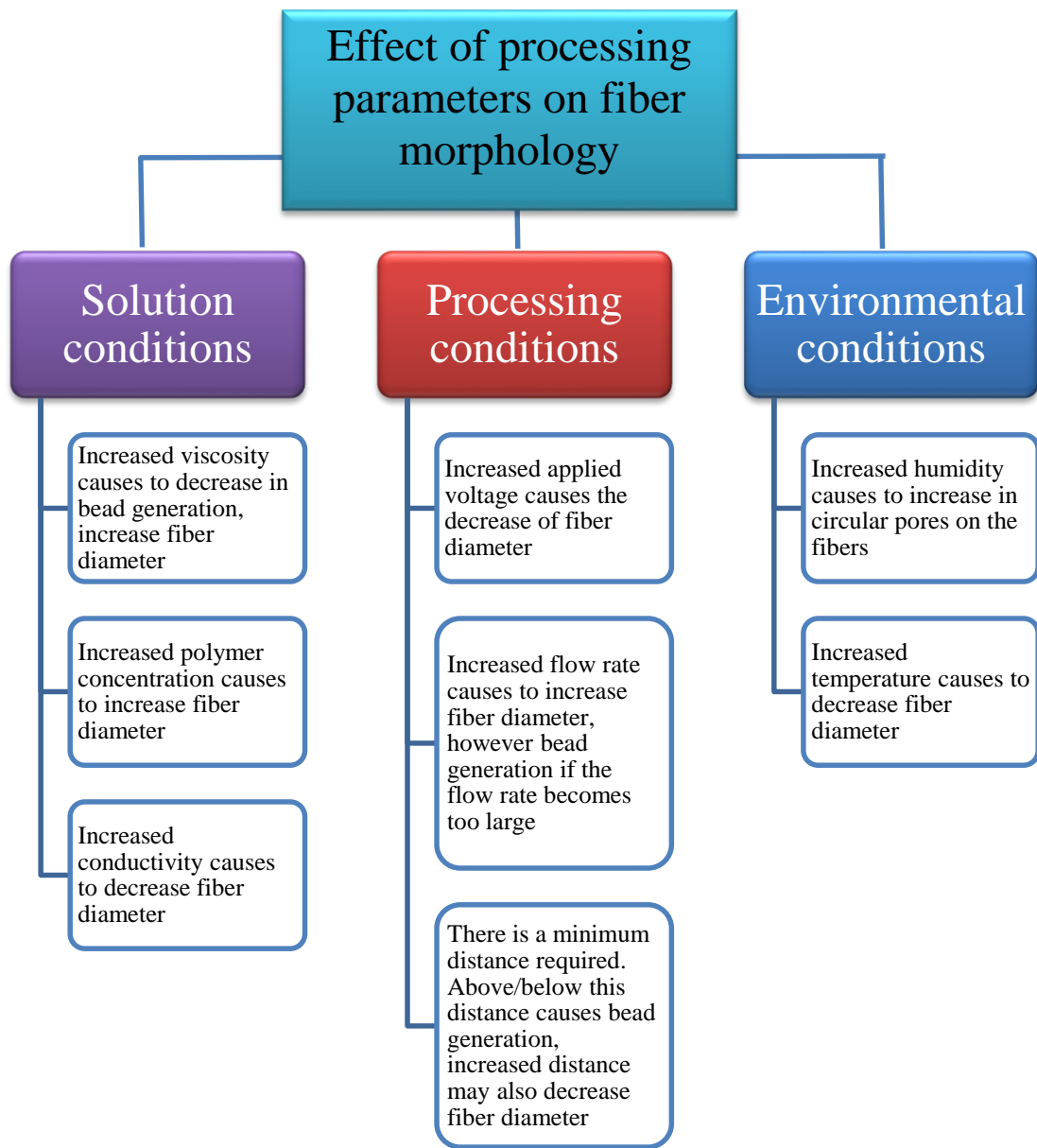


Figure 2. Overview of variables that can affect the electrospinning process and the fiber morphology^{12,22}

This technology was first discovered by Rayleigh in 1887, then studied by Zeleny in 1914 in more detail,²³ and later patented by Formhals in 1934.²⁴ However, the last twenty years research on electrospinning started to be more notorious, due to its promising utility in a broad range of fields, which resulted on the increase of the number of publications as shown in **Figure 3**.

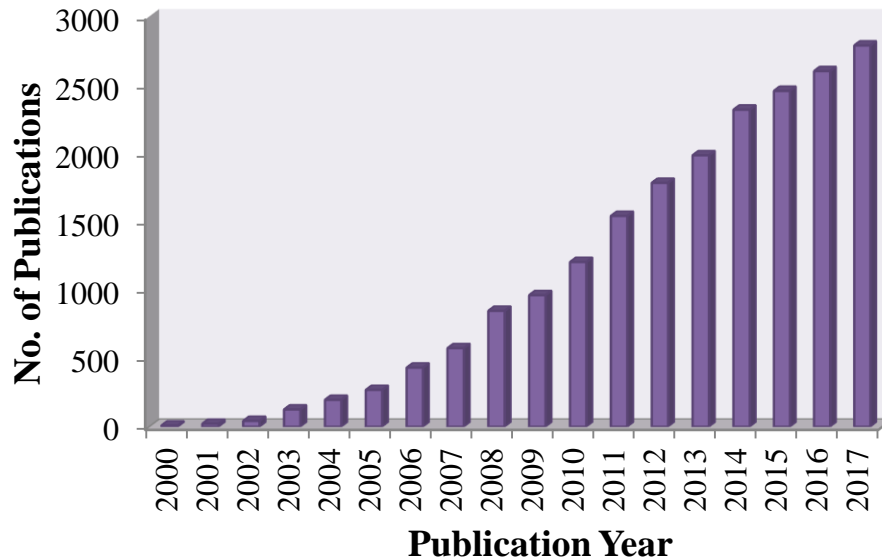


Figure 3. Number of publications in the last decade on electrospinning.

2.2. Materials used in electrospinning technology

A large variety of synthetic and biopolymers have been processed by electrospinning. Examples of synthetic polymers commonly used in electrospinning include Poly(α -hydroxy acids), such as lactic acids (PLA), glycolic acids (PGA) and their copolymers, Poly(caprolactone) (PCL), Poly(vinyl alcohol) (PVA), Polycarbonate, Poly(ethyleneglycol) (PEG), O Poly(urethane) (PU).²⁵ Synthetic polymers can often be electrospun more easily comparatively to biopolymers, however the last ones are preferred to be used in pharmaceutical or food applications due to health and safety issues.^{26,27} Moreover, many synthetic polymers lack the biocompatibility and degradability required for specific (life science) applications. Thus, the electrospinning of biopolymers, have been increasingly investigated,²⁸ and will be discussed in the following sections.

2.2.1. Biopolymers and biomolecules

Electrospun biopolymers include two main classes: proteins and polysaccharides.

Proteins (e.g. zein, gelatin, whey, casein, amaranth, soy, and egg and fish protein) are a class of biopolymers with unique properties/functionalities that can interact with a broad range of hydrophobic and hydrophilic bioactive compounds.²⁹ To be electrospun, proteins need to be unfolded in order to increase polymer chain entanglements,¹ which can be achieved by changing protein structure/aggregation and intra/inter-molecular disulfide bonds.¹

Polysaccharides (e.g. pullulan, dextran, chitosan, starch, alginate, cellulose, cyclodextrin, xanthan gum) are biopolymers consisting of repeating monomeric units of monosaccharides. They are often classified accordingly their charge into anionic, neutral and cationic, but also accordingly to their origin (bacterial, plants, seaweeds).

The electrospinning of polysaccharides, which is part of the main focus of this thesis, is also challenging,¹ and depends on many factors, including chemical properties (e.g. molecular weight, functional groups, charges of the polysaccharide) and the selection of the solvent. Those features will lead to different conductivities, extensional and intrinsic viscosities, surface tension and vapour pressure³⁰ necessary to produce fibers. The formation of electrospun polysaccharide fibers is dependent on the degree of their chain entanglements³⁰ and requires a weak shear thinning behavior.³⁰

Although most of the electrospinning studies focus on the use of (bio) macromolecules, recently some studies using biomolecules such as phospholipids have been reported.

The thesis focuses on the electrospinning of the polysaccharides xanthan gum, and chitosan, as well as phospholipids, which will be discussed in the following sections.

2.2.1.1. Xanthan Gum

Xanthan gum was discovered in the late 1950s by American Scientists and is that the first biopolymer made industrially. Xanthan gum is an extracellular biopolymer produced by the bacterium *Xanthomonas campestris*, consisting of pentasaccharide units containing glucose, mannose and glucuronic acid at a 2:2:1 relation respectively.^{31,32} Due to the presence of pyruvate residues at the terminal mannose moiety and the acetyl groups at D-Mannose unit linked to the main chain, xanthan gum has a polyanionic character. Moreover molecular modeling studies have demonstrated that xanthan for specific concentrations, temperature and pH, can assume a helical conformation, with the side branches positioned almost parallel to the helix axis that stabilizes the structure. Subsequently xanthan forms very viscous aqueous solutions, and at sufficiently high polymer concentration, it exhibits weak gel-like properties. Consequently, it has been widely used and investigated in areas such as food, pharmaceutical, cosmetics, biomedical, tissue engineering and oil industries as thickeners or stabilizers.^{33,34-38}

Stijnman and co-authors reported that xanthan gum could not be electrospun in water because of insufficient entanglement during electrospinning.³⁰ However due to the relevance of this polymer in different fields of research and industry, one of the main objectives of this thesis was to investigate the electrospinning of xanthan gum, by using formic acid as solvent.

2.2.1.2. Chitosan

Chitosan's (deacetylated chitin) are the second plentiful polysaccharides found in nature.³⁹ Chitosan(s) are constituted of glucosamine and N-acetyl glucosamine units. Properties of chitosan rely on its molecular weight (MW), degree of deacetylation (DDA), the distribution of acetylation patterns.⁴⁰ Chitosan's are insoluble in water due to its rigid crystalline structure^{41,42} and soluble in aqueous acidic solutions (for pH below their pK_a of 6.5). At a higher pH than 6.5, chitosan's molecules tend to precipitate owing to deprotonating of the amino groups and lose of its charges.⁴⁰ Chitosan has been widely used in food, biomedical, cosmetic, chemical and pharmaceutical industries due to its nontoxicity, bio functionality, biocompatibility, biodegradability and antimicrobial properties.^{41,42}

The electrospinning of chitosan into a fibrous structure is also challenging^{12,43} and the production of electrospun chitosan nanofibers are known to be dependent of the electrospinning conditions (distance, voltage, flow rate), the physico-chemical properties of chitosan (e.g. Mw, DA) and the solvent.⁴⁴⁻⁴⁷ Ohkawa and collaborators⁴⁸ electrospun chitosan using solvents mixtures of TFA/DCM into homogeneous and uniform nanofibers with an average diameter within the submicron range. However these fibers presented limited applicability, as they easily dissolve in neutral and weak basic aqueous solvents^{49,50} due to the high solubility of the TFA-chitosan salt residues. Efforts to enhance chitosan nanofiber stability have been reported through the neutralization of electrospun chitosan fiber mats with saturated solutions of Na₂CO₃,⁵¹ and crosslinking of chitosan electrospun fibers with glutaraldehyde,⁵² genipin, hexamethylene-1,6-diaminocarboxysulphonate (HDACS) and epi- chlorohydrin (ECH)⁵³. Nevertheless, the methods mentioned follow a two-step protocol or use components with latent cytotoxicity, which cannot suits applications within life sciences.

Table 1. Electrospinning of chitosan blended with other polymers.

Polymer	Molecular weight (kDa)	Solvent	Average diameter	References
Synthetic Polymers				
Chitosan/PEO	654	AA Aq	80 nm to 180 nm	55
Chitosan/PEO	200	AA Aq	98 nm	54
Chitosan/PVA	120	AcrA Aq	90 to 590 nm	58
Chitosan/PVA	220	AA Aq	80 to 150 nm	59
Chitosan/PVA	94	AA Aq	125 to 300 nm	57
Chitosan/PVA	1600	AA Aq	100 nm	60
Chitosan/PVA	Low Molecular Weight	AA Aq	80 to 250 nm	67
Chitosan/Silk Fibroin	220	FA	100 to 500 nm	62
Chitosan/ Pectin /PVA	1600	AA Aq	191 nm	63
Biopolymers				
Chitosan/Pullulan	50–190	CA Aq	650 nm	64
Chitosan/ Zein	50–190	Ethanol and TFA	100 to 600 nm	65
Chitosan/Gelatin	50–190	TFA/DCM	250 to 470 nm	66
Chitosan/Collagen	1000	HFP/TFA	400 to 700 nm	69
Chitosan/Collagen	15	AA Aq	134 to 398 nm	67

Abbreviation: PEO, poly ethylene oxide; PVA, poly(ethylene oxide); AA Aq, acetic acid aqueous; AcrA Aq, acrylic acid aqueous; CA Aq, citric acid aqueous; FA, formic acid; TFA, trifluoroacetic acid; DCM, dichloromethane; HFP, 1,1,1,3,3,3 hexafluoro-2-propanol.

Alternatively, the production of electrospun chitosan based fibers has been carried out by blending this biopolymer with other polymers, which are listed in **Table 1**. Chitosan was mixed with other synthetic or biopolymers, such as PEO^{54–56} or polyvinyl alcohol (PVA),^{57–61} silk fibroin,⁶² Pectin,⁶³ pullulan,⁶⁴ Zein,⁶⁵ Gelatin⁶⁶ and collagen.^{67,68,69} For example, Duan et al.⁵⁶ reported the electrospinning of chitosan (654 kDa) mixed with PEOs (600 and 4000 kDa) using 2 wt% aqueous acetic acid solutions as the solvent. The lowest diameter nanofibers (less

than 150 nm) were produced from chitosan/PEO ratio of 2:1 and 1:1 using 1500 kDa PEO at polymer concentrations of 6 wt%.

Similarly, Zhou and his colleagues stated that 7 wt% of pure chitosan (120 kDa) solutions were not electrospinnable in aqueous acrylic acid, however the addition of 9 wt% PVA solutions favored the production of the electrospun fibers⁵⁸. Uniform fibers with average diameters ranging from 157 to 590 nm and 89–320 nm were fabricated using concentrated acrylic acid to dissolve chitosan/PVA at ratios of 9:1 and 5:5, respectively. Moreover Huang et al.⁵⁹ blended 9 wt% PVA (2.5 kDa) with 3 wt% of chitosan (220 kDa) in aqueous acetic acid solution at a ratio of 3:7, which resulted in fibers diameters ranging between 150 and 300 nm.

2.2.1.3. Phospholipids

Phospholipids have been used for preparing capsular structures (mainly vesicles or liposomes),^{70–73} for nano-microencapsulation of drugs⁷⁴ and mammalian cells,⁷⁵ and in food⁷⁶ as delivery carriers of nutrients, nutraceuticals, food additives and antimicrobials. Encapsulation of bioactives within lipid formulations offers enhanced stability and protection combined with superior biocompatibility and enhanced permeability, depending on the lipid composition and properties.^{77,78} Among other phospholipids, asolectin, a mixture of lecithin, cephalin and phosphatidylinositol, saturated fatty acids, mono-unsaturated and poly-unsaturated fatty acids has been used to develop nano-microstructures such as fibers,^{79–82} hydrogels⁸³ and liposomes^{76,84} for the encapsulation of bioactives.^{82,85} In addition, asolectin components have also been proven to display antioxidants properties.^{85–88}

The electrospinning of phospholipids was reported for the first time by Mckee and co-workers, where critical concentrations of phospholipids, using mixtures of DMF:CHCl₃ as solvents, were

required to favor the self-assembly of the phospholipids into wormlike micelles able to originate significant entanglements to produce electrospun phospholipid fibers.⁷⁹

Recently, electrospun asolectin fibers with average diameters of $2.57 \pm 0.59 \mu\text{m}$, $\sim 3\text{-}8 \mu\text{m}$, $\sim 4\text{-}5 \mu\text{m}$ and $14.3 \pm 2.7 \mu\text{m}$ were produced using chloroform:dimethylformamide, isooctane, cyclohexane and limonene as solvents. The use of co-axial solvent electrospinning was tested, by using individual solvents in the outer needle and solutions of phospholipids dissolved in CHCl_3 : DMF in the inner needle. The average diameter of the fibers was observed to be reduced to the nanoscale, when DMF (a solvent with a high dielectric constant) was used as a sheath solvent. The dielectric constant of the solvents was found to have a strong influence on the the jet split properties and to play an important role on the morphology of the electrospun phospholipid fibers.⁸⁰ Furthermore, the mechanical properties of phospholipid fibers, prepared using isooctane as a solvent, were evaluated by nanoindentation using Atomic Force Microscopy.⁸¹ Their elastic modulus was found to be approximately 17.261 MPa. At a cycle of piezo expansion-retraction (loading-unloading) of a silicon tip on a fiber, relatively high adhesion was observed during unloading.⁸¹ The phospholipid fibers were shown to be stable in ambient conditions, preserving the modulus of elasticity up to 24 h. In another study, Yu et al.⁸⁹ used polyvinylpyrrolidone (PVP) with soybean lecithin to create a electrospun fibers. They observed liposomes and vesicles with a very narrow distribution (between 120–370 nm) after immersion of lecithin/PVP fibers in water. Zhang and co-authors applied a hybridization strategy to produce electrospun cholesteryl-succinyl silane (CSS) nanofibers to increase stability of electrospun lipid.⁹⁰

2.3. Applications of Electrospinning

The unique properties of electrospun nano-microfibers, such as high surface area per unit mass, high porosity, tunable pore size and surface properties, layer thinness, high permeability and cost-effectiveness^{11,91} has led to the increased interest on this this technology. Furthermore, electrospinning can be processed at room temperature; enables encapsulation of bioactive ingredients or functional compounds with high encapsulation efficiency, the final product is collected on dry state and requires low energy consumption and investment.

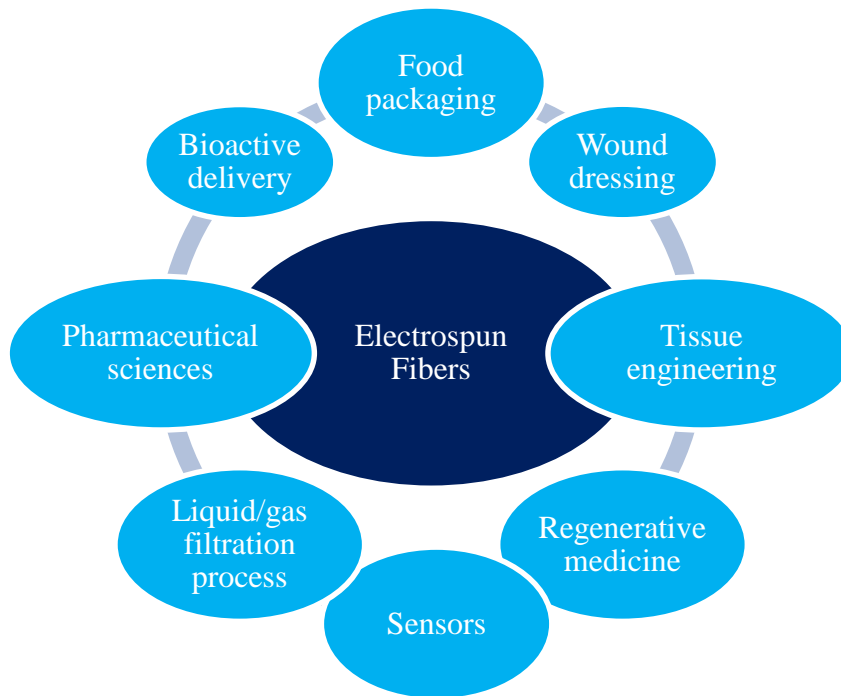


Figure 4. Examples of applications of electrospun fibers.

Therefore, electrospinning technology has been explored in a wide range of applications including food, drug delivery, tissue engineering, biomedicine, sensors, textile, filtration, composites, electronics, among others^{22,92} (**Figure 4**).

2.3.1. Encapsulation of bioactives within electrospun fibers

Food and pharmaceutical industries are searching for novel food products containing health-promoting bioactive compounds, with little or no synthetic ingredients. However, some bioactives are sensitive to the ambient factors such as light, temperature, pressure, and pH media, among others. The interactions of sensitive bioactives with ambient factors, might affect their chemical instability and degradation, leading to undesirable reactions with other compounds or formation of strong and unpleasant odor and/or flavors,⁹³ which affects their functionality and usage. In this context, encapsulation emerges as a solution to overcome these problems, and to control the release and delivery of the bioactives. Electrospinning facilitates the encapsulation of a broad range of bioactives using a variety of food ingredients (e.g. proteins, polysaccharides and phospholipids), at room temperature with a very high encapsulation efficiency. In addition, the encapsulation of bioactives within electrospun fibers with controlled diameters, morphologies, porosities and overall functionality, can further facilitate their delivery and improve their bioavailability.

Examples of bioactives include vitamins, omega-3 polyunsaturated fatty acids, probiotics, and polyphenolic compounds.⁹⁴ Polyphenols belongs to a class of antioxidants and are the most abundant in human diet.⁵⁶ Because of their antioxidant,⁹⁵ antimutagenic,⁹⁶ antimicrobial,⁹⁷ and anticarcinogenic properties,^{98,99} polyphenols have recently attracted the research towards the study of the metabolism and absorption mechanisms across the gut barrier.¹⁰⁰ Polyphenols are categorized according to the chemical structure of their carbon skeleton, and the most abundant classes in our diet are phenolic acids and flavonoids. Examples of polyphenols are caffeic acid, ferulic acid, epicatechin gallate, epicatechin, epigallocatechin gallate, curcumin and gallic acid

and the encapsulation of the three last polyphenols within electrospun fibers will be discussed in the following sections.

2.3.1.1. Vanillin

Vanillin (4-hydroxy-3-methoxybenzaldehyde) is a phenolic compound, which can either be extracted from pods of *Vanilla Planifolia* or synthesized chemically. It has been widely used in the food industry as a flavor, but also as a food preservative, due to its antioxidant, antimicrobial, anticarcinogenic and antimutagenic properties.^{101,102} However, its high volatility and thermal instability are the main drawbacks for its use and processing in food industry.^{103–105}

The encapsulation of vanillin using electrospinning technology has been investigated by Uyar and co-workers using cyclodextrins as carrier CD.^{101,106} For instance, electrospun PVA nanofibers with diameters of 200 nm incorporating vanillin/cyclodextrin inclusion complex (vanillin/CD-IC) were shown to prolong the shelf-life and the high temperature stability of vanillin.¹⁰⁶ In another study, vanillin/cyclodextrin inclusion complex nanofibers were successfully obtained from three modified CD types (HP β CD, HP γ CD and M β CD) in three different solvent systems (water, DMF and DMAc) via electrospinning processing, without using a polymer carrier.¹⁰¹ The authors demonstrated that these fibers allowed the loading of high amounts of vanillin, while improving its antioxidant property. Maximum encapsulation efficiency of vanillin (~85% w/w) was observed for vanillin/M β CD-IC nanofibers, however still considerable amount of vanillin (~75% w/w) was encapsulated in vanillin/HP β CD-IC nanofibers and vanillin/HP γ CD-IC nanofibers. Electrospun PVA nanofibers loaded with ethyl vanillin with diameters in the range 100–1700 nm, were also produced. PVA/ethyl vanillin nanofibers were

observed to be mechanically stable and to influence the thermal properties of vanillin comparatively to the free flavor.¹⁰⁷

2.3.1.2. Curcumin

Curcumin is another phenolic compound derived from the turmeric herb *Curcuma longa* L., with biological and pharmacological properties, such as antioxidant, anti-inflammatory, antimicrobial, antimalarial, and anticarcinogenic.¹⁰⁸ It has been also used in food industry as colorant.² As an hydrophobic molecule, curcumin has very low solubility in water and its chemical stability has been reported to be affected by external factors such as pH, exposure to light, temperature and oxygen.^{109,110} Moreover, curcumin has poor bioavailability due to inefficient absorption at the intestinal track and for that reason² it is commonly administered with carriers to transport this phenolic compound to the epithelial tissue.¹⁰⁹

Therefore, the production of curcumin delivery carriers has been attempted using electrospinning. For example, encapsulated curcumin in polyvinyl alcohol (PVA) nanofibers with and without β -cyclodextrin (CD) was investigated by Zhu Sun.¹⁰⁸ They demonstrated that the solubility and stability of curcumin was improved in PVA/curcumin and PVA/CD–curcumin complex nanofibers (containing 5 to 50% wt % of curcumin) which favored the delivery of curcumin more rapidly than the pristine drug. This study suggested the potential to utilize electrospun fibers with curcumin in anti-cancer therapies.

Furthermore, Rüzgar et al.,¹¹¹ produced electrospun polyethylene oxide (PEO)/ hydroxypropyl methylcellulose (HPMC) fibers loaded with curcumin. *In vitro* solubility tests showed that curcumin loaded within nanofibers dissolved in both distilled water and buffer (pH 1.2), and thus

curcumin- PEO/HPMC nanofibers can be a promising system for the oral delivery of curcumin.¹¹¹

Wang et al.¹¹² also produced homogeneous and smooth surface polyvinyl pyrrolidone (PVP) nanofibers loaded with curcumin by electrospinning. *In vitro* dissolution profiles have been shown that curcumin encapsulated within PVP nanofibers could be fast released in phosphate-buffered saline (pH 7.4) solution, while insignificant dissolution was detected in pure curcumin sample.¹¹² Thus, the bioavailability of curcumin was enhanced by using this electrospun fiber matrix, which was confirmed also with *in vitro* cell studies and *in vivo* animal tests.

Moreover, Aytac and Uyar¹¹³ developed electrospun core-shell nanofibers using cyclodextrin (core) and polylactic acid (shell) for the encapsulation of curcumin. They found that greater amount of curcumin was released from both CD/PLA and PLA nanofibers at pH 1 (simulated gastric fluid) compared to pH 7.4 (simulated intestinal fluid) due to increased solubility of curcumin at low pH. However, the released curcumin from CD/PLA core-shell fibers was higher than curcumin released from PLA due to the enhancement of solubility,¹¹³ suggesting that the core-shell nanofiber structure has the potential to be used for the delivery of hydrophobic drugs. Another study described the fabrication of curcumin-loaded gum tragacanth (GT)/poly (vinyl alcohol) (PVA) nanofibers.¹¹⁴ Other studies reported the encapsulation of curcumin with electrospun silk fibroin, polyvinylpyrrolidone, zein and amaranth-pullulan fibers to modulate the solubility, antioxidant, bioavailability and release properties of the bioactive compound.¹¹⁵⁻

118

2.3.1.3. Epigallocatechin gallate (EGCG)

EGCG is one of the most abundant polyphenolic compounds, and has recently received increasing attention in food and pharmaceutical applications due to its antioxidative properties, antimicrobial activities, and health benefits.¹¹⁹ However, it is not stable under alkaline conditions and may undergo oxidation, polymerization, and epimerization during processing.^{120–122} In addition, as many other polyphenols, EGCG has a poor bioavailability, due to its high hydrophilicity that limits EGCG permeability across intestinal epithelium.¹²³ Several studies have demonstrated a high and specific accumulation of tea flavonoids in epithelial Caco-2 cells or epithelial cells along the aerodigestive tract,^{124–126} which have been recognized as major sites for biological activity of flavonoids.

The development of electrospun poly (lactic-co-glycolic acid) (PLGA) nanofibers to encapsulate and control the release of EGCG was reported by Shin *et al.*¹²⁷ EGCG/PLGA fibers with diameter of 300–500 nm allowed the sustained release of EGCG over 28 days in the phosphate-buffered saline (pH 7.4). The release was mainly controlled by the diffusion of the EGCG and the degradation PLGA nanofibers.¹²⁷ In another study, zein nanofibers (with diameters ranging from 150 to 600nm) have been used to study the encapsulation and preservation of EGCG in aqueous media.¹²⁸ It was found that the recovery of EGCG increased significantly after its immersion in water (98 %) when the fibers have been stored for at least 1 day at 0 % relative humidity (RH), compared to fresh nanofibers (82 %), while at 75 % RH, a considerable loss of EGCG in water was observed. Based on the FTIR data, Li and co-workers concluded that the high amount of immobilized EGCG within the nanofibers was due to hydrogen bonding, hydrophobic interactions and possibly physical encapsulation, which caused in the retaining of EGCG within the zein fibers that are immersed in water.¹²⁸

Furthermore, Lee and co-workers¹²⁹ have developed hyaluronic acid/ lactic-co-glycolic acid (HA/PLGA) core/shell fibers for the encapsulation of EGCG. The studies suggested that the release of EGCG from HA/PLGA was controlled by the diffusion of the bioactive and the degradation of PLGA matrix over 4 weeks.¹²⁹ Other studies have also reported the use of electrospun fibers to create proper EGCG release carriers.^{130–132}

2.3.1.4. Gallic acid (GA)

GA, also known as 3,4,5-trihydroxybenzoic acid, is one of the main phenolic compounds found in plants, mostly in tea leaves,¹³³ vegetables, grapes, and pomegranates. It has been widely used as additive in food and pharmaceutical industries and its known by its antioxidant, antimicrobial, anti-inflammatory and anticancer activities.^{134–136} Several studies have demonstrated that only small amounts of orally administered GA are absorbed through the intestine due to its low permeability, poor water solubility (11.5 mg/mL) and chemical instability, as it easily oxidize.^{136–138}

Electrospun fibers have been used as a delivery carrier of GA. Due to high surface area of nanofibers, one would expect that the fibers improve the solubility and release of GA as well as protect it from oxidation. For example, Neo et al.¹³⁹ encapsulated GA in zein-based nanofibers to increase its stability. Moreover, cellulose acetate (CA),¹³⁶ and poly (L-lactic acid) (PLLA)/GA fibers¹⁴⁰ have been developed as an encapsulation matrices of GA.

Futhermore, Aytac et al.¹³⁷ developed an inclusion complex of GA in cyclodextrin (CD), that was then electrospun withing polylactic acid (PLA) nanofibers. They have studied the release behavior of GA into three different mediums: water, 10% ethanol and 95% ethanol, which were aqueous, alcoholic and fatty food simulants, respectively. They found that the release of GA

from PLA/GA nanofibers with and without CD showed similar behavior in all three mediums, however higher amount of GA release was achieved from PLA/GA/CD nanofibers in aqueous solution and 10% ethanol compared to PLA/GA nanofibers, due to the higher solubility of GA in water. Overall, it was suggested that the nanofibers with encapsulated GA displayed a high antioxidant activity which might be appropriate as a food packaging material, to rise the shelf life of food products and to improve the quality of foods.¹³⁷

2.3.2. Caco-2 cell model – the oral delivery system

Oral delivery is the one of the most adequate and safe means for administration of the bioactive compounds because of its appropriateness and easiness of administration. Electrospun fibers has been studied as oral delivery and oral cavity delivery systems,^{141–143} with promising results. The large surface to volume ratio of electrospun fibers can be utilized to improve the rate of dissolution and thus to increase the release of bioactive compounds.^{144–146} However, the oral delivery of the bioactive compounds at the intestine using electrospun nanofibers has not assessed in detail.

The Caco-2 cell model is used frequently to mimic the epithelial layer in the small intestine, and thus to evaluate the absorption of bioactive compounds *in vitro* assays.¹⁴⁷ The Caco-2 cells, which are originally from a human colon cell line, can polarize and express receptors that resemble the intestinal absorptive cells found in the small intestine when cultured under specific conditions.¹⁴⁸ *In vitro* permeability studies have been employed using Caco-2 cells, to assess the cytotoxicity and the permeation of bioactive compounds using a particular delivery system.^{149,150}

Figure 5 shows an illustration of the setup employed for the permeation assays of phenolic compounds curcumin, EGCG and GA that used for the studied described at Papers II and IV.

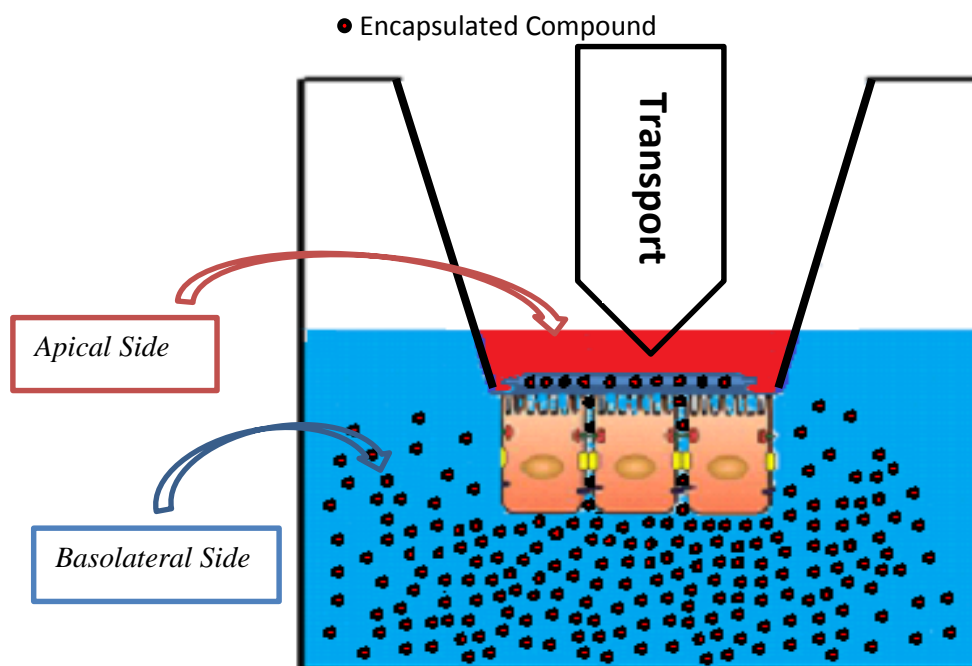


Figure 5. Illustration of a Transwell® setup with seeded Caco-2 cells. Electrospun fiber with an encapsulated compound was located on top of the cells. The compound was released and permeated the monolayer. The accumulated amount of permeated compounds was determined by taking out samples from the basolateral side and apical side, and analyzing them using spectrophotometry.

Furthermore, the stability of ions across the cell monolayer could be investigated by the transepithelial electrical resistance (TEER), to examine the mechanism behind the transepithelial permeation of the bioactive compound. The variations in TEER can designate the mechanism by which a molecule is transported; a reduced TEER values often indicates a paracellular transport facilitated by opening of the tight junctions - provided that the cell viability is not compromised.

The viability of the Caco-2 cells can be studied by measuring the relative metabolism of treated cells, in relation to untreated cells. The MTS/PMS (3-(4,5-dimethylthiazol-2-yl)-5-(3-carboxymethoxyphenyl)-2-(4-sulfophenyl)-2H-tetrazolium/phenazinemethosulfate) assay is viability colorimetric assay, where the cell viability is evaluated by monitoring a reduction of MTS, to a colored formazan product using absorbance spectroscopy. The reduction of MTS is only possible by viable cells, and the relative viability can therefore be quantified by comparison to a positive control.

Only few studies have evaluated the intestinal delivery properties of electrospun nanofibers with encapsulated bioactive compounds assessed using the Caco-2 cells model.^{151–153} Studies by Stephansen *et al.*¹⁵² from our group using a Caco-2 cell permeability assay found that electrospun fish sarcoplasmic proteins (FSP) nanofibers could be used as novel oral delivery system of biopharmaceuticals. In particular, encapsulation of insulin into the FSP fibers provided protection against chymotrypsin degradation (suitable for oral administration), and the interactions between fibers and epithelial cells led to opening of the tight junctions, which promoted an increased transepithelial transport of insulin without compromising cellular viability. Moreover, Tibolla *et al.*¹⁵¹ have shown that cellulose nanofibers (CNFs), isolated from an agro-industrial waste (unripe banana peel), were not cytotoxic to Caco-2 cells and can be safely used in food packaging applications. Lin *et al.*¹⁵³ also studied the anticancer efficiency of magnetic electrospun chitosan nanofibers by assessing the Caco-2 cell viability. It was found, that magnetic electrospun chitosan nanofibers have a potential therapeutic modality in tumor administration.

3. Results and discussion

This section has been separated into two parts; part A concerns electrospinning of xanthan, xanthan-chitosan and phospholipid (asolectin), and is composed of five parts organized by Paper I to Paper V. Part B concerns co-assembly of chitosan and phospholipids in to hydrogel, and is composed of one part organized by Paper VI.

3.1. Part A – electrospinning

3.1.1. Development of xanthan nanofibers- Paper I

Electrospinning of Xanthan Polysaccharide

Elhamalsadat Shekarforoush,¹ Adele Faralli,¹ Sokol Ndoni,^{2,3} Ana C. Mendes,¹ Ioannis S. Chronakis¹

1 Nano-Bio Science Research Group, DTU-Food, Technical University of Denmark, Søtofts plads, Building 227, 2800 Kgs. Lyngby, Denmark.

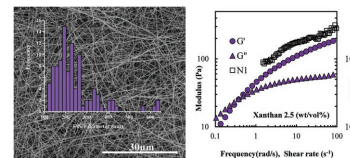
2 DTU-Nanotech, Technical University of Denmark, DK-2800 Kgs. Lyngby, Denmark.

3 Center for Nanostructured Graphene - CNG, Technical University of Denmark, DK-2800 Kgs. Lyngby, Denmark.

Electrospinning of Xanthan Polysaccharide

Elhamalsadat Shekarforoush, Adele Faralli, Sokol Ndoni, Ana C. Mendes, Ioannis S. Chronakis*

Electrospun pure xanthan polysaccharide nanofibers are prepared using formic acid as a solvent. Morphological studies by scanning electron microscopy show that uniform fibers with average diameters ranging from 128 ± 36.7 to 240 ± 80.7 nm are formed depending on the polysaccharide concentration (0.5 to 2.5 wt/vol%). The correlation between the concentration and the rheological properties of xanthan solutions, with the morphology of the nanofibers is investigated. At the polysaccharide concentrations where nanofiber formation is observed, an increase of the elastic modulus and first normal stress differences is observed. The typical “weak gel-like” and thixotropic properties known for aqueous xanthan solutions, are not observed for the xanthan solutions in formic acid. The Fourier transform infrared spectroscopic and circular dichroism studies verify that an esterification reaction takes place, where formic acid reacts with the pyruvic acid groups of xanthan. Hence, formate groups neutralize the pyruvic charges which in turn stabilize the helical conformation of xanthan. The results obtained from size-exclusion chromatography reveal a small difference in the molecular weight of the polysaccharide when dissolved in distilled water or in formic acid.



1. Introduction

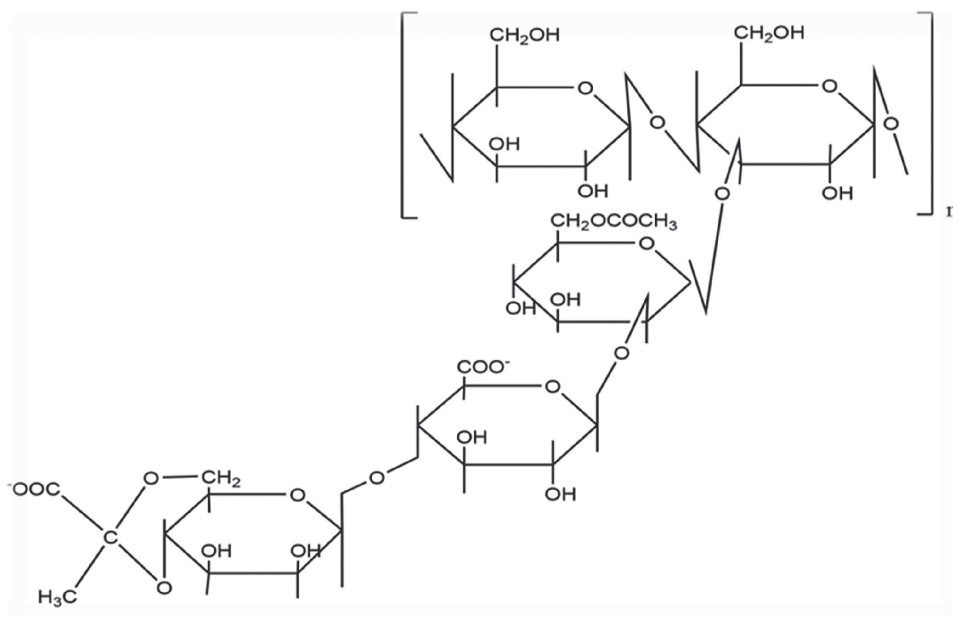
Studies related to the electrospinning of polysaccharides such as chitosan, starch, alginate, cellulose and cellulose derivatives, pullulan, dextran, and cyclodextrins are of growing interest the last years.^[1] It is known that the concentration, the chemical structure, and the shear thinning properties of the polysaccharides, affect their electrospinning processing.^[1,2] Typically, the formation of electrospun polysaccharide fibers is dependent on the degree of

their chain entanglements, the viscosity of the solution, and requires weak shear thinning properties to favor the breakdown of the liquid jet when pulled and extended by the electric field.^[2,3] For a number of polysaccharides, including xanthan gum, gellan gum, arabic gum, and carrageenan, it has been challenging to electrospun,^[2] and thus water-soluble polymers such as poly(ethylene oxide) and poly(vinyl alcohol) were used as “carriers.”^[4–6]

Xanthan gum is an extracellular heteropolysaccharide produced by the bacterium *Xanthomonas campestris*, containing glucose, mannose, and glucuronic acid (Figure 1) in the molar ratio 2:2:1.^[7,8] Due to the presence of pyruvic and acetic residues, xanthan has a polyanionic character.^[9,10] In its native state, xanthan adopts a helical structure as single or double helix. Upon high salt and polymer concentrations, intra- and intermolecular interactions promote double-helix ordering state.^[11]

Solutions of xanthan prepared using various molecular weights of the polysaccharide, concentrations, temperature, solvents, and pH have been widely studied in terms of their rheological properties.^[12–21] The “weak gel-like” properties of xanthan solutions arise from lateral association of ordered chain sequences to form extended junction zones comparable to those in true gels but much

E. Shekarforoush, Dr. A. Faralli, Dr. A. C. Mendes,
Prof. I. S. Chronakis
Nano-BioScience Research Group, DTU-Food
Technical University of Denmark
Søtofts plads, Building 227, 2800 Kgs. Lyngby, Denmark
E-mail: ioach@food.dtu.dk
Dr. S. Ndoni
DTU-Nanotech
Technical University of Denmark
2800 Kgs. Lyngby, Denmark
Dr. S. Ndoni
Center for Nanostructured Graphene – CNG
Technical University of Denmark
2800 Kgs. Lyngby, Denmark



■ Figure 1. Repeating structure of xanthan gum.

weaker, since the network structure may be broken down under stress conditions.^[22–24] The distinct shear thinning behavior of xanthan is associated with its molecular conformation, which at low shear stress association of chains is induced by hydrogen bonding resulting in high viscosity. However, disruption of the intra- and intermolecular hydrogen bonding at high shear stress, leads to the decrease of its viscosity.^[18,25,26]

Previous studies suggested that xanthan could not be electrospun due to the insufficient entanglements during electrospinning.^[2] In the present study we report for the first time the formation of electrospun xanthan nanofibers using formic acid as a solvent. The electrospinnability and the morphology of the resultant nanofibers were correlated with the rheological properties and the molecular conformation of xanthan solutions.

2. Experimental Section

2.1. Materials

Xanthan gum (Cosphaderm X 34), from *Xanthomonas campestris*, was kindly provided by Cosphatec GmbH (Drehbahn, Hamburg, Germany). All chemicals, including formic acid, were obtained from Sigma-Aldrich (Denmark) and used as received. Xanthan was dissolved in formic acid at final concentrations of 0.5, 1, 1.5, 2, and 2.5 wt/vol% (weight/volume%) and vigorously stirred overnight at room temperature.

2.2. Rheological Properties of Xanthan Solutions

The viscoelastic properties, elastic (G') and viscous modulus (G'') of xanthan solutions in formic acid were examined by low

amplitude oscillatory measurements using a controlled stress HAAKE MARS rheometer (Thermo Scientific Inc., Germany). A cone and plate probe (cone diameter 60 mm, angle 1° and gap 0.53 mm) were utilized. The sample was loaded on the rheometer plate and frequency sweeps (0.01 to 100 rad s^{-1}) were carried out using a constant shear stress of 1 Pa (within the linear viscoelastic region). Flow measurements were performed afterward in which the shear rate was increased from 0.1 to 100 s^{-1} and instantaneously decreased from 100 to 0.1 s^{-1} . The samples were covered with silicone oil to avoid evaporation. All measurements were carried out at room temperature (25°C) in triplicate for each sample.

2.3. Conductivity

Electrical conductivity of xanthan solutions was determined using WTW LF323-B conductivity meter (WTW GmbH, Weilheim, Germany). All measurements were carried out at room temperature ($25 \pm 2^\circ\text{C}$) in triplicate for each sample.

2.4. Circular Dichroism (CD)

CD measurements were performed on a Jasco J-810 spectropolarimeter connected to a temperature controller (Jasco PTC-423S). CD spectra of 0.5 wt/vol% xanthan solutions were collected in the wavelength range of 192–250 nm, at $20 \pm 1^\circ\text{C}$ using a scan speed of 10 nm min^{-1} , data pitch of 0.1 nm and bandwidth of 1 nm. Five scans were accumulated for each sample using a 0.1 cm path length quartz cuvette.

In order to evaluate the effect of formic acid on the molecular conformation of xanthan chains, 0.5 wt/vol% xanthan was dissolved in water or in formic acid at room temperature overnight under vigorous stirring. Subsequently, the samples were snap-frozen in liquid nitrogen and incubated overnight

in a vacuum chamber (Christ Alpha 1–2 ld. plus) at 0.75 mbar. The xanthan powders were both redissolved in water at a final concentration of 0.5 wt/vol% and kept under vigorous stirring at room temperature overnight. A 0.5 wt/vol% xanthan aqueous solution was used as a control without freeze-drying the sample.

2.5. Fourier Transform Infrared Spectroscopy

The Fourier transform infrared spectroscopic (FTIR) analysis was performed using a Perkin Elmer Spectrum 100 spectrometer based on a universal attenuated total reflectance-FTIR sensor. A crystal composed of diamond in the upper layer and zinc selenide focusing element was utilized for the analysis of xanthan samples in their solid state (pellet). Solid samples were analyzed on a measurement area of 2 mm in diameter enabling good contact between sample and crystal surface. 130 N force gauge was applied on the sample through a pressure arm. Measurements of native xanthan, freeze-dried xanthan previously dissolved in water, freeze-dried xanthan first dissolved in formic acid, and electrospun xanthan fibers after formic acid evaporation were recorded in a wavenumber range of 4000–700 cm^{-1} in the transmission mode. A total of four scans for each sample were accumulated at room temperature at a resolution of 1 cm^{-1} . The infrared peaks were identified using Spectrum 10 software using 1%T peak threshold. Spectra were plotted as percentage transmittance (%T) against wavenumber (cm^{-1}) with Origin Pro SR1 software.

2.6. Size-Exclusion Chromatography (SEC)

SEC has been used to evaluate the absolute molecular weight of xanthan solutions. A solution of xanthan dissolved in water, as well as freeze-dried xanthan previously dissolved in formic acid and resolubilized in water, were analyzed by SEC at the same concentration (0.05 wt/vol%). Such low concentration of xanthan was used to avoid the clogging of the filter located just before the detector units. A Shimadzu 10A HPLC instrument was operated with two SEC columns attached: a TSK-guard column PWH (internal diameter of 7.5 mm and length of 7.5 cm), and a TSKgel G6000PW column from Tosoh Bioscience (with particle size of 17 μm , internal diameter of 7.5 mm, and length of 30.0 cm). After the columns, the solution was analyzed by two detectors, a Shimadzu RID-10A differential refractive index detector and a Viscotek model 270 light scattering detector. The eluent (0.8 M NaNO_3 aqueous solution) was pumped through the columns at a flow rate of 0.5 mL min^{-1} and the measurement and detection units were kept at room temperature (20 $^\circ\text{C}$). The injection volume was 400 μL and triplicate analysis was done for each sample. The analytical columns were calibrated with two pulvular standards ($M_w = 107$ and 344 kDa, Polymer Standards Service, Germany) and a dextran standard with a molecular weight of 1750 kDa (American Polymer Standards, US). Data analysis was performed with Viscotek TriSEC GPC V3.0 software. For the evaluation of xanthan molecular weight, a refractive index increment dn/dc of 0.153 mL g^{-1} was used, which is typical for polysaccharides.^[27]

2.7. Electrospinning Process

The electrospinning setup included a high voltage generator (ES50P-10W, Gamma High Voltage Research, Inc., USA) to provide a voltage of 20 kV, and syringe pump (New Era Pump Systems, Inc., USA) to feed the xanthan solution at a flow rate of 0.01 mL min^{-1} . Xanthan fibers were collected on a steel plate covered with aluminum foil placed at a distance of 8 cm from the end of the needle. The electrospinning process was carried out at ambient conditions.

2.8. Morphology

The morphology of electrospun xanthan fibers was monitored using a Quanta FEG 3D scanning electron microscope (SEM). For SEM analysis, a small amount of fibers was attached on SEM specimen by a double-sided carbon adhesive tape, and sputter coated with 6 nm of gold (Leica Coater ACE 200). The Fibermetric application (Phenom Pro Suite software) was used to obtain the histograms with the diameter distribution of the nanofibers (measured at 100 different points for each image).

2.9. Statistical Analysis

All determinations were carried out in triplicate and results were stated as the mean values \pm of standard deviations. Significant differences ($p < 0.05$) among samples were assessed with analysis of variance (one-way ANOVA with Fisher's multiple comparison test), using the statistical Minitab software version 16 (Minitab Inc. State College, PA, USA).

3. Results and Discussions

3.1. Electrospinning of Xanthan Nanofibers

Xanthan nanofibers were obtained by the electrospinning of 1.5–2.5 wt/vol% polysaccharide solutions in formic acid (Figure 2). The nanofibrous structure is composed of individual, uniform, and randomly oriented fibers with average diameters ranging from 128 ± 36.7 to 240 ± 80.7 nm. Decrease of the xanthan concentration below 1 wt/vol% resulted in the formation of electrospun beaded fibers, and beads (at 0.5 wt/vol%), denoting that the polysaccharide concentration is critical for the formation of uniform nanofibers. Xanthan solutions beyond 2.5 wt/vol% were highly viscous and it was not possible to electrospun higher polysaccharide concentrations of this molecular weight.

Figure 3 shows the average nanofiber diameter (D) dependence with the concentration [c] of xanthan that can be described as

$$D = 0.127[c]^{0.69} \quad (1)$$

The dependence of the nanofiber diameter with the polysaccharide concentration is related to the intermolecular conformation and association of xanthan in formic acid and it will be discussed below.

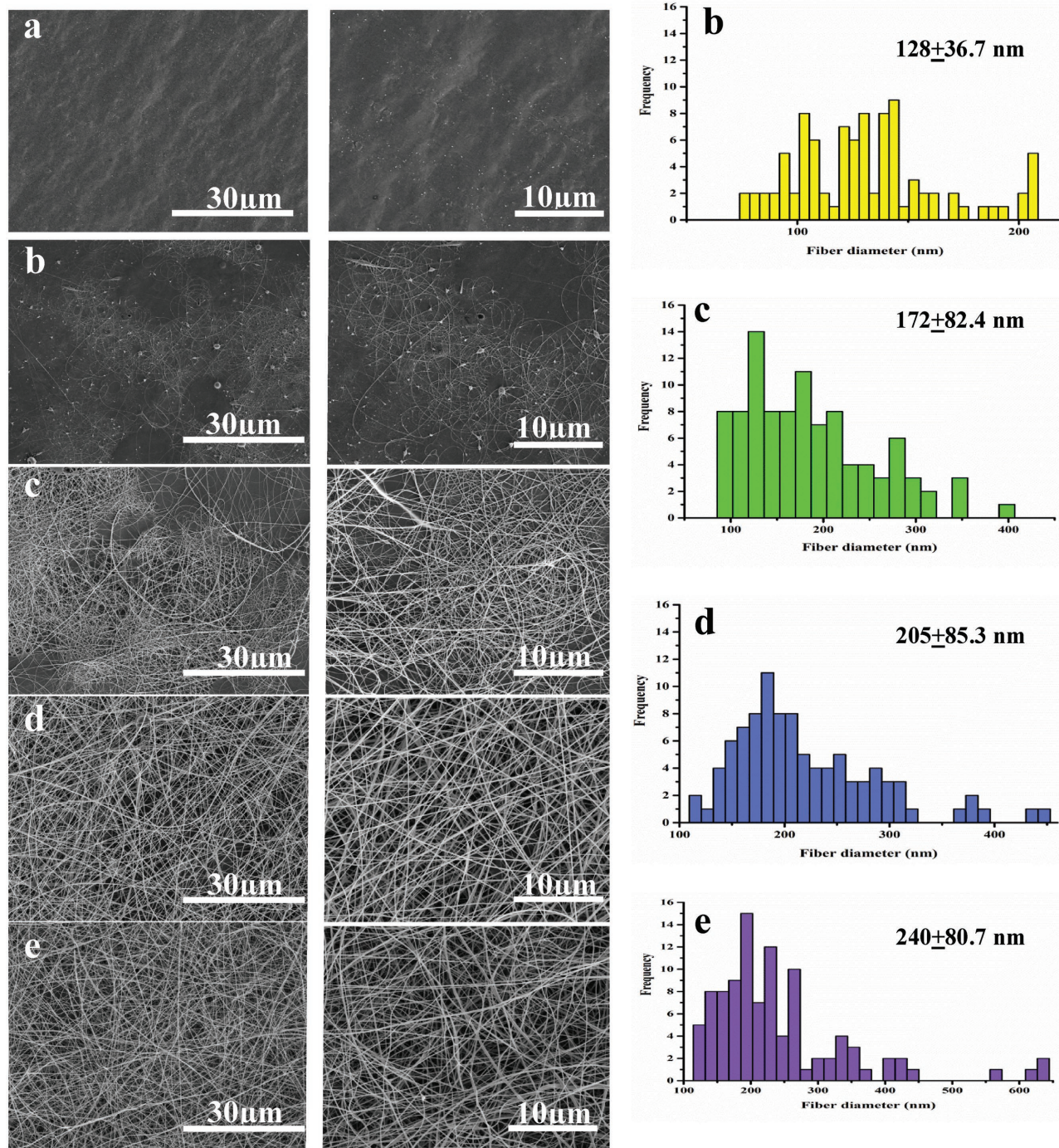


Figure 2. SEM images of electrospun xanthan nanofibers from different concentrations in formic acid: a) 0.5 wt/vol%, b) 1 wt/vol%, c) 1.5 wt/vol%, d) 2 wt/vol%, and e) 2.5 wt/vol%. The histograms summarize the diameter distribution of the nanofibers.

The electrical conductivity of xanthan solutions was increased significantly ($p < 0.05$) with the increase of the polysaccharide concentration (Table 1), as result of the increase of xanthan negative charges at higher concentrations.^[28] Such an increase of the solution conductivity induces greater transfer of the surface charges of the polymer jet, enhanced electrostatic repulsion, promoting

elongation, stretching, and the formation of electrospun nanofibers.^[29–33] Moreover, the high dielectric constant of formic acid (57.9) contributes positively to the development of charges within the jet, facilitating the formation of electrospun xanthan nanofibers.

Furthermore, a significant parameter influencing the electrospinnability is the viscoelasticity of the

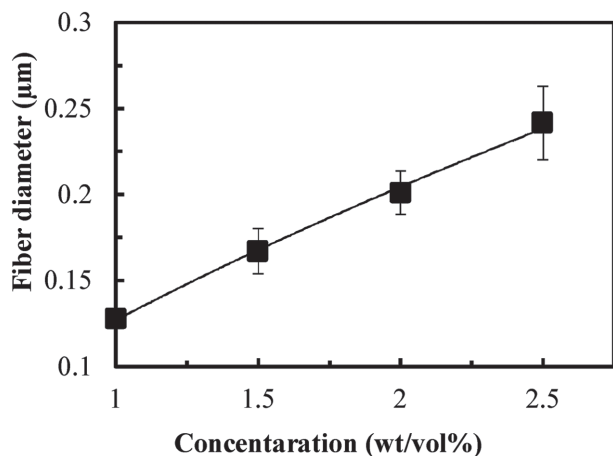


Figure 3. Dependence of the average nanofiber diameter with the concentration of xanthan ($R^2 = 0.998$).

polysaccharide solution. The solution must have a concentration and viscoelasticity high enough to cause polysaccharide chain entanglements, yet not so high that the viscoelasticity prevents the motion induced by the electric field. In the next section, we have studied the viscoelastic properties of different concentrations of xanthan solutions in formic acid.

3.2. Rheological Properties of Xanthan Solutions in Formic Acid

3.2.1. Oscillatory Measurements

The frequency (ω) dependence of the elastic (G') and loss modulus (G'') of the xanthan solutions is presented in Figure 4a. The values of both dynamic moduli gradually increased with the increase of xanthan concentration. For the lowest xanthan concentration (0.5 wt/vol%) the loss modulus was predominant over the elastic modulus ($G'' > G'$) within the frequency range of 0.1–100 rad s^{-1} . At higher polysaccharide concentrations (2 and 2.5 wt/vol%), the G' was marginally dominant over the G'' , with relatively high frequency dependence for both moduli

Table 1. Electrical conductivity of xanthan solutions in formic acid.

Xanthan [wt/vol%]	Conductivity [$\mu\text{s cm}^{-1}$]
0.5	$134.3 \pm 4.0^{\text{a}}$
1	$265.7 \pm 5.1^{\text{b}}$
1.5	$356.7 \pm 1.5^{\text{c}}$
2	$436.0 \pm 3.6^{\text{d}}$
2.5	$551.0 \pm 4.6^{\text{e}}$

^{a–e}Significant different at $p < 0.05$.

(Figure 4a). The crossover of the dynamic moduli appeared to shift toward lower frequencies with increasing xanthan concentration, in agreement with previous studies using dilute aqueous xanthan solutions.^[34–36] Previous studies, however, showed that for ordered conformation of xanthan aqueous solutions, G' dominates G'' over most of the frequencies (weak “gel-like” behavior), in agreement with the rheological behavior of most of the rigid polymers at relatively concentrated solutions.^[37] Overall, oscillatory rheological studies indicate that 0.5–2.5 wt/vol% xanthan in formic acid forms very “weak” viscoelastic solutions with high frequency dependence of G' and G'' .

Moreover, the $\tan \delta$ value ($\tan \delta = G''/G'$) provides a convenient index of the proportion of elastic-like character (Figure 4b). Clearly, the $\tan \delta$ value decreased more than seven times at the frequency of 0.1 rad s^{-1} by varying the xanthan concentration from 1 to 1.5 wt/vol%, the concentration at which electrospun nanofibers formation was observed. The $\tan \delta$ value was found to decrease with the

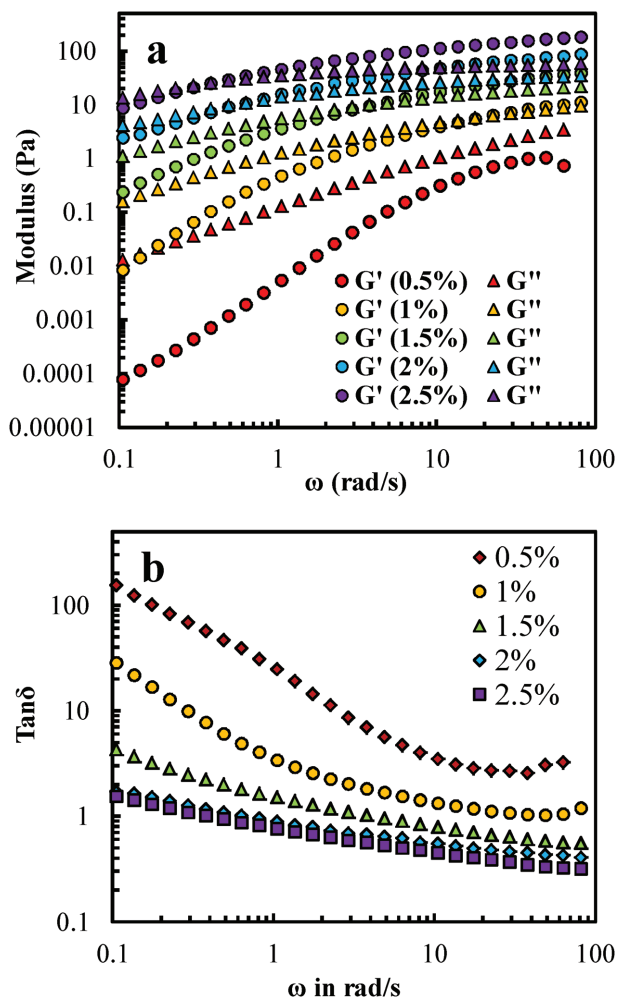


Figure 4. a) Elastic (G') and viscous (G'') modulus as a function of frequency, and b) $\tan \delta$ values as a function of frequency, for xanthan solutions (wt/vol%) in formic acid at 25 °C.

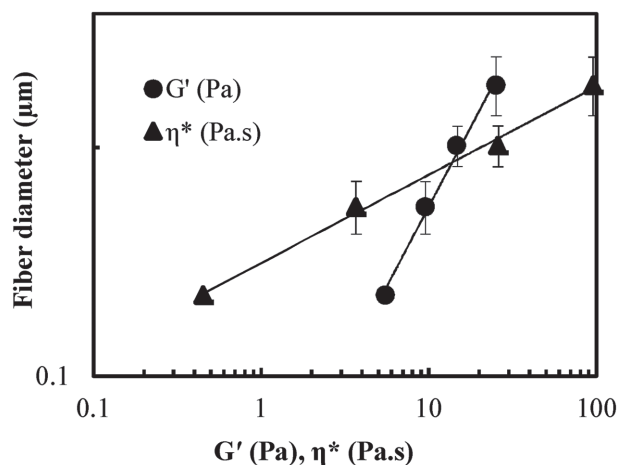


Figure 5. Dependence of the diameter of xanthan nanofibers with the elastic modulus (G') ($R^2 = 0.995$) and dynamic complex viscosity (η^*) ($R^2 = 0.993$) at 25 °C.

increase of xanthan concentration and to be around 0.4 at 10 rad s^{-1} for the 2.5 wt/vol% xanthan in formic acid. It is to note that for other biopolymer hydrogels such as gelatin, agarose, and carrageenan the $\tan \delta$ value was found to range from about 0.02 to 0.07.^[38,39]

Figure 5 shows the dependence of the average nanofiber diameter (D) of xanthan with the elastic modulus (G') (or viscous modulus, G'') and dynamic complex viscosity (η^*), at the cross-over frequency of the moduli (Figure 4a). The dependence can be described as

$$D = 0.14[G']^{0.12} \quad (2)$$

$$D = 0.06[\eta^*]^{0.42} \quad (3)$$

where the fiber diameter is in micrometers. Obviously, an increase in the viscoelastic parameters of the polysaccharide (as concentration increased) resulted to a larger number of entanglements, thus causing the formation of electrospun nanofibers with higher average diameters.

3.2.2. Flow Properties

As shown in Figure 6, flow rheological studies reveal that xanthan in formic acid has a shear thinning behavior, which is observed for xanthan and other aqueous polysaccharide solutions. No hysteresis were observed for the viscosity during increasing and decreasing of the imposed shear rate, suggesting that the xanthan solutions were not thixotropic with fast relaxation times, in contrast with aqueous preparations of xanthan that are thixotropic.^[40] Thus, disruption and reformation of weaker linkages could be responsible for the reversible shear thinning behavior of xanthan in formic acid. It is to note the strong increase of the viscosity beyond 1 wt/vol% (the concentration at which the formation of electrospun nanofibers was initiated); at

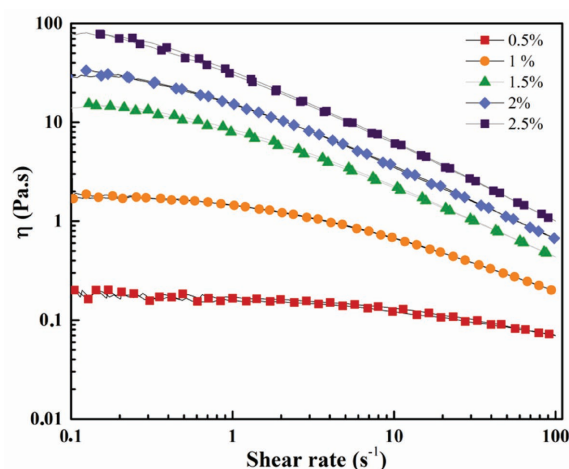


Figure 6. Flow curves for xanthan solutions (wt/vol%) in formic acid at 25 °C.

the low shear rate of 0.1 s^{-1} , the 1 wt/vol% of xanthan solution displayed ten times higher viscosity than the 0.5 wt/vol%.

Moreover, xanthan follows a power-law thinning behavior of $\eta = m \cdot \dot{\gamma}^{n-1}$ where η is the apparent viscosity, $\dot{\gamma}$ is shear rate, and m is the flow index. The flow index (m), which is a rheological parameter that reflects the values of the viscosity, was substantially increased above 1 wt/vol%. The power law index values (n) were in the range of 0.761–0.236 (Table 2). This behavior is close to that of aqueous xanthan gum behavior ($n = 0.24$) which is known to be caused by forming aggregates through hydrogen bonds and polymer entanglements, resulting in a high viscosity at low shear rates.^[41,42] Power law index values (n) in the range of 0.15–0.25, implying high shear thinning behavior, have been also reported for high concentrations of other polysaccharide solutions.^[40] Such a shear thinning behavior is critical for the extension of the polysaccharide jet by the electric field and for the formation of electrospun xanthan nanofibers.

Figure 7, shows an exponential relationship of the solution (apparent) viscosity with the increase of xanthan concentration in formic acid. Similar exponential

Table 2. Power law parameters from the shear thinning properties of xanthan solutions in formic acid (25 °C).

Xanthan [wt/vol%]	n	K	R^2
0.5	0.761	0.214	0.999
1	0.473	2.274	0.998
1.5	0.317	10.617	0.993
2	0.299	17.286	0.995
2.5	0.236	35.588	0.999

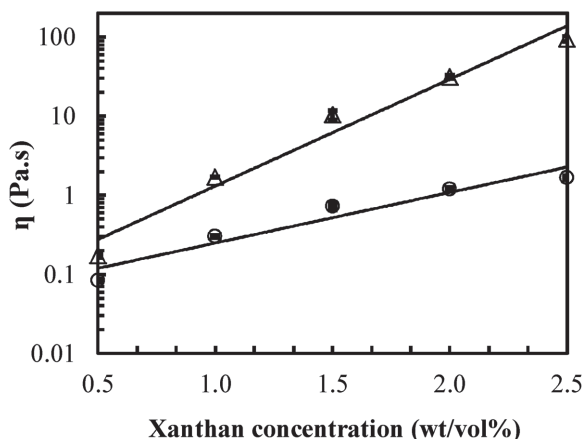


Figure 7. Semilogarithmic representation of the relation of the viscosity with xanthan concentration (circles: $50 \pm 5 \text{ s}^{-1}$; triangles: $0.2 \pm 0.02 \text{ s}^{-1}$). The solid lines represent exponential concentration dependence.

concentration dependence was also observed for aqueous xanthan solutions higher than 0.2 wt/vol%, both at 20 and 80 °C.^[43] Garcia-Ochoa et al.,^[44] also reported an exponential correlation of the viscosity of aqueous xanthan concentrations in the range from 0.1 to 0.2 wt/vol% with the addition of 0.1 wt/vol% of NaCl.

3.2.3. Normal Stress Difference

The first normal stress difference ($N1$) as a function of shear rate at different xanthan solutions is illustrated in Figure 8. For xanthan concentrations beyond 1.5 wt/vol%, the viscoelastic forces increased as the shear rate was increased, due to the stretching of xanthan chains within the flow field, resulted in an increased $N1$ values. The $N1$ values of xanthan in formic acid were highly dependent on the shear rate above the concentration of 1.5 wt/vol%

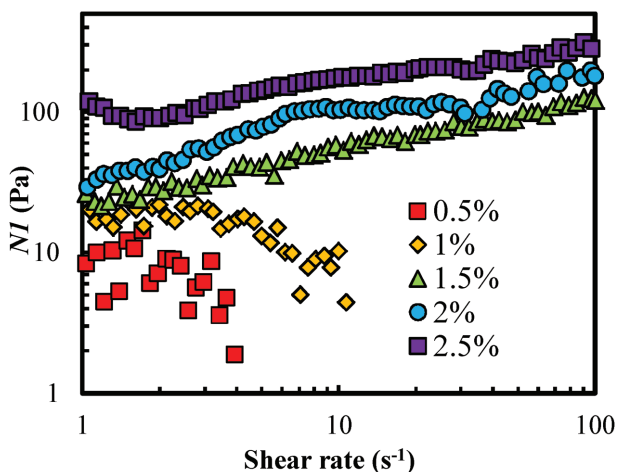


Figure 8. First normal stress difference ($N1$) upon increasing shear rate for xanthan solutions (wt/vol%) in formic acid at 25 °C.

(at which nanofiber formation was observed) and exhibited a power-law dependence ($N1 = A \cdot \dot{\gamma}^B$). For the shear rate of 10–100 s^{-1} the B values were 0.85, 1.06, and 1.49 for the 1.5, 2, and 2.5 wt/vol% xanthan concentrations, respectively. Comparatively, $N1$ values of aqueous xanthan solutions were less dependent on shear rate ($B = 0.09$).^[45,46] Overall, the data clearly indicate that at higher concentrations xanthan solutions in formic acid are elastic with strong entanglements among the molecular chains, resulting in a noticeable increase of $N1$.

3.2.4. Comparison between Apparent Viscosity and Dynamic Complex Viscosity

Figure 9 shows that the complex viscosity (η^*) values of xanthan in formic acid are slightly higher than the apparent viscosity values (η) for the concentrations of 2 and 2.5 wt/vol%. At the concentration range of 0.5–1 wt/vol%, it was observed that (η^*) was superimposed with (η). This suggests that xanthan in formic acid at high concentrations, deviate slightly from the “Cox–Merz” rule, which typically applies to most viscoelastic systems with physical entanglements and relates linear and nonlinear viscoelastic properties. A deviation from the Cox–Merz rule is generally attributed to the structural decay due to strain deformation applied to the system (i.e., low in oscillatory shear and high in steady shear).^[47–49] For the majority of polysaccharide solutions, the complex viscosity is almost always higher than the apparent viscosity at the same numerical values of frequency and shear rate, and their difference becomes increasingly larger with decreasing

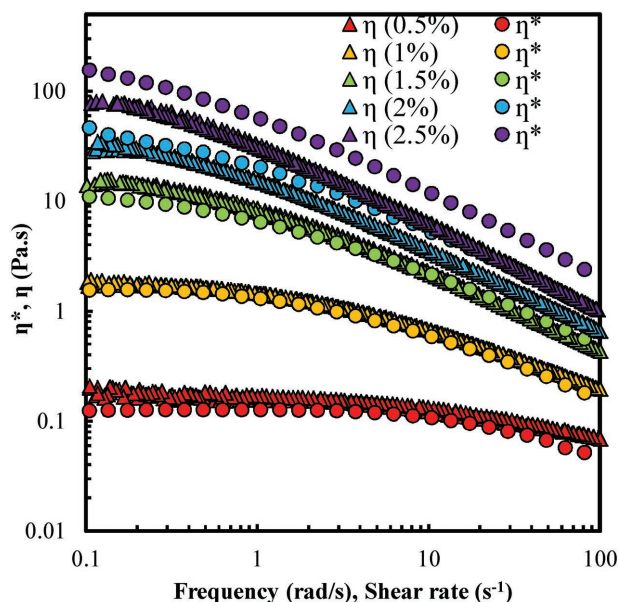


Figure 9. Complex viscosity (circles) and apparent viscosity (triangles) as a function of frequency of oscillation and shear rate for xanthan solutions at 25 °C.

frequencies and shear rates.^[47–49] The agreement with this empirical rule in the case of xanthan in formic acid at low concentrations and the slight deviation at higher concentrations is in contrast with the case of typical aqueous xanthan solutions, where structural features such as entanglements and/or aggregates and hydrogen bonding are responsible for the significant deviation from the Cox–Merz rule.

3.3. Molecular Conformation of Xanthan

Xanthan chains are subjected to a conformational transition from helix to random coils depending on the changes in concentration, pH, temperature, and solvent ionic strength.^[44,50,51] At low temperature (below 40 °C)^[44] or high ionic strength (less than 1 M NaCl),^[51] xanthan chains adopt ordered structures such as single or double helix.^[52] When the polysaccharide is subjected to high temperature or low ionic strength, disordered, and highly dynamic chain structures were found.^[53,54]

Although CD spectroscopy is a powerful technique for evaluating molecular conformations and the content of secondary structures, the analysis is limited toward analytes dissolved in solvents that do not interfere with circularly polarized light. Indeed, the evaluation of xanthan conformation when dissolved in formic acid was problematic because of the solvent optical activity, and the corresponding CD spectrum was found noisy (data not shown). Accordingly, xanthan solutions were prepared in water and in formic acid, freeze-dried, and resolubilized in water. As a control, the CD spectrum of xanthan in water without prior freeze-drying was also recorded. In Figure 10, the helix conformation of xanthan chains in solution is represented by the positive ellipticity at ≈ 200 nm and the negative ellipticity at ≈ 223 nm. These bands are attributed to the optically active carboxylic or carboxylate groups of the D-glucuronic acid and the pyruvate groups (band at ≈ 200 nm), and to the acetate groups (band at ≈ 223 nm).^[50] The CD spectrum of freeze-dried xanthan, previously dissolved in water and resolubilized in water (Figure 10, red line) shows a slight ellipticity shift in the positive band from 200 to 202 nm, indicating no significant effect of the ordered conformation, whereas the ellipticity intensity is comparable to that obtained from not freeze-dried xanthan solution in water (Figure 10, black line). On the other hand, the CD spectrum of freeze-dried xanthan, previously dissolved in formic acid and resolubilized in water shows a marked decrease in the ellipticity at 200 nm suggesting a reduction or a partial destruction of helix structures (Figure 10, blue line). However, the decrease of ellipticity in the range between 220 and 250 nm indicates diminished random coil content.

Hence, the CD analysis of xanthan solutions revealed that freeze-drying does not affect the conformational stability

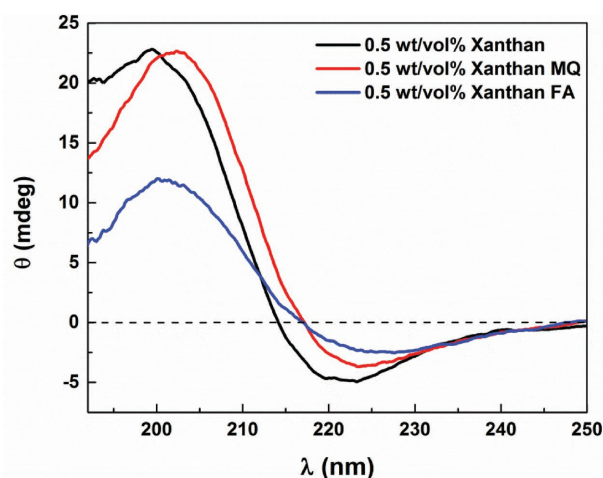


Figure 10. CD spectra of xanthan aqueous solution (0.5 wt/vol%, black line); xanthan aqueous solution (MQ) subjected to freeze-dry and redissolved in water (0.5 wt/vol%, red line); xanthan in formic acid (FA), freeze-dried, and redissolved in water (0.5 wt/vol%, blue line).

of xanthan chains and moreover, formic acid influences the xanthan secondary structure inducing an alteration of the helix content. Interestingly, a helix conformation recovery might occur when freeze-dried xanthan chains, first dissolved in formic acid are resolubilized in water. To elucidate the formic acid effect on the molecular conformation of xanthan, SEC and FTIR were also employed.

3.4. Fourier Transform Infrared Spectroscopy

Figure 11 shows the infrared spectra of native xanthan, freeze-dried xanthan previously dissolved in water, freeze-dried xanthan first dissolved in formic acid and electrospun xanthan fibers after formic acid evaporation. The IR peaks (numbered from 1 to 9 in Figure 11) and the group frequencies were assigned for all samples according to reported data.^[8,55,56] The broad peak in the region of 3000–3500 cm^{-1} was ascribed to O–H stretching (peak 1), and the band around 2900 cm^{-1} to the axial deformation of CH of CH_2 groups (peak 2). In Figure 11b, the region between 2000 and 700 cm^{-1} was enlarged for a better peaks visualization. Here, the stretching vibration of C=O was distinguished as three peaks: one band attributed to carbonyl functionalities (peak 3), a second one corresponding to symmetrical stretching of carboxylic groups (peak 4) of pyruvate and glucuronic acid, and a third band ascribed to the carboxylate asymmetric stretching (peak 5).^[8,55,56] Polysaccharide structure also presented a weak peak due to O–H in-plane deformation around 1250 cm^{-1} (peak 6), and as indicated by the red arrows in Figure 11b, the intensities of this band are much lower for xanthan powder previously dissolved in formic acid. Other characteristic peaks were found in the region of 1200–1000 cm^{-1} : peak 7

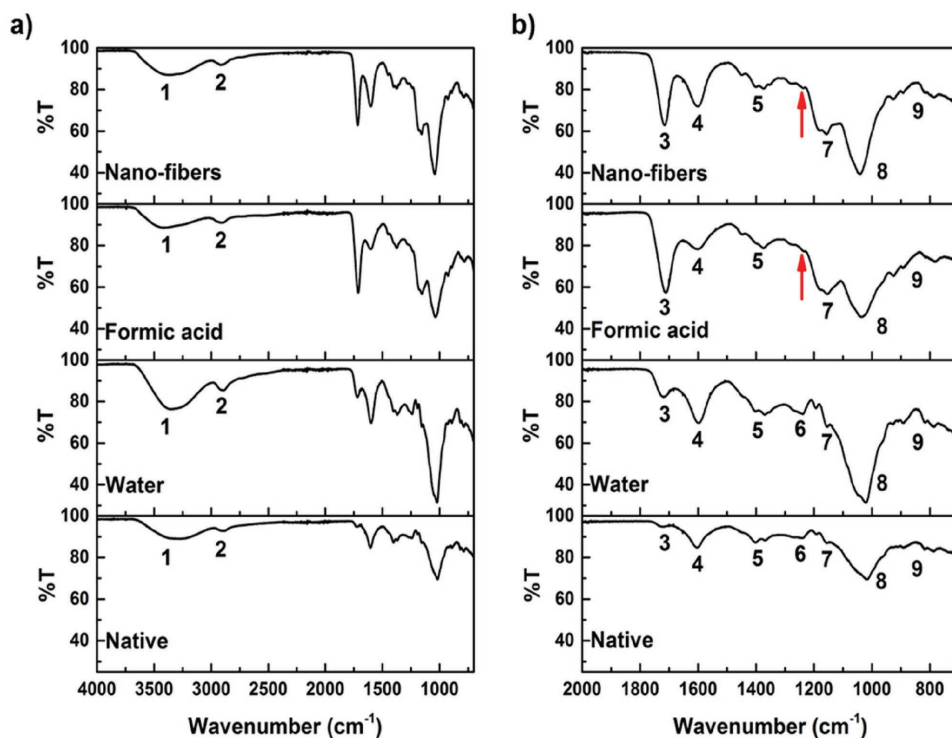


Figure 11. FTIR spectra of xanthan at different conditions: native, dissolved in water and freeze-dried, dissolved in formic acid and freeze-dried, and electrospun polysaccharide fibers after formic acid evaporation. a) FTIR spectra recorded in the wavenumber range from 4000 to 700 cm^{-1} and b) the corresponding enlarged plots in the region between 2000 and 700 cm^{-1} . FTIR peaks are labeled with numbers (1)–(9), and red arrows indicate missing peaks.

corresponds to O–H and C–O–C stretching of tertiary alcohols and esters, and peak 8 to O–H stretching of primary alcohols. In the wavenumber range between 900 and 750 cm^{-1} , the vibrational mode of backbone β -glycosidic linkages and the bending mode of C–H and O–H out-of-plane were assigned (peak 9).

Consequently, the esterification process of xanthan polysaccharide molecules dissolved in formic acid may explain the decrease in intensity of the O–H in-plane peak. The presence of formate groups at the hydroxyl positions 4 and 6 of glucose units might also explain the intensity increase of the IR peak 3 which corresponds to the carbonyl functionalities. Previous studies using various polysaccharides (such as starch, guar gum, chitin, and cellulose), dissolved in formic acid also revealed that an esterification reaction taking place at the hydroxyl groups in position 4 and 6 of glucose units.^[57]

3.5. Size-Exclusion Chromatography

The results obtained from size-exclusion chromatography revealed a small difference in molecular weight of the polysaccharide when dissolved in water or in formic acid. In Figure 12, the refractive index and the light scattering peaks of standard and xanthan solutions were plotted as a function of the retention volume.

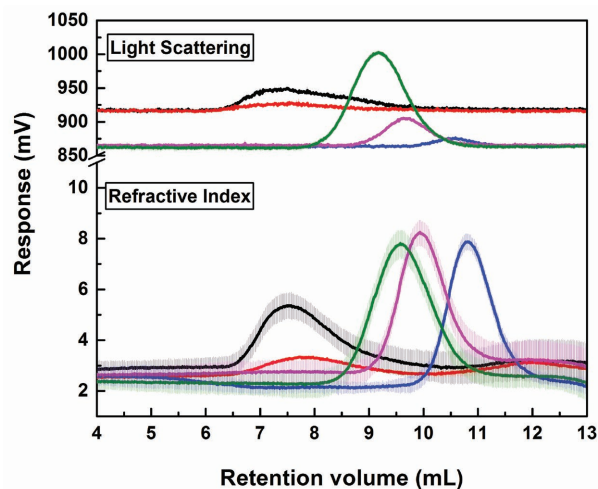


Figure 12. Size exclusion chromatograms of pullulan with a molecular weight of 107 and 344 kDa (blue line and magenta line, respectively); dextran with molecular weight of 1750 kDa (green line); xanthan dissolved in water (red line), and xanthan previously dissolved in formic acid for 15 h, freeze-dried, and resolubilized in water (black line). Standards (0.01 wt/vol%) and xanthan (0.05 wt/vol%) samples were dissolved in ultrapure milliQ water. In the plot, the refractive index (RI) and the light scattering (LS) of samples are reported as a function of retention volume (mL). Measurements were repeated three times (light colors along the curves indicate the standard deviation).

Indeed, xanthan dissolved in water was found to have a molecular weight approximately of 990 kDa with a polydispersity of 1.03 while the molecular weight of xanthan dissolved in formic acid corresponded approximately to 1030 kDa (polydispersity = 1.03). The absolute molecular weight of xanthan in the solutions were calculated by the respective ratios between the peak areas of light scattering and the refractive index traces given by the following equations^[58,59]

$$A_{\text{RI}} = k_{\text{RI}} \left(\frac{dn}{dc} \right) m \quad (4)$$

$$A_{\text{LS}} = k_{\text{LS}} \left(\frac{dn}{dc} \right)^2 m \overline{M_w} \quad (5)$$

where A_{RI} and A_{LS} are the areas underneath the refractive index peak and the light scattering peak, respectively. k_{RI} and k_{LS} are parameters that depend on the instrument and on the eluent used, not on the analyzed polymer; dn/dc is the differential refractive index increment ($dn/dc = 0.153 \text{ mL g}^{-1}$ for xanthan eluted with 0.8 M NaNO_3 aqueous solution at $\lambda = 633 \text{ nm}$); m is the injected mass and it is given by multiplying the injection volume with the mass concentration of a certain solution; $\overline{M_w}$ is the weight average molecular weight. The parameters k_{RI} and k_{LS} were determined from relations^[9,10] applied to the SEC chromatograms of the dextran and pullulan standards (with known $\overline{M_w}$, dn/dc , and m), and then applied for the calculation of $\overline{M_w}$ for the xanthan samples. Given the similar chemical composition, the values of dn/dc for the analyzed polysaccharides are expected to be very similar. This is supported by the observation that, with the exception of xanthan sample dissolved in water, the values of the A_{RI} in Figure 12 are directly proportional to the sample concentrations, as expected from relation at unchanged dn/dc .^[9] The similarity of the calculated $\overline{M_w}$ values for the xanthan in water and in formic acid is an indication that the obtained distribution of molecular masses was not significantly distorted. Notice that the $A_{\text{LS}}/A_{\text{RI}}$ is independent of the concentration. Interestingly, the results obtained from the size exclusion chromatography suggest a slight increase in molecular weight of the xanthan dissolved in formic acid of $\approx 40 \text{ kDa}$, confirming the hypothesis that during polysaccharide dissolution in formic acid an esterification reaction occurs.

4. Conclusions

Electrospun xanthan polysaccharide nanofibers with an average diameter of 128 ± 36.7 to $240 \pm 80.7 \text{ nm}$ were prepared using formic acid as a solvent. The correlation between the concentration and the rheological properties of xanthan solutions with the morphology of the nanofibers was investigated. At xanthan concentrations

above 1 wt/vol% chain entanglements leads to an increase of its elastic modulus, apparent viscosity, and first normal stress differences (N_1), resulting to the stabilization of the xanthan jet during electrospinning and formation of electrospun fibers. The typical “weak gel-like” properties of aqueous xanthan solutions, with junction zones comparable to those in true gels but much weaker, were not observed for xanthan solutions in formic acid. From the FTIR studies it was observed that an esterification reaction takes place; most probably formic acid reacts with the pyruvic acid groups of xanthan. As the esterification of pyruvic acid to pyruvil formate induces a decrease of the negative charges of xanthan, it neutralizes and stabilizes the helical conformation of xanthan. The results obtained from SEC revealed a small difference in molecular weight of the polysaccharide when dissolved in distilled water or in formic acid. Further studies are required to investigate the effect of different solvents, ionic conditions, and polysaccharide properties (e.g., molecular weight) for the formation of electrospun xanthan nanofibers.

Acknowledgements: The authors are grateful to Cosphatec GmbH (Drehbahn, Hamburg, Germany) and to Dr. Markus Schroeder for providing the xanthan samples. Support by the Danish Strategic Research Council (DSF-10-93456) and the Danish National Research Foundation (Project No. DNRF103) is acknowledged.

Received: February 6, 2017; Revised: March 6, 2017;
Published online: ; DOI: 10.1002/mame.201700067

Keywords: electrospinning process; formic acid; nanofibers; rheological properties; xanthan gum

- [1] A. C. Mendes, K. Stephansen, I. S. Chronakis, *Food Hydrocolloids* **2017**, *68*, 53.
- [2] A. C. Stijnman, I. Bodnar, R. Hans Tromp, *Food Hydrocolloids* **2011**, *25*, 1393.
- [3] S. Ramakrishna, K. Fujihara, W.-E. Teo, T.-C. Lim, Z. Ma, *An Introduction to Electrospinning and Nanofibers*, **2005**, World Scientific Publishing Co. Pte. Ltd., Singapore, pp. 46–47.
- [4] N. Bhattarai, M. Zhang, *Nanotechnology* **2007**, *18*, 455601.
- [5] J. W. Lu, Y. L. Zhu, Z. X. Guo, P. Hu, J. Yu, *Polymer* **2006**, *47*, 8026.
- [6] K. Park, S. Park, G. Kim, W. Kim, *Polymer* **2008**, *32*, 206.
- [7] S. Rosalam, R. England, *Enzyme Microb. Technol.* **2006**, *39*, 197.
- [8] S. Fariaa, C. L. O. Petkowicz, S. A. L. Morais, M. G. H. Terronesc, M. M. Resendea, F. P. Françad, V. L. Cardoso, *Carbohydr. Polym.* **2011**, *86*, 469.
- [9] I. H. Smith, K. C. Symes, C. J. Lawson, E. R. Morris, *Int. J. Biol. Macromol.* **1981**, *3*, 129.
- [10] P. A. Sandford, J. E. Pittsley, C. A. Knutson, P. R. Watson, M. C. Cadmus, A. Jeanes, in *Extracellular Microbial Polysaccharides*, (Eds: P. A. Sandford, A. Laskin) ACS, Washington, DC **1977**.
- [11] D. M. Goodall, in *Frontiers in Carbohydrate Research*, Vol. 2 (Ed: R. Chandrasekaran), Elsevier Applied Science, New York **1992**, p. 141.
- [12] Z. Wang, S. Y. Xu, J. Tang, *J. Food Sci.* **1986**, *51*, 96.

- [13] J. I. Horinaka, R. Yasuda, T. Takigawa, *J. Appl. Polym. Sci.* **2012**, *123*, 3023.
- [14] Z. Hong, F. Bo, L. Yongjun, Q. Xiaohui, J. Hao, L. Yuting, W. Liwei, T. Meng, L. Kejing, *J. Dispersion Sci. Technol.* **2017**, *38*, 361.
- [15] C. J. Carriquea, E. J. Amis, J. L. Schrag, J. D. Ferry, *J. Rheol.* **1993**, *37*, 469.
- [16] T. Coviello, K. Kajiwara, V. Crescenzi, *Macromolecules* **1986**, *19*, 2826.
- [17] T. Coviello, W. Burchard, M. Dentini, V. Crescenzi, *Macromolecules* **1987**, *20*, 1102.
- [18] C.-E. Brunchi, M. Bercea, S. Morariu, M. Dascalu, *J. Polym. Res.* **2016**, *23*, 123.
- [19] A. B. Rodd, D. E. Dunstan, D. V. Boger, *Carbohydr. Polym.* **2000**, *42*, 159.
- [20] B. Tinland, G. Maret, M. Rinaudo, *Macromolecules* **1990**, *23*, 596.
- [21] M. A. Zirnsak, D. V. Boger, V. Tirtaatmadja, *J. Rheol.* New York, US **1999**, *43*, 627.
- [22] D. A. Rees, E. J. Welsh, *Angew. Chem., Int. Ed.* **1977**, *16*, 214.
- [23] S. Ross-Murphy, *Trends Food Sci. Technol.* **1994**, *5*, 126.
- [24] S. B. Ross-Murphy, V. J. Morris, E. R. Morris, *Faraday Symp. Chem. Soc.* **1983**, *18*, 115.
- [25] B. Katzbauer, *Polym. Degrad. Stab.* **1998**, *59*, 81.
- [26] G. O. Phillips, P. A. Williams, in *Handbook of Hydrocolloids* (Eds: G. O. Phillips, P. A. Williams), CRC Press, New York **2000**, pp. 1–19.
- [27] A. Theisen, C. Johann, M. P. Deacon, S. E. Harding, *Refractive Increment Data-Book for Polymer and Biomolecular Scientists*, Nottingham University Press, Nottingham, UK **2000**.
- [28] R. Rošic, J. Pelipenko, P. Kocbek, S. Baumgartner, M. Bešter-Rogač, J. Kristl, *Eur. Polym. J.* **2012**, *48*, 1374.
- [29] S. Alborzi, L. T. Lim, Y. Kakuda, *J. Food Sci.* **2010**, *75*, 100.
- [30] A. Frenot, I. S. Chronakis, *Current Opinion in Colloid and Interface Science*, **2003**, *8*, 64.
- [31] K. Moomand, L. T. Lim, *Food Hydrocolloids* **2015**, *46*, 191.
- [32] L. Tang, P. Kebarle, *Anal. Chem.* **1991**, *63*, 2709.
- [33] A. C. Vega-Lugo, L. T. Lim, *J. Polym. Sci., Part B: Polym. Phys.* **2012**, *50*, 1188.
- [34] S. Talwar, J. Hinestroza, B. Pourdeyhimi, S. A. Khan, *Macromolecules* **2008**, *41*, 4275.
- [35] R. J. English, *J. Rheol.* New York, US **1997**, *41*, 427.
- [36] R. J. English, J. H. Laurer, R. J. Spontak, S. A. Khan, *Ind. Eng. Chem. Res.* **2002**, *41*, 6425.
- [37] E. Pelletier, C. Viebke, J. Meadows, P. A. Williams, *Biopolymers* **2001**, *59*, 339.
- [38] I. S. Chronakis, J. L. Doublier, L. Piculell, *Int. J. Biol. Macromol.* **2000**, *28*, 1.
- [39] I. S. Chronakis, L. Piculell, J. Borgström, *Carbohydr. Polym.* **1996**, *31*, 215.
- [40] B. Launay, J. L. Doublier, G. Cuvelier, in *Functional Properties of Food Macromolecules* (Eds: J. R. Mitchell, D. A. Ledward), Elsevier Applied Science Publ. London, New York **1985**, p. 1–78.
- [41] K. W. Song, Y. S. Kim, G. S. Chang, *Fibers Polym.* **2006**, *7*, 129.
- [42] B. Wei, L. Romero-Zerón, D. Rodrigue, *J. Pet. Explor. Prod. Technol.* **2014**, *4*, 113.
- [43] L. Zhong, M. Oostrom, M. J. Truex, V. R. Vermeul, J. E. Szecsody, *J. Hazard. Mater.* **2013**, *244*, 160.
- [44] F. Garcia-Ochoa, V. E. Santos, J. A. Casas, E. Gómez, *Biotechnol. Adv.* **2000**, *18*, 549.
- [45] B. Wei, L. Romero-Zeron, D. Rodrigue, *J. Macromol. Sci., Part B: Phys.* **2014**, *53*, 625.
- [46] P. J. Whitcomb, C. W. Macosko, *J. Rheol.* New York, US **1978**, *22*, 493.
- [47] D. R. Picout, S. B. Ross-Murphy, *Sci. World J.* **2003**, *3*, 105.
- [48] E. K. Chamberlain, M. A. Rao, *Carbohydr. Polym.* **1999**, *40*, 251.
- [49] W. E. Rochefort, S. Middleman, *J. Rheol.* New York, US **1987**, *31*, 337.
- [50] A. Bejenariu, M. Popa, L. Picton, D. Le Cerf, *Rev. Roum. Chim.* **2010**, *55*, 147.
- [51] V. B. Bueno, D. F. S. Petri, *Carbohydr. Polym.* **2014**, *101*, 897.
- [52] R. Lapsin, S. Prich, *Rheology of Industrial Polysaccharides: Theory and Applications*, Blackie, London **1995**.
- [53] B. Tinland, M. Rinaudo, *Macromolecules* **1989**, *22*, 1863.
- [54] *Polysaccharides: Structural Diversity and Functional Versatility* (Ed: S. Dumitriu), CRC Press, Boca Raton, FL **2004**.
- [55] D. Osiro, R. W. A. Franco, L. A. Colnago, *Artic. J. Braz. Chem. Soc.* **2011**, *22*, 1339.
- [56] S. N. Yuen, S. M. Choi, D. L. Phillips, C. Y. Ma, *Food Chem.* **2009**, *114*, 1091.
- [57] H. Tarkow, A. J. Stam, *J. Phys. Chem.* **1952**, *56*, 266.
- [58] A. Gamini, J. de Bleijser, J. C. Leyte, *Carbohydr. Res.* **1991**, *220*, 33.
- [59] M. Holmberg, K. B. Stibius, S. Ndoni, N. B. Larsen, P. Kingshott, X. L. Hou, *Anal. Biochem.* **2007**, *361*, 120.

3.1.2. Application of xanthan nanofibers- Paper II

Enhanced transepithelial permeation of gallic acid and (-)-epigallocatechin gallate across human intestinal Caco-2 cells using electrospun xanthan nanofibers

Adele Faralli, Elhamalsadat Shekarforoush, Ana C. Mendes, Ioannis S. Chronakis

Nano-Bio Science Research Group, DTU-Food, Technical University of Denmark,
Kemitorvet, B202, 2800 Kgs. Lyngby, Denmark

This manuscript was submitted to Colloids and Surfaces B Journal in April 2018.

**Enhanced transepithelial permeation of Gallic acid and (-)-Epigallocatechin
Gallate across human intestinal Caco-2 cells using
electrospun xanthan nanofibers**

Adele Faralli, Elhamalsadat Shekarforoush, Ana C. Mendes, Ioannis S. Chronakis *

Nano-BioScience Research Group, DTU-Food, Technical University of Denmark,
Kemitorvet, B202, 2800 Kgs. Lyngby, Denmark

*Corresponding author: Ioannis S. Chronakis

Tel: +45 40 20 64 13

E-mail: ioach@food.dtu.dk

Abstract

Xanthan polysaccharide nanofibers (X) were prepared using electrospinning processing as an encapsulation and delivery system of the *poorly absorbed* polyphenols compounds gallic acid (GA) and (-)-epigallocatechin gallate (EGCG). Scanning electron microscopy was used to characterize the electrospun nanofibers, and controlled release studies were performed at pH 6.5 and 7.4 in saline buffer, suggesting that the release of polyphenols from xanthan nanofibers follows a non Fickian mechanism. Furthermore, the X-GA and X-EGCG nanofibers were incubated with Caco-2 cells, and the cell viability, transepithelial transport and permeability properties across cell monolayers were investigated. An increase of GA and EGCG permeabilities was observed when the polyphenols were loaded into xanthan nanofibers, compared to the free compounds. The observed *in vitro* permeability enhancement of GA and EGCG was induced by the presence of the polysaccharide nanofibers, that successfully inhibited efflux transporters, as well as by tight junctions opening.

Keywords: Xanthan gum, electrospinning, gallic acid, (-)-epigallocatechin gallate, apparent permeability coefficient, efflux.

1. Introduction

Polyphenols are the most abundant antioxidants in our diet and they are receiving increasing interest due to the established association between the intake of polyphenol-rich diet and the prevention of various diseases.^{1,2} Because of their antioxidant,³ antimutagenic⁴ and anticarcinogenic properties,^{5,6} polyphenols have recently attracted the research interest towards the study of their metabolism and absorption mechanisms across the gut barrier.⁷

Polyphenols are categorized according to the chemical structure of their carbon skeleton, and the most abundant classes in our diet are phenolic acids and flavonoids. The most encountered phenolic acids are caffeic acid, ferulic acid and gallic acid. The latter, also known as 3,4,5-trihydroxybenzoic acid, is one of the main endogenous phenolic acids found in plants, mostly in tea leaves.⁸ Gallic acid (GA), also found in vegetables, grapes, and pomegranates is a potent non-enzymatic antioxidant and has a natural antitumor activity against lung, prostate, colon, gastric, breast cancer and human pre-myelocytic leukemia.⁹⁻¹² It has been reported that the *in vitro* treatment of lung and HeLa cancer cells with gallic acid concentrations in the micromolar range induces cell death associated to the depletion of glutathione (GSH) as well as reactive oxygen species (ROS) level changes.^{13,14} The physiological impact and efficiency of GA is strictly dependent on its bioavailability, biochemical integrity and succeeding interaction with target tissues. Many studies have demonstrated that only small amounts of orally administered GA are absorbed through the intestine due to its low permeability, poor water solubility and chemical instability.

Flavonoids, the most abundant polyphenols in our diet together with phenolic acids, can be divided into several classes, and catechins are the main flavonols found in tea.¹ The major tea

catechins are (–)-epigallocatechin gallate (EGCG), (–)-epicatechin gallate (ECG), (–)-epicatechin (EC) and (–)-epigallocatechin (EGC).¹⁵ These natural compounds have demonstrated various health-beneficial properties, including antioxidant, anti-inflammatory and anticancer effects both in animals and humans.^{16,17} Indeed, an inverse association between tea consumption and colorectal cancer frequency as well as gastric cancer has been identified.^{18,19} A particular interests towards EGCG has led to an extensive investigation of the beneficial properties of this natural molecule in the cosmetic, nutritional and pharmaceutical fields. However, as gallic acid, EGCG has a poor oral bioavailability and poor biochemical stability.

In the light of these considerations, the oral administration of gallic acid and (–)-epigallocatechin gallate requires a formulation strategy able to protect and maintain their structural integrity, increase their bioavailability and water solubility, and deliver them to target tissues. Among the existing delivery and stabilization approaches, the encapsulation of sensitive compounds is considered to be the most effective strategy for improving the oral bioavailability and shelf-life of compounds.^{20–22} Nowadays, a plethora of encapsulation techniques are commonly use in oral delivery systems, and carrier systems for phenolic acids and flavonoids encapsulation have been found feasible approaches to overcome both enzymatic degradation and membrane permeation issues.^{7,17} The encapsulation of EGCG in niosomal formulation results in a significantly enhanced drug absorption, stronger stability and lower toxicity compared with the free EGCG.¹⁷ The *in vitro* apparent permeability P_{app} of EGCG niosome across Caco-2 cell monolayers was found to be around $1.42 \pm 0.24 \times 10^{-6}$ cm/s, almost 2-folds as free EGCG (P_{app} value around $0.88 \pm 0.09 \times 10^{-6}$ cm/s). Furthermore, GA-loaded mesoporous silica nanoparticles (MSNs-GA) were easily internalized into Caco-2 cells without deleterious effect on cell viability, and preserving the same antitumor properties of free GA.⁷ In addition, the topical and transdermal delivery of

GA loaded into poly(L-lactic acid) fiber mats resulted in a preserved radical scavenging activity of the released phenolic acid.²³ GA has been also encapsulated within electrospun fibers as delivery carriers using the protein zein²⁴, cellulose acetate²⁵, as well as polylactic acid (PLA) nanofibers including complexes of GA and cyclodextrin²⁶. The encapsulation and release of EGCG loaded into electrospun nanofibers has been also investigated using zein nanofibers²⁷, hyaluronic acid/ lactic-co-glycolic acid fibers (HA/PLGA, core/shell)²⁸ and cellulose electrospun nanofibrous mats coated with bilayers of chitosan and EGCG²⁹.

In the present study, we report the formation of electrospun xanthan nanofibers as an encapsulation and delivery system of the two polyphenols, GA and EGCG. The resulting GA- and EGCG-loaded nanofibers were incubated with Caco-2 cells, and the cell viability, transepithelial transport and permeability properties across cell monolayers were investigated.

2. Materials and Methods

2.1. Materials

The human colon adenocarcinoma cell line Caco-2 [Caco-2] (ATCC® HTB-37™) was obtained from the American Type Culture Collection (Rockville, MD). Dulbecco's modified Eagle's medium (DMEM) high glucose (4.5 g/L), L-glutamine (200 mM), nonessential amino acids (100X), penicillin-streptomycin (10,000 U/mL and 10 mg/mL in 0.9% sodium chloride, respectively), trypsin-EDTA (10X), Phosphate Buffered Saline (PBS), fluorescein sodium salt (FLUO), lucifer yellow dilithium salt (LY), methanesulfonic acid, MES (1 M; pH 5.5-6.7), 4-(2-hydroxyethyl)-1-piperazineethanesulfonic acid solution, HEPES (1 M; pH 7.0-7.6), gallic acid (GA) and (-)-epigallocatechin gallate (EGCG) were purchased from Sigma Aldrich (Brøndby, Denmark). Tissue culture 12-well plates and 12-mm polycarbonate cell culture inserts with an

area of 1.12 cm² and a pore size of 0.4 µm were purchased from Corning Costar® Corporation. Fetal bovine serum (FBS) and Hanks' balanced salt solution (HBSS) with calcium and magnesium and without phenol red were obtained from Thermo Fisher Scientific (Roskilde, Denmark). CellTiter 96® AQueous One Solution Cell Proliferation Assay (MTS) was purchased from Promega Biotech AB (Sweden). Xanthan gum (Cosphaderm X-34) from *Xanthomonas campestris* was kindly provided by Cosphatec GmbH (Drehbahn, Hamburg, Germany).³⁰

2.2. Fabrication of electrospun nanofibers

Xanthan was dissolved in formic acid at a final concentration of 2.5% w/v under vigorous stirring overnight at room temperature. Subsequently, GA and EGCG were added to the polysaccharide solution and further stirred for 30 min. The electrospinning setup consisted of a high voltage generator (ES50P-10W, Gamma High Voltage Research, Inc., USA) to provide a voltage of 20 kV, and a syringe pump (New Era Pump Systems, Inc., USA) to feed the xanthan solution at a flow rate of 0.01 mL/min using a 21 G needle gauge. Xanthan fibers were collected on a steel plate covered with an aluminum foil placed at a distance of 8 cm from the end of the needle. The electrospinning process was carried out at ambient conditions (20 °C and around 20% humidity).

2.3. Morphology of the nanofibers

The morphology of electrospun X, X-GA and X-EGCG nanofibers was studied using a Phenom Pro scanning electron microscope (Phenom World, Thermo Fisher Scientific, Netherlands). For SEM analysis, a small piece of nanofibers web was attached on SEM specimen stubs by a double-sided adhesive tape. The average fiber diameter of nanofibers was calculated using image

J analysis software (National Institutes of Health, MD, USA) measured at 100 different points for each image.

2.4. *In vitro* release of gallic acid and (–)-epigallocatechin gallate from electrospun nanofibers

The amount of gallic acid (GA) and (–)-epigallocatechin gallate (EGCG) loaded into xanthan nanofibers was evaluated by immersing the nanofibers in equal volumes of complete growth medium (DMEM-FBS) or HBSS solution at pH 6.5 or pH 7.4. Briefly, 1.0 mg of X-GA and X-EGCG fibers were immersed in 2 mL pre-warmed medium in a 48-well plate, and the release of molecules from nanofibers were conducted at 37 °C for 8 h. The withdrawn aliquots were analyzed by RP-HPLC with detection of GA and EGCG at 255 nm and 270 nm, respectively. The cumulative amount of each compound released from nanofibers was then considered as the maximum releasable GA and EGCG amounts from these nanofiber formulations at that condition. All data were expressed as mean ± SD of three independent experiments.

2.5. Caco-2 cell culture and subculture

Caco-2 cells were routinely seeded at a concentration of 1.0×10^5 cells/mL in T-75 cm² flasks and incubated at 37 °C in a humidified atmosphere of 5% CO₂. The complete cell medium, here indicated as DMEM-FBS, consisted of high glucose DMEM containing 10% heat-inactivated FBS, 2 mM L-glutamine, 1% nonessential amino acids, 100 U/mL penicillin and 100 µg/mL streptomycin. The medium was renewed every second day until cells reached approximately 90% confluence. Cells were passaged at a subcultivation ratio of 1:4 by treatment with 0.25% trypsin - 0.53 mM EDTA solution for 10 min at 37 °C. After trypsinization, the cells were suspended in complete growth medium and centrifuged for 5 min at 1000 rpm. After supernatant removal, the pellet was suspended in the growth medium and cell concentration was determined

with ORFLO Moxi Z Mini Automated Cell Counter using Type S cassette (Biofrontier Technology, Singapore). All Caco-2 cells were used between passages 9 - 15.

2.6. Compounds and electrospun nanofibers tested with Caco-2 cell monolayers

Xanthan (X), gallic acid-loaded xanthan (X-GA) and (-)-epigallocatechin gallate-loaded xanthan (X-EGCG) nanofibers were produced by electrospinning a solution of the mixed compounds dissolved in formic acid. These nanofibers were tested with Caco-2 cell monolayers to evaluate their toxicity and apparent permeability coefficient (P_{app}) after release from nanofibers and as free compounds. Before testing nanofiber mats with Caco-2 cells, the collected fibers were kept under air stream for 3 days allowing complete formic acid evaporation. Besides GA and EGCG, the transepithelial transport of fluorescein (FLUO) and Lucifer yellow (LY) across Caco-2 cell monolayers were also investigated as marker models for intestinal epithelial permeability and integrity.

2.7. Caco-2 cell viability assay

The *in vitro* Caco-2 cell viability after treatment with free GA, free EGCG, xanthan nanofibers (X), GA-loaded xanthan nanofibers (X-GA) and EGCG-loaded xanthan nanofibers was evaluated by using the MTS [3-(4,5-dimethylthiazol-2-yl)-5-(3-carboxymethoxyphenyl)-2-(4-sulfophenyl)-2H-tetrazolium inner salt] colorimetric bioassay. Different concentrations of free GA and EGCG ranging from 1 μ M to 1 mM were prepared in PBS and sterile-filter with a 0.22 μ m pore size. Furthermore, increasing amounts of dried X, X-GA and X-EGCG nanofibers were peeled off from the aluminum foils and incubated with cells. In a 48-well plate, a concentration of 1.5×10^5 cells/mL were seeded in a complete growth medium and incubated for 2 days at 37 °C in a humidified atmosphere of 5% CO₂. Then, the monolayers were washed with PBS and the

complete medium was renewed. Caco-2 cells were incubated with free GA and free EGCG solutions, X nanofibers, X-GA nanofibers, X-EGCG nanofibers and PBS as a control. The plates were incubated for 24 h at 37 °C in a humidified atmosphere of 5% CO₂. The following day, all supernatants including those with suspended nanofibers were removed, cells were washed with PBS and the medium was renewed. 40 µL of pre-warmed MTS solution was added to each well under dark conditions. After 3 h incubation at 37 °C, the absorbance of the reduced MTS (formazan product) was recorded at 490 nm through a well plate reader (Wallac 1420 Victor2 Multilabel Counter, Perkin Elmer, Waltham, MA).

2.8. Transepithelial transport experiments

The transepithelial transport of free fluorescein (FLUO), free lucifer yellow (LY), free gallic acid (GA), free (-)-epigallocatechin gallate (EGCG), free gallic acid in presence of empty xanthan nanofibers (X + GA), free (-)-epigallocatechin gallate in presence of empty xanthan nanofibers (X + EGCG), gallic acid-loaded xanthan nanofibers (X-GA) and (-)-epigallocatechin gallate-loaded xanthan nanofibers (X-EGCG) across Caco-2 cell monolayers were investigated according to the protocol reported by Artursson et al.³¹ The transport experiments were performed in both apical-to-basolateral (AB, absorptive) and basolateral-to-apical (BA, secretory) directions, under a proton gradient. In fact, in order to mimic the acid microclimate of the small intestine, an apical and basolateral pH around 6.5 and 7.4 were used, respectively. Briefly, 1.0×10^5 cells/insert were seeded onto pre-wetted 12-mm polycarbonate cell culture inserts with an area of 1.12 cm² and a pore size of 0.4 µm. The apical and basolateral compartments were filled with 0.5 mL cell suspension and 1.5 mL complete medium, respectively. The Caco-2 cells were incubated onto the filters overnight at 37 °C in a humidified atmosphere of 5% CO₂. The day after, the growth medium was replaced in both compartments

and the plates were incubated for 21 days at 37 °C in a humidified atmosphere of 5% CO₂, renewing the complete growth medium every second day. For the AB transport experiments, donor solutions of FLUO, LY, GA and EGCG at a concentration of 11 mM, 9.57 mM, 1.1 mM and 1.1 mM, respectively were prepared in sterile-filter HBSS at pH 6.5 buffered with 10 mM MES. Again, donor solutions of FLUO, LY, GA and EGCG at a concentration of 10.3 mM, 9 mM, 1.03 mM and 1.03 mM, respectively were prepared in sterile-filter HBSS at pH 7.4 buffered with 25 mM HEPES to evaluate their BA transport. A volume of 50 µL of each stock solution was added to the donor chamber (0.55 mL and 1.55 mL were the total volumes in A and B, respectively). The transport of GA and EGCG released from nanofibers and as free compounds in presence of empty X nanofibers was also investigated. For the AB transport, 0.2 mg X-GA, 1.0 mg X-EGCG, 0.2 mg and 1.0 mg X were used, and accordingly, 0.6 mg X-GA, 3.0 mg X-EGCG, 0.6 mg and 3.0 mg X were incubated with cell monolayers to evaluate their BA transport. Prior nanofibers incubation, the mats were peeled off from the aluminum foil and kept under air stream for 3 days. After 21 days cell growth, the complete DMEM medium was removed from the cell monolayers and replaced with HBSS at pH 6.5 and pH 7.4 at the apical and basolateral compartments, respectively. For the AB transport studies, 1.5 mL HBSS was used in the basolateral side and 0.55 mL of each donor solution and/or nanofibers were added to the apical side. Immediately, 200 µL aliquots were withdrawn from each donor compartment (time=0). Aliquots from the acceptor side were then withdrawn at different time intervals, and the volume was replaced with fresh HBSS at pH 7.4 maintaining the well plates at 37 °C in a humidified atmosphere of 5% CO₂. A final aliquot from the donor chamber was taken as last time point. BA transport studies were conducted using the same procedure and incubating 0.5 mL HBSS at pH 6.5 in the apical side and 1.55 mL of donor solution and/or nanofibers in the

basolateral chamber. During the transport experiments, all cell media were pre-warmed at 37 °C. Each transport experiment was performed for a time interval of 8 h in triplicates (n=3). After 8 h transport studies and TEER measurements, both apical and basolateral chambers were washed twice with PBS and cell monolayers were detached from the insert membrane with 0.25% trypsin - 0.53 mM EDTA solution for 10 min at 37 °C. The collected Caco-2 cell lysates were centrifuged for 5 min at 1000 rpm and supernatants were discarded. Furthermore, the semipermeable membranes were carefully removed from the insert using a scalpel and collected into Eppendorf tubes in 500 µL HBSS at pH 6.5 (apical conditions). Cell pellets as well were resuspended in 500 µL HBSS at pH 6.5 and both cells and membranes were sonicated for 3 h using an ultrasonic bath (Branson Ultrasonic Corp., VWR, Denmark). The collected samples were then centrifuged for 15 min at 10000 rpm and supernatants were analyzed by HPLC. The same procedure was used to quantify the compound amounts adsorbed (X+GA and X+EGCG) or remained encapsulated (X-GA and X-EGCG) into the nanofibers at the end of transport experiments. The tested nanofibers were removed from the donor chamber and suspended in 500 µL of HBSS (pH 6.5 for AB transport and pH 7.4 for BA transport). After sonication and centrifugation, the molecules found in the supernatants were quantified by HPLC.

2.9. Measurement of transepithelial electrical resistance (TEER)

The Transepithelial Electrical Resistance (TEER) was measured at room temperature before and after permeability experiments with an epithelial volt-ohmmeter equipped with an STX2 “chopstick” electrodes (EVOM2™, World Precision Instruments, Sarasota, FL, USA). Before measuring the resistance values of each well, the cell monolayers and the basolateral chamber were washed twice with pre-warmed HBSS at pH 6.5 and HBSS at pH 7.4, respectively. The resistance values of the semipermeable membrane without cells (R_{BLANK}) were recorded and

subtracted from the resistance values obtained from the measurement of each cell monolayers onto semipermeable membrane (R_{TOTAL}). The specific cell resistance values (R_{TISSUE}) were calculated by:

$$R_{TISSUE} (\Omega) = R_{TOTAL} (\Omega) - R_{BLANK} (\Omega) \quad [1]$$

TEER values of cellular monolayers were expressed in $\Omega \times \text{cm}^2$ and calculated by:

$$TEER_{TISSUE} (\Omega \text{ cm}^2) = R_{TISSUE} (\Omega) \times A_{MEMBRANE} (\text{cm}^2) \quad [2]$$

2.10. Quantification of compounds

Donor solutions of FLUO, LY, GA and EGCG were prepared and sterile-filter in HBSS at pH 6.5 and pH 7.4 to perform transepithelial studies. Standard curves of GA and EGCG dissolved in HBSS at pH 6.5 and pH 7.4 were obtained by HPLC analysis. 200 μL samples withdrawn from the donor and acceptor compartments during transport experiments across cell monolayers were quantitatively analyzed using RP-HPLC (Thermo Fisher Scientific, Denmark). A C18 column (3.0 x 100 mm) and 0.5 mL/min flow rate were used. GA and EGCG were quantified with detection at 255 nm and 270 nm, respectively. FLUO and LY aliquots were instead analyzed by UV-vis spectrometry (Nanodrop One^C, Thermo Fisher Scientific, Denmark), recording their absorbance at 490 nm and 430 nm, respectively. The amount of each compound transported across the cell monolayers within a time interval of 8 h was calculated for both apical-to-basolateral (AB) and basolateral-to-apical (BA) directions. FLUO, LY, GA and EGCG that remained entrapped within cell monolayers, insert membranes and nanofibers were likewise quantified at the end of permeability studies.

2.11. FLUO, LY, GA and EGCG distribution after transport experiments and mass balance.

After transport experiments in both AB and BA directions, the amount of each compound collected at the apical and basolateral chambers were quantified. Donor concentrations at time=0 ($C_{D,t=0h}$), donor and acceptor concentrations at time=8h ($C_{D,t=8h}$ and $C_{A,t=8h}$), compound concentrations remained inside cell monolayer at time=8h ($C_{Caco-2,t=8h}$), within membrane filters at time=8h ($C_{insert,t=8h}$), and adsorbed or remained encapsulated into nanofibers at time=8h ($C_{fibers,t=8h}$) were experimentally measured. Therefore, the mass balance of each compound was calculated as follow:

$$C_{D,t=0h} = C_{D,t=8h} + C_{A,t=8h} + C_{Caco-2,t=8h} + C_{insert,t=8h} + (C_{fibers,t=8h}) \quad [3]$$

Mass balance values of >90% were found for all tested compounds.

2.12. Calculation of the apparent permeability coefficients $P_{app, AB}$ and $P_{app, BA}$.

The absorptive apparent permeability coefficient ($P_{app, AB}$) and the secretory apparent permeability coefficient ($P_{app, BA}$) were calculated by:

$$P_{app} = \frac{dC}{dt} * \frac{V}{A * C_0} \quad [4]$$

where, dC/dt ($\mu M/s$) is the change in concentration on the acceptor chamber over time; V (cm^3) is the volume of the solution in the acceptor compartment; A (cm^2) is the area of the semipermeable membrane; C_0 (μM) is the initial concentration in the donor chamber. The results presented in this study were expressed as mean \pm SD of three independent experiments. PDR, or permeability directional ratio, is a measure of compound polarization in Caco-2 cell monolayers, and was calculated by:

$$\text{PDR} = \frac{P_{\text{app,BA}}}{P_{\text{app,AB}}} \quad [5]$$

3. Results

3.1. Morphological characterization and stability of xanthan nanofibers

Xanthan nanofibers were obtained by electrospinning a 2.5% w/v xanthan solution in formic acid (**Figure 1**). The nanofibrous structures are composed of individual, uniform and randomly oriented fibers with average diameters of 235 ± 49 nm. The average diameter of electrospun X-GA and X-EGCG nanofibers was slightly increased to 327 ± 119 nm and 270 ± 95 nm, respectively, when 2 mM of phenolic compound was added to the polysaccharide solution.

3.2. *In vitro* release of GA and EGCG from xanthan nanofibers

The cumulative *in vitro* release of GA and EGCG from xanthan nanofibers was investigated by immersing the fibers in complete growth medium (DMEM-FBS), HBSS at pH 6.5 and HBSS at pH 7.4 (**Figure 2**). The total amount of GA and EGCG released from fibers was 69.01% and 70.53% in HBSS at pH 6.5, 58.47% and 83.44% in HBSS at pH 7.4, respectively. Slightly different release values emerged from the immersion of fibers in the complete growth medium, which had an experimentally measured pH value of 7.28. It is to note that electrospun X, X-GA, and X-EGCG nanofibers remained intact in all release media and no morphological changes were observed during the experimental studies (data not shown). It is suggested that the presence of several salts in both DMEM-FBS and HBSS, successfully prevented the dissolution of X, X-GA and X-EGCG nanofibers.

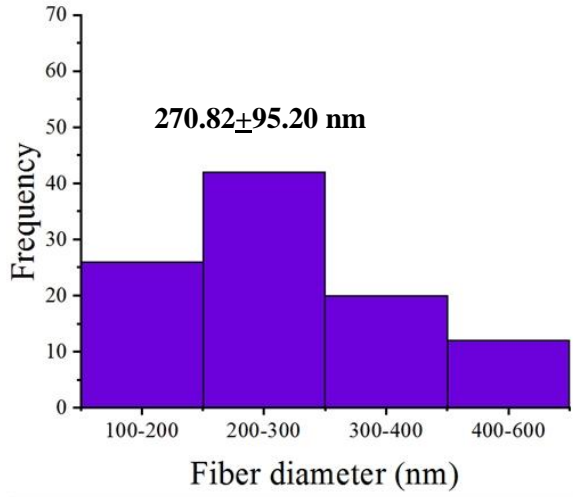
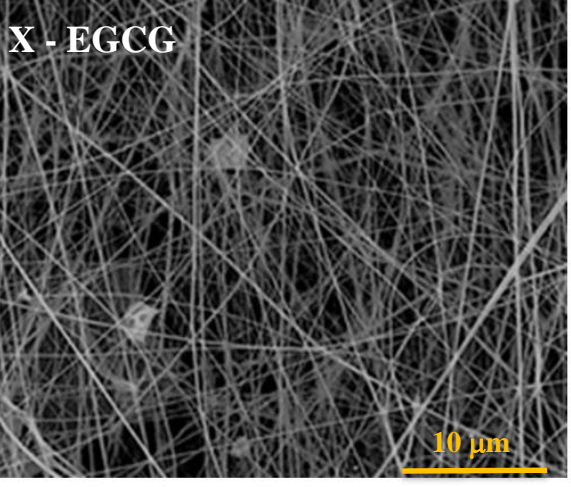
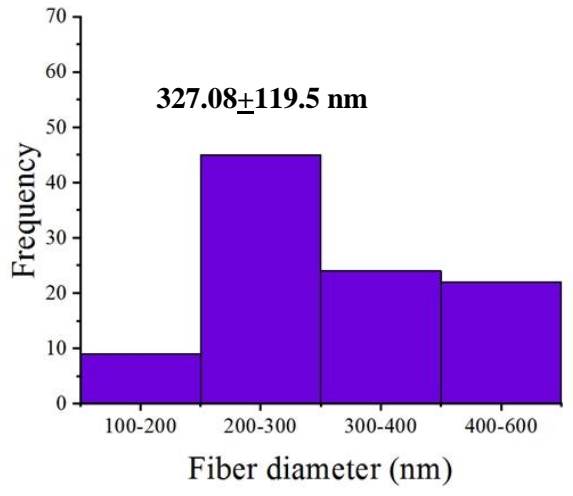
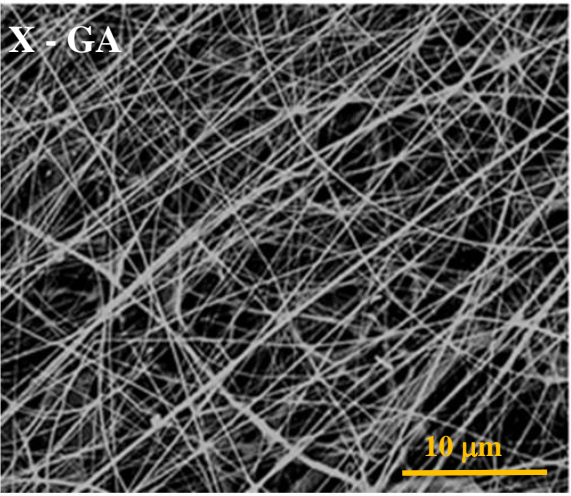
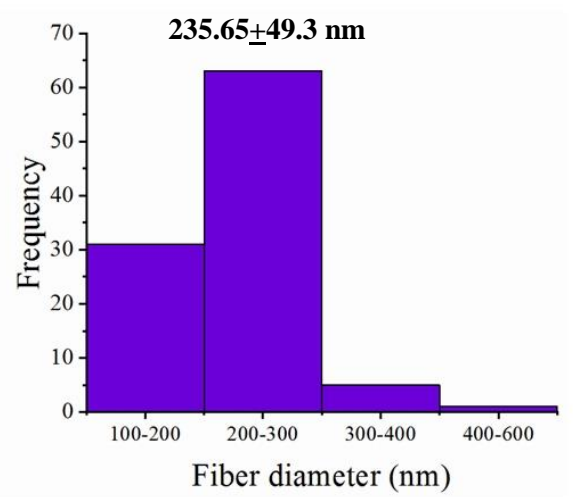
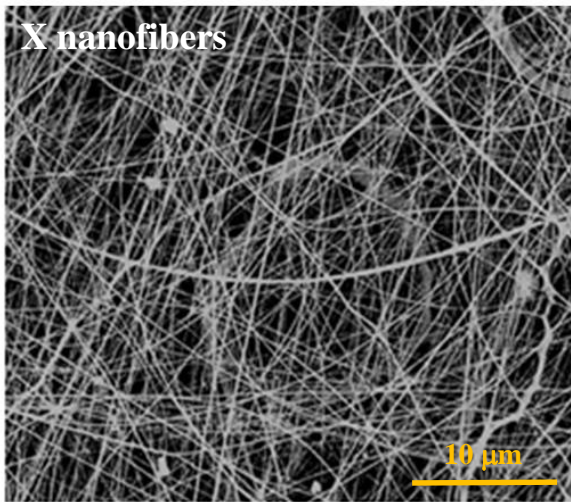


Figure 1. Morphological analysis by scanning electron microscopy and average fiber diameter distributions of electrospun X nanofibers, X-GA and X-EGCG nanofibers.

The mechanism of GA and EGCG release from X nanofibers in pH 6.5 and 7.4 media were fitted by Korsmeyer-Peppas kinetic model ($C = kt^n$), where, C is amount of compound released within the time t ; k is the rate constant and n the release exponent. The constant value of k is usually related to the characteristics of the delivery system and drug; while n is the diffusion exponent which characterizes the transport mechanism of the drug and it depends on the type of transport, geometry, and polydispersity. The n values of the kinetic model in pH 6.5 and 7.4 media for the release of GA were 0.85 and 0.83, respectively. In the case of EGCG release, the n values in pH 6.5 and 7.4 media were 0.84 and 0.77, respectively. These results confirm that the release of the studied phenolic compounds is governed by the non Fickian mechanism.

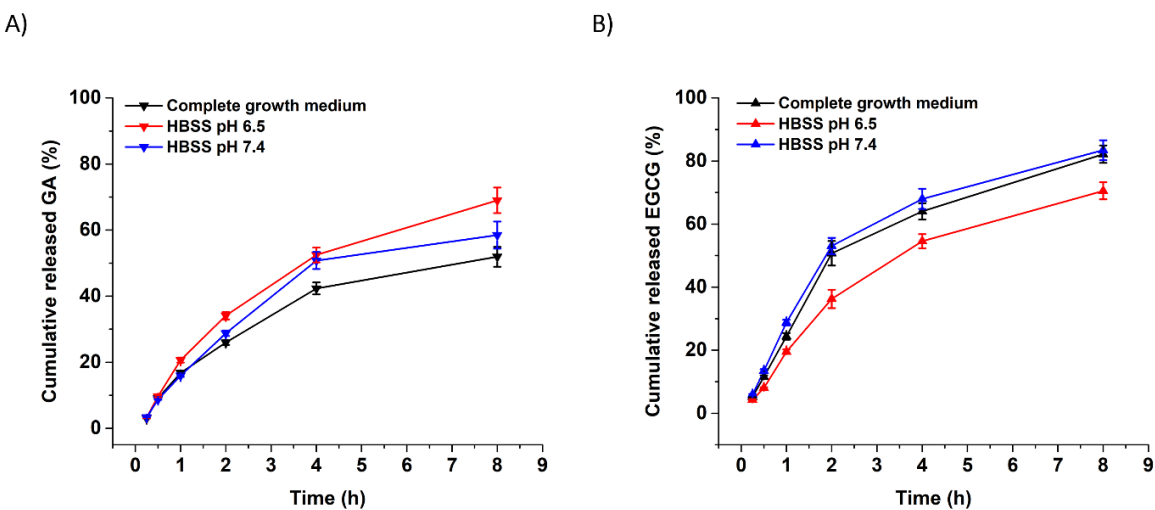


Figure 2. Cumulative *in vitro* release of GA (A) and EGCG (B) from xanthan nanofibers. All data were the mean \pm SD of three independent experiments.

3.3. Effect of GA, EGCG and their nanofiber forms on Caco-2 cell viability

The viability of Caco-2 cells after 24 h treatment with free GA, EGCG and PBS as control was evaluated through MTS bioassay (**Figure 3**). The MTS tetrazolium compound is normally reduced by living cells into a colored formazan product that is soluble in culture medium and quantified recording its absorbance at 490 nm. This conversion is accomplished by dehydrogenase enzymes in metabolically active cells; therefore MTS conversion is directly proportional to the number of living cells.

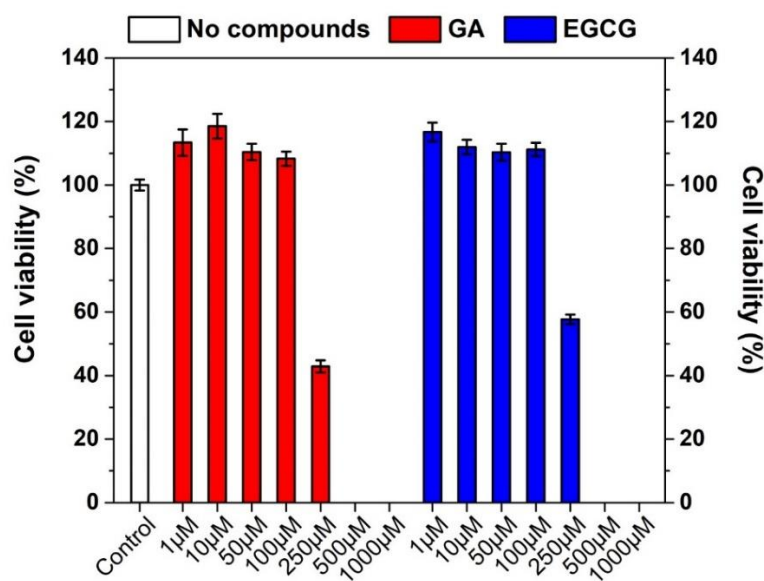


Figure 3. Viability bioassay of Caco-2 cells incubated with PBS (control, white bar) and increasing concentrations of free GA (red bars) and free EGCG (blue bars) diluted in PBS ranging from 1 μM to 1 mM. After 24 h incubation with the compounds, the cell viability was evaluated through MTS assay. Data were the mean ± SD of four independent experiments.

When Caco-2 cells were incubated with free GA or EGCG in the concentration range between 1-100 μM , an increase in the cell viability confirmed the beneficial properties of these polyphenols. By contrast, concentrations above 100 μM resulted in a drastically decrease of cell viability, with a 50% or even higher cell mortality. The IC_{50} of free GA after 24 h incubation was estimated to be around 180 μM .⁷ The concentration-dependent toxic effect of GA and EGCG was taken into account in order to perform transepithelial transport across proliferating cell monolayers. Indeed, the amount of X-GA and X-EGCG fibers was carefully calculated to obtain a final released GA and EGCG concentration lower or equal to 100 μM .

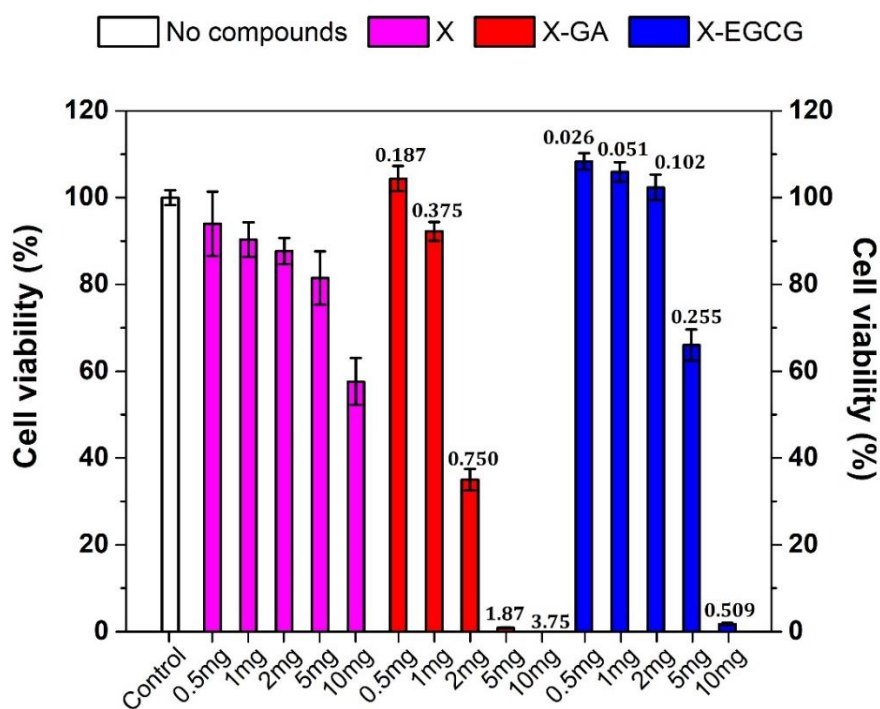


Figure 4. MTS viability bioassay of Caco-2 cells after 24 h incubation with complete growth medium (Control, white bar) and increasing amounts of empty xanthan nanofibers (X, magenta bars), gallic acid-loaded xanthan nanofibers (X-GA, red bars) and (-)-epigallocatechin gallate-loaded xanthan nanofibers (X-EGCG, blue bars). The numbers reported on top of the red and

blue bars represent the maximum releasable concentration (mM) of GA and EGCG in a 1.2 mL volume of complete growth medium. Data were the mean \pm SD of four independent experiments.

The viability of Caco-2 cells after 24 h treatment with increasing amount of empty X, X-GA and X-EGCG nanofibers was also investigated to establish the amount of fibers (in milligrams) to be used for transepithelial transport studies. As shown in **Figure 4**, the incubation of empty X fibers induced a directly proportional decrease of cell viability, reaching around 60% cell viability for 10 mg X nanofibers. However, this reduction was found to be more pronounced when cells were treated with X-GA and X-EGCG fibers. The release of GA from 2.0 mg X-GA fibers caused a cell mortality around 70% and down until 98% for 5 mg X-GA fibers. The same effect was also confirmed after EGCG release from X-EGCG fibers, even though 95% cell mortality was observed for 10 mg fibers. Consequently, the reduction of cell viability induced by X-GA and X-EGCG fibers was mainly attributed to GA and EGCG releases, as confirmed in **Figure 3**, and only partially caused by X nanofibers. Altogether, the *in vitro* release profile of GA and EGCG from nanofibers, the incubation time of fibers with cells, and the encapsulation efficiency must be taken into account.

3.4. Assessment of cell monolayers integrity

The cell monolayers integrity is a fundamental determinant for the study of compound transport across the intestinal barrier, especially when passive transport through tight junctions is involved.³² To ensure reliable *in vitro* permeability experiments across Caco-2 cell monolayers, the transport of non-radiolabeled markers, fluorescein and lucifer yellow, and transepithelial electrical resistance measurement were conducted to quantitatively investigate the integrity of monolayers after 21 days growth on 12-mm polycarbonate inserts. The average TEER value for

Caco-2 cell monolayers randomly chosen for transport studies was $370.74 \pm 15.81 \Omega \text{ cm}^2$. The TEER values of monolayers before and after transport of FLUO and LY were found in the range of $300\text{-}500 \Omega \text{ cm}^2$ (**Figure 5**), indicating an “intermediate” tightness of the gastrointestinal epithelium.³³

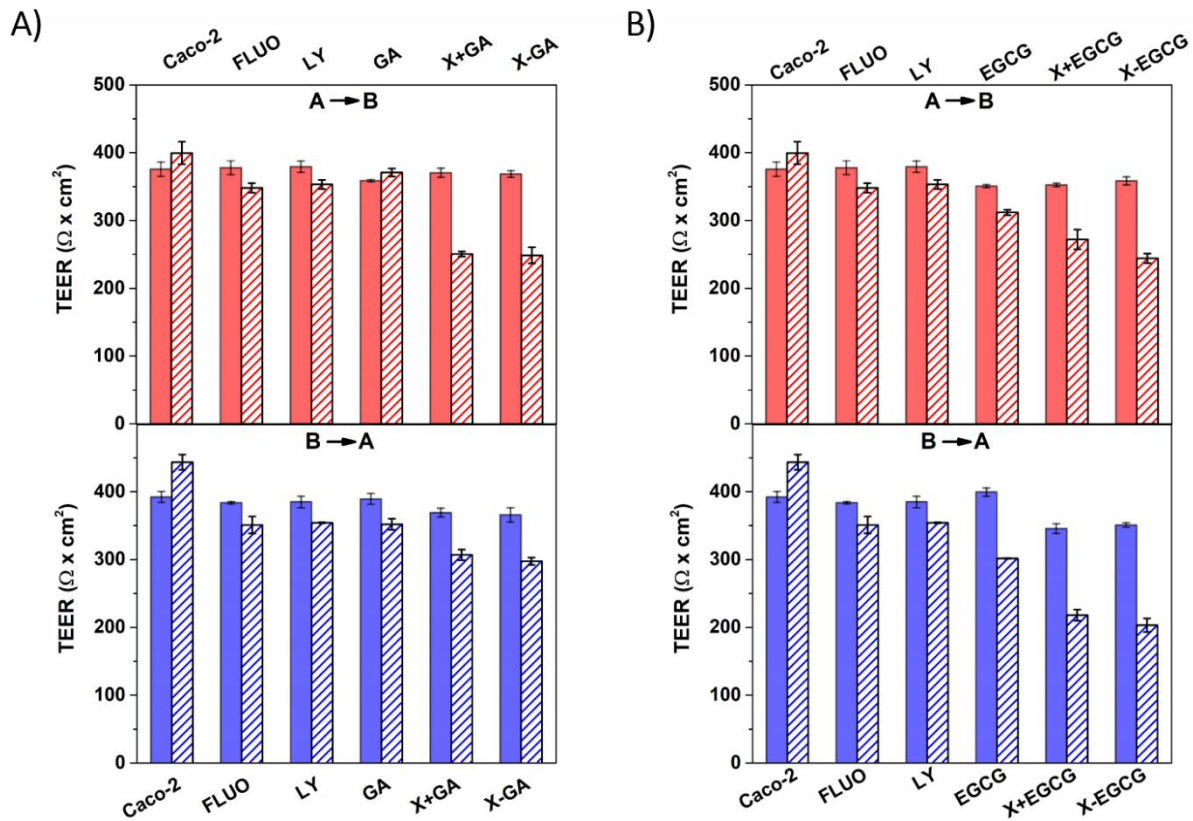


Figure 5. Transepithelial electrical resistance (TEER) measurements of cell monolayers before (full colored bars) and after (patterned bars) apical-to-basolateral (AB) and basolateral-to-apical (BA) studies for a time interval of 8 h. TEER values were recorded for GA, X+GA, X-GA (A) and EGCG, X+EGCG and X-EGCG (B). All data were the mean \pm SD of three independent experiments.

Given that, the AB and BA transepithelial transports of FLUO and LY across Caco-2 monolayers under a proton gradient were investigated, resulting in a pH-dependent transport of FLUO. The apparent permeability coefficients of FLUO were $P_{app,AB} = 3.31 \times 10^{-6}$ cm/s and $P_{app,BA} = 2.01 \times 10^{-6}$ cm/s, whereas much lower values were observed from the LY transport: $P_{app,AB} = 1.13 \times 10^{-7}$ cm/s and $P_{app,BA} = 1.21 \times 10^{-7}$ cm/s (**Figure 6C**). Because of the lipoid nature of polarized epithelial cell layers, the transport of ions and hydrophilic compounds is restricted through the membrane. Indeed, the hydrophilic LY was transported across epithelial cells solely via tight junctions, whereas the lipophilic nature of FLUO permitted its permeation through transcellular transport.³⁴⁻³⁶ Thus, the TEER and permeability observations suggested that the integrity and tightness of epithelial cell monolayers were maintained after 21 days culturing.

3.5. Transepithelial transport and distribution of free GA, EGCG and their nanofiber forms

The transported amounts of GA and EGCG, their apparent permeability coefficient and their permeability directional ratio were assessed for both AB and BA directions under a proton gradient. In addition, the compounds were incubated at the donor chamber in a free form (GA and EGCG), in a free form in presence of empty xanthan nanofibers (X+GA and X+EGCG), and in the nanofiber forms (X-GA and X-EGCG).

Figure 6 summarizes all the above-mentioned parameters. First and foremost, the amounts of molecules transported in the acceptor chamber were higher in the AB direction than BA. Secondly, the addition of empty or loaded xanthan nanofibers enhanced the transport of GA and EGCG in the AB direction (**Figure 6 B-D**).

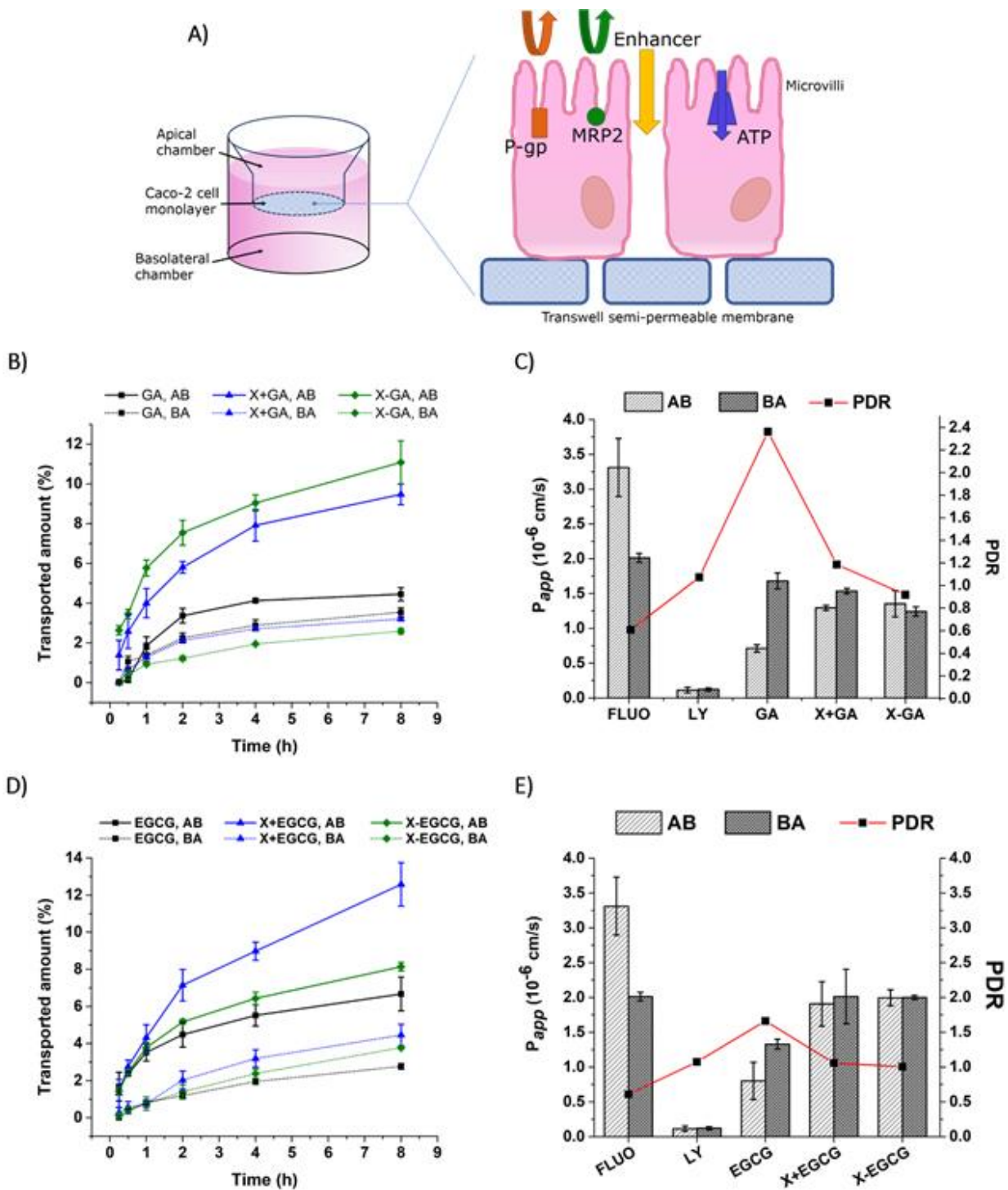


Figure 6. Transepithelial transport of GA and EGCG across Caco-2 monolayers. Illustration of the efflux transporters expressed on the apical membrane of epithelial cells (A). Transported amount of GA, X+GA and X-GA (B), and EGCG, X+EGCG and X-EGCG (D) in both AB and

BA directions. Apparent permeability coefficient, P_{app} and PDR of GA, X+GA and X-GA (C), and EGCG, X+EGCG and X-EGCG (E). All data were the mean \pm SD of three independent experiments.

Indeed, the permeated amount of gallic acid in the X+GA and X-GA formulations was 2-fold and 2.5-fold higher than that of free GA. The same results were obtained for the transported EGCG in the AB direction, but on the contrary, the X+EGCG form was the most effective (a 1.9-fold the free EGCG). These results suggested that the permeation of the compounds was greatly enhanced by the presence of xanthan nanofibers, either as empty nanostructures or loaded with polyphenols. Accordingly, the apparent permeability coefficients of GA and EGCG incubated with nanofibers were at least 2-fold than of these without fibers in the donor chamber. The GA and X-GA permeability values in the AB direction were $P_{app, AB} = 7.12 \times 10^{-7}$ cm/s and $P_{app, AB} = 1.96 \times 10^{-6}$ cm/s, respectively (**Figure 6C**). The same increase in permeability was calculated also for the EGCG nanofiber form, where EGCG and X-EGCG had a $P_{app, AB} = 7.99 \times 10^{-7}$ cm/s and $P_{app, AB} = 1.99 \times 10^{-6}$ cm/s, respectively (**Figure 6E**). An increment of the apparent permeability coefficient values was also found in the BA direction, even though less pronounced than in the AB direction.

The fate of GA and EGCG during 8 h transepithelial transports in both AB and BA directions was monitored by quantifying their concentration in the donor and acceptor compartments, and also in the cell lysate, insert membrane (filter), and within xanthan nanofibers (adsorbed or unreleased).

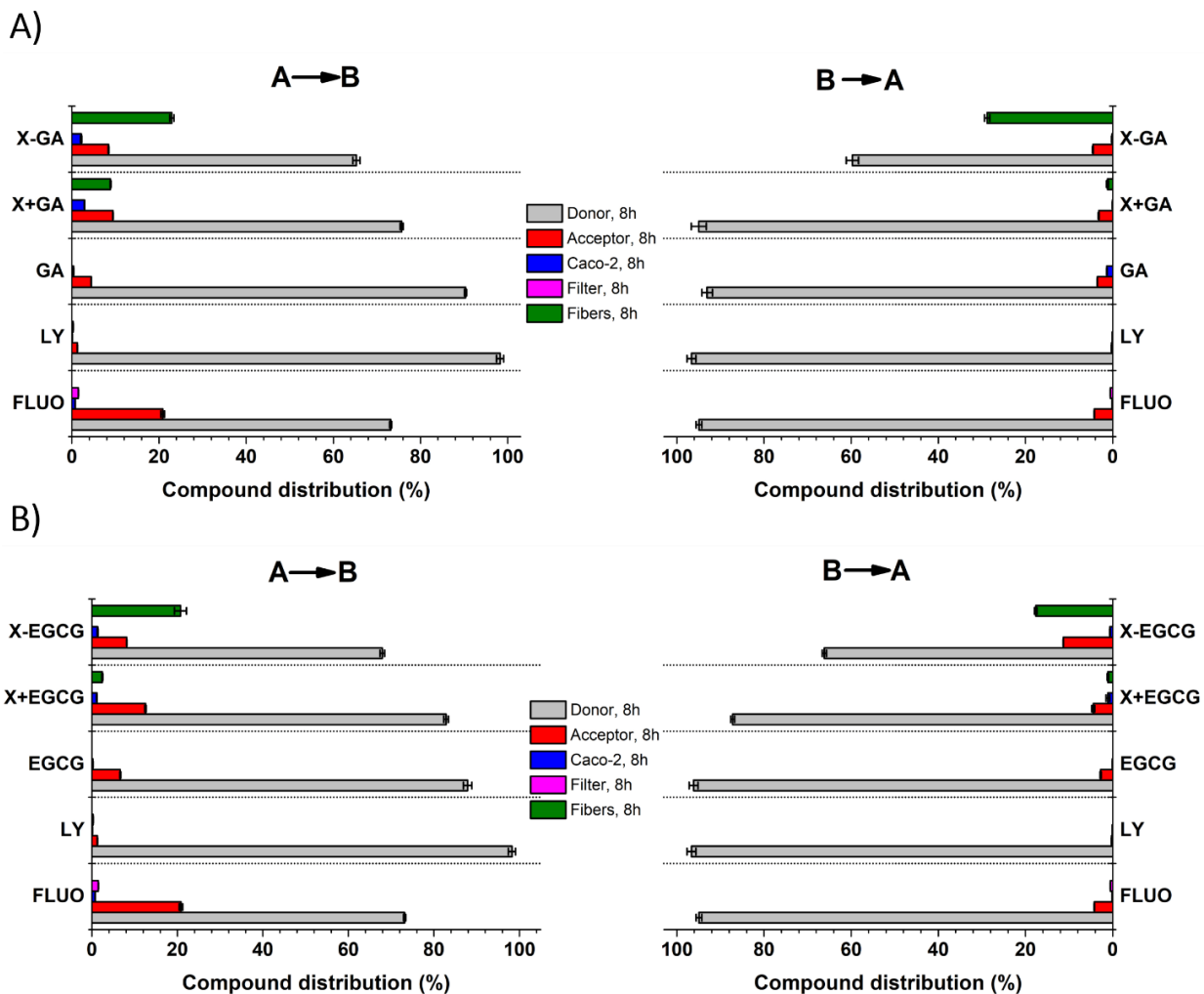


Figure 7. Quantification of GA (A) and EGCG (B) distribution in the donor side, acceptor side, cell lysate, membrane insert and fibers, after 8 h transepithelial transport in both AB and BA directions. All data are the mean \pm SD of three independent experiments.

Figure 7 shows the distribution of the tested compounds in the above-mentioned compartments. As first, after 8 h experiment, most of the incubated compounds were still found in the donor chamber ($\geq 60\%$ of the concentration at time=0h), and only less than 20% were detected in the acceptor side. However, the yields of GA and EGCG recorded in A were higher when incubated with xanthan nanofibers than in absence. Small amounts of GA and EGCG were also detected

inside the epithelial monolayers (3% and 1.3%, respectively), and adsorbed to or unreleased from xanthan nanofibers (28.79% and 20.71%, respectively).

4. Discussion

In this study, the human differentiated epithelial Caco-2 cells were chosen as an established *in vitro* cell model for the prediction of bioactive compounds absorption and transport mechanism.³⁷ The Caco-2 cells possess many features, among which their ability to slowly differentiate into monolayers forming microvilli and tight junctions at the apical side, and to express brush border transporters and enzymes involved in the metabolism and transport of several substrates.^{31,38,39} Therefore, transepithelial transport studies of GA and EGCG were performed across Caco-2 monolayers in the apical-to-basolateral and basolateral-to-apical direction under proton gradient. The two polyphenols investigated in this study are characterized by a poor intestinal absorption due to their high hydrophilicity; in fact, they can hardly penetrate the cell membrane and only passive diffusion seems to be involved in permeation.¹⁷

In our previous study, the electrospinning processing of xanthan polysaccharide solutions dissolved in formic acid was investigated.³⁰ The developed xanthan nanofibers were morphologically stable over a wide pH range in saline buffers, thus in the present study xanthan polysaccharide nanofibers was used to encapsulate and release the GA and EGCG bioactives. The 24 h incubation of nanofibers with Caco-2 cells revealed a proliferative effect in cell viability for amount lower or equal to 0.5 mg X-GA and 2.0 mg X-EGCG; drastic cell mortality was observed for doses above this range. In addition, the treatment of Caco-2 cells with increasing amount of empty xanthan nanofibers resulted in a dose-dependent reduction of cell viability, near to 60% for 10.0 mg X amount. However, this observed effect in cell viability was

expected to be less pronounced for the transepithelial transport studies, since the cell monolayers were exposed to X, X-GA and X-EGCG for 8 h interval rather than 24 h. The transepithelial transport of GA and EGCG in the acceptor compartment was successfully enhanced by the presence of xanthan, both as empty nanostructure and as nanocarrier, and the permeability coefficients were higher than those calculated for free compounds. In addition, the PDR values estimated for free GA and free EGCG were both higher than 1.5 (2.4 and 1.7, respectively). These results suggest that the transport of GA and EGCG is modulated by an active transport pathway, and more specifically by efflux. Several studies have described the mechanism and the efflux transporters involved in the unidirectional transport of GA and EGCG across epithelial barrier.^{15,17,40-42} Enterocytes express several transporters on the apical and basolateral membrane which can actively transport a wide range of structurally diverse compounds into (influx) or out (efflux) of the cell. GA and EGCG, as depicted in **Figure 6A**, are actively transported outside cells through P-glycoprotein (P-gp), multidrug resistant protein 2 (MRP2) and the ATP binding cassette (ATP) transporters that are expressed on the apical membrane of Caco-2 monolayers.^{39,42} These efflux pumps restrict therefore the influx of GA and EGCG in the acceptor chamber, rather promoting their efflux from enterocytes. Several efflux pump inhibitory compounds, such as indomethacin, verapamil, MK-571^{17,41} have been thoroughly investigated, resulting to an increase in oral absorption. In this study, the calculated PDR values obtained for free GA and free EGCG transport were higher than 1.5, confirming their efflux from monolayers. However, the PDR values of X+GA, X-GA, X+EGCG and X-EGCG were all lower than 1.5 (**Figure 6C-E**). Hence, the incubation of xanthan nanofibers in the donor compartment greatly improved the absorption of GA and EGCG across epithelial barrier, suggesting an inhibitory effect of xanthan on efflux transporters. Indeed, it has been demonstrated that

naturally occurring polymers and polysaccharides, such as dextran, anionic gums as well as polysaccharides in Aloe vera, can inhibit efflux pumps.^{42,43} For instance, the effect of 0.5 mg/mL xanthan gum have shown increased concentration of P-gp substrates such as vinblastine and doxorubicin, pointing out its inhibitory activity.⁴² Additionally, polysaccharides consisting of linear chains of glucose and mannose units, and acetylated mannose residues, like Aloe vera polysaccharides and xanthan gum, have shown a reversible intestinal tight junctions opening behavior, enhancing the paracellular permeability and thus, the bioavailability of drugs.⁴³ Such effect of xanthan nanofibers on tight junctions opening was also confirmed by a moderate decrease of TEER after transepithelial transports.

5. Conclusion

Uniform and homogeneous xanthan nanofibers were fabricated using electrospinning processing and the encapsulation and release of two poorly absorbed polyphenol compounds, GA and EGCG, was investigated. It was found that X, X-GA and X-EGCG nanofibers remained stable in aqueous HBSS medium at different pH (6.5 and pH 7.4). The total amount of GA and EGCG released from xanthan nanofibers was 69.01% and 70.53% in HBSS at pH 6.5, and 58.47% and 83.44% in HBSS at pH 7.4, respectively. Moreover, the nanofibers were incubated with Caco-2 cells and the cell viability, transepithelial transport and GA and EGCG permeability properties across cell monolayers were investigated. At least a 2-fold increase of GA and EGCG permeability was observed in the presence of X-GA and X-EGCG nanofibers, in comparison with the free- phenolic compounds. Indeed, the polysaccharide nanofibers enhanced the GA and EGCG permeability by opening the tight junctions of Caco-2 monolayers, as well as inhibiting the efflux transporters. These findings are extremely relevant to promote the delivery not only of polyphenols but also of other poorly absorbed bioactives.

Acknowledgment

The project was supported by a third of a PhD stipend (to ES) from the Technical University of Denmark.

References

1. Scalbert, A. & Williamson, G. Dietary intake and bioavailability of polyphenols. *J. Nutr.* **130**, 2073S–85S (2000).
2. Kühnau, J. The flavonoids. A class of semi-essential food components: their role in human nutrition. *World Rev. Nutr. Diet.* **24**, 117–91 (1976).
3. Inoue, M. *et al.* Antioxidant, Gallic Acid, Induces Apoptosis in HL-60RG Cells. *Biochem. Biophys. Res. Commun.* **204**, 898–904 (1994).
4. Inoue, M. *et al.* Selective induction of cell death in cancer cells by gallic acid. *Biol. Pharm. Bull.* **18**, 1526–30 (1995).
5. Gali, H. U., Perchellet, E. M. & Perchellet, J. P. Inhibition of tumor promoter-induced ornithine decarboxylase activity by tannic acid and other polyphenols in mouse epidermis in vivo. *Cancer Res.* **51**, 2820–5 (1991).
6. Gali, H. U., Perchellet, E. M., Klish, D. S., Johnson, J. M. & Perchellet, J. P. Antitumor-promoting activities of hydrolyzable tannins in mouse skin. *Carcinogenesis* **13**, 715–8 (1992).
7. Rashidi, L. *et al.* A cellular uptake and cytotoxicity properties study of gallic acid-loaded mesoporous silica nanoparticles on Caco-2 cells. *J. Nanoparticle Res.* **16**, 2285 (2014).
8. KONISHI, Y., KOBAYASHI, S. & SHIMIZU, M. Transepithelial Transport of *p* - Coumaric Acid and Gallic Acid in Caco-2 Cell Monolayers. *Biosci. Biotechnol. Biochem.*

- 67, 2317–2324 (2003).
9. Huang, P.-J. *et al.* In vitro and in vivo activity of gallic acid and *Toona sinensis* leaf extracts against HL-60 human promyelocytic leukemia. *Food Chem. Toxicol.* **50**, 3489–3497 (2012).
 10. Inoue, M., Sakaguchi, N., Isuzugawa, K., Tani, H. & Ogihara, Y. Role of reactive oxygen species in gallic acid-induced apoptosis. *Biol. Pharm. Bull.* **23**, 1153–7 (2000).
 11. Kaur, M., Velmurugan, B., Rajamanickam, S., Agarwal, R. & Agarwal, C. Gallic Acid, an Active Constituent of Grape Seed Extract, Exhibits Anti-proliferative, Pro-apoptotic and Anti-tumorigenic Effects Against Prostate Carcinoma Xenograft Growth in Nude Mice. *Pharm. Res.* **26**, 2133–2140 (2009).
 12. Pal, C. *et al.* Gallic acid prevents nonsteroidal anti-inflammatory drug-induced gastropathy in rat by blocking oxidative stress and apoptosis. *Free Radic. Biol. Med.* **49**, 258–267 (2010).
 13. You, B. R. & Park, W. H. Gallic acid-induced lung cancer cell death is related to glutathione depletion as well as reactive oxygen species increase. *Toxicol. Vitro.* **24**, 1356–1362 (2010).
 14. You, B. R., Moon, H. J., Han, Y. H. & Park, W. H. Gallic acid inhibits the growth of HeLa cervical cancer cells via apoptosis and/or necrosis. *Food Chem. Toxicol.* **48**, 1334–1340 (2010).
 15. Vaidyanathan, J. B. & Walle, T. Cellular Uptake and Efflux of the Tea Flavonoid (-)Epicatechin-3-gallate in the Human Intestinal Cell Line Caco-2. *J. Pharmacol. Exp. Ther.* **307**, 745–752 (2003).
 16. Katiyar, S. & Mukhtar, H. Tea in chemoprevention of cancer. *Int. J. Oncol.* **8**, 221–38

- (1996).
17. Song, Q. *et al.* Enhanced uptake and transport of (+)-catechin and (-)-epigallocatechin gallate in niosomal formulation by human intestinal Caco-2 cells. *Int. J. Nanomedicine* **9**, 2157 (2014).
 18. Ji, B. T. *et al.* Green tea consumption and the risk of pancreatic and colorectal cancers. *Int. J. cancer* **70**, 255–8 (1997).
 19. Su, J. & Arab, L. Tea consumption and the reduced risk of colon cancer – results from a national prospective cohort study. doi:10.1079/PHN2001314
 20. Munin, A. & Edwards-Lévy, F. Encapsulation of Natural Polyphenolic Compounds; a Review. *Pharmaceutics* **3**, 793–829 (2011).
 21. Dube, A., Ng, K., Nicolazzo, J. A. & Larson, I. Effective use of reducing agents and nanoparticle encapsulation in stabilizing catechins in alkaline solution. *Food Chem.* **122**, 662–667 (2010).
 22. Caddeo, C., Teskač, K., Sinico, C. & Kristl, J. Effect of resveratrol incorporated in liposomes on proliferation and UV-B protection of cells. *Int. J. Pharm.* **363**, 183–191 (2008).
 23. Chuysinuan, P., Chimnoi, N., Techasakul, S. & Supaphol, P. Gallic acid-loaded electrospun poly(L-lactic acid) fiber mats and their release characteristic. *Macromol. Chem. Phys.* **210**, 814–822 (2009).
 24. Neo, Y. P. *et al.* Encapsulation of food grade antioxidant in natural biopolymer by electrospinning technique: A physicochemical study based on zein-gallic acid system. *Food Chem.* **136**, 1013–1021 (2013).
 25. Phiriyawirut, M. & Phaechamud, T. Gallic Acid-loaded Cellulose Acetate Electrospun

- Nanofibers: Thermal Properties, Mechanical Properties, and Drug Release Behavior. *Open J. Polym. Chem.* **2**, 21–29 (2012).
26. Aytac, Z., Kusku, S. I., Durgun, E. & Uyar, T. Encapsulation of gallic acid/cyclodextrin inclusion complex in electrospun polylactic acid nanofibers: Release behavior and antioxidant activity of gallic acid. *Mater. Sci. Eng. C* **63**, 231–239 (2016).
 27. Li, Y., Lim, L.-T. & Kakuda, Y. Electrospun Zein Fibers as Carriers to Stabilize (–)-Epigallocatechin Gallate. *J. Food Sci.* **74**, C233–C240 (2009).
 28. Lee, E. J. *et al.* Hyaluronic acid/poly(lactic-co-glycolic acid) core/shell fiber meshes loaded with epigallocatechin-3-O-gallate as skin tissue engineering scaffolds. *J. Nanosci. Nanotechnol.* **14**, 8458–63 (2014).
 29. Tian, J. *et al.* Antimicrobial application of nanofibrous mats self-assembled with chitosan and epigallocatechin gallate. *Colloids Surfaces B Biointerfaces* **145**, 643–652 (2016).
 30. Shekarforoush, E., Faralli, A., Ndoni, S., Mendes, A. C. & Chronakis, I. S. Electrospinning of Xanthan Polysaccharide. *Macromol. Mater. Eng.* **302**, 1–11 (2017).
 31. Hubatsch, I., Ragnarsson, E. G. E. & Artursson, P. Determination of drug permeability and prediction of drug absorption in Caco-2 monolayers. *Nat. Protoc.* **2**, 2111–2119 (2007).
 32. Srinivasan, B. *et al.* TEER Measurement Techniques for In Vitro Barrier Model Systems. *J. Lab. Autom.* **20**, 107–126 (2015).
 33. Amidon, G. L., Lee, P. I. & Topp, E. M. *Transport processes in pharmaceutical systems.* (M. Dekker, 2000).
 34. Högerle, M. L. & Winne, D. Drug absorption by the rat jejunum perfused in situ. Dissociation from the pH-partition theory and role of microclimate-pH and unstirred layer.

- Naunyn. Schmiedebergs. Arch. Pharmacol.* **322**, 249–55 (1983).
35. Bock, U. *et al.* Transport of proteolytic enzymes across Caco-2 cell monolayers. *Pharm. Res.* **15**, 1393–400 (1998).
 36. Konishi, Y., Hagiwara, K. & Shimizu, M. Transepithelial Transport of Fluorescein in Caco-2 Cell Monolayers and Use of Such Transport in In Vitro Evaluation of Phenolic Acid Availability. *Biosci. Biotechnol. Biochem.* **66**, 2449–2457 (2002).
 37. Artursson, P., Palm, K. & Luthman, K. Caco-2 monolayers in experimental and theoretical predictions of drug transport. *Adv. Drug Deliv. Rev.* **46**, 27–43 (2001).
 38. Yee, S. In vitro permeability across Caco-2 cells (colonic) can predict in vivo (small intestinal) absorption in man--fact or myth. *Pharm. Res.* **14**, 763–6 (1997).
 39. Naruhashi, K. *et al.* Comparison of the expression and function of ATP binding cassette transporters in Caco-2 and T84 cells on stimulation by selected endogenous compounds and xenobiotics. *Drug Metab. Pharmacokinet.* **26**, 145–53 (2011).
 40. Hoosain, F. G. *et al.* Bypassing P-Glycoprotein Drug Efflux Mechanisms: Possible Applications in Pharmaco-resistant Schizophrenia Therapy. doi:10.1155/2015/484963
 41. Mao, X. *et al.* Transport of Corilagin, Gallic Acid, and Ellagic Acid from Fructus Phyllanthi Tannin Fraction in Caco-2 Cell Monolayers. *Evid. Based. Complement. Alternat. Med.* **2016**, 9205379 (2016).
 42. Werle, M. Expert Review Natural and Synthetic Polymers as Inhibitors of Drug Efflux Pumps. (2007). doi:10.1007/s11095-007-9347-8
 43. Beneke, C., Viljoen, A. & Hamman, J. Sci Pharm In Vitro Drug Absorption Enhancement Effects of Aloe vera and Aloe ferox. *za (J. H. Hamman) Sci Pharm* **80**, 475–486 (2012).

3.1.3. Development of xanthan-chitosan nanofibers- Paper III

Electrospun Xanthan gum-Chitosan nanofibers as delivery carrier of hydrophobic bioactives

Elhamalsadat Shekarforoush,¹ Fatemeh Ajalloueiian,¹ Guanghong Zeng,² Ana C. Mendes,¹ Ioannis S. Chronakis¹

1 Nano-BioScience Research Group, DTU-Food, Technical University of Denmark, Kemitorvet B202, 2800 Kgs. Lyngby, Denmark

2 Danish National Metrology Institute, Kogle Alle 5, DK-2970 Hoersholm, Denmark



Electrospun xanthan gum-chitosan nanofibers as delivery carrier of hydrophobic bioactives



Elhamalsadat Shekarforoush^a, Fatemeh Ajalloueiian^a, Guanghong Zeng^b, Ana C. Mendes^{a,*}, Ioannis S. Chronakis^a

^aNano-BioScience Research Group, DTU-Food, Technical University of Denmark, Kemitorvet B202, 2800 Kgs. Lyngby, Denmark

^bDanish National Metrology Institute, Kogle Alle 5, DK-2970 Hoersholm, Denmark

ARTICLE INFO

Article history:

Received 27 March 2018

Received in revised form 25 May 2018

Accepted 11 June 2018

Available online 15 June 2018

Keywords:

Xanthan gum

Chitosan

Electrospinning

Drug delivery

Curcumin

ABSTRACT

Viscoelastic gels of xanthan gum-chitosan(X-Ch) in formic acid were electrospun to produce nanofibers, stable in aqueous media, for the encapsulation and release of curcumin (Cu). After 120 h, the nanofibers released lower amount of curcumin (~20%) at pH 2.2 comparatively to the release in neutral media (~50%), suggesting that X-Ch nanofibers could be used as a carrier for the encapsulation of hydrophobic bioactive compounds with long-term pH-stimulated release properties.

© 2018 Elsevier B.V. All rights reserved.

1. Introduction

The efficient delivery of hydrophobic bioactives, requires proper encapsulation to overcome concerns related with their low solubility and instability in aqueous body fluids, and limited bioavailability. Electrohydrodynamic (electrospinning and electro spray) methods have been widely studied due to their high encapsulation efficiency, low process temperature using a range broad food bioactive and shell ingredient [1]. Moreover, electrospun fibers comes along with high surface area, tunable diameter and surface functionality, which makes them very attractive for encapsulation and controlled bioactive release [1,2].

Curcumin is a phenolic compound recognized by its pharmaceutical properties as an antioxidant, antimicrobial, anti-inflammatory agent and inhibitor of tumorigenesis and metastasis [3,4]. Due to its hydrophobicity and subsequent poor bioavailability, new delivery carriers have been investigated using electrospinning technology [5–7].

Chitosan (Ch) is a cationic polysaccharide consisting of N-acetyl glucosamine and glucosamine known for its biocompatibility, biodegradability, and mucoadhesivity [8] and ability to enhance gastrointestinal drug absorption [9]. Xanthan (X) gum is an anionic polysaccharide known for its peculiar physico-chemical properties

[10] and has been used as encapsulating matrix [11]. A recent study from our group found that X-Ch-Cu nanofibers incubated with Caco-2 cells, resulted in enhancement of the *in vitro* absorption of Cu across cell monolayers, with a 3-fold increase of Cu permeability, compared to free-curcumin. This work aims to investigate the X-Ch nanofiber development, morphological and encapsulation properties and evaluate its potential as a Cu release carrier in various pH media.

2. Experimental

2.1. Materials

All chemicals including xanthan gum (Mw about 2000 kDa [12], chitosan (Mw 28 kD, degree of deacetylation (DD) of 89% and degree of polymerization (DP) of 175), curcumin and formic acid, were obtained from Sigma-Aldrich (Denmark).

2.2. Preparation and characterization of electrospun solutions and fibers

Xanthan (0.75% w/v) and chitosan (3% w/v) were dissolved in formic acid under vigorous stirring overnight at room temperature. Curcumin (2% w/v) was added to X-Ch solution, and stirred for 30 min. X, Ch and X-Ch (with and without curcumin) rheological properties were determined as described at [13]. X-Ch

* Corresponding author.

E-mail address: anac@food.dtu.dk (A.C. Mendes).

and X-Ch-Cu solutions were electrospun at 25 kV (ES50P-10 W, Gamma High Voltage Research, Inc., USA), feed rate of 0.01 mL/min (syringe pump, New Era Pump Systems, USA) using a 21G needle (Proto Advantage, Canada). Fibers were collected on a stainless steel plate, placed 10 cm from the needle tip. Scanning electron microscopy (SEM) and fiber diameter distribution analyses (100 data points) followed the protocol described in [5]. Atomic force microscopy (AFM) was performed on Multimode 8 in PeakForce QNM mode. TAP150A probes with normal spring constant of 5 N/m were used. To measure the adhesion force, deflection sensitivity calibration was performed on sapphire and spring constant (determined by thermal tuning). Adhesion map was formed by plotting the adhesion forces at each point, obtained from the retraction part of each force-distance curve. The encapsulation efficiency (EE) of the Cu within X-Ch nanofibers was determined by Cu fiber extraction using methanol in a sonication bath [5].

2.3. In vitro release studies

X-Ch-Cu nanofibers (3.0 mg) were suspended in 2 mL of Tris buffered saline solution (pH 2.2, 6.5 and 7.6) at 37 °C in a thermostaker water bath. Supernatant aliquots (100 μ L) were withdrawn and replaced with the same volume of fresh media. The amount of Cu released was determined using a NanoDrop One UV-Vis Spectrophotometer (Thermo Fisher Scientific, Denmark) at the optical wavelength of 420 nm. Triplicates were conducted for each sample.

3. Results and discussions

Formation of a viscoelastic network with elastic modulus values (G') higher than the viscous modulus (G'') was observed for the X-Ch mixture in formic acid after 12.5 h (Fig. 1a). Individual xanthan and chitosan solutions exhibited G'' higher than G' . The $\tan \delta$ value ($\tan \delta = G''/G'$) for individual chitosan and xanthan solutions was 2,533 and 1,17, respectively, denoting a liquid-like behaviour, whereas the $\tan \delta$ of X-Ch mixture was 0.144, confirming a gel-like behaviour as reported for other biopolymers gels [13].

Flow rheological studies (Fig. 1b) reveal that xanthan in formic acid has a shear thinning behaviour [13]. The chitosan solution shows nearly Newtonian behaviour at the shear rates of 0.1–100 s^{-1} , and higher viscosity values than xanthan solution. However, a substantial viscosity increase was observed for X-Ch mixture. X and X-Ch mixture followed a power-law thinning behaviour of $\eta = m \cdot \gamma^{n-1}$ where η is the apparent viscosity, γ the shear rate, and m the flow index. The power law index values (n) were in the range of 0.551–0.437 for X-Ch and X-Ch-Cu, which are necessary to produce electrospun fibers [13]. The formation of a viscoelastic gel network, and an apparent viscosity increase of the X-Ch mixture is due to the oppositely charged X-Ch polyelectrolytes electrostatic interactions [14].

Fig. 2 shows individual, uniform and randomly oriented X-Ch nanofibers with average diameters of 750 nm. Note that both individual xanthan and chitosan solutions at the aforementioned concentrations could not be electrospun into fibers. The average diameter of electrospun xanthan-chitosan nanofibers slightly increased to 910 nm with the addition of 2% curcumin, due to the increase of the solution viscosity (Fig. 1b). The EE of Cu within X-Ch nanofibers was $69.4 \pm 4.1\%$.

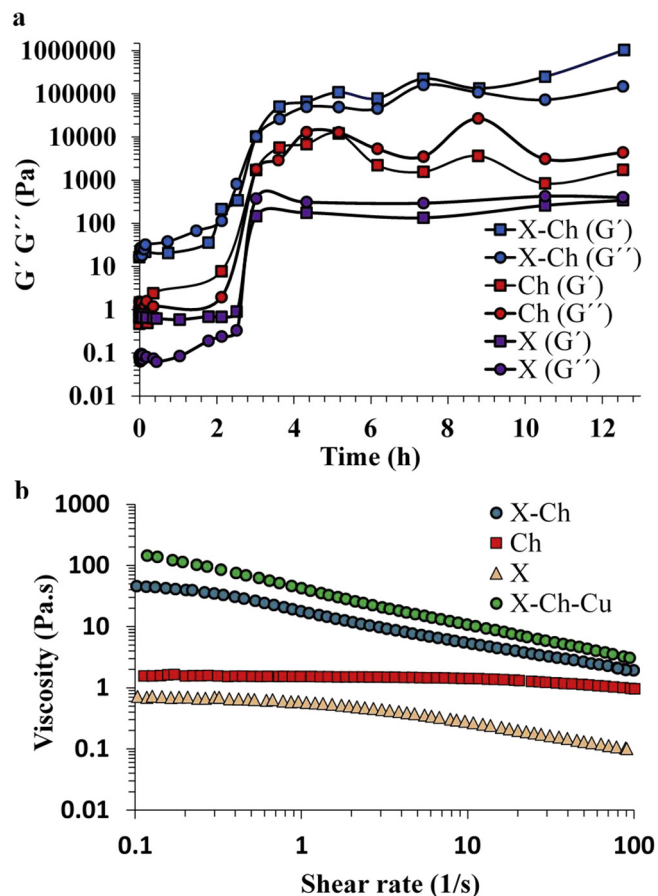


Fig. 1. Viscoelastic properties over time (a) and flow curves (b) of X, Ch, X-Ch and X-Ch-Cu solution.

The X-Ch and X-Ch-Cu fibers' adhesive properties were quantified by Peakforce QNM, which measures adhesion force between the AFM tip (silicon) and nanofibers at each pixel (Fig. 3). Adhesion forces from the top of the nanofibers are shown in the line profiles of X-Ch and X-Ch-Cu, with the average values of 10 nN, and 4 nN, respectively. X-Ch nanofibers displayed adhesive properties that decreased with the encapsulation of curcumin, due to the hydrophobic nature of this bioactive. The adhesive maps indicate that curcumin is incorporated homogeneously within X-Ch-Cu nanofibers.

Fig. 4 shows an 8–10% sustained release of curcumin from X-Ch nanofibers over 12 h for all pH studied (2.2, 6.5 and 7.4) with no burst effect [6]. Beyond that, the release of curcumin at pH 2.2 was much lower than the other media, with no significant increase for up to 120 h. On the other hand, the Cu release conducted in media at pH 7.4 and 6.5 was increased beyond 12 h up to 45 and 50% respectively [6]. It is to note that X-Ch and X-Ch-Cu nanofibers remained intact in all release media after 10–12 h at 37 °C (data not shown). However, after 120 h X-Ch-Cu nanofibers slightly swelled in buffer at pH 6.5 and 7.4 (about 3.5 times the initial fiber diameter), while at pH 2.2 the diameter increased about 1.5 times.

It is suggested, that the oppositely charged xanthan-chitosan mixture in formic acid is associated electrostatically [14]. When the electrospun nanofibers are immersed in the release media at different pH(s), the electrostatic equilibrium for both

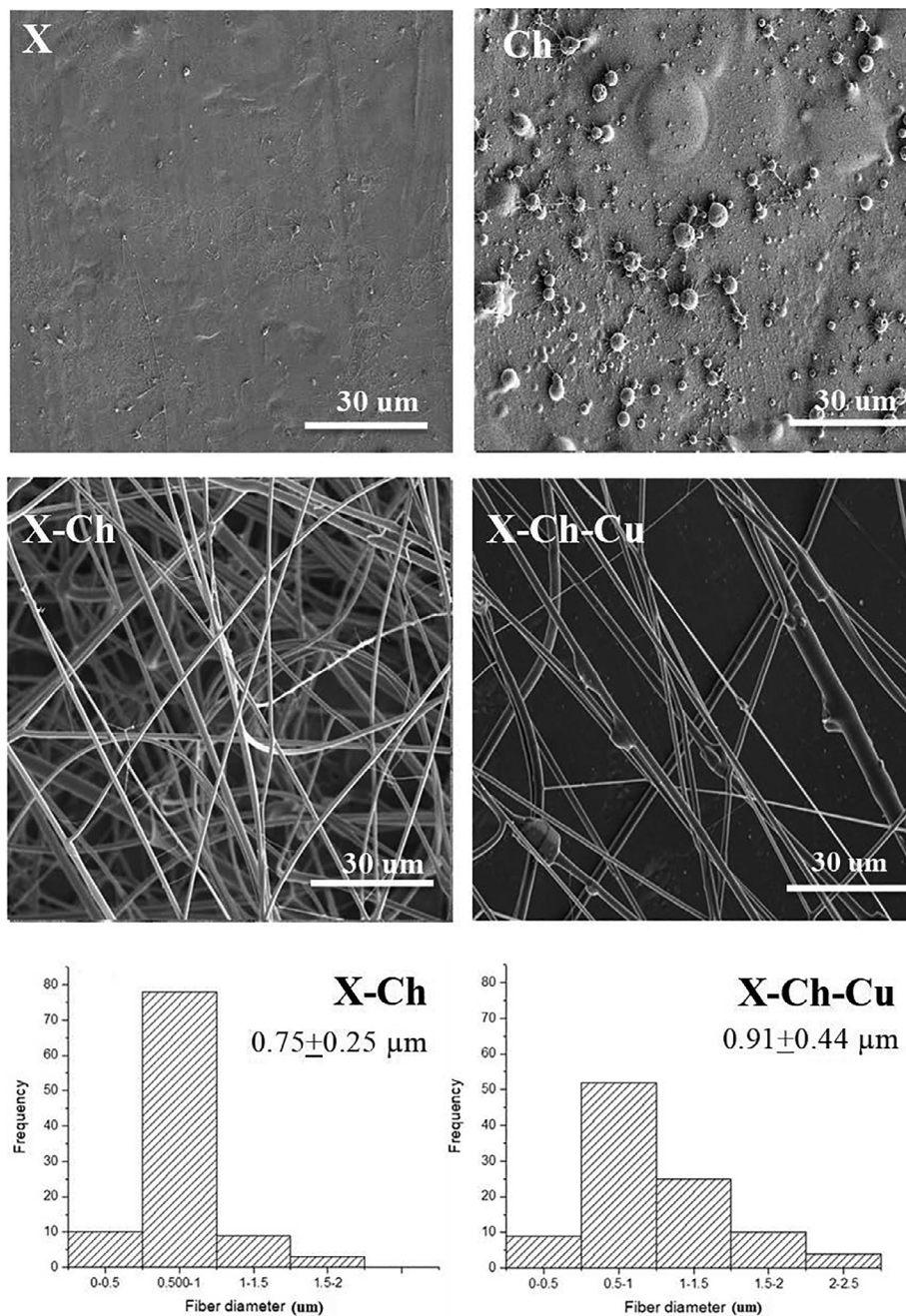


Fig. 2. SEM images of electrospun X, Ch, X-Ch and X-Ch-Cu solutions and histograms displaying nanofibers diameter distribution.

polyelectrolytes is expected to change. Consequently, at pH values below the pKA of chitosan (about 6.5), such as pH 2.2, stronger interactions chitosan-xanthan are expected [15], resulting in denser nanofibers with lower swelling and lower diffusion of the bioactive. Korsmeyer-Peppas model [16], confirmed that the release of Cu at neutral pH followed non Fickian mechanism, an indicator of drug diffusion in the hydrated matrix and polymer relaxation (release exponents “ n ” of 0.70 (pH 6.5) and 0.71 (pH 7.4)). At pH 2.2 the release of Cu is described by the Higuchi mathematical model ($C = kt^{0.5}$), with k value of 2.13.

4. Conclusions

Stable nanofibers in aqueous were produced by the electrospinning of X-Ch viscoelastic gels for the encapsulation and release of curcumin. The adhesion properties of the fibers were reduced with the addition of Cu, due to its hydrophobic properties. The release of curcumin was controlled by the pH of the release media. At pH 2.2 the nanofibers released lower amount of curcumin (~20%) compared to the release in neutral media (~50%) after 120 h due to the higher swelling of the matrix. The results indicated that

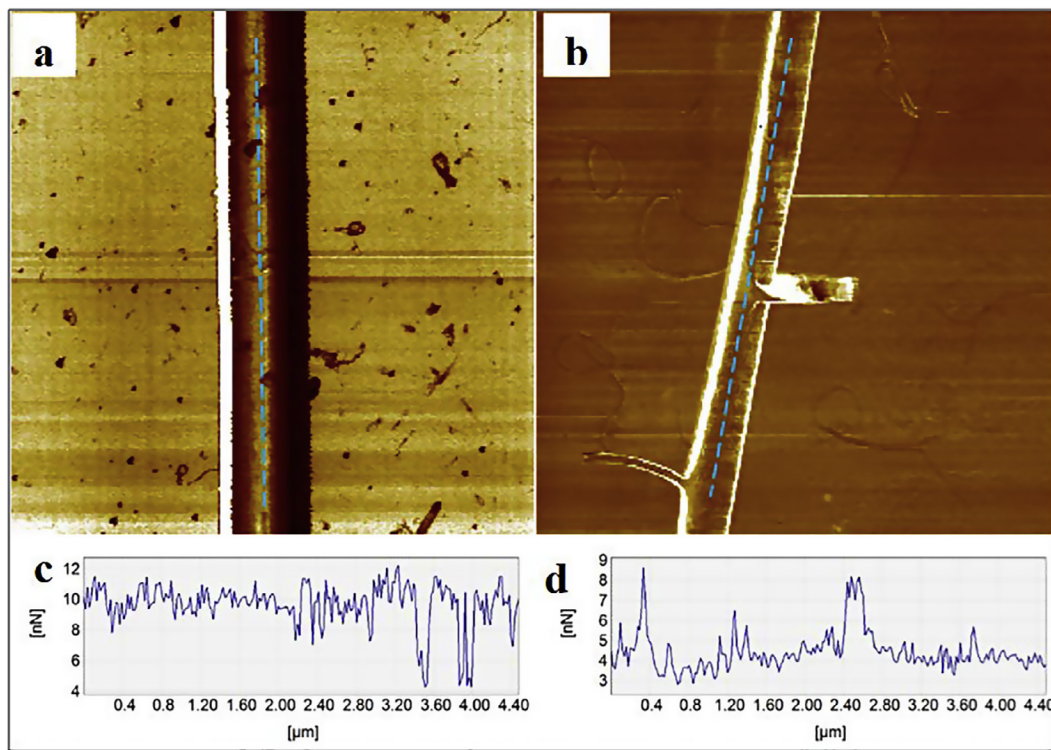


Fig. 3. AFM adhesion maps of X-Ch (a), and X-Ch-Cu (b), and corresponding line profiles for X-Ch (c) and X-Ch-Cu (d).

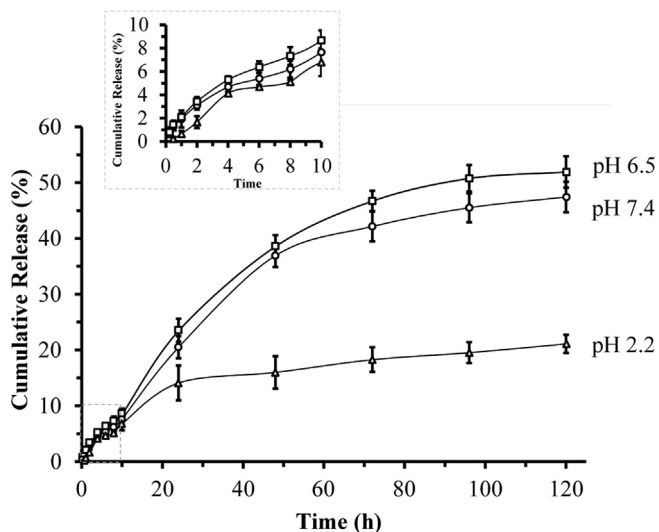


Fig. 4. Release of Curcumin from X-Ch nanofibers in TRIS buffer solution, 37 °C, pH 2.2, 6.5, 7.4.

electrospun X-Ch nanofibers could be used as a carrier for the encapsulation of hydrophobic bioactive compounds with high encapsulation efficiency, physical stability in aqueous media, and with long-term pH-stimulated release properties.

Acknowledgments

ES thanks DTU-Food for supporting her PhD stipend. GZ thanks the Danish Agency for Institutions and Educational Grants.

References

- [1] A.C. Mendes, K. Stephansen, I.S. Chronakis, Electrospinning of food proteins and polysaccharides, *Food Hydrocoll.* 68 (2017) 53–68, <https://doi.org/10.1016/j.foodhyd.2016.10.022>.
- [2] C. Jacobsen, P.J. Garcia-Moreno, A.C. Mendes, R.V. Mateiu, I.S. Chronakis, Use of electrospinning for encapsulation of sensitive bioactive compounds and applications in food, *Annu. Rev. Food Sci. Technol.* 9 (2018) 1–25.
- [3] X.Z. Sun, G.R. Williams, X.X. Hou, L.M. Zhu, Electrospun curcumin-loaded fibers with potential biomedical applications, *Carbohydr. Polym.* 94 (2013) 147–153, <https://doi.org/10.1016/j.carbpol.2012.12.064>.
- [4] D. Perrone, F. Ardito, G. Giannatempo, M. Dioguardi, G. Troiano, L. Lo Russo, A. De Lillo, L. Laino, L. Lo Muzio, Biological and therapeutic activities, and anticancer properties of curcumin, *Exp. Ther. Med.* 10 (2015) 1615–1623, <https://doi.org/10.3892/etm.2015.2749>.
- [5] E. Shekarforoush, A. Mendes, V. Baj, S. Beerens, I. Chronakis, Electrospun phospholipid fibers as micro-encapsulation and antioxidant matrices, *Molecules* 22 (2017) 1708, <https://doi.org/10.3390/molecules22101708>.
- [6] A.C. Mendes, C. Gorzelanny, N. Halter, S.W. Schneider, I.S. Chronakis, Hybrid electrospun chitosan-phospholipids nanofibers for transdermal drug delivery, *Int. J. Pharm.* 510 (2016) 48–56, <https://doi.org/10.1016/j.ijpharm.2016.06.016>.
- [7] A. Blanco-Padilla, A. Lopez-Rubio, G. Loarca-Pina, L.G. Gomez-Mascaraque, S. Mendoza, Characterization, release and antioxidant activity of curcumin-loaded amaranth-pullulan electrospun fibers, *LWT – Food Sci. Technol.* 63 (2015) 1137–1144, <https://doi.org/10.1016/j.lwt.2015.03.081>.
- [8] G. Borchard, H.L. Lueßen, A.G. de Boer, J.C. Verhoef, C.-M. Lehr, H.E. Junginger, The potential of mucoadhesive polymers in enhancing intestinal peptide drug absorption. III: effects of chitosan-glutamate and carbomer on epithelial tight junctions in vitro, *J. Control. Release* 39 (1996) 131–138, [https://doi.org/10.1016/0168-3659\(95\)00146-8](https://doi.org/10.1016/0168-3659(95)00146-8).
- [9] A. Portero, C. Remuñán-López, H.M. Nielsen, The potential of chitosan in enhancing peptide and protein absorption across the TR146 cell culture model in vitro model of the buccal epithelium, *Pharm. Res.* 19 (2002) 169–174.
- [10] B. Katzbauer, Properties and applications of xanthan gum, *Polym. Degrad. Stab.* 59 (1998) 81–84, [https://doi.org/10.1016/S0141-3910\(97\)00180-8](https://doi.org/10.1016/S0141-3910(97)00180-8).
- [11] A.C. Mendes, T. Strohmenger, F. Goycoolea, I.S. Chronakis, Electrostatic self-assembly of polysaccharides into nanofibers, *Colloids Surfaces A Physicochem. Eng. Asp.* 531 (2017) 182–188, <https://doi.org/10.1016/j.colsurfa.2017.07.044>.
- [12] C.S. Wang, G. Natale, N. Virgilio, M.C. Heuzey, Synergistic gelation of gelatin B with xanthan gum, *Food Hydrocoll.* 60 (2016) 374–383, <https://doi.org/10.1016/j.foodhyd.2016.03.043>.
- [13] E. Shekarforoush, A. Faralli, S. Ndoni, A.C. Mendes, I.S. Chronakis, Electrospinning of xanthan polysaccharide, *Macromol. Mater. Eng.* 201700067 (2017) 1700067, <https://doi.org/10.1002/mame.201700067>.

- [14] M. Takahashi M. Iijima K. Kimura T. Hatakeyama H. Hatakeyama thermal and viscoelastic properties of xanthan gum/chitosan complexes in aqueous solutions 85 2006 669–674.
- [15] H. Chen, Y. Song, N. Liu, H. Wan, N. Liao, G. Shu, Effect of complexation conditions on microcapsulation of *B. bifidum* BB01 in xanthan-chitosan polyelectrolyte complex gels, *J. Chem. Pharm. Res.* 6 (2014) 1355–1360, <https://doi.org/10.1016/j.foodhyd.2007.12.011>.
- [16] R.W. Korsmeyer, R. Gurny, E. Doelker, P. Buri, N.A. Peppas, Mechanisms of solute release from porous hydrophilic polymers, *Int. J. Pharm.* 15 (1983) 25–35, [https://doi.org/10.1016/0378-5173\(83\)90064-9](https://doi.org/10.1016/0378-5173(83)90064-9).

3.1.4. Application of xanthan-chitosan nanofibers- Paper IV

***In vitro* permeability enhancement of curcumin across Caco-2 cells monolayers using electrospun xanthan-chitosan nanofibers**

Adele Faralli, Elhamalsadat Shekarforoush, Fatemeh Ajalloueian, Ana C. Mendes, Ioannis S. Chronakis

Nano-Bio Science Research Group, DTU-Food, Technical University of Denmark, Kemitorvet, B202, 2800 Kgs. Lyngby, Denmark

This manuscript was submitted to Carbohydrate Polymers Journal in April 2018.

***In vitro* permeability enhancement of curcumin across Caco-2 cells
monolayers using electrospun xanthan-chitosan nanofibers**

Adele Faralli, Elhamalsadat Shekarforoush, Fatemeh Ajalloueian, Ana C. Mendes,

Ioannis S. Chronakis *

Nano-BioScience Research Group, DTU-Food, Technical University of Denmark,

Kemitorvet, B202, 2800 Kgs. Lyngby, Denmark

*Corresponding author: Ioannis S. Chronakis

Tel: +45 40 20 64 13

E-mail: ioach@food.dtu.dk

Abstract

Xanthan-Chitosan (X-Ch) polysaccharides nanofibers were prepared using electrospinning processing as an encapsulation and delivery system of curcumin (Cu). The X-Ch-Cu nanofibers remained stable in aqueous HBSS medium at pH 6.5 and pH 7.4, mainly due to the ability of oppositely charged xanthan-chitosan polyelectrolytes to form ionically associated electrospun nanofibers. The xanthan-chitosan-curcumin nanofibers were incubated with Caco-2 cells, and the cell viability, transepithelial transport and permeability properties across cell monolayers were investigated. After 24 h of incubation, the exposure of Caco-2 cell monolayers to X-Ch-Cu nanofibers resulted in a cell viability of ~80%. A 3-fold increase of curcumin permeability was observed when the polyphenol was loaded into X-Ch nanofibers, compared to the free curcumin. This increased *in vitro* transepithelial permeation of curcumin without compromising cellular viability was induced by interactions upon contact between the nanofibers and the Caco-2 cells, leading to the opening of the tight junctions. The results obtained revealed that X-Ch nanofibers can be used for oral delivery applications of poorly water-soluble compounds at the gastrointestinal tract.

Keywords: Xanthan gum; Chitosan; Electrospinning; Fibers; Drug delivery; Curcumin

1. Introduction

Curcumin (Cu) is a polyphenolic compound obtained from the dietary spice turmeric found in the Asian plant *Curcuma longa*. Due to its variety of biological properties such as anti-inflammatory, analgesic, potent antioxidant capacity,^{1,2} antimicrobial³ and anticarcinogenic,⁴ it has been used for centuries as dietary supplement and medicine.^{5,6} Several studies in animal models and humans have reported that no serious toxicity is observed when curcumin is administered even at high doses, and clinical phase I studies have shown a high tolerance to repeated ingestions of 12 g of curcumin per day.⁷ Many of the curcumin benefits are also found at a cellular level as regulator of cellular enzymes such as cyclooxygenase and glutathione S-transferases, immuno-modulation, inhibitor of several cell signaling pathways, and cell-cell adhesion.⁶ Despite the established beneficial effects of curcumin as bioactive compound, curcumin has a poor aqueous solubility, intense staining color, and very low bioavailability.^{7,8} In fact, after oral administration of curcumin for up to 12 g/day, plasma and tissue levels of curcumin were found very low (in the range of nanogram per milliliter).⁷ The major reasons causing such low gastrointestinal bioavailability of curcumin have been ascribed to poor absorption, chemical instability, rapid metabolism and systemic elimination, and accumulation within epithelial cells of the intestine.^{7,9} Furthermore, in the hepatic and intestinal tissues of rats and humans, curcumin undergoes phase I and phase II metabolism,^{10,11} similar to *in vitro* investigations.^{8,12} A stepwise reduction of the olefinic double bonds of curcumin takes place in the phase I metabolism leading to tetrahydro-, hexahydro-, and octahydro-curcumin metabolites. A further biotransformation of curcumin and its metabolites involves the conjugation to glucuronic acid, sulfate, and glutathione under cell-free conditions and also in human Caco-2

cells¹³. Moreover, it has also been documented that curcumin undergoes degradation in aqueous solution and at neutral pH, and hydrolyzed under alkaline pH.^{14,15}

In order to overcome some of the major drawbacks of curcumin, different promising strategies have been undertaken aiming a higher permeability, resistance to metabolic processes, and enhancement of its solubility. A wide range of adjuvants such as piperine,¹⁶ quercetin,¹⁷ epigallocatechin-3-gallate (EGCG)¹⁸ and genistein¹⁹ have been proposed to modulate the permeability of curcumin and to increase its bioavailability. More recently, a wide variety of nano- and micro-delivery systems such as nanoparticles,²⁰ micelles,^{21,22} liposomes, and phospholipid complexes²³ have emerged as solutions to enhance the bioavailability of various therapeutic agents.⁷ However, very few studies have been published reporting improved delivery properties of curcumin-loaded systems. Nanoencapsulation of curcumin using natural and synthetic polymers²⁰ and liposomal nanoparticles have been the most explored strategies because of their suitability for the encapsulation of a highly hydrophobic compound like curcumin, the prevention of curcumin degradation processes, and the enhancement of curcumin chemical stability. Lately, mucoadhesive nanostructured lipid carriers (NLCs) coated with polyethylene glycol 400 (PEG400) and polyvinyl alcohol (PVA) have been employed as a candidate system for oral delivery of curcumin.²⁴ The authors have demonstrated that polymer-coated curcumin-loaded NLCs improved curcumin water solubility more than 60-folds, as compared to curcumin dispersion. In addition, curcumin was protected from degradation processes, and the *in vitro* apparent permeability (P_{app}) of curcumin across Caco-2 monolayers was higher than that obtained from uncoated NLCs.²⁴ Another approach to overcome the low curcumin oral bioavailability has been proposed by Frank *et al.*²⁵ The preparation of nanoscaled micellar formulations based on Tween 80 for curcumin delivery has revealed an increase on the

apparent permeability through the intestinal barrier, resulting in a P_{app} value of 2.11×10^{-6} cm/s, compared to a P_{app} value of 0.56×10^{-6} cm/s for free native curcumin.²⁵ Furthermore, curcumin has been also encapsulated within electrospun fibers as delivery carriers, developed using phospholipid²⁶, as well as biopolymers such as gelatin²⁷ and blends of amaranth protein isolate – pullulan.²⁸

Electrospun fibers hold great promises as oral delivery systems. The large surface to volume ratio, the tunable surface functionality as well as the high encapsulation efficiency of the electrospun fibers, favor the diffusion and the dissolution rate of the bioactive compounds, and thus enhance their delivery.^{29,30} However, the delivery of the bioactive compounds at the intestine using electrospun fibers has not been assessed.

Furthermore, the Caco-2 cell model is used frequently to mimic the epithelial layer in the small intestine, and thus to evaluate the absorption of bioactive compounds *in vitro* assays.³¹ The Caco-2 cells, which are originally from a human colon cell line, can polarize and express receptors that resemble the intestinal absorptive cells found in the small intestine when cultured under specific conditions. *In vitro* permeability studies have been employed the Caco-2 cells model, to assess the cytotoxicity and the permeation of bioactive compounds such as intestinal absorption of peptide drugs.³² To the best of our knowledge, only few studies have assessed the intestinal delivery properties of bioactive compounds encapsulated within electrospun nanofibers using the Caco-2 cells model. A recent study from our group using a Caco-2 cell permeability assay found that electrospun fish sarcoplasmic proteins (FSP) nanofibers could be used as novel oral delivery system of biopharmaceuticals.³³ Lin *et al.* also studied the anticancer efficiency of magnetic electrospun chitosan nanofibers by assessing the Caco-2 cell viability. It was found, that

magnetic electrospun chitosan nanofibers have a potential therapeutic modality in tumor administration.³⁴

Chitosan is a cationic polysaccharide consisting of N-acetyl glucosamine (GlcNAc) and glucosamine (GlcN), and it has been widely used in the food, pharmaceutical and biomedical fields because of its biocompatibility, biodegradability, and mucoadhesivity.³⁵ One of the most interesting properties is the ability of chitosan to enhance gastrointestinal drug absorption.³⁶ However, the chemical stability of chitosan is limited to a basic environment such as in the intestine and colon, whereas in neutral environments the polymer loses its charge and precipitate resulting in an ineffective absorption enhancer.³⁷ In order to chemically stabilize chitosan for applications that demands enhanced drug absorption, chitosan derivatives such as water-soluble quaternary ammonium chitosan,³⁷ and chitosan-glutamate,³⁶ have been synthesized.

Alternatively, stable polyelectrolyte complexes of chitosan with xanthan have showed favorable properties as intestinal delivery systems. For instance, xanthan-chitosan hydrogels³⁸⁻⁴¹ and xanthan-chitosan nanoparticles³⁸ have been studied as oral delivery carriers for a range of drug and bioactive compounds.

In the present study, we report the formation of electrospun xanthan-chitosan nanofibers as an encapsulation and delivery system of curcumin. The resulting curcumin-loaded nanofibers were incubated with Caco-2 cells, and the cell viability, transepithelial transport and permeability properties across cell monolayers were investigated. A consistent enhancement of the *in vitro* intestinal absorption of curcumin across cell monolayers was observed when the polyphenol was loaded into xanthan-chitosan nanofibers compared to the free curcumin.

2. Materials and Methods

2.1. Methods

Xanthan (X), chitosan (Ch), curcumin (Cu) from *Curcuma longa* (Turmeric) and formic acid were obtained from Sigma-Aldrich (Denmark) and used as received. Xanthan gum from *Xanthomonas campestris* (product nr. G1253), with molecular weight ~ 2000 kDa was used.³⁹ The selected chitosan polysaccharide (product nr. 448869) has a molecular weight of ~ 28 kDa, degree of deacetylation (DD) of 89% and degree of polymerization (DP) of 175.

The human colon adenocarcinoma cell line Caco-2 [Caco-2] (ATCC® HTB-37™) was obtained from the American Type Culture Collection (Rockville, MD). Dulbecco's modified Eagle's medium (DMEM) high glucose (4.5 g/L), L-glutamine (200 mM), nonessential amino acids (100X), penicillin-streptomycin (10,000 U/mL and 10 mg/mL in 0.9% sodium chloride, respectively), trypsin-EDTA (10X), Dulbecco's Phosphate Buffered Saline 1X (DPBS) without calcium chloride and magnesium chloride, dimethyl sulfoxide 99.5% purity (DMSO), fluorescein sodium salt (FLUO), lucifer yellow dilithium salt (LY), , methanesulfonic acid, MES (1 M; pH 5.5-6.7), 4-(2-hydroxyethyl)-1-piperazineethanesulfonic acid solution, HEPES (1 M; pH 7.0-7.6) were purchased from Sigma Aldrich (Brøndby, Denmark). Tissue culture 12-well plates and 12-mm polycarbonate cell culture inserts with an area of 1.12 cm² and a pore size of 0.4 μm were purchased from Corning Costar® Corporation. Fetal bovine serum (FBS) and Hanks' balanced salt solution (HBSS) with calcium and magnesium and without phenol red were obtained from Thermo Fisher Scientific (Roskilde, Denmark). CellTiter 96® AQueous One Solution Cell Proliferation Assay (MTS) was purchased from Promega Biotech AB (Sweden).

2.2 Preparation of polysaccharides mixtures

Xanthan and Chitosan mixtures with curcumin were prepared by dissolving 3% w/v chitosan powder with 0.75% w/v xanthan powder in formic acid under vigorous stirring overnight at room temperature. Subsequently, curcumin (2% w/v) was added to the solubilized mixture of polysaccharides, and further stirred for 30 min.

The electrical conductivity of xanthan, chitosan and xanthan-chitosan, and xanthan-chitosan-curcumin solutions was determined using WTW LF323-B conductivity meter (WTW GmbH, Weilheim, Germany). All measurements were carried out at room temperature (25 ± 2 °C) in triplicate for each sample.

2.3. Electrospinning setup

The electrospinning setup included a high voltage generator (ES50P-10W, Gamma High Voltage Research, Inc., USA) to provide a voltage of 25 kV, and a syringe pump (New Era Pump Systems, Inc., USA) to feed the xanthan-chitosan and curcumin mixtures at a flow rate of 0.01 mL/min. A 21 G needle (Proto Advantage, Canada) with inner diameter 0.813 mm was used. Nanofibers were collected on a steel plate covered with aluminium foil placed at a distance of 10 cm from the edge of the needle. The electrospinning process was carried out at ambient conditions and samples were stored in an exicator until further analysis.

2.4. Morphology

The morphology of electrospun nanofibers was monitored using a Quanta FEG 3D scanning electron microscope (SEM) as described by Shekarforoush *et al.*⁴⁰ Briefly, a small amount of fibers was attached on SEM specimen by a double-sided carbon adhesive tape, and sputter coated with 6 nm of gold layer (Leica Coater ACE 200). Image J software (National Institute of

Health, USA) was used to analyse the average diameter of the nanofibers (measured at 100 different points for each image).

2.5. Encapsulation efficiency

The encapsulation efficiency of Cu within X-Ch electrospun nanofibers was determined by extracting the Cu from the fibers using methanol in a sonication bath for 30 min, and collecting the amount of loaded curcumin from supernatants after centrifugation at 4500 rpm for 15 min. The concentration of curcumin in the supernatant was determined using a UV-vis spectrometry (Nanodrop OneC, Thermo Fisher Scientific, Roskilde, DK), by recording its absorbance at 280 and 420 nm. Standard curves for curcumin were prepared with concentrations ranging from 0–100 µg/mL. The encapsulation efficiency was calculated using the following equation:

$$\% \text{ Encapsulation Efficiency} = \frac{\text{Calculated curcumin concentration}}{\text{Theoretical curcumin concentration}} \times 100 \quad [1]$$

2.6. *In vitro* release of curcumin

The *in vitro* release of curcumin from xanthan-chitosan nanofibers was evaluated by suspending 3.0 mg of X-Ch-Cu fibers in 2 mL pre-warmed HBSS at pH 6.5 and pH 7.4, respectively. The curcumin release was conducted for a time interval of 8 h at 37 °C without stirring. Supernatant aliquots were withdrawn and analyzed by UV-vis spectrometry by recording the curcumin absorption at 280 and 420 nm. The cumulative amount of curcumin released from X-Ch-Cu nanofibers was then considered as the maximum releasable curcumin from the nanofibers structure.

2.7. Caco-2 cell culture and subculture

Caco-2 cells were routinely seeded at a concentration of 1.0×10^5 cells/mL in T-75 cm² flasks and incubated at 37 °C in a humidified atmosphere of 5% CO₂. The complete cell medium consisted of high glucose DMEM containing 10% heat-inactivated FBS, 2 mM L-glutamine, 1% nonessential amino acids, 100 U/mL penicillin, and 100 µg/mL streptomycin. The medium was renewed every second day until cells reached approximately 90% confluence. Cells were passaged at a subcultivation ratio of 1:4 by treatment with 0.25% trypsin – 0.53 mM EDTA solution for 10 min at 37 °C. After trypsinization, the cells were suspended in complete growth medium and centrifuged for 5 min at 1000 rpm. After supernatant removal, the pellet was suspended in the growth medium and the cell concentration was determined with ORFLO Moxi Z Mini Automated Cell Counter using Type S cassette (Biofrontier Technology, Singapore). All Caco-2 cells were used between passages 6 - 12.

2.8. Compounds and electrospun nanofibers used for the cell studies

Xanthan-chitosan (X-Ch) and curcumin-loaded xanthan-chitosan (X-Ch-Cu) electrospun nanofibers were tested with Caco-2 cells to evaluate their toxicity and to determine the apparent permeability coefficient (P_{app}) of curcumin loaded into the nanofibers, and as free compound. Before testing the nanofibers with Caco-2 cells, the collected fibers were kept under air stream for 3 days allowing complete formic acid evaporation.

Besides curcumin, the transepithelial transport of fluorescein (FLUO) and Lucifer yellow (LY) across Caco-2 cell monolayers were also investigated as markers for intestinal epithelial permeability and integrity. The physicochemical properties and the expected mechanisms involved on molecules permeation across Caco-2 monolayers are listed in **Table 1**.

Table 1.

Physicochemical properties of compounds and their expected transepithelial transport across Caco-2 cell monolayers.

Compound	MW (Da)	ACDLogP ^a	ACDpK _a ^a	λ _{Abs} ^b (nm)	Transepithelial transport across Caco-2 cell monolayers
Curcumin, Cu	368.39	3.07	8.11	280 and 420	<ul style="list-style-type: none"> • Extremely poor gastrointestinal absorption. • Undergoes phase I and II bio-transformations.^c • Passive transport.^c
Fluorescein, FLUO	376.27	4.81	4.40	490	<ul style="list-style-type: none"> • pH-dependent transport. • Influx ratio ~ 10.^d • Carrier-mediated unidirectional transcellular transport.^{d,e}
Lucifer Yellow, LY	457.25	-5.06	-0.9	430	<ul style="list-style-type: none"> • pH-independent transport. • No observed influx-efflux. • Paracellular pathway.^{d,f}

^a Values for LogP and pK_a were obtained from the ACD database.

^b Experimentally determined wavelength.

^c Results published by Dempe *et al.*⁸

^d Results published by Konishi *et al.*⁴¹

^e Results published by Berginc *et al.*⁴²

^f Results published by Hashimoto *et al.*⁴³

2.9. Caco-2 cell viability assay

The *in vitro* Caco-2 cell viability after treatment with free curcumin (Cu), xanthan-chitosan nanofibers (X-Ch), and curcumin-loaded xanthan-chitosan nanofibers (X-Ch-Cu) was evaluated by using the MTS [3-(4,5-dimethylthiazol-2-yl)-5-(3-carboxymethoxyphenyl)-2-(4-sulfophenyl)-2H-tetrazolium inner salt] colorimetric bioassay. A stock solution of 50 mM curcumin was prepared in 0.5 M NaOH and immediately diluted to 5 mM in PBS. The curcumin solution was filtered through sterile-filters (with a 0.22 μm pore size). In a 96-well plate, a concentration of 2.0×10^4 cells/100 μL were seeded in a complete growth medium and incubated for 2 days at 37 $^{\circ}\text{C}$ in a humidified atmosphere of 5% CO_2 . Then the cells were washed with PBS, and the complete medium was renewed. Caco-2 cells were incubated with free curcumin solution (150 and 500 μM), X-Ch nanofibers (0.5 mg), X-Ch-Cu nanofibers (0.5 mg), and PBS as a control. Caco-2 cells were incubated for one day at 37 $^{\circ}\text{C}$ in a humidified atmosphere of 5% CO_2 . The following day, the nanofibers were removed from the wells, cells were washed with PBS and the medium was renewed (100 μL). 20 μL MTS solution was added to each well under dark conditions. After 3 h incubation at 37 $^{\circ}\text{C}$, the absorbance of the reduced MTS (formazan product) was recorded at 490 nm through a well plate reader (Wallac 1420 Victor2 Multilabel Counter, Perkin Elmer, Waltham, MA).

2.10. Transepithelial transport experiments

The transport of free fluorescein (FLUO), free lucifer yellow (LY), free curcumin (Cu), free curcumin in presence of xanthan-chitosan nanofibers (X-Ch + Cu), and curcumin-loaded xanthan-chitosan nanofibers (X-Ch-Cu) across Caco-2 cell monolayers were investigated according to the protocol reported by Artursson *et al.*⁴⁴ The transepithelial transport experiments

were performed in both apical-to-basolateral (AB, absorptive) and basolateral-to-apical (BA, secretory) directions, under a proton gradient. In fact, in order to mimic the acidic microclimate of the small intestine, an apical pH of 6.5 and a basolateral pH of 7.4 were used. Briefly, 1.0×10^5 cells/insert were seeded onto pre-wetted 12-mm polycarbonate cell culture inserts (area of 1.12 cm^2 and a pore size of $0.4 \text{ }\mu\text{m}$). The apical and basolateral compartments were filled with 0.5 mL cell suspension and 1.5 mL complete medium, respectively. The Caco-2 cells plates were incubated overnight at $37 \text{ }^\circ\text{C}$ in a humidified atmosphere of 5% CO_2 . The day after, the growth medium was replaced in both compartments and the plates were incubated for 21 days at $37 \text{ }^\circ\text{C}$ in a humidified atmosphere of 5% CO_2 , renewing the complete growth medium every second day. For the AB transport experiments, donor solutions of fluorescein, lucifer yellow, and curcumin at a concentration of 11 mM, 9.57 mM, and 1.65 mM, respectively were prepared in sterile-filter HBSS at pH 6.5 buffered with 10 mM MES. Again, donor solutions of fluorescein, lucifer yellow, and curcumin at a concentration of 10.3 mM, 9 mM, and 1.55 mM, respectively were prepared in sterile-filter HBSS at pH 7.4 buffered with 25 mM HEPES to evaluate their BA transport across cell monolayers. X-Ch and X-Ch-Cu nanofibers have been also investigated, and 3.0 mg of nanofibers for AB transport and 9.0 mg of nanofibers for BA transport were used. After 21 days cell growth, the complete DMEM medium was removed from the Caco-2 cell monolayers and was replaced with HBSS at pH 6.5 and pH 7.4 at the apical and basolateral compartments, respectively. For the AB transport studies, 1.5 mL HBSS was used in the basolateral side and 0.55 mL of each donor solutions and/or nanofibers were added to the apical side. Immediately, 50 μL aliquots were withdrawn from each donor compartment (time=0). The aliquots were then withdrawn from the acceptor side at different time intervals, and the volume was replaced with fresh pre-warmed HBSS at pH 7.4 maintaining the well plates at $37 \text{ }^\circ\text{C}$ in a

humidified atmosphere of 5% CO₂. A final aliquot from the donor chamber was taken as last time point. BA transport studies were conducted by using 0.5 mL HBSS at pH 6.5 in the apical side, and 1.55 mL of donor solution and/or nanofibers in the basolateral chamber. Again, a 50 µL aliquot was immediately withdrawn from the donor compartment (time=0), and the plates were kept at 37 °C in a humidified atmosphere of 5% CO₂. At different time intervals, 50 µL aliquots from the acceptor compartment were collected and the volume was replaced with fresh pre-warmed HBSS at pH 6.5. A final aliquot was taken from the donor side at last time point. During the transport experiments, all cell media and solutions were pre-warmed at 37 °C. Each transport experiment was performed for a time interval of 8h, in triplicates (n=3). After 8 h transport studies both apical and basolateral chambers were washed twice with PBS, and cell monolayers were detached from the insert membrane with 0.25% trypsin – 0.53 mM EDTA solution for 10 min at 37 °C. The collected Caco-2 cell lysates were centrifuged for 5 min at 1000 rpm and supernatants were discarded. Furthermore, the semipermeable membranes were carefully removed from the insert using a scalpel and collected into Eppendorf tubes in 500 µL HBSS at pH 6.5 (apical conditions). Cell pellets as well were re-suspended in 500 µL HBSS at pH 6.5 and both cells and membranes were sonicated for 3 h using an ultrasonic bath (Branson Ultrasonic Corp., VWR, Denmark). The collected samples were then centrifuged for 5 min at 10 000 rpm and the supernatants were analyzed by UV-vis spectroscopy. The same procedure was used to quantify the amount of curcumin adsorbed (X-Ch + Cu) or encapsulated (X-Ch-Cu) into the nanofibers at the end of transport experiments. The tested nanofibers were removed from the donor chamber and suspended in 500 µL of HBSS (pH 6.5 for AB transport and pH 7.4 for BA transport). After sonication and centrifugation, the curcumin found in the supernatants was quantified by absorbance measurement.

Measurement of transepithelial electrical resistance (TEER)

The Transepithelial Electrical Resistance (TEER) was measured at room temperature before and after permeability experiments with an epithelial volt-ohmmeter equipped with an STX2 “chopstick” electrodes (EVOM2™, World Precision Instruments, Sarasota, FL, USA). Before measuring the resistance values of each well, the cell monolayers and the basolateral chamber were washed twice with pre-warmed HBSS at pH 6.5 and HBSS at pH 7.4, respectively. The resistance values of the semipermeable membrane without cells (R_{BLANK}) were recorded and subtracted from the resistance values obtained from the measurement of cell monolayers on the semipermeable membrane (R_{TOTAL}). The specific cell resistance values (R_{TISSUE}) were obtained from the following equation:

$$R_{\text{TISSUE}} (\Omega) = R_{\text{TOTAL}} (\Omega) - R_{\text{BLANK}} (\Omega) \quad [2]$$

TEER values of cellular monolayers were expressed in $\Omega \times \text{cm}^2$ and calculated according to the following equation:

$$\text{TEER}_{\text{TISSUE}} (\Omega \text{ cm}^2) = R_{\text{TISSUE}} (\Omega) \times A_{\text{MEMBRANE}} (\text{cm}^2) \quad [3]$$

2.11. Quantification of compounds

Donor solutions of fluorescein, lucifer yellow, and curcumin were prepared and sterile-filter in HBSS at pH 6.5 and pH 7.4 to perform transepithelial studies. Standard curves of FLUO, LY, and Cu dissolved in HBSS at pH 6.5 and pH 7.4 were obtained through UV-vis spectroscopic analysis (Nanodrop One^C, Thermo Fisher Scientific, Roskilde, DK). The aliquots withdrawn from the donor and acceptor compartments during transport experiments across cell monolayers

were quantified by UV-vis spectrometry recording the absorbance values at 490 nm for FLUO, 430 nm for LY, and 280 nm and 420 nm for Cu (**Table 2**). The amount of each compound transported across the cell monolayers within a time interval of 8 h was calculated for both apical-to-basolateral (AB) and basolateral-to-apical (BA) directions. FLUO, LY, and curcumin that remained entrapped within cell monolayers, insert membranes and nanofibers were likewise quantified at the end of permeability studies after sonication treatment.

Table 2

Tested compounds and relative concentrations used for transepithelial transport studies (AB and BA) across Caco-2 cell monolayers.

Compound	AB transport		BA transport		λ_{Abs} (nm)
	[] _A (μM)	V _A (μL)	[] _B (μM)	V _B (μL)	
Fluorescein, FLUO	1000	50	1000	150	490
Lucifer Yellow, LY	870	50	870	150	430
Free Curcumin, Cu	150	50	150	150	280 and 420
Free Curcumin + nanofibers, Cu+X- Ch	150 μM +3.0 mg fibers	50	150 μM +9.0 mg fibers	150	280 and 420
Curcumin loaded nanofibers, X-Ch-Cu	3.0 mg fibers (150 μM releasable Cu)	0	9.0 mg fibers (150 μM releasable Cu)	0	280 and 420

2.12. FLUO, LY, and Cu distribution after transport experiments and mass balance

After transport experiments in both AB and BA directions, the amount of each compound in the apical and basolateral compartments was quantified by UV-vis spectrometry. Donor concentrations at time=0 ($C_{D,t=0h}$), donor and acceptor concentrations at time=8h ($C_{D,t=8h}$ and $C_{A,t=8h}$, respectively), compound concentrations remained within cell monolayer at time=8h ($C_{Caco-2,t=8h}$), membrane filters at time=8h ($C_{insert,t=8h}$), and adsorbed or encapsulated into nanofibers at time=8h ($C_{fibers,t=8h}$) were experimentally measured by UV-vis spectroscopy. Therefore, the mass balance of each compound was calculated as follow:

$$C_{D,t=0h} = C_{D,t=8h} + C_{A,t=8h} + C_{Caco-2,t=8h} + C_{insert,t=8h} + (C_{fibers,t=8h}) \quad [4]$$

Mass balance values of >90% were found for all tested compounds.

2.13. Calculation of the apparent permeability coefficients $P_{app, AB}$ and $P_{app, BA}$.

The absorptive apparent permeability coefficient ($P_{app, AB}$) and the secretory apparent permeability coefficient ($P_{app, BA}$) were determined according to the equation:

$$P_{app} = \frac{dC}{dt} * \frac{V}{A * C_0} \quad [5]$$

where, dC/dt ($\mu\text{M/s}$) is the change in concentration on the acceptor chamber over time; V (cm^3) is the volume of the solution in the acceptor compartment; A (cm^2) is the area of the semipermeable membrane; C_0 (μM) is the initial concentration in the donor chamber. The results presented in this study were the averages of three experiments and were expressed as the mean \pm standard deviation.

3. Results and Discussions

3.1. Electrospinning of Xanthan - Chitosan nanofibers

Xanthan-Chitosan nanofibers were obtained by electrospinning mixtures of X at the concentration of 0.75% w/v with 3% w/v Ch dissolved in formic acid (**Figure 1**). The obtained nanofibrous structures are composed of individual, uniform and randomly oriented fibers with an average diameter of 750 ± 250 nm. Note that chitosan solution (3% w/v) in formic acid (without xanthan) could not be electrospun into fibers. The average diameter of electrospun xanthan-chitosan nanofibers slightly increased to 900 ± 440 nm with the addition of 2% w/v curcumin (**Figure 1**). The encapsulation efficiency of Cu within X-Ch nanofibers was $69.4 \pm 4.1\%$. Furthermore, the electrical conductivity of 0.75 % w/v xanthan and 3% w/v chitosan solutions in formic acid was 0.19 ± 0.01 mS/cm and 1.23 ± 0.06 mS/cm, respectively. However the electrical conductivity of the X-Ch mixture (0.75-3 % w/v) and X-Ch-Cu (0.75-3-2 % w/v) was enhanced significantly to 5.5 ± 0.08 mS/cm and 5.71 ± 0.09 mS/cm, respectively, as an indication of an organizational change in the structure of the polysaccharides mixture. Such an increase of the solution conductivity induces greater transfer of the surface charges of the polysaccharides jet, enhanced electrostatic repulsion, promoting elongation, stretching, and the formation of electrospun X-Ch-Cu nanofibers.⁴⁵

Moreover, the X-Ch-Cu nanofibers remained stable in aqueous HBSS medium at different pH (6.5 and pH 7.4), due to the ability of oppositely charged xanthan-chitosan mixture to form ionically associated electrospun nanofibers.⁴⁶ The features of xanthan-chitosan-curcumin nanofibers were not further examined in the present study.

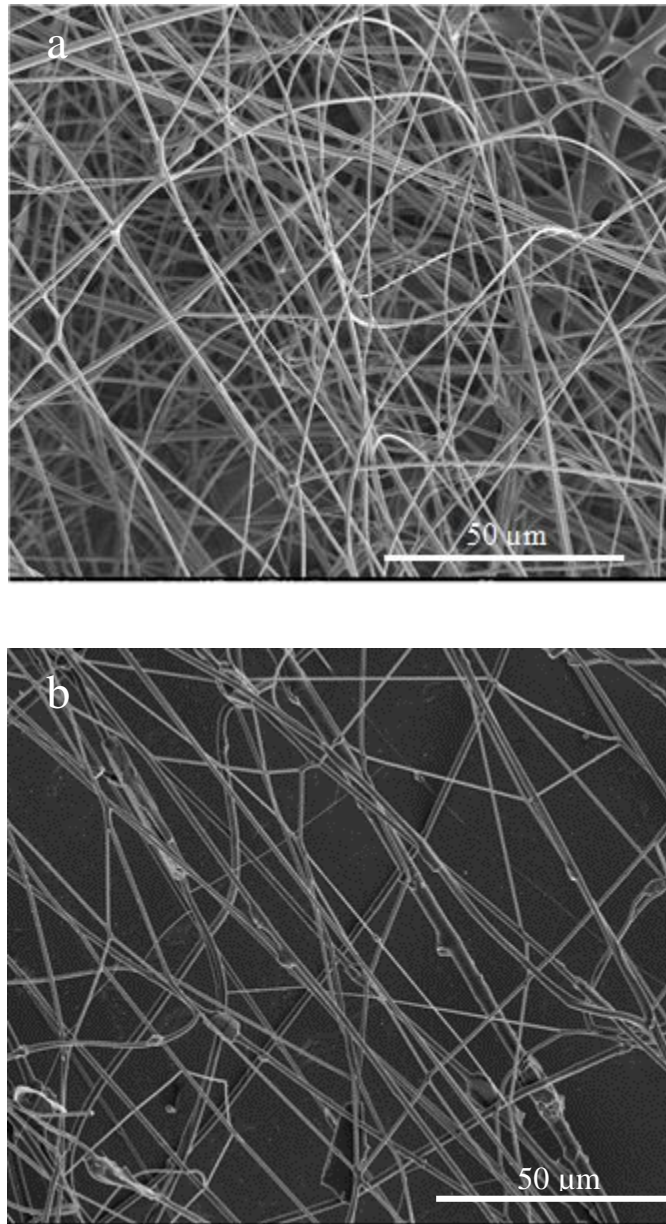


Figure 1. SEM images of electrospun nanofibers of (a) xanthan-chitosan (0.75 - 3% w/v) and (b) xanthan-chitosan-curcumin (0.75 - 3 -2% w/v) mixtures in formic acid.

3.2. *In vitro* release study

The cumulative release profile of curcumin from the electrospun X-Ch nanofibers at two different pH (7.4 and 6.5) at 37 °C is shown in **Figure 2**. A sustained release of curcumin from X-Ch nanofibers was observed over a period of 4 h for both pH with no significant burst effect. Approximately 4% of curcumin was released from X-Ch nanofibers after 4 h and beyond that, no significant changes in the cumulative release of Cu were found up to 8 h. The slow release of curcumin is due to its hydrophobic nature. FTIR studies confirmed the absence of physical or chemical interactions between curcumin molecules and xanthan-chitosan fibers matrix (data not shown).

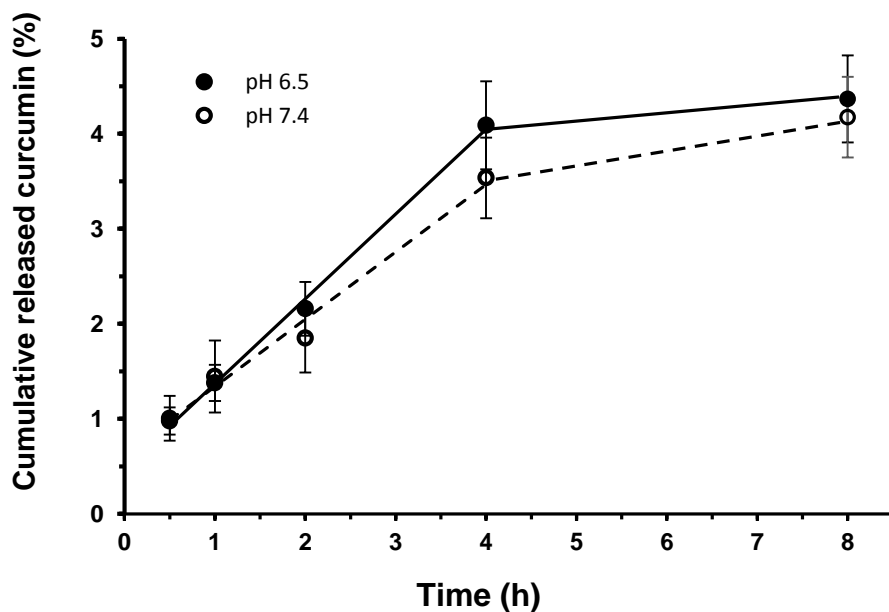


Figure 2. Release of curcumin from X-Ch-Cu nanofibers suspended in HBSS medium at pH 6.5 (solid line), and pH 7.4 (dashed line) at 37 °C. All data are the mean \pm SD of three independent experiments.

3.3. Caco-2 cell studies

In our previous studies, we have observed a significant effect on the permeation of a model protein (insulin) across Caco-2 cells upon contact with electrospun fish sarcoplasmic protein fibers (FSP).³³ Encapsulation of insulin into the FSP fibers provided protection against chymotrypsin degradation (suitable for oral administration), and the interactions between fibers and epithelial cells led to opening of the tight junction, which promoted an increased transepithelial transport of insulin without compromising cellular viability.³³ This approach of using electrospun nanofibers is superior to the typical approach of administering solely nanoparticles for intestinal delivery of bioactives (typically nanoparticles are distributed over the entire surface, having a short retention time, and low bioactive penetration).

The Caco-2 cell system has been recommended by the US Food and Drug Administration (FDA) as being an established *in vitro* cell model for the prediction of oral drug absorption and drug transport mechanism across human differentiated epithelial cell monolayers³¹. The human colon carcinoma cell line Caco-2 was chosen because of the many similar features with the intestinal epithelial cells. In fact, Caco-2 cells can slowly differentiate into monolayers forming microvilli and tight junctions at the apical side, and expressing brush border enzymes for phase I and phase II metabolism and transport proteins^{44,47,48}. In the present study, the Caco-2 cell system was selected as a tool to investigate the *in vitro* absorption and the transports (both apical-to-basolateral (AB) and basolateral-to-apical (BA)) of curcumin across cell monolayers.

3.4. Evaluation of cell viability

The viability of Caco-2 cells after 24-h treatment with free curcumin (Cu), Xanthan-Chitosan nanofibers (X-Ch), curcumin-loaded Xanthan-Chitosan nanofibers (X-Ch-Cu), and PBS was

evaluated through MTS bioassay (**Figure 3**). The MTS tetrazolium compound is reduced by cells into a colored formazan product that is soluble in tissue culture medium and quantified recording its absorbance at 490 nm. This conversion is accomplished by dehydrogenase enzymes in metabolically active cells, therefore MTS conversion is directly proportional to the number of living cells ⁴⁹. The incubation of Caco-2 cells with 0.5 mg X-Ch nanofibers, 0.5 mg X-Ch-Cu nanofibers, and free curcumin (Cu, 150 μ M) was non-toxic to the cells, and cell viability was found to be $\geq 80\%$. By contrast, when cells were exposed to 500 μ M free curcumin, the cell viability value was decreased to $\sim 20\%$, indicating a concentration-dependent toxic effect of curcumin in cell viability. According to the encapsulation efficiency of curcumin into nanofibers and the *in vitro* release profile of curcumin from X-Ch-Cu nanofibers at pH 7.4, the amount of releasable curcumin from 0.5 mg X-Ch-Cu nanofibers was assumed to be 150 μ M. Therefore, this concentration was selected to determine the apical-to-basolateral and basolateral-to-apical transports of curcumin across Caco-2 cell monolayers.

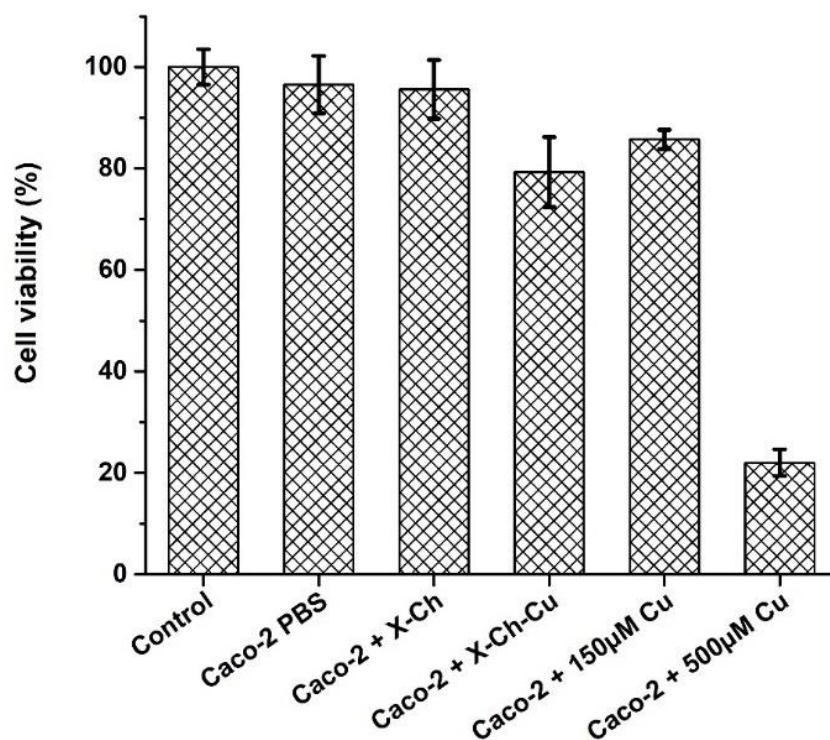


Figure 3. MTS cell viability bioassay. Caco-2 cells were seeded in 96-well plates at a concentration of 2.0×10^4 cells/mL for 48 h. Then cells were incubated with: PBS (also used for curcumin dilution), 0.5 mg Xanthan-Chitosan nanofibers (X-Ch), 0.5 mg curcumin-loaded Xanthan-Chitosan nanofibers (X-Ch-Cu), 150 μ M curcumin diluted in PBS (Cu), and 500 μ M curcumin diluted in PBS (Cu). After 24 h incubation, the cell viability was evaluated through MTS assay. Data are the mean \pm SD of six independent experiments.

3.5. Evaluation of Caco-2 cell monolayers integrity

To perform reliable *in vitro* permeability experiments across Caco-2 cell monolayers, the transport of non-radiolabeled markers, fluorescein and lucifer yellow, and the transepithelial electrical resistance measurements were conducted to quantitatively investigate the integrity and permeability of cell monolayers after 21 days growth on 12-mm polycarbonate inserts. The monolayers integrity is a fundamental determinant of the study of drugs transport via the intestinal membrane, especially when the passive transport of substances through tight junctions is involved.⁵⁰ Therefore, the AB and BA transepithelial transports of fluorescein (FLUO) and lucifer yellow (LY) across Caco-2 monolayers under a proton gradient were investigated (**Figure 4**). The average of TEER values for Caco-2 cell monolayers measured at 37 °C was $422 \pm 30 \Omega \text{ cm}^2$ and the TEER values of Caco-2 cell monolayers before and after transport of FLUO and LY were found to be in the range of 350-500 $\Omega \text{ cm}^2$ (**Figure 4a**) indicating an “intermediate” tightness of the gastrointestinal epithelium, as established by the GI epithelia classification based on TEER values.⁵¹ **Figure 4b** and **4c** show the cumulative permeated amount of the two markers after apical-to-basolateral and basolateral-to-apical transport across Caco-2 cell monolayers in presence of a proton gradient (pH 6.5 in A and pH 7.4 in B), and the FLUO and LY distribution within the cell model system, respectively. The permeation of fluorescein across the monolayers increased over time and it was higher when a lower pH of the donor solution was used. In fact, after 8h the amount of fluorescein at the acceptor chamber was 20% and 12% for the AB and BA transport respectively, suggesting a pH-dependent transport of fluorescein. Consequently, most of the fluorescein at the donor side was still found at time=8h (~78%), and this value was even higher for BA transport. Only small amounts of FLUO were detected within the cell lysate and insert membrane (0.74 and 0.58%, respectively). Contrarily, the permeation of LY was weakly

affected by pH and the cumulative amounts transferred across cell monolayers were less than 1.5% for both AB and BA transports, resulting in a highly poor absorption of LY (98% of the initial donor concentration remained there). The values of the apparent permeability coefficients of FLUO were $P_{app,AB} = 9.52 \times 10^{-6}$ and $P_{app,BA} = 1.89 \times 10^{-6}$ cm/s, whereas much lower values were calculated for the LY transport: $P_{app,AB} = 6.26 \times 10^{-7}$ and $P_{app,BA} = 1.46 \times 10^{-7}$ cm/s (**Figure 4d**). These results demonstrate that the different physical-chemical properties of FLUO and LY are strongly reflected in their permeation across the cell monolayers and the transport mechanism involved in the absorption. The main features of a compound influencing its permeation are logP, pK_a, molecular weight, and ionization (**Table 1**).⁵² Fluorescein is a small and lipophilic molecule (logP_{o/w} = 4.81) and possesses two ionization groups having a pK_{a1} = 4.36 and pK_{a2} = 6.38. By contrast, lucifer yellow is a small hydrophilic compound (logP_{o/w} = -5.06) and has a pK_a = -0.9. According to the results presented in **Figure 4**, P_{app} values of FLUO increased with the decreasing pH of the donor solution, at which the compound is ionized at a smaller extent, while the high hydrophilicity and ionization of LY prevent its absorption through cell monolayers. The apical membrane of polarized epithelial cell layers has a lipid nature thus it restricts the transport of ions and hydrophilic molecules. Therefore, lipophilic compounds like FLUO, across the cell barrier through a passive transcellular transport following their pH partitioning into the apical membrane and diffusing through the cytoplasm reaching the basolateral membrane⁵³. For more hydrophilic compounds like LY, transcellular diffusion is often prevented and depending on the pK_a of molecules at the donor pH, the transport of these solutes across epithelial cells can occur via tight junctions (paracellular transport). In the light of these considerations, the results obtained from AB and BA transport of FLUO and LY suggested that the integrity and tightness

of Caco-2 cell monolayers after 21 days were maintained, and further studies using X-Ch-Cu nanofibers have been investigated using this approach.

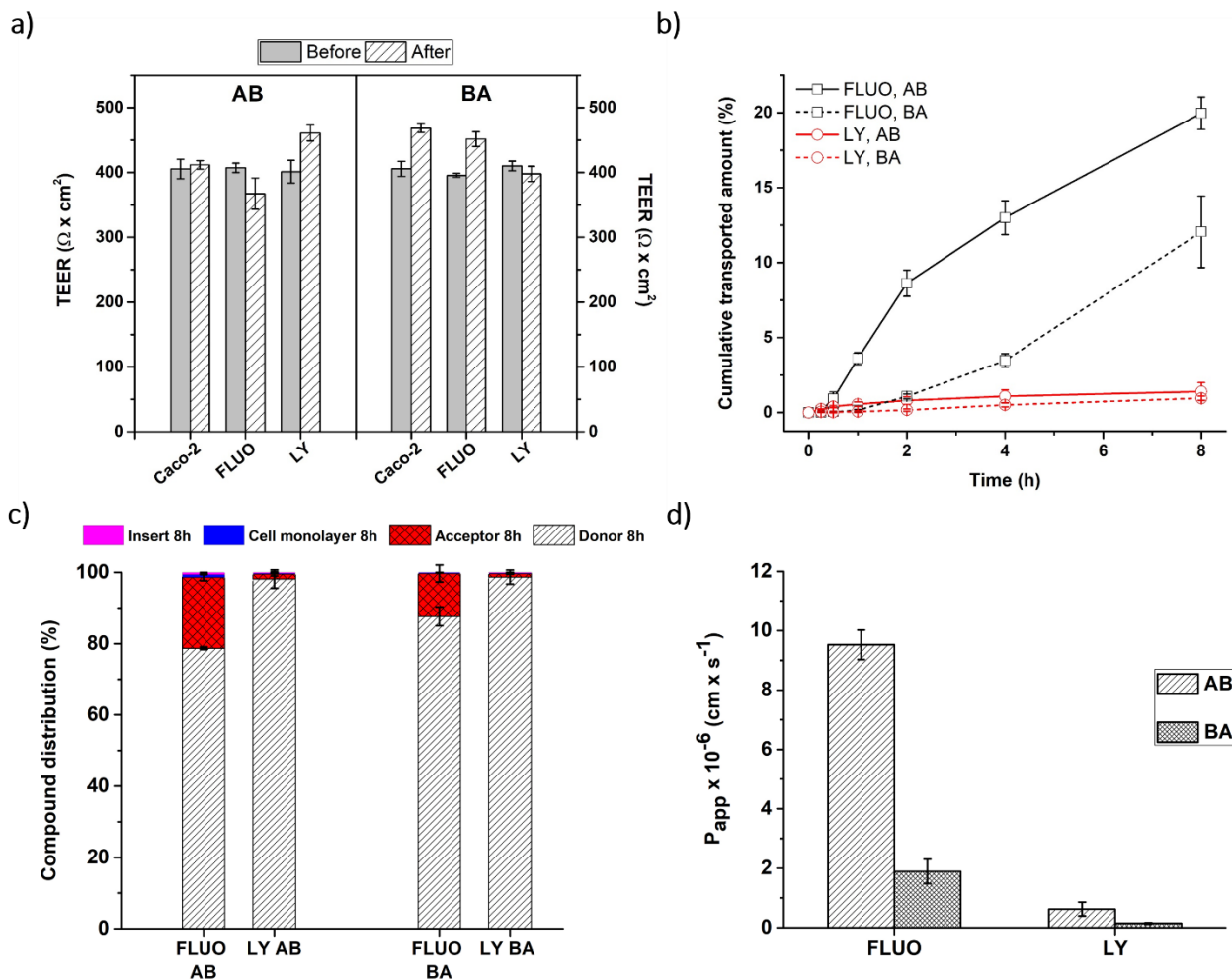


Figure 4. Quantitative evaluation of Caco-2 cell monolayers integrity. Fluorescein (FLUO) and lucifer yellow (LY) were used as non-radiolabeled permeability markers and the transepithelial electrical resistance values (TEER) of cell monolayers were measured before and after apical-to-basolateral (AB) and basolateral-to-apical (BA) studies for a time interval of 8 h. **a)** TEER values of Caco-2 monolayers incubated respectively with a transport medium, 1 mM FLUO, and 870 μM LY at the donor chamber, before and after AB and BA transport processes. **b)** Percentage of the cumulative transported amount of FLUO and LY over time, for both AB and BA studies. **c)**

FLUO and LY distribution after 8 h transport experiments in the acceptor chamber, donor chamber, Caco-2 cell monolayer, and insert membrane. **d)** Apparent permeability coefficient (P_{app}) of FLUO and LY calculated for both AB and BA transports. All data are the mean \pm SD of three independent experiments.

3.6. Caco-2 cell monolayers treatments

The low aqueous solubility, poor intestinal absorption and extensive metabolism and excretion are crucial parameters that affect curcumin bioavailability. In order to overcome some of these limiting factors, Xanthan-Chitosan electrospun nanofibers as curcumin delivery system were produced and investigated. In the present study, the restricted use of chitosan as an *in vitro* absorption enhancer in epithelial cell monolayers was overcome by mixing the chitosan with xanthan gum polysaccharide. As reported by Dempe *et al.*,⁸ Caco-2 cell monolayers express the enzymes involved in phase I and II metabolism of curcumin. In fact, curcumin metabolites such as hexahydro- and octahydro-curcumin, as well as their glucuronide and sulfate conjugates were identified as major metabolites at the donor and acceptor side.⁸ Thus, in the present study, the quantification of curcumin at the apical and basolateral side was conducted recording the absorbance of native curcumin at 420 nm, and also measuring the absorbance of curcumin metabolites at 280 nm, as suggested by Dempe *et al.*⁸ Therefore, the data obtained for curcumin transepithelial transport studies, include the contribution of both transported native curcumin and its metabolites.

The 24 h exposure of Caco-2 cell monolayers to X-Ch and X-Ch-Cu nanofibers resulted in a cell viability >90% and ~80%, respectively (**Figure 3**). In addition to that, the incubation of cell monolayers with 150 μ M free Cu and X-Ch-Cu nanofibers ended up to a comparable cell

viability value, indicating that the amount of curcumin loaded into the nanofibers was similar to the free curcumin (150 μ M), and that the small decrement in cell viability (~80%) was attributed to the curcumin dose and not to the presence of X-Ch nanofibers (>90%). In order to investigate the presumed enhancement of curcumin absorption across epithelial cell monolayers in presence of Xanthan-Chitosan nanofibers, the AB and BA transport of free Cu (Cu), X-Ch nanofibers + free Cu (X-Ch + Cu), and curcumin-loaded X-Ch nanofibers (X-Ch-Cu) were performed (**Figure 5a and b**). As depicted in the illustrations, the free curcumin and/or nanofibers were incubated at the donor chamber and the transported amount of curcumin was withdrawn from the acceptor side over a period of 8h under a proton gradient. The addition of Xanthan-Chitosan nanofibers to free curcumin was found to enhance curcumin permeation of nearly 2-fold compared to free curcumin alone, and such enhancement was even higher for X-Ch-Cu nanofibers reaching 3.4-fold. For X-Ch-Cu nanofibers, the total amount of curcumin transported across cell monolayers for AB and BA transports was 32.81% and 46.94% of the releasable curcumin, respectively. The observed slight reduction of TEER values for AB transport of X-Ch + Cu and X-Ch-Cu was found to be more pronounced for BA transport of X-Ch + Cu and X-Ch-Cu (**Figure 5c and d**). Taken together, the observed results suggest that the presence of Xanthan-Chitosan nanofibers positively affect curcumin permeation since a 3-fold higher concentration of curcumin was detected in the acceptor chamber. The decrease in TEER values supports that the tight junctions were affected by the electrospun fibers, and direct contact between the fibers and cell monolayers. This is in agreement with our previous study on the permeation of a model protein (insulin) across Caco-2 cells upon contact with electrospun fish protein fibers.³³ Indeed, we found that direct interaction between the nanofibers and the monolayer induces changes in the tight junctions, and thus an increase in permeation at local hot spots on the epithelial barrier.

Moreover, the reduction of TEER values could be also attributed in part to the presence of chitosan within the electrospun nanofibers, which is responsible for the tight junctions opening, thus promoting paracellular transport. In addition to that, no cell-damaging was detected after 24 h treatment with X-Ch and X-Ch-Cu. In fact, the effect of chitosan and its derivatives on Caco-2 cell monolayers has been extensively studied,^{35,37} and TEER measurements have shown that chitosan induces an immediate reduction of TEER in a dose-dependent effect on tight junction permeability. However, a recovery of TEER values in the time range of few hours up to one day could be observed after chitosan polymer solution removal.^{35,37} In these studies, a paracellular transport of [¹⁴C]-mannitol across Caco-2 monolayers was recorded only when a certain TEER threshold value was reached.³⁵

The fate of curcumin during transepithelial transport in both AB and BA directions was monitored by quantifying (after 8 h) the amount of curcumin in the donor and acceptor side, Caco-2 cell lysate, insert membrane, and within X-Ch nanofibers. **Figure 6a** shows the distribution of curcumin in the above-mentioned compartments when free Cu, X-Ch + Cu, and X-Ch-Cu nanofibers were incubated in the donor chamber. Although significant amounts of curcumin were still detected in the donor side after 8h transport, curcumin concentrations $\geq 10\%$ of the donor initial concentration were detected in the acceptor side. Only small amounts of curcumin were found into cell lysate, $< 3\%$, and insert membrane, $< 1.5\%$, while considerable curcumin amounts remained loaded into X-Ch-Cu nanofibers even after 8h release (28% into X-Ch-Cu in the AB study, and 13% into X-Ch-Cu in the BA study).

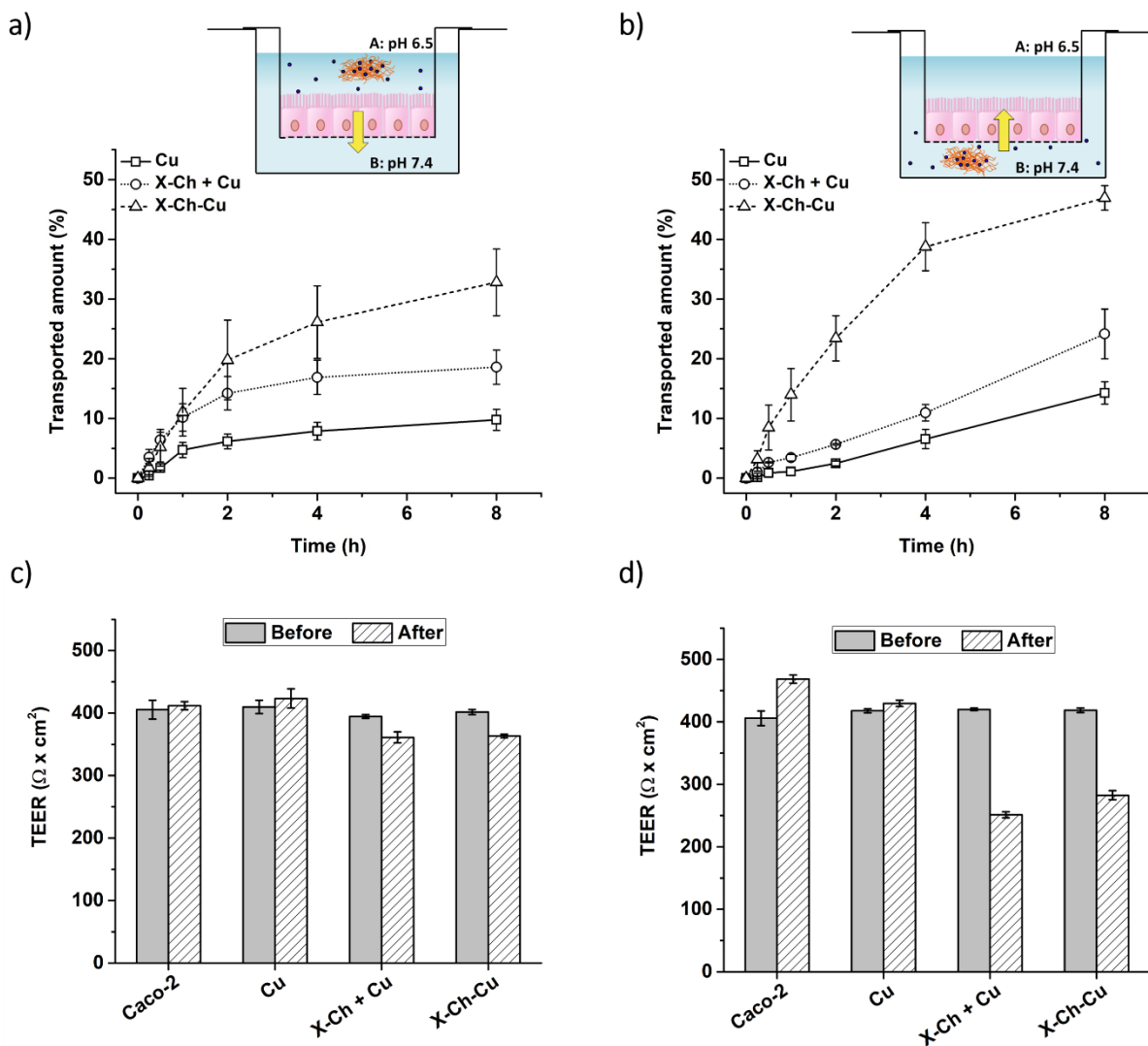


Figure 5. Study of the transepithelial transport across Caco-2 cell monolayers of free curcumin (Cu, 150 μ M), free curcumin (150 μ M) + 3.0 mg Xanthan-Chitosan nanofibers (X-Ch + Cu), and 9.0 mg curcumin-loaded Xanthan-Chitosan nanofibers (X-Ch-Cu, fibers amount that corresponded to 150 μ M released curcumin) at the donor chamber. Apical-to-basolateral (AB) and basolateral-to-apical (BA) transport were conducted for a time interval of 8 h under a proton gradient, pH= 6.5 at the apical side and pH= 7.4 at the basolateral chamber. **a)** and **b)** Percentage of the transported amount of Cu over time for AB and BA studies, respectively. **c)** and **d)** TEER

values of Caco-2 cell monolayers before and after AB and BA transport, respectively. All data are the mean \pm SD of three independent experiments.

Nevertheless, the proposed curcumin delivery system showed the highest amount of curcumin permeating the epithelial cell monolayers with a $P_{app, AB} = 1.49 \times 10^{-5}$ cm/s and a $P_{app, BA} = 7.00 \times 10^{-6}$ cm/s (**Figure 6c**), and a 2-fold permeability enhancement was measured when Xanthan-Chitosan nanofibers were added to a free curcumin solution in the donor side compared to free curcumin without fibers. In addition, after 8 h, the morphology of the tested nanofibers was analyzed by microscopy (data not shown), and besides a loss of yellow-orange coloration due to the released curcumin, no morphological variations were observed.

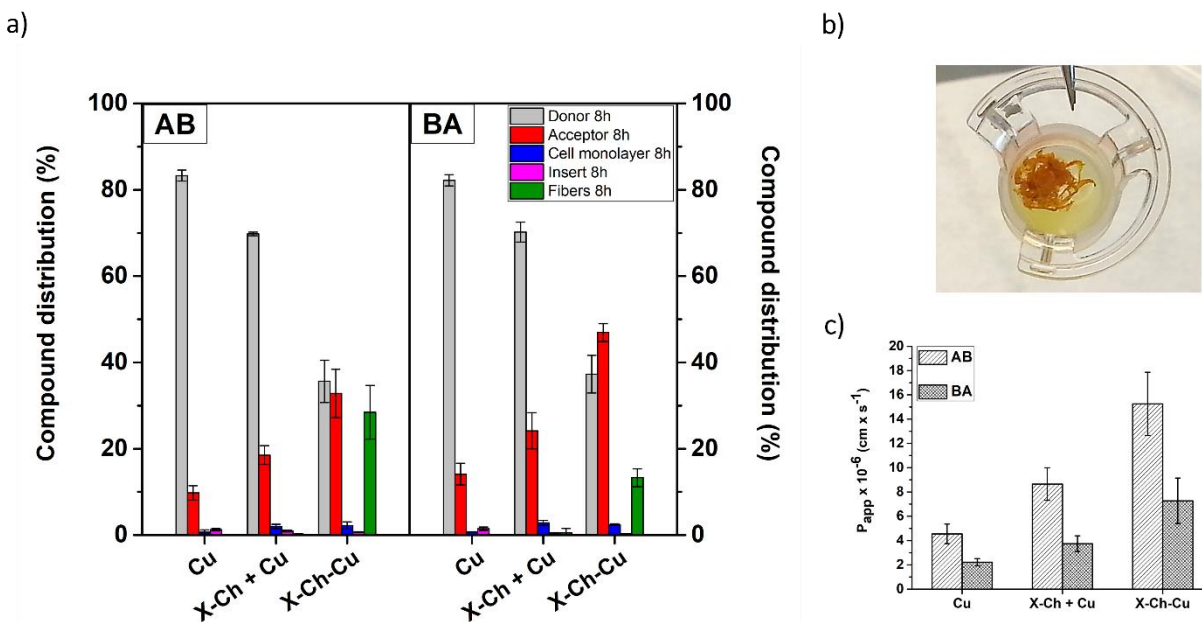


Figure 6. Study of the transepithelial transport of 150 μ M free curcumin (Cu), 3.0 mg Xanthan-Chitosan nanofibers + 150 μ M free Cu (X-Ch + Cu), and 9.0 mg curcumin-loaded Xanthan-Chitosan nanofibers (X-Ch-Cu) across Caco-2 cell monolayers. **a)** Cu distribution after 8 h transport experiments in the acceptor chamber, donor chamber, Caco-2 cell monolayer, insert

membrane, and within X-Ch nanofibers. **b)** Image of a Caco-2 cell monolayer cultured for 21 days in a 12-mm polycarbonate semipermeable membrane containing a solution of HBSS at pH 6.5 and 9.0 mg X-Ch-Cu nanofibers. The yellow medium indicates the presence of released curcumin from X-Ch-Cu nanofibers that has a strong orange color. **c)** Apparent permeability coefficient (P_{app}) of Cu calculated for both AB and BA transports. All data are the mean \pm SD of three independent experiments.

4. Conclusions

Uniform and homogeneous Xanthan-Chitosan nanofibers were fabricated using electrospinning processing and investigated as an encapsulation and delivery system of curcumin, a poor water soluble polyphenolic compound. It was found that X-Ch-Cu nanofibers remained stable in aqueous HBSS medium at different pH (6.5 and pH 7.4). Moreover, X-Ch-Cu nanofibers were incubated with Caco-2 cells, and cell viability, transepithelial transport and curcumin permeability properties across cell monolayers were investigated. After 24 h of incubation, the exposure of Caco-2 cell monolayers to X-Ch and X-Ch-Cu nanofibers resulted in a cell viability of >90% and ~80%, respectively. A 3.4-fold increase of curcumin permeability was observed in the presence of X-Ch fibers, in comparison with free-curcumin. The X-Ch nanofibers interacted with intestinal Caco-2 cells and caused tight junctions opening, demonstrated by a decrease in TEER values, which promoted increased transepithelial permeation of curcumin without compromising cellular viability. Hence, the interactions between electrospun fibers and the epithelial cells, could be used to promote increased uptake of bioactives. Furthermore, *in vivo* experiments are required to fully demonstrate the efficiency of these nanofibers for oral delivery applications of poorly water-soluble compounds at the gastrointestinal tract.

Acknowledgments

The project was supported by a PhD stipend (to ES) from the Technical University of Denmark. Part of this work was also supported by the European Union funded project “Nano3Bio” (grant agreement no 613931) under FP7.

References

1. Aftab, N. & Vieira, A. Antioxidant activities of curcumin and combinations of this curcuminoid with other phytochemicals. *Phyther. Res.* **24**, n/a-n/a (2009).
2. Ak, T. & Gülçin, İ. Antioxidant and radical scavenging properties of curcumin. *Chem. Biol. Interact.* **174**, 27–37 (2008).
3. Zorofchian Moghadamtousi, S. *et al.* A Review on Antibacterial, Antiviral, and Antifungal Activity of Curcumin. *Biomed Res. Int.* **2014**, 1–12 (2014).
4. Perrone D, Ardito F, Giannatempo G, Dioguardi M, Troiano G, Lo Russo L, De Lillo A, Laino L, L. M. L. Biological and therapeutic activities, and anticancer properties of curcumin. *Exp. Ther. Med.* **10**, 1615–1623 (2015).
5. Gupta, S. C., Patchva, S. & Aggarwal, B. B. Therapeutic roles of curcumin: lessons learned from clinical trials. *AAPS J.* **15**, 195–218 (2013).
6. Sharma, R. A., Gescher, A. J. & Steward, W. P. Curcumin: The story so far. *Eur. J. Cancer* **41**, 1955–1968 (2005).
7. Anand, P., Kunnumakkara, A. B., Newman, R. A. & Aggarwal, B. B. Bioavailability of Curcumin: Problems and Promises. *Mol. Pharm.* **4**, 807–818 (2007).

8. Dempe, J. S., Scheerle, R. K., Pfeiffer, E. & Metzler, M. Metabolism and permeability of curcumin in cultured Caco-2 cells. *Mol. Nutr. Food Res.* **57**, 1543–1549 (2013).
9. Wahlang, B., Pawar, Y. B. & Bansal, A. K. Identification of permeability-related hurdles in oral delivery of curcumin using the Caco-2 cell model. *Eur. J. Pharm. Biopharm.* **77**, 275–282 (2011).
10. Sharma, R. A., Steward, W. P. & Gescher, A. J. PHARMACOKINETICS AND PHARMACODYNAMICS OF CURCUMIN. in *The Molecular Targets and Therapeutic Uses of Curcumin in Health and Disease* **595**, 453–470 (Springer US, 2007).
11. Hoehle, S. I., Pfeiffer, E., Sólyom, A. M. & Metzler, M. Metabolism of Curcuminoids in Tissue Slices and Subcellular Fractions from Rat Liver. *J. Agric. Food Chem.* **54**, 756–764 (2006).
12. Pfeiffer, E. *et al.* Curcuminoids Form Reactive Glucuronides In Vitro. *J. Agric. Food Chem.* **55**, 538–544 (2007).
13. Usta, M. *et al.* Human Glutathione S-Transferase-Mediated Glutathione Conjugation of Curcumin and Efflux of These Conjugates in Caco-2 Cells. *Chem. Res. Toxicol.* **20**, 1895–1902 (2007).
14. Wang, Y. J. *et al.* Stability of curcumin in buffer solutions and characterization of its degradation products. *J. Pharm. Biomed. Anal.* **15**, 1867–76 (1997).
15. Tønnesen, H. H. & Karlsen, J. Studies on curcumin and curcuminoids. VI. Kinetics of curcumin degradation in aqueous solution. *Z. Lebensm. Unters. Forsch.* **180**, 402–4 (1985).

16. Shoba, G. *et al.* Influence of Piperine on the Pharmacokinetics of Curcumin in Animals and Human Volunteers. *Planta Med.* **64**, 353–356 (1998).
17. Cruz–Correa, M. *et al.* Combination Treatment With Curcumin and Quercetin of Adenomas in Familial Adenomatous Polyposis. *Clin. Gastroenterol. Hepatol.* **4**, 1035–1038 (2006).
18. Balasubramanian, S. & Eckert, R. L. Green Tea Polyphenol and Curcumin Inversely Regulate Human Involucrin Promoter Activity via Opposing Effects on CCAAT/Enhancer-binding Protein Function. *J. Biol. Chem.* **279**, 24007–24014 (2004).
19. Verma, S. P., Salamone, E. & Goldin, B. Curcumin and Genistein, Plant Natural Products, Show Synergistic Inhibitory Effects on the Growth of Human Breast Cancer MCF-7 Cells Induced by Estrogenic Pesticides. *Biochem. Biophys. Res. Commun.* **233**, 692–696 (1997).
20. Lee, W.-H. *et al.* Recent advances in curcumin nanoformulation for cancer therapy. *Expert Opin. Drug Deliv.* **11**, 1183–1201 (2014).
21. Kocher, A., Schiborr, C., Behnam, D. & Frank, J. The oral bioavailability of curcuminoids in healthy humans is markedly enhanced by micellar solubilisation but not further improved by simultaneous ingestion of sesamin, ferulic acid, naringenin and xanthohumol. *J. Funct. Foods* **14**, 183–191 (2015).
22. Schiborr, C. *et al.* The oral bioavailability of curcumin from micronized powder and liquid micelles is significantly increased in healthy humans and differs between sexes. *Mol. Nutr. Food Res.* **58**, 516–527 (2014).
23. Cuomo, J. *et al.* Comparative Absorption of a Standardized Curcuminoid Mixture and Its

- Lecithin Formulation. *J. Nat. Prod.* **74**, 664–669 (2011).
24. Chanburee, S. & Tiyaboonchai, W. Enhanced intestinal absorption of curcumin in Caco-2 cell monolayer using mucoadhesive nanostructured lipid carriers. *J. Biomed. Mater. Res. Part B Appl. Biomater.* (2017). doi:10.1002/jbm.b.33884
 25. Frank, J. *et al.* Transepithelial Transport of Curcumin in Caco-2 Cells Is significantly Enhanced by Micellar Solubilisation. *Plant Foods Hum. Nutr.* **72**, 48–53 (2017).
 26. Shekarforoush, E., Mendes, A. C., Baj, V., Beeren, S. R. & Chronakis, I. S. Electrospun phospholipid fibers as micro-encapsulation and antioxidant matrices. *Molecules* **22**, 1–16 (2017).
 27. Deng, L., Kang, X., Liu, Y., Feng, F. & Zhang, H. Effects of surfactants on the formation of gelatin nanofibres for controlled release of curcumin. *Food Chem.* **231**, 70–77 (2017).
 28. Blanco-Padilla, A., López-Rubio, A., Loarca-Piña, G., Gómez-Mascaraque, L. G. & Mendoza, S. Characterization, release and antioxidant activity of curcumin-loaded amaranth-pullulan electrospun fibers. *LWT - Food Sci. Technol.* 1–8 (2015). doi:10.1016/j.lwt.2015.03.081
 29. Ignatious, F., Sun, L., Lee, C.-P. & Baldoni, J. Electrospun Nanofibers in Oral Drug Delivery. *Pharm. Res.* **27**, 576–588 (2010).
 30. Li, X., Kanjwal, M. A., Lin, L. & Chronakis, I. S. Electrospun polyvinyl-alcohol nanofibers as oral fast-dissolving delivery system of caffeine and riboflavin. *Colloids Surfaces B Biointerfaces* **103**, 182–188 (2013).
 31. Artursson, P., Palm, K. & Luthman, K. Caco-2 monolayers in experimental and

- theoretical predictions of drug transport. *Adv. Drug Deliv. Rev.* **46**, 27–43 (2001).
32. Araújo, F. & Sarmiento, B. Towards the characterization of an in vitro triple co-culture intestine cell model for permeability studies. *Int. J. Pharm.* **458**, 128–134 (2013).
 33. Stephansen, K., García-Díaz, M., Jessen, F., Chronakis, I. S. & Nielsen, H. M. Bioactive protein-based nanofibers interact with intestinal biological components resulting in transepithelial permeation of a therapeutic protein. *Int. J. Pharm.* **495**, 58–66 (2015).
 34. Lin, T.-C., Lin, F.-H. & Lin, J.-C. In vitro feasibility study of the use of a magnetic electrospun chitosan nanofiber composite for hyperthermia treatment of tumor cells. *Acta Biomater.* **8**, 2704–2711 (2012).
 35. Borchard, G. *et al.* The potential of mucoadhesive polymers in enhancing intestinal peptide drug absorption. III: Effects of chitosan-glutamate and carbomer on epithelial tight junctions in vitro. *J. Control. Release* **39**, 131–138 (1996).
 36. Portero, A., Remuñán-López, C. & Nielsen, H. M. The potential of chitosan in enhancing peptide and protein absorption across the TR146 cell culture model-an in vitro model of the buccal epithelium. *Pharm. Res.* **19**, 169–74 (2002).
 37. Kowapradit, J. *et al.* In vitro Permeability Enhancement in Intestinal Epithelial Cells (Caco-2) Monolayer of Water Soluble Quaternary Ammonium Chitosan Derivatives. *AAPS PharmSciTech* **11**, 497–508 (2010).
 38. Kulkarni, N., Wakte, P. & Naik, J. Development of floating chitosan-xanthan beads for oral controlled release of glipizide. *Int. J. Pharm. Investig.* **5**, 73–80 (2015).
 39. Wang, C. S., Natale, G., Virgilio, N. & Heuzey, M. C. Synergistic gelation of gelatin B

- with xanthan gum. *Food Hydrocoll.* **60**, 374–383 (2016).
40. Shekarforoush, E., Faralli, A., Ndoni, S., Mendes, A. C. & Chronakis, I. S. Electrospinning of Xanthan Polysaccharide. *Macromol. Mater. Eng.* **302**, 1–11 (2017).
 41. Konishi, Y., Hagiwara, K. & Shimizu, M. Transepithelial Transport of Fluorescein in Caco-2 Cell Monolayers and Use of Such Transport in In Vitro Evaluation of Phenolic Acid Availability. *Biosci. Biotechnol. Biochem.* **66**, 2449–2457 (2002).
 42. Berginc, K., Žakelj, S., Levstik, L., Uršič, D. & Kristl, A. Fluorescein transport properties across artificial lipid membranes, Caco-2 cell monolayers and rat jejunum. *Eur. J. Pharm. Biopharm.* **66**, 281–285 (2007).
 43. Hashimoto, K., Matsunaga, N. & Shimizu, M. Effect of Vegetable Extracts on the Transepithelial Permeability of the Human Intestinal Caco-2 Cell Monolayer. *Biosci. Biotechnol. Biochem.* **58**, 1345–1346 (1994).
 44. Hubatsch, I., Ragnarsson, E. G. E. & Artursson, P. Determination of drug permeability and prediction of drug absorption in Caco-2 monolayers. *Nat. Protoc.* **2**, 2111–2119 (2007).
 45. Frenot, A. & Chronakis, I. S. Polymer nanofibers assembled by electrospinning. *Curr. Opin. Colloid Interface Sci.* **8**, 64–75 (2003).
 46. Shekarforoush, E., Ajalloueiian, F., Zeng, G., Mendes, A. C. & Chronakis, I. S. Electrospun xanthan gum-chitosan nanofibers as delivery carrier of hydrophobic bioactives. *Mater. Lett.* **228**, 322–326 (2018).
 47. Yee, S. In vitro permeability across Caco-2 cells (colonic) can predict in vivo (small

- intestinal) absorption in man--fact or myth. *Pharm. Res.* **14**, 763–6 (1997).
48. Naruhashi, K. *et al.* Comparison of the expression and function of ATP binding cassette transporters in Caco-2 and T84 cells on stimulation by selected endogenous compounds and xenobiotics. *Drug Metab. Pharmacokinet.* **26**, 145–53 (2011).
 49. Cory, A. H., Owen, T. C., Barltrop, J. A. & Cory, J. G. Use of an aqueous soluble tetrazolium/formazan assay for cell growth assays in culture. *Cancer Commun.* **3**, 207–12 (1991).
 50. Srinivasan, B. *et al.* TEER Measurement Techniques for In Vitro Barrier Model Systems. *J. Lab. Autom.* **20**, 107–126 (2015).
 51. Amidon, G. L., Lee, P. I. & Topp, E. M. *Transport processes in pharmaceutical systems.* (M. Dekker, 2000).
 52. Camenisch, G., Folkers, G. & van de Waterbeemd, H. Review of theoretical passive drug absorption models: historical background, recent developments and limitations. *Pharm. Acta Helv.* **71**, 309–27 (1996).
 53. Högerle, M. L. & Winne, D. Drug absorption by the rat jejunum perfused in situ. Dissociation from the pH-partition theory and role of microclimate-pH and unstirred layer. *Naunyn. Schmiedeberg's. Arch. Pharmacol.* **322**, 249–55 (1983).

3.1.4. Application of Asolection phospholipid microfiber- Paper V

Electrospun Phospholipid Fibers as Micro-Encapsulation and Antioxidant Matrices



Elhamalsadat Shekarforoush ¹, Ana C. Mendes ^{1,*}, Vanessa Baj ², Sophie R. Beeren ² and Ioannis S. Chronakis ¹

1 Nano-Bio Science Research Group, DTU-Food, Technical University of Denmark, Kemitorvet 202, 2800 Kongens Lyngby, Denmark.

2 DTU-Chemistry, Technical University of Denmark, Kemitorvet 207, 2800 Kongens Lyngby, Denmark.

Article

Electrospun Phospholipid Fibers as Micro-Encapsulation and Antioxidant Matrices

Elhamalsadat Shekarforoush ¹, Ana C. Mendes ^{1,*} , Vanessa Baj ², Sophie R. Beeren ²  and Ioannis S. Chronakis ¹

¹ Nano-Bio Science Research Group, DTU-Food, Technical University of Denmark, Kemitorvet 202, 2800 Kongens Lyngby, Denmark; elsh@food.dtu.dk (E.S.); ioach@food.dtu.dk (I.S.C.)

² DTU-Chemistry, Technical University of Denmark, Kemitorvet 207, 2800 Kongens Lyngby, Denmark; vanbaj@kemi.dtu.dk (V.B.); sopbee@kemi.dtu.dk (S.R.B.)

* Correspondence: anac@food.dtu.dk; Tel.: +45-9351-8947

Received: 9 September 2017; Accepted: 9 October 2017; Published: 17 October 2017

Abstract: Electrospun phospholipid (asolectin) microfibers were investigated as antioxidants and encapsulation matrices for curcumin and vanillin. These phospholipid microfibers exhibited antioxidant properties which increased after the encapsulation of both curcumin and vanillin. The total antioxidant capacity (TAC) and the total phenolic content (TPC) of curcumin/phospholipid and vanillin/phospholipid microfibers remained stable over time at different temperatures (refrigerated, ambient) and pressures (vacuum, ambient). ¹H-NMR confirmed the chemical stability of both encapsulated curcumin and vanillin within phospholipid fibers. Release studies in aqueous media revealed that the phenolic bioactives were released mainly due to swelling of the phospholipid fiber matrix over time. The above studies confirm the efficacy of electrospun phospholipid microfibers as encapsulation and antioxidant systems.

Keywords: phospholipids; electrospinning; microfibers; antioxidants; encapsulation; vanillin; curcumin

1. Introduction

Phospholipids have been used for preparing biomimetic capsular structures (mainly vesicles or liposomes) [1–4], for several life science applications, including nano-micro encapsulation of drugs [5] and mammalian cells [6], and in food [7] as delivery carriers of nutrients, nutraceuticals, food additives and antimicrobials. Encapsulation of bioactives within lipid formulations often offers enhanced stability and protection, combined with superior biocompatibility and enhanced permeability, depending on the lipid composition and properties [8,9]. Among other phospholipids, asolectin, constituted by a mixture of lecithin, cephalin and phosphatidylinositol, saturated fatty acids, mono-unsaturated and poly-unsaturated fatty acids has been used to develop nano-microstructures such as fibers [10–13], hydrogels [14] and liposomes [7,15] for the encapsulation of bioactives [13,16]. In addition, asolectin components have also been proven to display antioxidant properties [16–19]. Pan and co-workers [16] evaluated the effect of the antioxidant properties of lecithin emulsifier on the oxidative stability of encapsulated bioactive compounds. They demonstrated that the antioxidant activity of lecithin emulsifier can significantly reduce the saturation of free radicals across the interface of oil-in-water emulsions, as well as the rate of oxidation of the bioactive encapsulate (curcumin), thus increasing its shelf life. The antioxidant effect of lecithins was also tested on several oils and fats varying in FA composition and tocopherol content [17]. They found that lecithins, at specific concentrations, exhibited a good protective effect against oxidation on several oils and fats with varying FA composition. These antioxidant properties were enhanced in samples containing tocopherols, due to the synergistic interactions between amino-alcohol phospholipids and γ - and δ -tocopherols.

Furthermore, Doert and co-authors [20] studied the synergistic effect of lecithins with tocopherols and observed that phospholipids synergistically enhance the antioxidant effect of phenolic antioxidants.

Phenolic compounds are known for the inhibition of free radical formation and/or for the interruption of the propagation of autoxidation [21]. Vanillin (4-hydroxy-3-methoxybenzaldehyde) is a phenolic compound, which can either be extracted from pods of *Vanilla Planifolia* or synthesized chemically, and has been widely used in the food industry as a flavor, but also as a food preservative, due to its antioxidant, antimicrobial, anticarcinogenic and antimutagenic properties [22,23]. However, its high volatility and thermal instability are the main drawbacks for its use and processing. Curcumin is another phenolic compound derived from the turmeric of the herb *Curcuma longa* L., with biological and pharmacological properties, such as antioxidant, anti-inflammatory, antimicrobial, antimalarial, and anticarcinogenic properties [24]. Due to its hydrophobic nature, curcumin has very low solubility in water and its chemical stability has been reported to be affected by external factors such as pH, exposure to light, temperature and oxygen [25,26]. Curcumin has poor bioavailability due to inefficient absorption at the intestinal track and for that reason it is commonly administered with digestible lipids that facilitate the solubilization and transport of this phenolic compound to the epithelial tissue [25].

Electrospinning processing is suitable for the production of continuous and functional nano-microfibers, from a wide range of (bio)polymers [27] and small molecules such as phospholipids [10–12]. The fabrication of electrospun phospholipid fibers has been initially reported using DMF:CHCl₃ solvents [11]. Recently, it was demonstrated that the morphological properties of electrospun phospholipid fibers could be controlled using solvents with different polarities such as isooctane, cyclohexane and limonene and by the application of a co-axial solvent electrospinning [11]. The mechanical properties of phospholipid microfibers were investigated by nanoindentation using Atomic Force Microscopy [12]. It was found that these fibers have an elastic modulus of 17.26 MPa and were stable in ambient conditions, preserving the modulus of elasticity up to 24 h [12]. In another study, Yu et al. [28] mixed polyvinylpyrrolidone (PVP) with soybean lecithin to create a fibrous network by electrospinning. Formation of liposomes and vesicles with a very narrow distribution between 120–370 nm was observed after immersion of lecithin/PVP fibers in water. To increase the stability of electrospun lipid based systems, Zhang et al. applied a hybridization strategy to produce electrospun cholesteryl-succinyl silane (CSS) nanofibers [29].

Electrospun fibers have been used for encapsulation and controlled release of bioactives [27]. The encapsulation of curcumin within electrospun fibers using Chitosan/Phospholipids [13], polylactic acid (PLA) [30,31], polyvinyl pyrrolidone [32], blends of amaranth protein isolate/pullulan [33], and cellulose acetate [34], as well as the encapsulation of the vanillin/cyclodextrin inclusion complex (vanillin/CD-IC) within electrospun polyvinyl alcohol (PVA) [35] fibers has been reported.

This study aimed to develop electrospun phospholipid microfibers to encapsulate vanillin and curcumin as model phenolic compounds and investigate their morphology, release and antioxidant properties.

2. Results and Discussion

2.1. Morphology

Phospholipid microfibers were obtained by electrospinning using limonene and isooctane solvents, as reported previously [11,12]. The fibrous structure (Figure 1a,b) is composed of individual, uniform and randomly oriented fibers with average diameters of $15.74 \pm 4.68 \mu\text{m}$ and $4.51 \pm 1.27 \mu\text{m}$ for limonene and isooctane, respectively.

The higher average diameter of electrospun asolectin phospholipid using limonene as solvent in comparison with isooctane is related to the dielectric constant (ϵ solvent) and the evaporation point (Bp solvent) of the solvents. Limonene has a higher evaporation point and dielectric constant (176 °C; 2.3) compared to isooctane (99 °C, 1.92), thus slower evaporation takes place resulting in fibers with higher average diameter as discussed in our previous studies [11].

Electrospun phospholipid fibers loaded with vanillin and curcumin were also developed with average diameters of $20.36 \pm 5.4.5 \mu\text{m}$ and $4.42 \pm 1.71 \mu\text{m}$, respectively (Figure 1c,d). The inclusion of

vanillin and curcumin on phospholipid solutions did not significantly change the morphology of electrospun phospholipid fibers, suggesting that the bioactives were efficiently encapsulated and well distributed within the microfibers. The increase in fiber diameter after encapsulation of bioactives within electrospun fibers has been well reported [13,36].

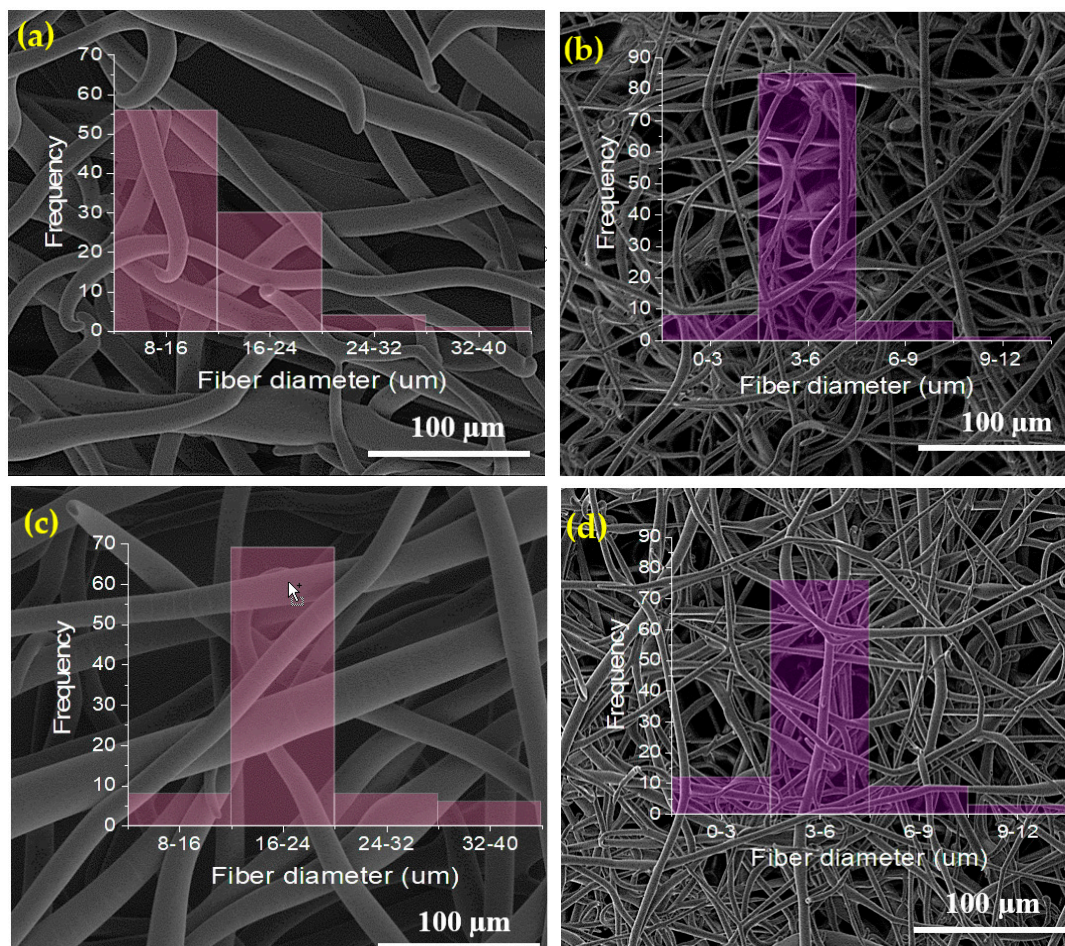


Figure 1. SEM images and corresponding histograms of the diameter distribution of electrospun phospholipid fibers prepared using limonene (a) and isooctane (b) as solvents encapsulating vanillin (c) and curcumin (d).

2.2. FTIR Analysis

Figure 2a,b shows the FTIR spectra of asolectin, vanillin, curcumin, asolectin electrospun fibers made with isooctane and limonene (controls) and asolectin fibers with encapsulated vanillin and curcumin, respectively. Table 1 lists the assigned peaks.

The FTIR spectrum of pure asolectin powder showed the peaks at 3000 and 2800 cm^{-1} corresponding to the C-H stretching of CH_2 groups, and the peaks at 1730 cm^{-1} and 1240 cm^{-1} corresponded to C=O stretching and PO_2^- groups, respectively (Figure 2a) [37]. The features for asolectin fibers remained the same as the pure asolectin powder before the electrospinning process in both solvents, suggesting that the electrospinning process and the solvents did not change the physico-chemical properties of asolectin.

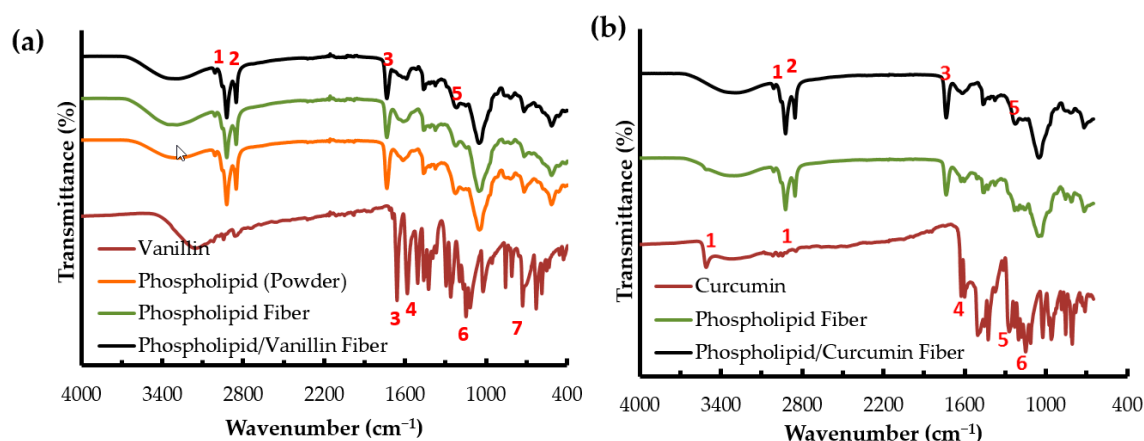


Figure 2. FTIR spectra of vanillin powder, asolectin powder, electrospun asolectin fiber and electrospun asolectin/vanillin fiber prepared using limonene (a) and curcumin powder, electrospun asolectin fiber and electrospun asolectin/curcumin fiber prepared using isooctane (b) as solvents. The red numbers in the figure are the assigned peaks listed in Table 1.

The FTIR spectrum of pure vanillin powder indicates characteristic peaks at 731, 1510 and 1590 cm^{-1} which correspond to the stretching vibration absorption of the benzene ring. The peak at 1660 cm^{-1} is attributed to the stretching vibration of C=O of the aldehyde group [38]. Also, the peak at 1150 cm^{-1} shows the presence of ether groups in pure vanillin (Figure 2a) [23,39].

For curcumin, the bands observed at 3085–3552 cm^{-1} , 1601 cm^{-1} , 1273 cm^{-1} , and 1152 cm^{-1} are respectively attributed to the phenolic O-H stretching, stretching vibrations of the benzene ring, aromatic C-O stretching and C-O-C stretching modes (Figure 2b) [24].

The FTIR spectra of electrospun asolectin fibers loaded with both vanillin and curcumin showed the same main peaks; therefore, it is assumed that both phenolic compounds were efficiently loaded within asolectin fibers and no interactions between the bioactives and the matrix occurred.

Table 1. IR peak assignment of the electrospun phospholipid (Phos) fibers.

Peak Number	Group Frequency (cm^{-1})							Assignment
	Vanillin Powder	Curcumin Powder	Phos Powder	Phos (Limonene) Fiber	Phos (Isooctane) Fiber	Phos/Vanillin Fiber	Phos/Curcumin Fiber	
1	-	3085–3552	3001	3000	3000	3000	3000	phenolic O-H stretching
2	-	-	2920 2850	2922 2852	2930 2859	2908 2847	2923 2853	C-H stretching of CH_2 groups
3	1660	-	1730	1735	1746	1725	1740	C=O stretching of carbonyl groups
4	1590 1510	1601	-	-	-	-	-	stretching vibrations of the benzene ring
5	-	1273	1240	1230	1243	1205	1229	PO_2^- groups; aromatic C-O stretching
6	1150	1152	-	-	-	-	-	C-O-C stretching
7	731	-	-	-	-	-	-	stretching vibrations of the benzene ring

2.3. Encapsulation Efficiency (EE)

The encapsulation efficiency of vanillin and curcumin within asolectin microfibers was found to be of $85.23 \pm 1.19\%$ and $96.39 \pm 2.81\%$, respectively. The relatively high encapsulation efficiency is related to the high solubility of vanillin and curcumin in limonene and isooctane, respectively. Consequently, the bioactives could be efficiently dispersed within the fibers and well encapsulated.

The encapsulation efficiency of vanillin using electrospun almond gum/polyvinyl alcohol (PVA) composite nanofibers was reported to range from 68% to 75% for vanillin concentrations of 1% to 3% (*w/w*) respectively [40]. The EE of vanillin loaded within microcapsules of spray dried soy protein isolate/maltodextrin was 58.3% [41].

The EE of curcumin encapsulated within cellulose acetate electrospun fibers at concentrations of 5, 10, 15, and 20% *w/v* was reported to be of $101.9 \pm 0.8\%$, $95.6 \pm 2.5\%$, $91.4 \pm 0.4\%$, and $90.8 \pm 0.4\%$, respectively [34]. In another study, the EE of curcumin within liposomes was determined to range from $80.77 \pm 4.12\%$ to $82.32 \pm 3.91\%$ [42].

2.4. Total Antioxidant Capacity (TAC) Assay

Figure 3 presents the effect of storage conditions (time, temperature and pressure) on the total antioxidant capacity of the both asolectin fibers with and without phenolic compounds. TAC was measured through the formation of the phosphomolybdenum complex and the reduction of Mo (VI) to Mo (V) by the antioxidant components in the phospholipid and phospholipid/bioactive specimens [34]. Several methods are available to measure the antioxidant capacity of food and biological systems [43,44]. The phosphomolybdenum method is used for extensive screening of the total antioxidant capacity of samples of very different origins and composition (hydrophobic and hydrophilic) from natural sources [45]. This is a simple low-cost method [46,47] and has been utilized for the determination of the antioxidant capacity of various compounds such as vitamin E [45], quercetin [29], curcumin [48], and flavonoid fractions of *Pistacia atlantica* fruit [43].

Electrospun asolectin fibers produced using limonene exhibited antioxidant capacity ranging from 76 to 89 μg Galic Acid Equivalent/mg of microfibers ($\mu\text{gGAE}/\text{mg}$) for samples stored at 4 °C, and from 75 to 86 $\mu\text{gGAE}/\text{mg}$ when stored at ambient temperature (Figure 3). Similarly, the TAC determined for asolectin fibers prepared using isooctane ranged from 76 to 80 $\mu\text{gGAE}/\text{mg}$ (4 °C) and from 71 to 80 $\mu\text{gGAE}/\text{mg}$ (ambient temperature). These data suggested that the solvent does not play a significant role in TAC of phospholipid fibers. It is noteworthy that the slight differences of the TAC values of the (control) asolectin fibers prepared using limonene or isooctane as solvents, are related to the differences of the molecular mass of the solvents that has to be considered when using this analytical method. Phospholipids are known for their antioxidant properties [18,19,49] and asolectin that contains lecithin, cephalin and other phospholipids display antioxidant activity, as demonstrated previously [16,17].

For pure vanillin and curcumin powders (non-encapsulated), a decrease in TAC was observed over 15 days of storage. The TAC of vanillin stored at 4 °C was decreased by 23 (low pressure) and 25% (ambient pressure) from day 1 to day 15. At ambient temperature, the TAC of vanillin stored at low pressure and ambient pressure decreased by 30% and 26% respectively from 1 to day 15. After 15 days, curcumin stored at 4 °C was observed to significantly decrease its TAC to about 28% and 44% when stored at low pressure and ambient pressure, respectively. At room temperature non-encapsulated curcumin lost around 38% (at low pressure) and 33% (at room pressure) of its total antioxidant capacity from day 1 to day 15. Curcumin is a bioactive susceptible to oxidation [16] and its stability is known to be negatively affected by oxygen exposure [25,26].

However, after encapsulation of phenolic compounds, the TAC of asolectin fibers loaded with both curcumin and vanillin was found to be constant over time (Figure 3), suggesting that the antioxidant stability of the compounds can be maintained. Moreover, an increase in TAC was observed for fibers loaded with curcumin and vanillin, suggesting an improvement of antioxidant activity due to the combination of phospholipids with phenolic compounds. This is in accordance with previous studies

where an improvement of TAC was confirmed by synergistic interactions of lecithins with other phenolic compounds such as tocopherols [17,50].

Previous studies showed that encapsulated curcumin could retain higher antioxidant stability in lecithin (antioxidant) stabilized emulsions compared to curcumin in Tween 20 (non-antioxidant) stabilized emulsions. The higher antioxidant activity of emulsifier could significantly lower the rate of radical permeation and consequently reduce the rate of oxidation of the encapsulated curcumin [16]. Figure 3 shows the TAC of curcumin/asolectin and curcumin/vanillin fibers over 15 days. The TAC assay was also conducted for 45 days and no evidence of reduction of TAC was observed (data not shown), suggesting that the phospholipids fibers and phospholipids/phenolic compounds fibers preserve their antioxidant activity for extended periods of time.

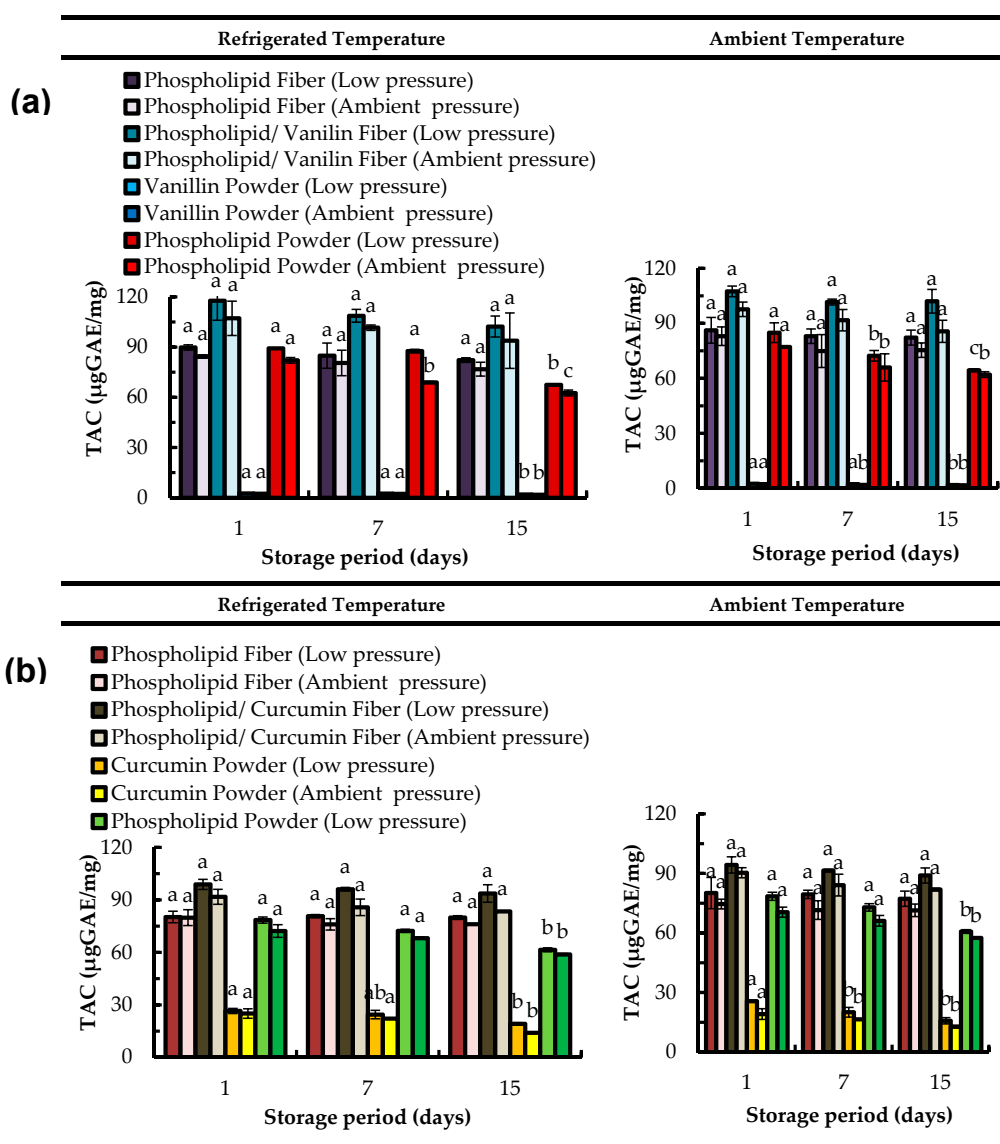


Figure 3. Total antioxidant capacity (TAC) over time of electrosun phospholipid fibers prepared using limonene (top graphs (a)) and isoctane (bottom graphs (b)) as solvent; Data are represented as mean \pm SD [N = 3]; a–c: significant difference at $p \leq 0.05$ in terms of total antioxidant capacity of each storage condition during storage time.

Antioxidant activity of phenolic compounds is known to be affected by the presence of oxygen and temperature. Figure 3 shows that no significant differences were observed for the TAC when

microfibers-bioactives were stored at different temperatures (refrigerated, ambient) and pressures (vacuum, ambient pressure). However, the most favorable storage conditions for both curcumin and vanillin loaded in electrospun asolectin fibers were refrigerated temperature and low pressure, as slightly higher TAC values were determined.

The total phenolic content (TPC) within the fibers over time was also determined based on the electron transfer from phospholipid and phospholipid/bioactive specimens to the complexed Mo (IV) present in the Folin–Ciocalteu reagent [51,52] (Figure 4). Similar to TAC (Figure 3), the total phenolic content was not changed significantly over time for the phenolics encapsulated within electrospun phospholipid fibers. However, for the non-encapsulated curcumin, a reduction of TPC by 40% from day 1 to day 15 was determined when this bioactive was stored in ambient pressure and refrigerated temperature (11.9 $\mu\text{gGAE}/\text{mg}$). The encapsulated curcumin displayed a TPC of 24.5 $\mu\text{gGAE}/\text{mg}$ for the same storage conditions.

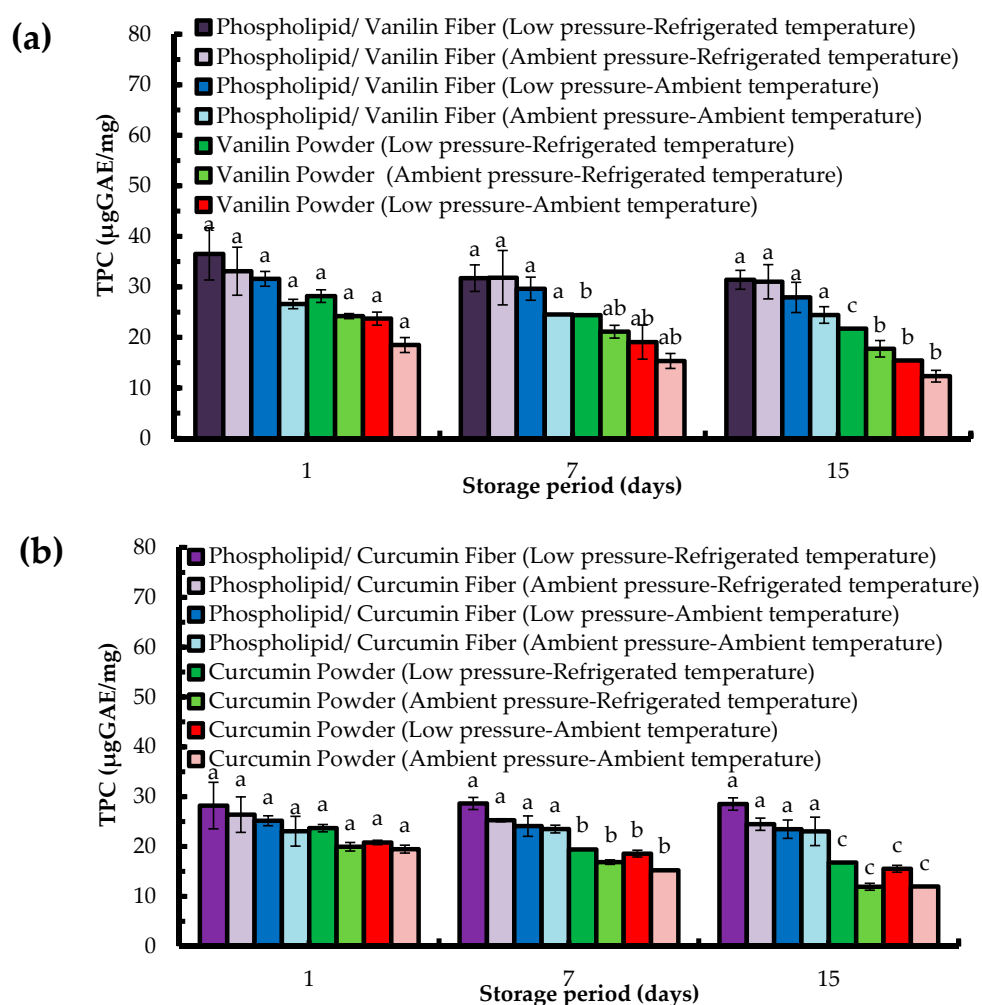


Figure 4. Total phenolic content (TPC) over time of electrospun phospholipid fibers prepared using limonene (a) and isooctan (b) as solvents; Data are represented as mean \pm SD [N = 3]; a–c: significant difference at $p \leq 0.05$ in terms of total phenolic content of each storage condition during storage time.

The TPC of non-encapsulated vanillin was observed to decrease by about 35% when this compound was stored at reduced pressure and room temperature, reaching the values of 15 $\mu\text{gGAE}/\text{mg}$ after 15 days. The encapsulated vanillin stored at reduced pressure and room temperature exhibited a TPC of 28 $\mu\text{gGAE}/\text{mg}$ (Figure 4).

Hence, TAC and TPC data demonstrate the potential of asolectin fibers to be used as antioxidant systems as well as efficient matrices for the encapsulation of phenolic compounds. Cases of preservation of TPC within electrospun fibers have been reported [53–55].

2.5. Stability of Phenolic Compounds Test under Storage by $^1\text{H-NMR}$

The composition of the electrospun asolectin fibers with encapsulated curcumin or vanillin was analyzed using $^1\text{H-NMR}$ spectroscopy. The chemical stability of vanillin and curcumin and the retention of these encapsulated phenolic compounds in the fibers upon storage were monitored. $^1\text{H-NMR}$ spectra of the fibers in $\text{DMSO-}d_6$ solution were obtained after increasing storage times at room temperature ranging from 1 day to 30 days (Figure 5). Figure 5a(i),b(i) shows the assigned $^1\text{H-NMR}$ spectra of vanillin and curcumin as references. Figure 5a(ii),b(ii) shows the spectra for each fiber after 1 day of storage. In the region 0.5–3 ppm, several peaks corresponding to the aliphatic tails of the phospholipids can be seen. Highlighted in red are the peaks corresponding to the phenolic compounds. After 30 days of storage (Figure 5a(iii),b(iii)), the spectra have not altered. This suggests that not only are the encapsulated curcumin and vanillin chemically stable over the 30 days storage time, but the concentration of encapsulated phenolic compounds does not decrease under the storage conditions. This finding is in agreement with the total phenolic content data (TPC) measured at room temperature and pressure (Figure 3), suggesting that asolectin fibers were effective matrices to prolong the stability of vanillin and curcumin.

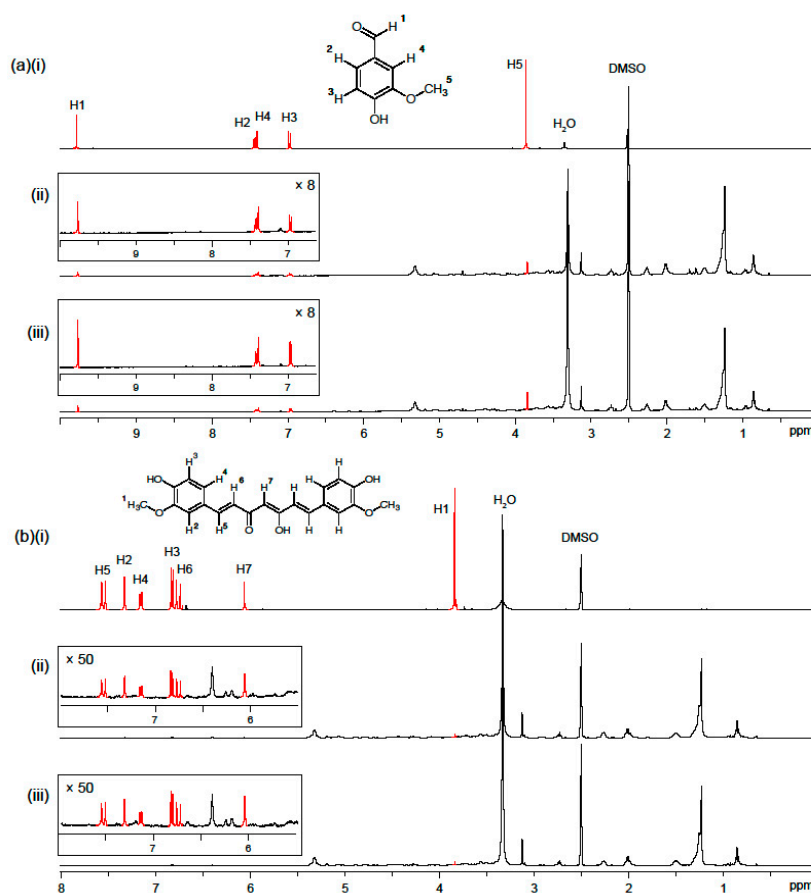


Figure 5. $^1\text{H-NMR}$ spectra (298 K, 400 MHz) in $\text{DMSO-}d_6$ of vanillin (a(i)) and curcumin (b(i)); and electrospun phospholipid fibers with encapsulated vanillin and curcumin analyzed at different storage times: (ii) 1 day and (iii) 30 days.

2.6. In Vitro Release Study

The release profiles at 37 °C of vanillin and curcumin from asolectin microfibers are shown in Figure 6. For both vanillin and curcumin, a steady increase in the release of the bioactives was observed up to 240 min. At this time, the released amount of vanillin was 95% while the released amount of curcumin was 70%. From 240 to 300 min, only a slight increase of the released bioactives was observed.

The lower percentage of released curcumin compared to vanillin could be attributed to its hydrophobic nature. Similar curcumin release profiles showing a steady increase of curcumin released from electrospun nanofibers, produced using chitosan/phospholipid [13], blends of amaranth protein isolate (API)/pullulan [33] and PLGA copolymer solutions [56] have been reported. On the other hand, a higher percentage of release (near 100%) of vanillin from almond gum/polyvinyl alcohol (PVA) electrospun fibers has been observed in aqueous media, due to the higher solubility and higher swelling degree of almond gum/PVA/vanillin nanofiber in distilled water [40].

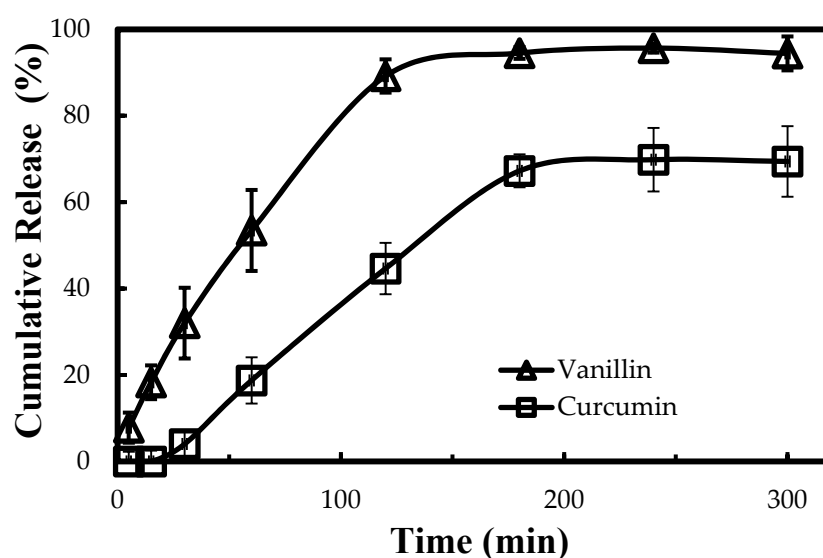


Figure 6. Cumulative release of vanillin and curcumin from phospholipid fibers into phosphate buffered saline (PBS), pH = 7.6 (n = 3). The error bars in the figure represent the standard deviation (SD).

The release mechanism of the phenolic compounds from electrospun asolectin fibers was analyzed using the Korsmeyer–Peppas model [57]. This model concerns the release of drugs from cylindrical structures and predicts whether the release of the compound from a matrix follows Fickian diffusion, through determination of the coefficient “n” estimated from linear regression of the log(Cumulative Release) as a function of log(Time). The “n” determined from both release curves was above 0.45, with a correlation value (R^2) of 0.98 and 0.99 for vanillin and curcumin respectively, suggesting that the release mechanism of both bioactives was mainly due to the swelling of the phospholipid fibers that influenced the release of bioactives. Wongsasulak and co-authors [58] also reported that the swelling of the matrix (electrospun polymers of zein, poly(ethylene oxide), and chitosan) triggered the release of the bioactive (α -tocopherol) according to Korsmeyer–Peppas model. To confirm the changes in morphology of phospholipid fibers after immersion in PBS, Environmental SEM (ESEM) photographs were taken at different time points of immersion (Figure 7). After one hour in PBS, fibers were observed to slightly increase their diameter as a result of the swelling of the matrix. At the end of 2 h, the progressive water absorption was observed (Figure 7c) resulting in the loss of fibril-like shape, that was further observed at the end of 4 hours of immersion in PBS (Figure 7d). It is to be noted that a previous study suggested that electrospun phospholipid scaffolds, made from lethicin solutions, lack physical stability as a consequence of hydration and further breakdown of fibril-like structures in the presence of moisture [59].

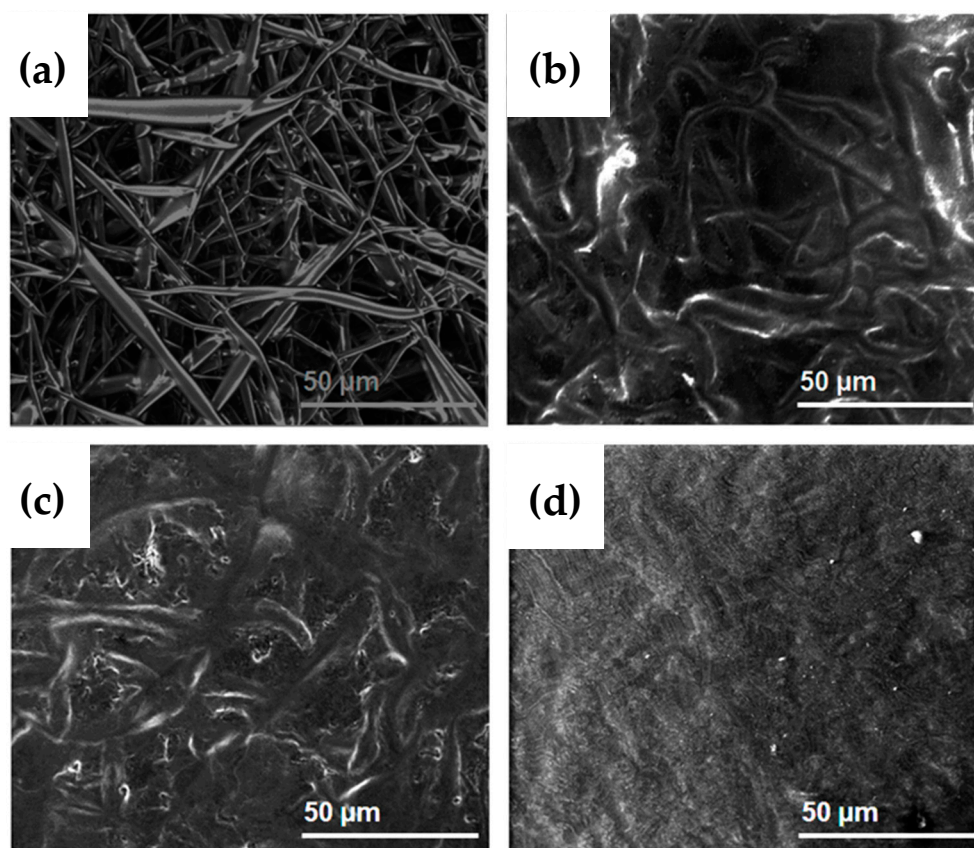


Figure 7. Environmental SEM (ESEM) images of electrospun asolectin microfiber fibers (a); showing its morphology after immersion in PBS for 1 h (b); 2 h (c) and 4 h (d).

Yu and co-authors reported the fabrication of electrospun composite fibers made of polyvinylpyrrolidone (PVP) and soybean lecithin [27] and observed the collapse of composite fibers after contact with water within less than one minute as a result of changes in the hydrophilic/hydrophobic nature. Our system was observed to last longer which allowed the sustained release of encapsulated bioactives for 360 min (Figure 6).

3. Materials and Methods

3.1. Materials

Asolectin from soybean (Sigma-Aldrich product nr: 11145, lot nr: BCB66221V) was used as received. It contains approximately lecithin (25–33%), cephalin and phosphatidylinositol, saturated fatty acids (24%), mono-unsaturated (14%) and poly-unsaturated fatty acids (62%). Methyl-4-(1-methylethenyl)-cyclohexene (limonene), isooctane, curcumin and vanillin were obtained from Sigma-Aldrich and used as received without further purification.

3.2. Preparation of Electrospinning Solutions

A total of 60% (*wt/wt*) asolectin phospholipid was dissolved in limonene and isooctane at room temperature and then, vanillin (3%, *wt/v*) or curcumin (0.5% *wt/v*) were added, respectively, and stirred for 15 min before electrospinning processing. Solutions of 60% (*wt/wt*) asolectin were also prepared in both limonene and isooctane without phenolic compounds. Isooctane and Limonene were selected as solvents due to their capability produce electrospun phospholipid fibers [11] and to dissolve curcumin and vanillin, respectively.

3.3. Electrospinning Processing

The electrospinning setup included a high voltage generator (ES50P-10W, Gamma High Voltage Research, Inc., Ormond Beach, FL, USA) to provide a voltage of 21 kV, and syringe pump (New Era Pump Systems, Inc., Farmingdale, NJ, USA) to feed the solutions at a flow rate of 0.01 mL/min. Phospholipids fibers were collected on a steel plate covered with aluminium foil placed at a distance of 10 cm from the end of the needle. A blunt end stainless steel needle (Proto Advantage, Ancaster, ON, Canada) with inner diameters between 0.8 mm to 0.4 mm was used. The electrospinning process was carried out at ambient conditions.

3.4. Morphology

The morphology of the electrospun phospholipid, phospholipid/vanillin and phospholipid/curcumin fibers was investigated using a Quanta FEG 3D scanning electron microscope (SEM). Samples were attached on metal stubs with double-sided adhesive carbon tape and coated with 6 nm of gold for better conductivity using a sputter coater (Leica Coater ACE 200). The average fiber diameter was calculated using image J analysis software (National Institutes of Health, MD, USA) measured at 100 different points for each image. Changes in morphology of electrospun phospholipid fibers were further monitored after contact in PBS by Environmental SEM (ESEM). Samples were mounted on aluminium stubs and placed upside down immersed in PBS for 1, 2 and 4 h prior to the visualization in the Quanta FEG 3D SEM.

3.5. Fourier Transform Infrared (FTIR) Spectroscopy

FTIR spectra in the transmission mode were recorded using a Perkin 124 Elmer Spectrum 100 spectrometer based on a Universal Attenuated Total Reflectance sensor 125 (UATR-FTIR). The infrared peaks were identified using Spectrum™ 10 software using 1 %T peak threshold. Spectra were plotted as percentage transmittance (%T) against wavenumber (cm^{-1}).

3.6. Encapsulation Efficiency

The encapsulation efficiency of the phenolic compounds (vanillin and curcumin) in asolectin fibers was determined by extracting the bioactives from the fibers using water and ethanol in a sonication bath for 30 min prior to centrifugation at 4500 rpm for 15 min. The concentration of bioactives in the supernatant was determined using a UV-Vis spectrophotometer (U-1500, Hitachi, Tokyo, Japan), where absorbance of vanillin and curcumin were measured at wavelengths of 280 nm and 425 nm, respectively. Standard curves for vanillin and curcumin were prepared with concentrations ranging from 0–100 $\mu\text{g}/\text{mL}$. Encapsulation efficiency was calculated using the following Equation (1):

$$\% \text{ Encapsulation Efficiency} = \frac{\text{Phenolic compounds (encapsulated)}}{\text{Phenolic compounds (total)}} \times 100 \quad (1)$$

3.7. Total Antioxidant Capacity Assay (TAC)

Antioxidant capacities of phospholipid powder, vanillin powder, curcumin powder, phospholipid fibers, phospholipid/vanillin fibers and phospholipid/curcumin fibers were evaluated by the method of Jayaprakasha et al., 2006 [48]. Asolectin fibers (with and without phenolic compounds) were stored at different pressures (ambient and vacuum) and temperatures (refrigerated 4 °C and room temperature) and their TAC was evaluated after 1, 7 and 15 days storage. An amount of 300 μL of diluted extracted solution prepared in methanol was added to an Eppendorf tube containing 3 mL reagent solution (0.6 M sulfuric acid, 28 mM sodium phosphate and 4 mM ammonium molybdate). The Eppendorf tubes were capped and incubated in a water bath at 95 °C for 90 min. Then, samples were cooled to room temperature and the absorbance of each sample was measured at 695 nm against

a blank (1 mL of reagent solution and the appropriate volume of the same solvent used for the sample). Gallic acid was used as the reference.

3.8. Total Phenolic Content (TPC)

The total phenolic content of the stored samples at different pressures (ambient and vacuum) and temperatures (refrigerated at 4 °C and room temperature) were determined via a modified Folin–Ciocalteu method [51] for 1, 7, 15 and 45 days of their storage. Briefly, 0.3 mL of diluted extract solution (5 mg/mL) was mixed with 0.6 mL of deionized water and 0.5 mL of Folin–Ciocalteu reagent in a test tube and then 1.5 mL of 20% sodium carbonate aqueous solution was added and the volume was made up to 10 mL with deionized water. The samples were incubated for 30 min at room temperature in darkness and then absorbance measured at 760 nm using a UV–Vis spectrophotometer (U-1500, Hitachi, Tokyo, Japan). The determination of the phenolic content was obtained by using gallic acid as a standard.

3.9. Stability of Phenolic Compounds Test under Storage by $^1\text{H-NMR}$ Spectroscopy

Asolectin, asolectin/vanillin and asolectin/curcumin fibers were stored in ambient conditions at room temperature in the laboratory for 30 days. After 1, 15 and 30 days of storage, small samples of fibers were analyzed by $^1\text{H-NMR}$ spectroscopy (400 MHz NMR spectrometer, Bruker, Billerica, MA, USA) at 298 K in order to compare the amount of the remaining phenolic compounds in the samples during storage time. Samples for $^1\text{H-NMR}$ spectroscopic analysis were prepared in $\text{DMSO-}d_6$ at a concentration of 10 mg/mL. The samples were alternatively sonicated and heated in closed vials with a heat gun in order to dissolve the material. $^1\text{H-NMR}$ spectra of vanillin and curcumin were recorded as references.

3.10. In Vitro Release Study

The in vitro release of phenolic compounds from asolectin fibers was determined by UV–Vis spectroscopy [13]. Briefly, asolectin fibers (15 mg) were included in dialysis bags (SpectraLab with a MWCO 6–8 kDa) that were further sealed and placed into 20 mL phosphate buffer saline (pH~7.4) in a test tube in a shaking water bath at 37 °C for 360 min. The 2-mL samples were collected at each interval time point and replaced by fresh media (PBS, 2 mL). The amount of phenolic compounds released in the supernatant was determined afterwards using a UV–Vis spectrophotometer (U-1500, Hitachi, Tokyo, Japan) at optical wavelengths of 280 and 425 nm for vanillin and curcumin, respectively. A calibration curve of phenolic compounds in phosphate buffer saline (pH~7.4) was constructed with a concentration range from 0–100 $\mu\text{g/mL}$. The experiments were performed in triplicate and the results were reported as average values \pm standard deviation.

The mechanism of release was investigated following the Korsmeyer–Peppas model:

$$\frac{M_t}{M_\infty} = kt^n \quad (2)$$

where M_t/M_∞ is the fraction of drug released at time t , k is the rate constant and n is the release exponent. If $n \leq 0.45$, the release mechanism follows a Fickian diffusion and for $0.45 < n < 0.89$ the drug release follows a non-Fickian diffusion (anomalous transport) [35].

3.11. Statistical Analysis

Presented results are an average of at least three independent experiments and are presented as mean \pm standard deviation. The results were analyzed with one-way ANOVA using Fisher's test in Minitab software version 16 (Minitab Inc., State College, PA, USA). The significant differences between samples were considered at a significance level of $p \leq 0.05$.

4. Conclusions

In this study, electrospun phospholipid (asolectin) microfibers were investigated as encapsulation and antioxidant matrices for phenolic compounds, such as vanillin and curcumin. Asolectin fibers were observed to have antioxidant properties. Such antioxidant properties were improved after the encapsulation of the phenolic compounds, as observed from TAC and TPC assays. The antioxidant capacity of curcumin/phospholipid and vanillin/phospholipid microfibers was observed to remain stable over time at different temperatures (refrigerated, ambient) and pressures (vacuum, ambient), while the pristine non-encapsulated phenolic compounds decreased their TAC and TPC values. Moreover, the phospholipid matrix permitted the release of both curcumin and vanillin upon aqueous emersion, mainly due to the swelling of the phospholipid fibers that triggered the diffusion of bioactives. The above studies confirm the efficacy of electrospun phospholipid microfibers as encapsulation and antioxidant systems.

Acknowledgments: The authors are grateful to Hamed Safafar for fruitful discussions about antioxidant capacity of phospholipid fibers.

Author Contributions: A.C.M. and I.S.C. conceived and designed the experiments; E.S., A.C.M., V.B., S.R.B. performed the experiments; E.S., A.C.M., V.B., S.R.B., I.S.C. analyzed the data and wrote the manuscript.

Conflicts of Interest: The authors declare no conflict of interest.

References

1. Gosangari, S.L.; Watkin, K.L. Effect of preparation techniques on the properties of curcumin liposomes: Characterization of size, release and cytotoxicity on a squamous oral carcinoma cell line. *Pharm. Dev. Technol.* **2012**, *17*, 103–109. [[CrossRef](#)] [[PubMed](#)]
2. Maria, A.; Maria, B.; Sinico, C.; Sapienza, L.; Moro, P.A. Phospholipid-detergent systems: Effects of polysorbates on the release of liposomal caffeine. *Farmaco* **1998**, *53*, 650–654.
3. Shazly, G.; Nawroth, T.; Langguth, P. Comparison of dialysis and dispersion methods for in vitro release determination of drugs from multilamellar liposomes. *Dissolut. Technol.* **2008**, *15*, 7–10. [[CrossRef](#)]
4. Hühn, E.; Buchholz, H.-G.; Shazly, G.; Maus, S.; Thews, O.; Bausbacher, N.; Rösch, F.; Schreckenberger, M.; Langguth, P. Predicting the in vivo release from a liposomal formulation by IVIVC and non-invasive positron emission tomography imaging. *Eur. J. Pharm. Sci.* **2010**, *41*, 71–77. [[CrossRef](#)] [[PubMed](#)]
5. Huynh, N.T.; Passirani, C.; Saulnier, P.; Benoit, J.P. Lipid nanocapsules: A new platform for nanomedicine. *Int. J. Pharm.* **2009**, *379*, 201–209. [[CrossRef](#)] [[PubMed](#)]
6. Mendes, A.C.; Baran, E.T.; Reis, R.L.; Azevedo, H.S. Fabrication of phospholipid-xanthan microcapsules by combining microfluidics with self-assembly. *Acta Biomater.* **2013**, *9*, 6675–6685. [[CrossRef](#)] [[PubMed](#)]
7. Taylor, T.M.; Weiss, J.; Davidson, P.M.; Bruce, B.D. Liposomal nanocapsules in food science and agriculture. *Crit. Rev. Food Sci. Nutr.* **2005**, *45*, 587–605. [[CrossRef](#)] [[PubMed](#)]
8. Mouritsen, O.G. *Life—As A Matter of Fat: The Emerging Science of Lipidomics*; Springer: Heidelberg, Germany, 2005; ISBN 3540232486.
9. Mouritsen, O.G. Lipids, curvature, and nano-medicine. *Eur. J. Lipid Sci. Technol.* **2011**, *113*, 1174–1187. [[CrossRef](#)] [[PubMed](#)]
10. McKee, M.G.; Layman, J.M.; Cashion, M.P.; Long, T.E. Phospholipid nonwoven electrospun membranes. *Science* **2006**, *311*, 353–355. [[CrossRef](#)] [[PubMed](#)]
11. Jørgensen, L.; Qvortrup, K.; Chronakis, I.S. Phospholipid electrospun nanofibers: Effect of solvents and co-axial processing on morphology and fiber diameter. *RSC Adv.* **2015**, *5*, 53644–53652. [[CrossRef](#)]
12. Mendes, A.C.; Nikogeorgos, N.; Lee, S.; Chronakis, I.S. Nanomechanics of Electrospun Phospholipid Fiber. *Appl. Phys. Lett.* **2015**, *106*. [[CrossRef](#)]
13. Mendes, A.C.; Gorzelanny, C.; Halter, N.; Schneider, S.W.; Chronakis, I.S. Hybrid electrospun chitosan-phospholipids nanofibers for transdermal drug delivery. *Int. J. Pharm.* **2016**, *510*, 48–56. [[CrossRef](#)] [[PubMed](#)]

14. Mendes, A.C.; Shekarforoush, E.; Engwer, C.; Beeren, S.R.; Gorzelanny, C.; Goycoolea, F.M.; Chronakis, I.S. Co-assembly of chitosan and phospholipids into hybrid hydrogels. *Pure Appl. Chem.* **2016**, *88*, 905–916. [[CrossRef](#)]
15. De Sousa, R.S.; de Moraes Nogueira, A.O.; Marques, V.G.; Clementin, R.M.; de Lima, V.R. Effects of α -eleostearic acid on asolectin liposomes dynamics: Relevance to its antioxidant activity. *Bioorg. Chem.* **2013**, *51*, 8–15. [[CrossRef](#)] [[PubMed](#)]
16. Pan, Y.; Tikekar, R.V.; Nitin, N. Effect of antioxidant properties of lecithin emulsifier on oxidative stability of encapsulated bioactive compounds. *Int. J. Pharm.* **2013**, *450*, 129–137. [[CrossRef](#)] [[PubMed](#)]
17. Judde, A.; Villeneuve, P.; Rossignol-Castera, A.; Guillou, A. Antioxidant effect of soy lecithins on vegetable oil stability and their synergism with tocopherols. *J. Am. Oil Chem. Soc.* **2003**, *80*, 1209–1215. [[CrossRef](#)]
18. Cui, L.; Decker, E.A. Phospholipids in foods: Prooxidants or antioxidants? *J. Sci. Food Agric.* **2016**, *96*, 18–31. [[CrossRef](#)] [[PubMed](#)]
19. Choe, E.; Min, D.B. Mechanisms of Antioxidants in the Oxidation of Foods. *Compr. Rev. Food Sci. Food Saf.* **2009**, *8*, 345–358. [[CrossRef](#)]
20. Doert, M.; Jaworska, K.; Moersel, J.T.; Kroh, L.W. Synergistic effect of lecithins for tocopherols: Lecithin-based regeneration of α -tocopherol. *Eur. Food Res. Technol.* **2012**, *235*, 915–928. [[CrossRef](#)]
21. Brewer, M.S. Natural Antioxidants: Sources, Compounds, Mechanisms of Action, and Potential Applications. *Compr. Rev. Food Sci. Food Saf.* **2011**, *10*, 221–247. [[CrossRef](#)]
22. Celebioglu, A.; Kayaci-Senirmak, F.; Kusku, S.I.; Durgun, E.; Uyar, T. Polymer-free nanofibers from vanillin/cyclodextrin inclusion complexes: High thermal stability, enhanced solubility and antioxidant property. *Food Funct.* **2016**. [[CrossRef](#)] [[PubMed](#)]
23. Hundre, S.Y.; Karthik, P.; Anandharamkrishnan, C. Effect of whey protein isolate and β -cyclodextrin wall systems on stability of microencapsulated vanillin by spray-freeze drying method. *Food Chem.* **2015**, *174*, 16–24. [[CrossRef](#)] [[PubMed](#)]
24. Sun, X.Z.; Williams, G.R.; Hou, X.X.; Zhu, L.M. Electrospun curcumin-loaded fibers with potential biomedical applications. *Carbohydr. Polym.* **2013**, *94*, 147–153. [[CrossRef](#)] [[PubMed](#)]
25. Kharat, M.; Du, Z.; Zhang, G.; McClements, D.J. Physical and chemical stability of curcumin in aqueous solutions and emulsions: Impact of pH, temperature, and molecular environment. *J. Agric. Food Chem.* **2017**. [[CrossRef](#)] [[PubMed](#)]
26. Price, L.C.; Buescher, R.W. Decomposition of turmeric curcuminoids as affected by light, solvent and oxygen. *J. Food Biochem.* **1996**, *20*, 125–133. [[CrossRef](#)]
27. Mendes, A.C.; Stephansen, K.; Chronakis, I.S. Electrospinning of food proteins and polysaccharides. *Food Hydrocoll.* **2017**, *68*, 53–68. [[CrossRef](#)]
28. Yu, D.-G.; Branford-White, C.; Williams, G.R.; Blich, S.W.A.; White, K.; Zhu, L.-M.; Chatterton, N.P. Self-assembled liposomes from amphiphilic electrospun nanofibers. *Soft Matter* **2011**, *7*, 8239. [[CrossRef](#)]
29. Zhang, J.; Cohn, C.; Qiu, W.; Zha, Z.; Dai, Z.; Wu, X. Atomic force microscopy of electrospun organic-inorganic lipid nanofibers. *Appl. Phys. Lett.* **2011**, *99*, 103702. [[CrossRef](#)] [[PubMed](#)]
30. Mai, T.T.T.; Nguyen, T.T.T.; Le, Q.D.; Nguyen, T.N.; Ba, T.C.; Nguyen, H.B.; Phan, T.B.H.; Tran, D.L.; Nguyen, X.P.; Park, J.S. A novel nanofiber Cur-loaded polylactic acid constructed by electrospinning. *Adv. Nat. Sci. Nanosci. Nanotechnol.* **2012**, *3*, 25014. [[CrossRef](#)]
31. Dhurai, B.; Saraswathy, N.; Maheswaran, R.; Sethupathi, P.; Vanitha, P.; Vigneshwaran, S.; Rameshbabu, V. Electrospinning of curcumin loaded chitosan/poly (lactic acid) nanofilm and evaluation of its medicinal characteristics. *Front. Mater. Sci.* **2013**, *7*, 350–361. [[CrossRef](#)]
32. Wang, C.; Ma, C.; Wu, Z.; Liang, H.; Yan, P.; Song, J.; Ma, N.; Zhao, Q. Enhanced Bioavailability and Anticancer Effect of Curcumin-Loaded Electrospun Nanofiber: In Vitro and In Vivo Study. *Nanoscale Res. Lett.* **2015**, *10*, 439. [[CrossRef](#)] [[PubMed](#)]
33. Blanco-Padilla, A.; Lopez-Rubio, A.; Loarca-Pina, G.; Gomez-Mascaraque, L.G.; Mendoza, S. Characterization, release and antioxidant activity of curcumin-loaded amaranth-pullulan electrospun fibers. *LWT Food Sci. Technol.* **2015**, *63*, 1137–1144. [[CrossRef](#)]
34. Suwanton, O.; Opanasopit, P.; Ruktanonchai, U.; Supaphol, P. Electrospun cellulose acetate fiber mats containing curcumin and release characteristic of the herbal substance. *Polymer* **2007**, *48*, 7546–7557. [[CrossRef](#)]

35. Kayaci, F.; Uyar, T. Encapsulation of vanillin/cyclodextrin inclusion complex in electrospun polyvinyl alcohol (PVA) nanowebs: Prolonged shelf-life and high temperature stability of vanillin. *Food Chem.* **2012**, *133*, 641–649. [[CrossRef](#)]
36. Kanawung, K.; Panitchanapan, K.; Puangmalee, S.; Utok, W.; Kreua-ongarjnucool, N.; Rangkupan, R.; Meechaisue, C.; Supaphol, P. Preparation and Characterization of Polycaprolactone/Diclofenac Sodium and Poly(vinyl alcohol)/Tetracycline Hydrochloride Fiber Mats and Their Release of the Model Drugs. *Polym. J.* **2007**, *39*, 369–378. [[CrossRef](#)]
37. Lopes De Azambuja, C.R.; Dos Santos, L.G.; Rodrigues, M.R.; Rodrigues, R.F.M.; Da Silveira, E.F.; Azambuja, J.H.; Flores, A.F.C.; Horn, A.P.; Dora, C.L.; Muccillo-Baisch, A.L.; et al. Physico-chemical characterization of asolectin-genistein liposomal system: An approach to analyze its in vitro antioxidant potential and effect in glioma cells viability. *Chem. Phys. Lipids* **2015**, *193*, 24–35. [[CrossRef](#)] [[PubMed](#)]
38. Peng, H.; Xiong, H.; Li, J.; Xie, M.; Liu, Y.; Bai, C.; Chen, L. Vanillin cross-linked chitosan microspheres for controlled release of resveratrol. *Food Chem.* **2010**, *121*, 23–28. [[CrossRef](#)]
39. Rezaei, A.; Tavanai, H.; Nasirpour, A. Fabrication of electrospun almond gum/PVA nanofibers as a thermostable delivery system for vanillin. *Int. J. Biol. Macromol.* **2016**, *91*, 536–543. [[CrossRef](#)] [[PubMed](#)]
40. Rezaei, A.; Nasirpour, A.; Tavanai, H.; Fathi, M. A study on the release kinetics and mechanisms of vanillin incorporated in almond gum/polyvinyl alcohol composite nanofibers in different aqueous food simulants and simulated saliva. *Flavour Fragr. J.* **2016**, *31*, 442–447. [[CrossRef](#)]
41. Noshad, M.; Mohebbi, M.; Koocheki, A.; Shahidi, F. Microencapsulation of vanillin by spray drying using soy protein isolate-maltodextrin as wall material. *Flavour Fragr. J.* **2015**, *30*, 387–391. [[CrossRef](#)]
42. Chen, Y.; Wu, Q.; Zhang, Z.; Yuan, L.; Liu, X.; Zhou, L. Preparation of curcumin-loaded liposomes and evaluation of their skin permeation and pharmacodynamics. *Molecules* **2012**, *17*, 5972–5987. [[CrossRef](#)] [[PubMed](#)]
43. Belyagoubi-Benhammou, N.; Belyagoubi, L.; El Zerey-Belaskri, A.; Atik-Bekkara, F. In vitro antioxidant properties of flavonoid fractions from *Pistacia atlantica* Desf. subsp. *atlantica* fruit using five techniques. *J. Mater. Environ. Sci.* **2015**, *6*, 1118–1125.
44. Ali, S.S.; Kasoju, N.; Luthra, A.; Singh, A.; Sharanabasava, H.; Sahu, A.; Bora, U. Indian medicinal herbs as sources of antioxidants. *Food Res. Int.* **2008**, *41*, 1–15. [[CrossRef](#)]
45. Prieto, P.; Pineda, M.; Aguilar, M. Spectrophotometric quantitation of antioxidant capacity through the formation of a phosphomolybdenum complex: Specific application to the determination of vitamin E. *Anal. Biochem.* **1999**, *269*, 337–341. [[CrossRef](#)] [[PubMed](#)]
46. Tusevski, O.; Kostovska, A.; Iloska, A.; Trajkovska, L.; Simic, S.G. Phenolic production and antioxidant properties of some Macedonian medicinal plants. *Cent. Eur. J. Biol.* **2014**, *9*, 888–900. [[CrossRef](#)]
47. Chevolleau, S.; Mallet, J.F.; Ucciani, E.; Gamisans, J.; Gruber, M. Antioxidant activity in leaves of some mediterranean plants. *J. Am. Oil Chem. Soc.* **1992**, *69*, 1269–1271. [[CrossRef](#)]
48. Jayaprakasha, G.K.; Jaganmohan Rao, L.; Sakariah, K.K. Antioxidant activities of curcumin, demethoxycurcumin and bisdemethoxycurcumin. *Food Chem.* **2006**, *98*, 720–724. [[CrossRef](#)]
49. Saito, H.; Ishihara, K. Antioxidant activity and active sites of phospholipids as antioxidants. *J. Am. Oil Chem. Soc.* **1997**, *74*, 1531–1536. [[CrossRef](#)]
50. Bandarra, N.M.; Campos, R.M.; Batista, I.; Nunes, M.L.; Empis, J.M. Antioxidant synergy of alpha-tocopherol and phospholipids. *J. Am. Oil Chem. Soc.* **1999**, *76*, 905–913. [[CrossRef](#)]
51. Safafar, H.; van Wagenen, J.; Møller, P.; Jacobsen, C. Carotenoids, phenolic compounds and tocopherols contribute to the antioxidative properties of some microalgae species grown on industrial wastewater. *Mar. Drugs* **2015**, *13*, 7339–7356. [[CrossRef](#)] [[PubMed](#)]
52. Tavassoli-Kafrani, E.; Goli, S.A.H.; Fathi, M. Fabrication and characterization of electrospun gelatin nanofibers crosslinked with oxidized phenolic compounds. *Int. J. Biol. Macromol.* **2017**, *103*, 1062–1068. [[CrossRef](#)] [[PubMed](#)]
53. Yakub, G.; Toncheva, A.; Manolova, N.; Rashkov, I.; Kussovski, V.; Danchev, D. Curcumin-loaded poly(L-lactide-co-D,L-lactide) electrospun fibers: Preparation and antioxidant, anticoagulant, and antibacterial properties. *J. Bioact. Compat. Polym.* **2014**, *29*, 607–627. [[CrossRef](#)]
54. Neo, Y.P.; Ray, S.; Jin, J.; Gizdavic-Nikolaidis, M.; Nieuwoudt, M.K.; Liu, D.; Quek, S.Y. Encapsulation of food grade antioxidant in natural biopolymer by electrospinning technique: A physicochemical study based on zein-gallic acid system. *Food Chem.* **2013**, *136*, 1013–1021. [[CrossRef](#)] [[PubMed](#)]

55. Aytac, Z.; Kusku, S.I.; Durgun, E.; Uyar, T. Encapsulation of gallic acid/cyclodextrin inclusion complex in electrospun polylactic acid nanofibers: Release behavior and antioxidant activity of gallic acid. *Mater. Sci. Eng. C* **2016**, *63*, 231–239. [[CrossRef](#)] [[PubMed](#)]
56. Sampath, M.; Lakra, R.; Korrapati, P.; Sengottuvelan, B. Curcumin loaded poly (lactic-co-glycolic) acid nanofiber for the treatment of carcinoma. *Colloids Surf. B Biointerfaces* **2014**, *117*, 128–134. [[CrossRef](#)] [[PubMed](#)]
57. Korsmeyer, R.W.; Gurny, R.; Doelker, E.; Buri, P.; Peppas, N.A. Mechanisms of solute release from porous hydrophilic polymers. *Int. J. Pharm.* **1983**, *15*, 25–35. [[CrossRef](#)]
58. Wongsasulak, S.; Pathumban, S.; Yoovidhya, T. Effect of entrapped α -tocopherol on mucoadhesivity and evaluation of the release, degradation, and swelling characteristics of zein-chitosan composite electrospun fibers. *J. Food Eng.* **2014**, *120*, 110–117. [[CrossRef](#)]
59. Hunley, M.T.; McKee, M.G.; Long, T.E. Submicron functional fibrous scaffolds based on electrospun phospholipids. *J. Mater. Chem.* **2007**, *17*, 605. [[CrossRef](#)]

Sample Availability: Not available.



© 2017 by the authors. Licensee MDPI, Basel, Switzerland. This article is an open access article distributed under the terms and conditions of the Creative Commons Attribution (CC BY) license (<http://creativecommons.org/licenses/by/4.0/>).

3.2. Part B– Hydrogel (Supporting paper)

3.2.1. Nanostructures as hydrogels made from co-assembly of chitosan and phospholipids-

Paper VI

Co-assembly of chitosan and phospholipids into hybrid hydrogels

Ana C. Mendes¹; Elhamalsadat Shekarforoush¹, Christoph Engwer², Sophie Beeren³, Christian Gorzelanny⁴, Francisco M. Goycoolea², Ioannis S. Chronakis¹

¹Nano-BioScience Research Group, DTU-Food, Technical University of Denmark, Søtofts plads 227, 2800 Kgs. Lyngby, Denmark.

²Institute for Biology and Biotechnology of Plants (IBBP), Westfälische Wilhelms-Universität Münster, Schlossgarten 3, 48149 Münster, Germany.

³Experimental Dermatology, Medical Faculty Mannheim, Heidelberg University, Theodor-Kutzer-Ufer 1-3, 68167 Mannheim, Germany.

⁴DTU-Chemistry, Technical University of Denmark, Kemitorvet 207, 2800 Kgs. Lyngby, Denmark.

Conference paper

Ana C. Mendes*, Elhamalsadat Shekarforoush, Christoph Engwer, Sophie R. Beeren, Christian Gorzelanny, Francisco M. Goycoolea and Ioannis S. Chronakis

Co-assembly of chitosan and phospholipids into hybrid hydrogels

DOI 10.1515/pac-2016-0708

Abstract: Novel hybrid hydrogels were formed by adding chitosan (Ch) to phospholipids (P) self-assembled particles in lactic acid. The effect of the phospholipid concentration on the hydrogel properties was investigated and was observed to affect the rate of hydrogel formation and viscoelastic properties. A lower concentration of phospholipids (0.5% wt/v) in the mixture, facilitates faster network formation as observed by Dynamic Light Scattering, with lower elastic modulus than the hydrogels formed with higher phospholipid content. The nano-porous structure of Ch/P hydrogels, with a diameter of 260 ± 20 nm, as observed by cryo-scanning electron microscopy, facilitated the penetration of water and swelling. Cell studies revealed suitable biocompatibility of the Ch/P hydrogels that can be used within life sciences applications.

Keywords: biomaterials; carbohydrates; chitosan; colloids; EUCHIS-12; hydrogel; ICC-13; phospholipids; self-assembly.

Introduction

Hydrogels are three-dimensional (3D) structures made of chemical or physical crosslinked polymeric networks with a high ability to absorb and retain large amounts of water [1–5]. Hydrogel properties such as soft and rubbery consistency and diffusive transport characteristics [6], gives them the possibility to be used as scaffolds for cell growth and proliferation [1]. In addition, some hydrogels have mucoadhesive and bioadhesive characteristics [2]. Moreover, hydrogels offer the advantage of flexibility to deform and conform to the shape they are confined to, which makes them good candidates to be used in a broad range of food [7] and biomedical applications [1–5].

Among other natural derived polymers, chitosan(s) (polysaccharides made of glucosamine and N-acetyl glucosamine units), exhibit a set of remarkable biological properties such as biocompatibility, biodegradability, hemostatic activity, antibacterial, antimycotic and anticoagulant activity [8–11]. Furthermore, the degradation products of chitosan have been shown to be nontoxic, non-immunogenic and noncarcinogenic [12]. Consequently chitosan(s) have been widely formulated into several structures such as fibers, films,

Article note: A collection of invited papers based on presentations at the 12th Conference of the European Chitin Society (12th EUCHIS)/13th International Conference on Chitin and Chitosan (13th ICC), Münster, Germany, 30 August – 2 September 2015.


***Corresponding author: Ana C. Mendes**, Nano-BioScience Research Group, DTU-Food, Technical University of Denmark, Søtofts plads 227, 2800 Kgs. Lyngby, Denmark, e-mail: anac@food.dtu.dk

Elhamalsadat Shekarforoush and Ioannis S. Chronakis: Nano-BioScience Research Group, DTU-Food, Technical University of Denmark, Søtofts plads 227, 2800 Kgs. Lyngby, Denmark

Christoph Engwer and Francisco M. Goycoolea: Institute for Biology and Biotechnology of Plants (IBBP), Westfälische Wilhelms-Universität Münster, Schlossgarten 3, 48149 Münster, Germany

Sophie R. Beeren: DTU-Chemistry, Technical University of Denmark, Kemitorvet 207, 2800 Kgs. Lyngby, Denmark

Christian Gorzelanny: Experimental Dermatology, Medical Faculty Mannheim, Heidelberg University, Theodor-Kutzer-Ufer 1-3, 68167 Mannheim, Germany

 © 2016 IUPAC & De Gruyter. This work is licensed under a Creative Commons Attribution-NonCommercial-NoDerivatives 4.0 International License. For more information, please visit: <http://creativecommons.org/licenses/by-nc-nd/4.0/>

Bereitgestellt von | De Gruyter / TCS
Angemeldet
Heruntergeladen am | 15.11.16 15:49

particles and hydrogels and used in a wide range of biomedical applications such as drug delivery and tissue engineering [1, 13, 14]. Chitosan(s) physical hydrogels can be produced via non-covalent interactions e.g. electrostatic, hydrophobic, and hydrogen bonding forces between polymer chains [1]. The properties of physical hydrogels can be easily tuned by adjusting the concentration and nature of the components. Furthermore these hydrogels are prepared often in mild conditions (as they don't require toxic covalent crosslinkers), making their use safe for medical applications. Examples of chitosan physical hydrogels are numerous and have been well described elsewhere [1, 15].

Phospholipids, the self-assembling molecular building blocks of cell membranes, constituted by a charged polar head group and a hydrophobic tail, have been largely explored to produce nano-bio structures in the shape of nanoparticles, capsules/liposomes, emulsions [12] and organogels [16]. Organogels, the 3-D networks of entangled reverse cylindrical micelles and jelly-like phases, immobilizing macroscopic external organic phases [17], have been developed by using lecithins as building blocks [16].

The binding of chitosan to phospholipids is a phenomenon known to be caused by the destabilization of the phospholipid membrane bilayer when exposed to chitosans [18, 19] as a consequence of the binding of the negatively charged phosphate groups in phospholipids to chitosan(s) [20]. Formulation of hybrid stable films of chitosan-phospholipids for the release of paclitaxel [21] and docetaxel [22, 23], assembled nanoparticles [24, 25] and nanocapsules/nanoparticles to release capsaicin [26], have been reported. In addition, the biocompatibility of chitosans/phospholipids systems [12, 27] has been confirmed, highlighting the benefits of using these components to produce nanostructures to be used within life sciences. Recently our group explored the potential of combining chitosan with phospholipids to produce electrospun chitosan/phospholipids hybrids nanofibers for applications in drug delivery [28], demonstrating the potential of combining both components to develop functional chitosan/phospholipids hybrids. However, to the best of our knowledge, the co-assembly of chitosan and phospholipids to fabricate hydrogels has never been studied. Therefore, this study aimed to develop hybrid chitosan/phospholipids hydrogels and investigate their physicochemical properties and biocompatibility.

Materials and methods

Materials

Chitosan, with Molecular weight (Mw) of 385 kDa, Degree of Acetylation (DA) of 26% was obtained from GILLET CHITOSAN (product 111). Asolectin from soybean (containing approximately 25–33% of lecithin, cephalin and phosphatidylinositol, 24% saturated fatty acids, 14% mono-unsaturated and 62% poly-unsaturated fatty acids) and chemicals were obtained from Sigma-Aldrich, unless otherwise indicated. All of the consumable were used as received.

Fabrication of hybrid chitosan/phospholipids hydrogels

Asolectin was suspended in lactic acid (2 M) at concentrations of 0.5, 1 and 2% wt/v. Solutions of asolectin were centrifuged to remove undissolved components. Chitosan was added to asolectin solutions in order to reach a concentration of 2% wt/v. Samples were mixed until hydrogel formation took place (for about 4 min) and named as Ch/P0.5, Ch/P1 and Ch/P2, for phospholipids concentrations of 0.5, 1 and 2% wt/v, respectively.

¹H nuclear magnetic resonance (NMR) spectroscopy

¹H NMR spectra were recorded on an 800 MHz Bruker (Fällanden, Switzerland) Avance spectrometer equipped with a TCI Z-gradient CryoProbe and an 18.7 T magnet (Oxford Magnet Technology, Oxford, UK) and processed

with Topspin 3.0 (Bruker). The samples were prepared in the same manner as described for hydrogel preparation in D₂O. To facilitate the transfer of the hydrogel to the NMR tubes, the samples were warmed with a heat gun.

Dynamic light scattering (DLS) measurements

ζ-Potential and size measurements were performed using a Zetasizer NanoZS Instrument (ZEN 3600, Malvern Instruments, Worcestershire, UK). Prior the analyzes, phospholipids and chitosan/phospholipid solutions were prepared with the same concentrations used in the hydrogels. The solutions were filtered using a pyrogen free 0.45 mm disposable membrane filter (Schleicher and Schuell Bioscience, Germany). The intensity correlation function (ICF) was recorded at a fixed laser position (3 mm) and laser intensity (attenuator 7) was optimized prior to the measurements. The ICF was recorded over 100 seconds at 25 °C. The experiments were performed in three replicates. For data analysis, the ICF was normalized.

Rheological analysis

The viscoelastic properties (elastic (G') and viscous modulus (G'')) of hydrogel samples were examined by low amplitude oscillatory measurements using a Thermo Scientific™ Haake Mars II Rheometer System. A serrated PP 60Ti (plate–plate geometry) with a gap of 1 mm, at 25 °C was utilized. The sample was loaded on the rheometer plate and frequency sweep using a constant shear stress of 1 Pa (within the linear viscoelastic region) and stress sweep (at a frequency of 1 Hz) were carried out. The samples were covered with silicone oil to avoid evaporation. All experiments were prepared in triplicate for each sample.

Hydrogel morphology

The morphology of the hydrogels was evaluated by cryo-scanning electron microscopy (cryo-SEM). The cross-sections of the hydrogel were analyzed, applying a cryogenic technique to fracture the samples, before sputter-coating with gold prior the visualization on a scanning electron microscope with cryo-function coupled (Quanta FEG 3D SEM).

Water uptake

The amount of water uptake (swelling) was determined by immersion of the samples in PBS and incubation at 37 °C over a period of 1, 3, 6, 24 and 72 h in dynamic conditions. After each time point, samples were taken out of the solution, rinsed with distilled water, blotted on filter paper to remove surface water, and immediately weighed (mt , mass of wet sample). Afterwards, samples were dried until constant weight (mf) and the percentage of water uptake was determined following equation 1:

$$\text{WU (\%)} = \left(\frac{mt - mf}{mf} \right) \times 100 \quad (1)$$

Three replicates were performed for each sample [N = 3].

Weight loss

The stability of these hydrogels was evaluated through the determinations of weight loss (WL). Samples were weighed, immersed in PBS and incubated at 37 °C under dynamic conditions during 1, 3, 6, 24 and 72 h. After

each time point, samples were taken out of the solution, rinsed with distilled water, blotted on filter paper (to remove surface water) and then dried until constant weight in order to determine the percentages of weight loss following equation:

$$WL (\%) = \left(\frac{mf - m0}{m0} \right) \times 100 \quad (2)$$

where mf is the final mass after immersion and $m0$ is the initial mass prior the immersion in PBS. Three replicates were performed for each sample [$N = 3$].

Biological assessment. LDH assay

The assay was performed as previously reported [29]. Briefly, hydrogels were placed with a spatula to the center of a well of a 12-well plate. The covered area was in the range of 0.7 cm² corresponding to 20 % of the total growth area. Prior to the LDH analysis 0.15×10^6 mouse fibroblasts (L929) were seeded into each well and cultivated for 24 h and 48 h. L929 cells were maintained in RPMI 1640 medium supplemented with 10 % fetal calf serum (FCS), 1 % L-glutamine and 1 % penicillin/streptomycin. LDH was measured in the supernatants of cells using a cytotoxicity test kit (Roche Diagnostics, Mannheim, Germany) according to the manufacture's protocol. Fluorescence microscopy and cell cycle analysis. L929 cells were fixed with ice-cold methanol for 30 min, washed with HEPES-buffered Ringer solution (140 mM NaCl, 5 mM KCl, 1 mM MgCl₂; 1 mM CaCl₂, 5 mM glucose and 10 mM HEPES) and blocked for 1 h at room temperature with 2 % bovine serum albumin (BSA) dissolved in HEPES-buffered Ringer solution, supplemented with 0.3 % Triton X-100. F-actin was stained for 1 h with TRITC-paloidin (Sigma-Aldrich, St. Louis, US) applying a 1:2000 dilution in HEPES-buffered Ringer solution. Nuclei were stained for 10 min with 4,6-diamidino-2-phenylindole (DAPI) diluted in HEPES-buffered Ringer solution ($0.1 \mu\text{g mL}^{-1}$). Fluorescence microscopy was employed using a Zeiss Z.1 observer (Zeiss, Jena, Germany) using a 20× objective. As basis for the cell cycle analysis DNA concentration per cell was analyzed using image J [30].

Results and discussion

NMR spectroscopy

The ¹H-NMR spectrum of asolectin in lactic acid (2 M) was recorded at three different concentrations: 0.5, 1 and 2 % wt/v (Fig. 1). Aside from the dilution factor, the spectra were essentially identical and each

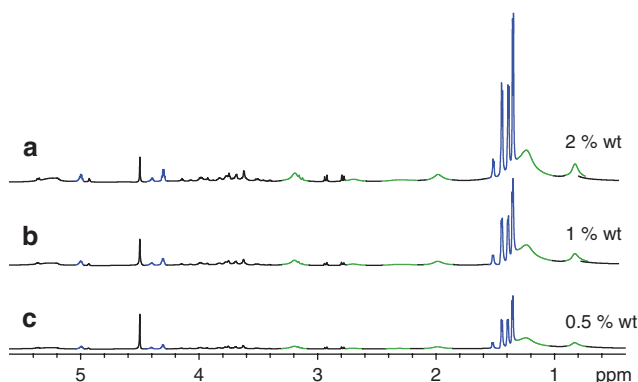


Fig. 1: ¹H-NMR spectra (800 MHz, 323 K) of asolectin/ lactic acid (2 M) in D₂O at varying concentrations: (a) 2 % wt/v; (b) 1 % wt/v and (c) 0.5 % wt/v.

showed broad signals for the hydrophobic tails of the phospholipids. When the phospholipids were present as monomers in solution, sharp signals with clear splitting patterns corresponding to each of the protons on the hydrocarbon tails of the phospholipids could be expected. The broad peaks suggest that instead the phospholipids have self-assembled into supramolecular particles. That the spectra are essentially identical indicates that the concentration of 0.5 % wt/v of asolectin in lactic acid solution is above the critical aggregation concentration and that the particles have similar structures within the concentration range studied.

The hydrogel and its individual constituent components were each analyzed using $^1\text{H-NMR}$ spectroscopy (Fig. 2). Figure 2a shows the $^1\text{H-NMR}$ spectrum of the 2 M lactic acid solution used to prepare the hydrogel. Both free D,L-lactic acid and D,L-lactic acid oligomers, which form reversibly in aqueous solution via an ester condensation reaction, were identified [31]. Figure 2b shows the spectrum of chitosan (0.5 % wt/v) in the lactic acid solution. The signals for chitosan are identifiable, but broad, most likely because this large polymer has reduced mobility in the solution, which leads to line broadening [32]. In the presence of chitosan, several signals from the lactic acid broaden and shift upfield. This is most likely a consequence of the proton transfer from the carboxylic acid of lactic acid to the amines on the chitosan polymer and a consequent, electrostatic interaction between the positively charged polymer and the negatively charged lactate counterions. The signals that shift and broaden correspond to protons adjacent to the carboxylate groups. Figure 2c shows the spectrum of a solution of asolectin (2 % wt/v) and lactic acid (2 M). As asolectin is a mixture of different phospholipids, the $^1\text{H-NMR}$ spectrum is complex and no attempt was made to assign all the signals. It is possible, however, to identify the broadened signals due to the aliphatic protons in the hydrophobic tails of the phospholipids (colored green). These so broad signals are an indication that the phospholipids self-assemble in aqueous solution, presumably due to the hydrophobic effect.

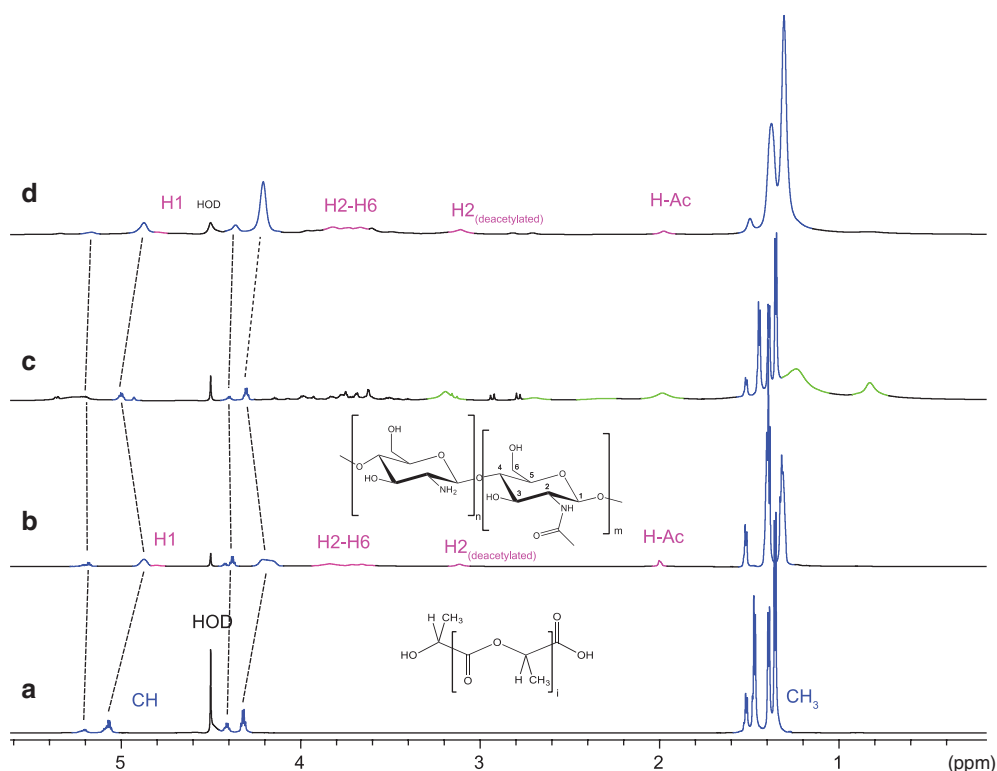


Fig. 2: $^1\text{H-NMR}$ spectra of (800 MHz, 323 K) of the hydrogel and its individual components in D_2O : (a) 2 M lactic acid; (b) chitosan (0.5 % wt/v) in 1 M lactic acid (the spectrum is amplified 2 times); (c) asolectin (2 % wt/v) in 2 M lactic acid; and (d) the hydrogel formed with 2 % wt/v chitosan, 2 % wt asolectin and 2 M lactic acid.

In the NMR spectrum of the hydrogel (Fig. 2d) it is possible to clearly identify broad signals due to the chitosan and lactic acid components. However, the signals due to the hydrophobic tails of the asolectin component are conspicuously absent. Signals for gelators frequently become invisible in ^1H -NMR spectroscopy upon hydrogel formation due to extensive line broadening [33]. Notably the chitosan and lactic acid signals are still visible which suggests these components, on the other hand, have sufficient thermal motion in the hydrogel to provide the ^1H NMR spectrum. The residual water signal at 4.5 ppm is also broadened in the spectrum of the hydrogel, which indicates that the water molecules are also part of the gel assembly, as expected.

DLS

DLS analysis suggests the presence of self-assembled asolectin particles in solutions of lactic acid (2 M), as observed using NMR spectroscopy (Fig. 1). Increasing the concentration of phospholipid leads to a decrease of ζ -potential (Fig. 3a) and an increase in average diameter (Fig. 3b). The ζ -potential is related to the stability of charged particles in suspension [34]. The greater value of the ζ -potential (-48.2 ± 1.5 mV) obtained at

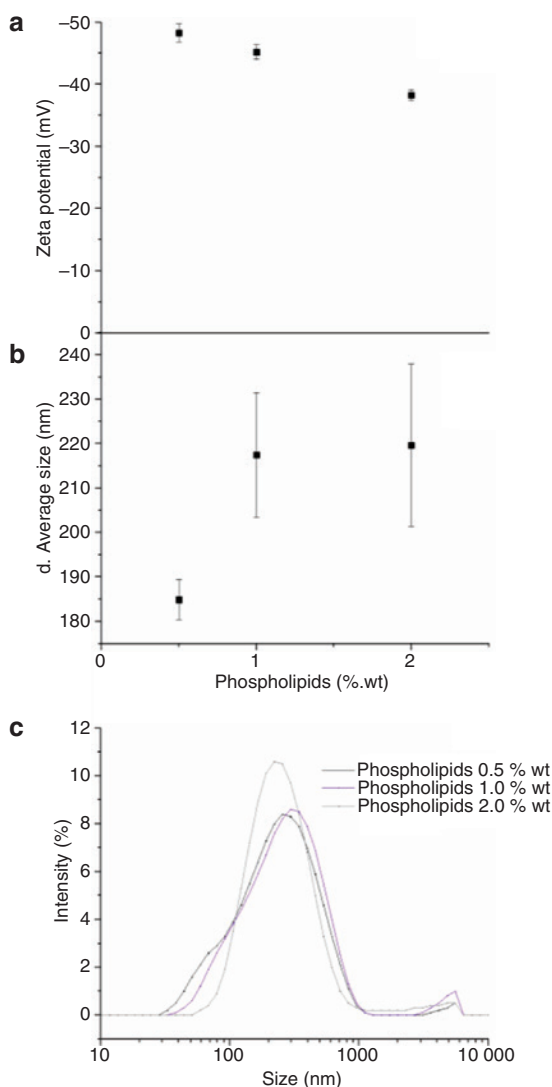


Fig. 3: The effect of the concentration of phospholipids on (a) zeta-potential, (b) d-particle size and (c) particle size distribution of self-assembled phospholipid nanoparticles at concentrations of 0.5, 1 and 2 % wt/v.

lower concentrations of phospholipids (Fig. 3a) might be related with the higher mobility of the phospholipid chains and thus favorable intermolecular interactions between them, leading to the formation of particles with a small average diameter of 185 ± 4.5 nm (Fig. 3b). Small and co-workers observed by DLS studies that the size of the lipid particles is proportional to the phospholipid concentration [35]. Furthermore, Chuah and co-workers [25] observed a similar trend: for higher concentrations of phospholipid molecules, the formation of larger and less stable particles was observed. At the highest concentration of phospholipid (2% wt/v) the ζ -potential was found to be of -38.9 ± 0.3 mV (Fig. 3a) and the particle size was found to be 220 ± 18 nm (Fig. 3b). DLS analysis shows a narrow size distribution, suggesting that the concentration of phospholipid doesn't affect significantly its dispersity in solution (Fig. 3c).

DLS was also used to analyze the dynamic processes occurring in dispersions using the intensity correlation function (ICF), $g^{(2)} - 1$ [36]. Figure 4a shows a similar decay of ICF for all the tested phospholipid solutions in lactic acid, corresponding to the population of vesicles in solution. However after the addition of chitosan to each phospholipid solution, the initial intensity of ICF (s) decreased and a noisy/oscillatory signal appeared for longer delay times (Fig. 4). The decrease of ICF initial intensity has been correlated with the crosslinking of polymeric chains during hydrogel formation [36]. The fluctuations observed after the decay of ICF are related to the onset time of gelation [36, 37]. The data presented in Fig. 4 clearly demonstrate that the amount of phospholipid affects hydrogel formation. The initial decrease of ICF intensity (from phospholipid solution to hydrogel) was found to be more accentuated for Ch/PO.5 hybrid hydrogel (Fig. 4b). For this ratio

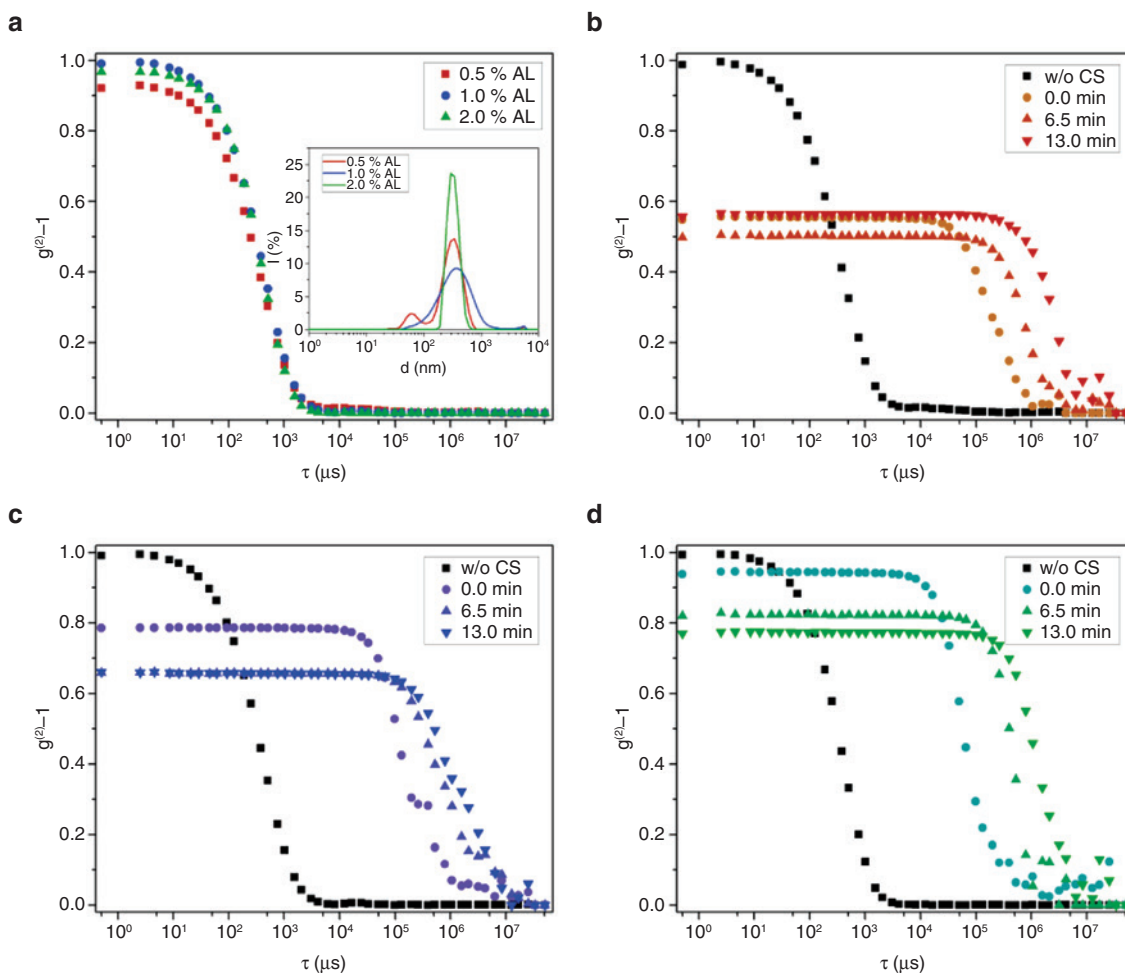


Fig. 4: Development of the intensity correlation function over time of different concentrations of (a) phospholipids; after the addition of chitosan and hydrogel formation using (b) 0.5 % wt/v, (c) 1 % wt/v and (d) 2 % wt/v of phospholipids.

the ICF intensity dropped from 0.99 to 0.56, while for Ch/P1 and Ch/P2 a decrease in the initial ICF intensity was observed from 0.99 to 0.79 and 0.93, respectively. This data suggests that the rate of gelation tend to decrease with increasing phospholipid content, as a result of increased viscosity and decreased mobility of the molecules in solution. The decrease of $g^{(2)} - 1$, when T tends to infinite (∞) was observed as result of a decrease of ergodicity and hydrogelation [38, 39].

Rheology

The viscoelastic properties of the Ch/P hybrid hydrogels were studied by oscillatory rheology as a function of frequency and shear stress (Fig. 5a and b). Within the frequency range tested, the solid-like response (G'), is dominant over the viscous-flow (G''), with high frequency dependence mostly for elastic modulus. Moreover, the $\tan \delta$ value ($\tan \delta = G''/G'$) provides a convenient index of the proportion of elastic-like character. The $\tan \delta$ value at the frequency of ~ 1 Hz is 0.277, 0.371 and 0.436 for Ch/P2, Ch/P1 and CH/P0.5 hydrogels, respectively. For other biopolymer hydrocolloid hydrogels such as gelatin, agarose, and carrageenan $\tan \delta$ value was found to range from about 0.02 to 0.07 [40].

The elastic and loss modulus followed the power law relation G' or $G''(\omega) = K \omega^A$ at the frequency range of 0.1 – 30 Hz and it can be used to describe the behavior of the G' and G'' in a comparable manner (Table 1). For hydrogels, the plots of $\log G'$ and $\log G''$ vs. $\log \omega$ have zero slope, whereas for weak elastic gels, the plots have positive slopes and the values of K' are higher than those of K'' with the frequency dependency, as found for the Ch/P hydrogels.

The response to increasing amplitude of oscillation is shown in Fig. 5b. The elastic and loss modulus remain independent of deformation at imposed strains up to ~ 100 Pa, with the samples effectively flowing beyond that. This dependence of shear moduli on oscillatory strain is characteristic of a weak elastic gel.

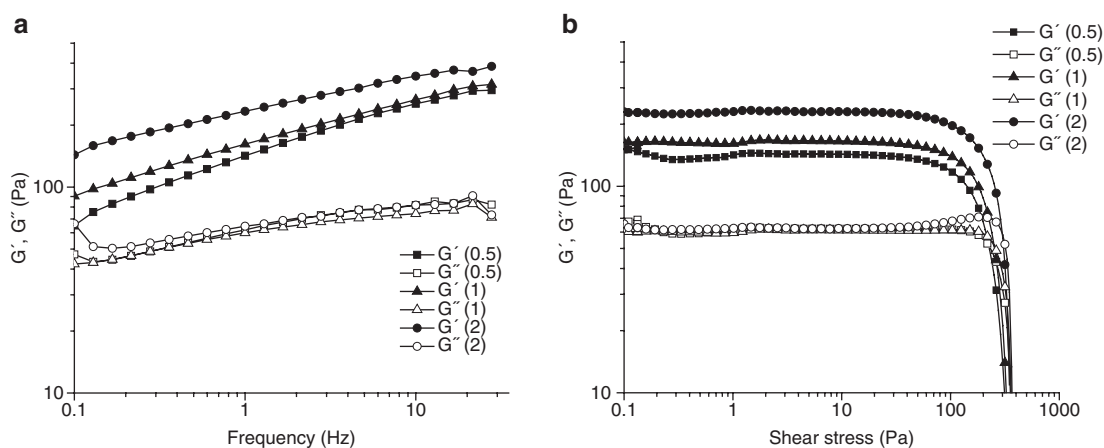


Fig. 5: Elastic (G') and viscous modulus (G'') of chitosan/phospholipids hybrid hydrogels as a function of frequency (a) and shear stress (b).

Table 1: Parameters from the power law relation $G(\omega) = K \omega^A$ determined from experimentally measured storage modulus and loss modulus for Ch/P hydrogels with different concentrations of phospholipids.

Sample designation	K'	A' (Pa s)	K''	A'' (Pa s)
Ch/P0.5	136.8	0.2669	60.0	0.1419
Ch/P1	158.5	0.2239	57.8	0.1216
Ch/P2	229.7	0.1717	63.5	0.1143

K' and A' refer to elastic modulus; K'' and A'' refer to viscous modulus.

Cryo-scanning electron microscopy (Cryo-SEM)

Figure 6, shows the internal microstructure of Ch/P hybrid hydrogels composed of a hierarchical porous structures, with porous diameter of 260 ± 20 nm. The different ratios of Ch/P provided similar morphology. Mertins and Dimova [20] have also observed that the adsorption of chitosan on the phospholipid membrane leads to the disruption of supramolecular phospholipids vesicles and pore formation. By phase contrast microscopy these authors observed the formation of microscopic pores during vesicle collapse and slower restructuring into microparticles resembling microgels [20].

Swelling

The swelling profile of the Ch/P hybrids over time is illustrated in the Fig. 7. Overall, it can be observed that the amount of phospholipid mediates the swelling capability of the Ch/P hybrid hydrogels. After 1 h, Ch/P0.5 absorbs about 0.62 that increased to 1.86 after 6 h in contact with PBS at 37 °C. Between 6 and 24 h the water uptake didn't change significantly and at the end of 72 h the swelling % was about 2.76. A similar profile was observed for Ch/P1 and Ch/P2 hybrid hydrogels. The relatively rapid initial swelling (between 1 and 6 h) is mainly caused by the porous structure (Fig. 6) which facilitated the permeation of the PBS inside the hydrogels [41, 42]. The increase of phospholipid content tends to increase the swelling capability of these hydrogels due to the hydrophilic nature of asolectin. This feature might facilitate the diffusion of water through the inner porous existent within the hydrogel nano-micro structure and thus facilitate water absorption.

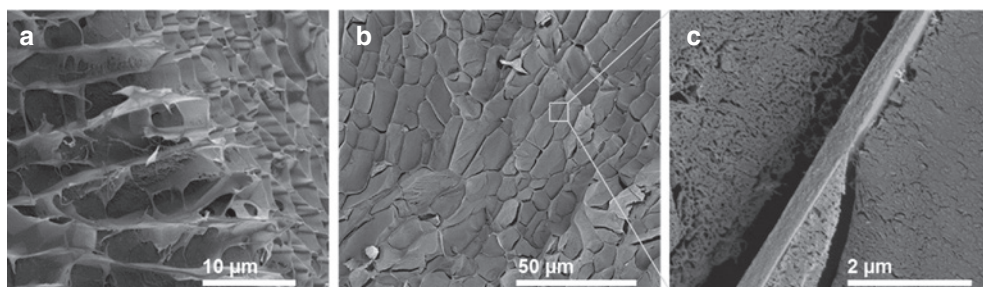


Fig. 6: Cryo-SEM images of the cross sections of Ch/P hybrid hydrogels, showing its internal porous micro (a) and nanostructures (b) and (c) at different magnifications.

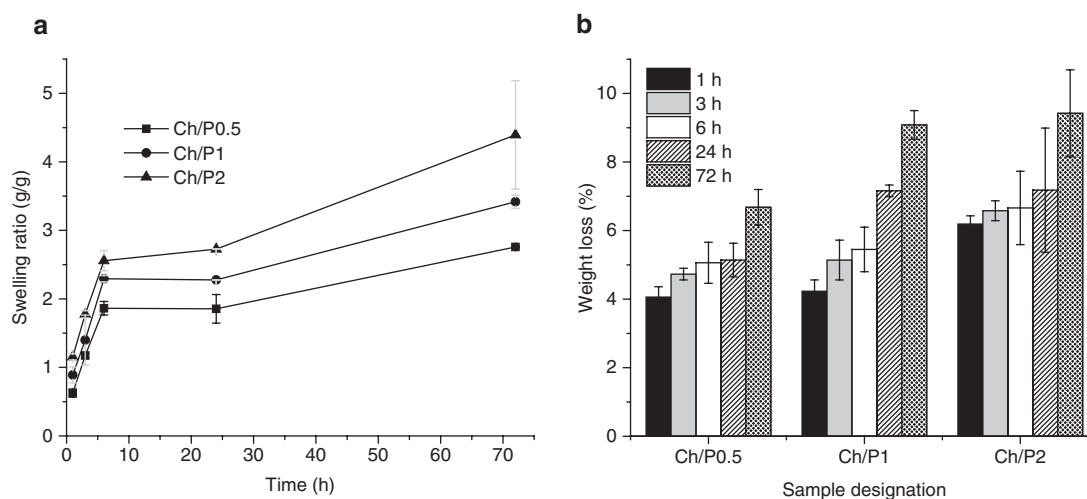


Fig. 7: The effect of the phospholipid content on the (a) swelling capability and (b) stability of the Ch/P hybrid hydrogels.

The stability of the Ch/P hybrid hydrogels was investigated by determination of their losses of weight. With the increase of the incubation time of the hydrogels in PBS, an increase in the percentage of the weight loss was observed. Thus, Ch/P0.5 lost about 4 % of its weight after 1 h of incubation within PBS and about 5 % after 24 h. At the end of the 72 h these hydrogels lost about 6.68 % of their weight. Comparable trends were

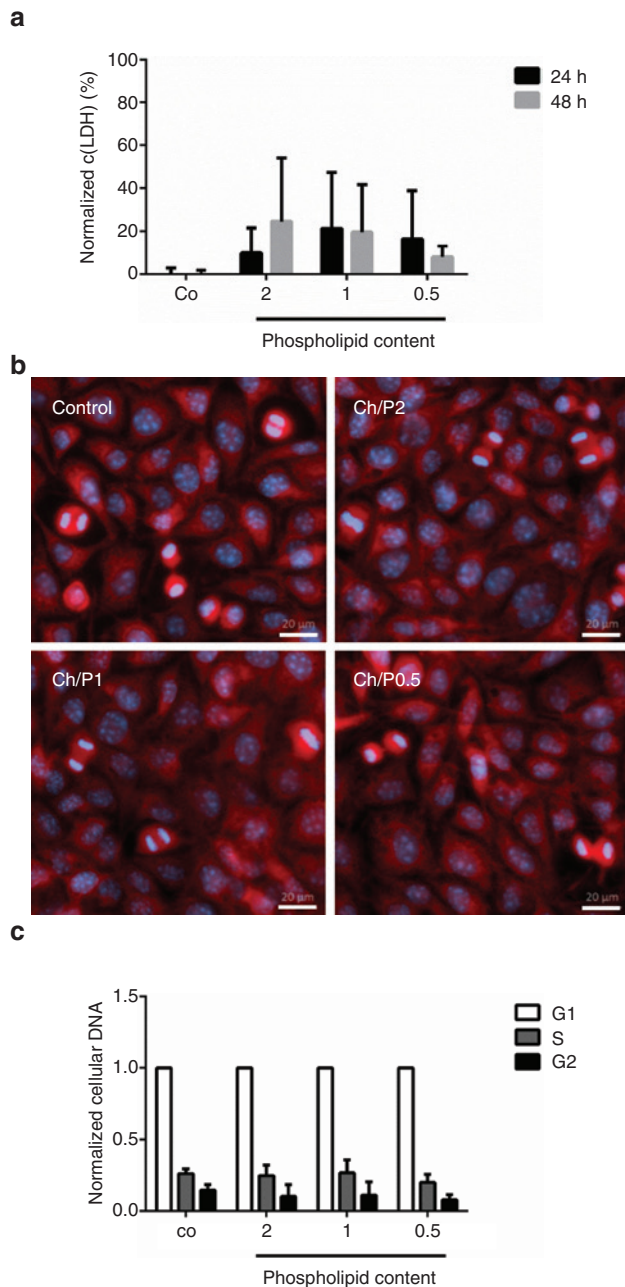


Fig. 8: Co-cultivation of chitosan/phospholipid hydrogels with fibroblasts (L929). (a) Concentration of lactate dehydrogenase (LDH) measured in the supernatants of cell cultivated for 24 h and 48 h in the presence or absence of hydrogels. Controls (co) were set to 0 %, cells treated with 0.1% triton-X100 inducing a maximal release of LDH were set to 100 %. (N=3); (b) Fluorescence microscopic analysis of cells co-cultivate with hydrogels that were on glass cover slips. Cells seeded on glass cover slips without hydrogel were used as control (co). F-actin was stained with TRITC-labeled phalloidin (red), DNA of cell nuclei were stained with DAPI (blue). Scale bar corresponds to 20 μm ; (c) DNA staining with DAPI was used to analyze the cell cycle status of L929 cells. (> 300 nuclei were analyzed of three independent experiments).

observed for the other hydrogel formulations (Ch/P1 and Ch/P2). Ch/P3 hydrogels lost about $1.4 \pm 0.1\%$ and Ch/P1 lost about $1.2 \pm 0.2\%$ more of their weigh compared to Ch/P0.5.

Biological assessment

Fibroblasts were co-cultivated with the phospholipid/chitosan hydrogels with different contents of phospholipids to investigate their biological compatibility. Potential cytotoxicity was accessed by measuring the amount of lactate dehydrogenase (LDH) released into the supernatants 24 h and 48 h after seeding the cells. In comparison to the control cells (cultivation on tissue culture treated polystyrene), increased levels of LDH released were detected in the supernatants of the cells co-cultivated with hydrogels. However, differences between the groups were not statistically significant (Fig. 8a). To further supplement these findings, immunofluorescence staining of the cells was analyzed by fluorescence microscopy (Fig. 8b). In preliminary experiments it was found that cells barely attached directly to the hydrogels but settle around the hydrogels. Therefore our examination was focused on areas next to the hydrogels. In agreement with the LDH measurements, no evident differences in cell morphologies or mitosis rate were found. These results were further confirmed by a cell cycle analysis indicating no negative impact of the hydrogels on the proliferative potential of L929 cells (Fig. 8c).

Conclusions

Asolectin phospholipid in 2 M lactic acid produced supramolecular particles with ζ -potential and size depending on the phospholipid concentration. The addition of chitosan (Mw 385 KDa, DA 26%) to phospholipid self-assembled particles in lactic acid formed stable hybrid hydrogels. The concentration of phospholipid particles affected the rate of the hydrogel formation and on their viscoelastic properties. The lower concentration of phospholipids (0.5% wt/v) facilitates faster network formation, with lower elastic modulus than the gels formed with higher phospholipid content. The internal structure of Ch/P hybrid hydrogels was found to involve nanoporous sections which in turn facilitated the penetration of water and swelling. Cell studies revealed that the cells didn't attach to the hydrogels, however they could perform their metabolic activity suggesting that these hybrid chitosan/phospholipids hybrid hydrogels have suitable biocompatibility to be used in life sciences applications.

Acknowledgments: This work was supported by the European Union funded project "Nano3Bio" (grant agreement no 613931) under FP7.

References

- [1] N. Bhattarai, J. Gunn, M. Zhang, *Adv. Drug Deliv. Rev.* **62**, 83 (2010).
- [2] N. A. Peppas, J. J. Sahlin, *Biomaterials* **17**, 1553 (1996).
- [3] N. A Peppas, P. Bures, W. Leobandung, H. Ichikawa, *Eur. J. Pharm. Biopharm.* **50**, 27 (2000).
- [4] J. M. Shapiro, M. L. Oyen, *J. Miner. Met. Mater. Soc.* **65**, 505 (2013).
- [5] D. Buenger, F. Topuz, J. Groll, *Prog. Polym. Sci.* **37**, 1678 (2012).
- [6] M. Hamidi, A. Azadi, P. Raffei, W. Hennink, C. van Nostrum, *Adv. Drug Deliv. Rev.* **54**, 13 (2002).
- [7] H. M. Shewan, J. R. Stokes, *J. Food Eng.* **119**, 781 (2013).
- [8] V. Balan, L. Verestiuc, *Eur. Polym. J.* **53**, 171 (2014).
- [9] R. Jayakumar, D. Menon, K. Manzoor, S. V. Nair, H. Tamura, *Carbohydr. Polym.* **82**, 227 (2010).
- [10] Y. Luo, Q. Wang, *Int. J. Biol. Macromol.* **64**, 353 (2014).
- [11] B. Menchicchi, A. Hensel, F. M. Goycoolea, *Curr. Pharm. Des.* **21**, 4888 (2015).
- [12] R. Souza, P. Zahedi, C. J. Allen, M. Piquette-Miller, *Biomaterials* **30**, 3818 (2009).
- [13] A. Anitha, S. Sowmya, P. T. Sudheesh Kumar, S. Deepthi, K. P. Chennazhi, H. Ehrlich, M. Tsurkan, R. Jayakumar, *Prog. Polym. Sci.* **39**, 1 (2014).

- [14] W. W. Thein-Han, W. F. Stevens, *Drug Dev. Ind. Pharm.* **30**, 397 (2004).
- [15] M. Dash, F. Chiellini, R. M. Ottenbrite, E. Chiellini, *Prog. Polym. Sci.* **36**, 981 (2011).
- [16] V. K. Singh, P. M. Pandeyb, T. Agarwalb, D. Kumara, I. Banerjeeb, A. Anisc, K. Palb, *J. Mech. Behav. Biomed. Mater.* **55**, 250 (2015).
- [17] A. Bhatia, B. Singh, K. Raza, S. Wadhwa, O. P. Katara, *Int. J. Pharm.* **444**, 47 (2013).
- [18] N. Fang, V. Chan, H. Q. Mao, K. W. Leong, *Biomacromolecules* **2**, 1161 (2001).
- [19] O. Mertins, R. Dimova, *Langmuir* **29**, 14545 (2013).
- [20] O. Mertins, R. Dimova, *Langmuir* **29**, 14552 (2013).
- [21] J. Grant, M. Blicher, M. Piquette-Miller, C. Allen, *J. Pharm. Sci.* **94**, 1512 (2005).
- [22] P. Zahedi, R. Souza, M. Piquette-Miller, C. Allen, *Int. J. Pharm.* **377**, 76 (2009).
- [23] E. A. Ho, V. Vassileva, C. Allen, M. Piquette-Miller, *J. Control. Release* **104**, 181 (2005).
- [24] F. Sonvico, A. Cagnani, A. Rossi, S. Motta, M. T. Di Bari, F. Cavatorta, M. J. Alonso, A. Deriu, P. Colombo, *Int. J. Pharm.* **324**, 67 (2006).
- [25] A. M. Chuah, T. Kuroiwa, S. Ichikawa, I. Kobayashi, M. Nakajima, *J. Food Sci.* **74**, N1 (2009).
- [26] F. M. Goycoolea, A. Valle-Gallego, R. Stefani, B. Menchicchi, L. David, C. Rochas, M. J. Santander-Ortega, M. J. Alonso, *Colloid Polym. Sci.* **290**, 1423 (2012).
- [27] P. Pereira, S. S. Pedrosa, A. Correia, C. F. Lima, M. P. Olmedo, Á. González-Fernández, M. Vilanova, F. M. Gama, *Toxicol. Vitr.* **29**, 638 (2015).
- [28] A. C. Mendes, C. Gorzelanny, N. Halter, S. W. Schneider, I. S. Chronakis, *Int. J. Pharm.* **510**, 48 (2016).
- [29] C. Gorzelanny, R. Kmeth, A. Obermeier, A. T. Bauer, N. Halter, K. Kümpel, M. F. Schneider, A. Wixforth, H. Gollwitzer, R. Burgkart, B. Stritzker, S. W. Schneider, *Sci. Rep.* **6**, 22849 (2016).
- [30] C. A. Schneider, W. S. Rasband, K. W. Eliceiri, *Nat. Methods* **9**, 671 (2012).
- [31] J. L. Espartero, I. Rashkov, S. M. Li, N. Manolova, M. Vert, *Macromolecules*, **9297**, 3535 (1996).
- [32] M. Lavertu, Z. Xia, A. N. Serreqi, M. Berrada, A. Rodrigues, D. Wang, M. D. Buschmann, A. Gupta, *J. Pharm. Biomed. Anal.* **32**, 1149 (2003).
- [33] Y. E. Shapiro, *Prog. Polym. Sci.* **36**, 1184 (2011).
- [34] A. C. Mendes, K. H. Smith, E. Tejada-Montes, E. Engel, R. L. Reis, H. S. Azevedo, A. Mata, *Adv. Funct. Mater.* **23**, 430 (2013).
- [35] D. M. Small, *Molecular Association in Biological and Related Systems* **84**, 31 (American Chemical Society, 1968).
- [36] W. A. de Moraes, M. R. Pereira, J. L. C. Fonseca, *Carbohydr. Polym.* **87**, 2376 (2012).
- [37] K. Yoshida, T. Yamaguchi, N. Osaka, H. Endo, M. Shibayama, *Chem. Phys.* **12**, 3260 (2010).
- [38] P. N. Pusey, W. Van Megen, *Phys. A Stat. Mech. its Appl.* **157**, 705 (1989).
- [39] T. Norisuye, M. Shibayama, R. Tamaki, Y. Chujo, *Macromolecules* **32**, 1528 (1999).
- [40] I. S. Chronakis, L. Piculell, J. Borgström, *Carbohydr. Polym.* **31**, 215 (1996).
- [41] F. Zhang, C. Hea, L. Cao, W. Feng, H. Wang, X. Moa, J. Wangd, *Int. J. Biol. Macromol.* **48**, 474 (2011).
- [42] S. D. Nath, C. Abueva, B. Kima, B. T. Lee, *Carbohydr. Polym.* **115**, 160 (2015).

4. Conclusions

In this PhD thesis, electrospun nano-microfibers of polysaccharides (xanthan gum, chitosan) and phospholipids were investigated as carriers for the encapsulation and release of phenolic bioactive compounds. These functional nano-microcarriers provide a sustained controlled released of the phenolic compounds (Papers I-V), with improved bioavailability in the GI tract (Papers II, IV), and an increased stability of the phenolic bioactives (with respect to temperature, oxygen, light and pressure) (Paper V).

One of the benefits of utilizing polysaccharides and phospholipids is their inherent biocompatibility. The biocompatibility of electrospun xanthan and xanthan-chitosan nanofibers was confirmed by *in vitro* cell studies. In particular, the exposure of Caco-2 cell monolayers to xanthan-chitosan-curcumin nanofibers resulted in a cell viability of ~80%. Another advantage of using biopolymers is their natural ability to interact with biological systems. The electrospun xanthan and xanthan-chitosan nanofibers interacted with Caco-2 cells by inhibiting the efflux transporters and opening the tight junctions. Consequently, an enhancement in the transepithelial permeability of the bioactive phenolic compounds was demonstrated, confirming the potential to utilize these nano-microcarriers to improve the poor bioavailability of phenolic compounds.

The findings in this PhD thesis expanded the current scientific knowledge on the development and utilization of electrospun nano-microfibers of polysaccharides (xanthan gum, chitosan) and phospholipids as novel nano-microdelivery systems of bioactive phenolic compounds, for a range of new food and pharmaceutical applications.

5. References

1. Mendes, A. C., Stephansen, K. & Chronakis, I. S. Electrospinning of food proteins and polysaccharides. *Food Hydrocoll.* **68**, 53–68 (2017).
2. Shekarforoush, E., Mendes, A. C., Baj, V., Beeren, S. R. & Chronakis, I. S. Electrospun phospholipid fibers as micro-encapsulation and antioxidant matrices. *Molecules* **22**, 1–16 (2017).
3. Gibbs, B. F., Kermasha, S., Alli, I. & Mulligan, C. N. Encapsulation in the food industry: A review. *Int. J. Food Sci. Nutr.* **50**, 213–224 (1999).
4. Rosenberg, M., Kopelman, I. J. & Talmon, Y. Factors Affecting Retention in Spray-Drying Microencapsulation of Volatile Materials. *J. Agric. Food Chem.* **38**, 1288–1294 (1990).
5. Scalbert, A. & Williamson, G. Dietary intake and bioavailability of polyphenols. *J. Nutr.* **130**, 2073S–85S (2000).
6. Kühnau, J. The flavonoids. A class of semi-essential food components: their role in human nutrition. *World Rev. Nutr. Diet.* **24**, 117–91 (1976).
7. Quettier-Deleu, C. *et al.* Phenolic compounds and antioxidant activities of buckwheat (*Fagopyrum esculentum* Moench) hulls and flour. *J. Ethnopharmacol.* **72**, 35–42 (2000).
8. Rahmanian, N., Jafari, S. M. & Wani, T. A. Bioactive profile, dehydration, extraction and application of the bioactive components of olive leaves. *Trends Food Sci. Technol.* **42**, 150–172 (2015).

9. Rahmanian, N., Jafari, S. M. & Galanakis, C. M. Recovery and removal of phenolic compounds from olive mill wastewater. *JAOCS, J. Am. Oil Chem. Soc.* **91**, 1–18 (2014).
10. Taghvaei, M. & Jafari, S. M. Application and stability of natural antioxidants in edible oils in order to substitute synthetic additives. *J. Food Sci. Technol.* **52**, 1272–1282 (2015).
11. Frenot, A. & Chronakis, I. S. Polymer nanofibers assembled by electrospinning. *Curr. Opin. Colloid Interface Sci.* **8**, 64–75 (2003).
12. Weiss, J., Kanjanapongkul, K., Wongsasulak, S. & Yoovidhya, T. *13 - Electrospun fibers: fabrication, functionalities and potential food industry applications. Nanotechnology in the Food, Beverage and Nutraceutical Industries* (Woodhead Publishing Limited, 2012). doi:<http://dx.doi.org/10.1533/9780857095657.2.362>
13. Reneker, D. H. & Chun, I. Nanometre diameter fibres of polymer, produced by electrospinning. *Nanotechnology* **7**, 216–223 (1996).
14. Chronakis, I. S. Novel nanocomposites and nanoceramics based on polymer nanofibers using electrospinning process - A review. *J. Mater. Process. Technol.* **167**, 283–293 (2005).
15. Chronakis, I. S. Micro-/nano-fibers by electrospinning technology: Processing, properties and applications. *Micro-Manufacturing Eng. Technol.* 264–286 (2010). doi:10.1016/B978-0-8155-1545-6.00016-8
16. Li, D. & Xia, Y. Electrospinning of nanofibers: reinventing the wheel? *Adv. Mater.* **16**, 1151–1170 (2004).
17. Carroll, C. P. & Joo, Y. L. Electrospinning of viscoelastic Boger fluids: Modeling and

- experiments. *Phys. Fluids* **18**, (2006).
18. Doshi, J. & Reneker, D. H. Electrospinning process and applications of electrospun fibers. *Conf. Rec. 1993 IEEE Ind. Appl. Conf. Twenty-Eighth IAS Annu. Meet.* **35**, 151–160 (1993).
 19. Reneker, D. H. & Chun, L. Nanometre diameters of polymer, produced by electrospinning. *Nanotechnology* **7**, 216–223 (1996).
 20. Supaphol, P., Mit-Uppatham, C. & Nithitanakul, M. Ultrafine electrospun polyamide-6 fibers: Effect of emitting electrode polarity on morphology and average fiber diameter. *J. Polym. Sci. Part B Polym. Phys.* **43**, 3699–3712 (2005).
 21. Han, S. O., Son, W. K., Youk, J. H. & Park, W. H. Electrospinning of Ultrafine Cellulose Fibers and Fabrication of Poly(butylene succinate) Biocomposites Reinforced by Them. *Polym. Polym. Compos.* **107**, 1954 (2008).
 22. Kriegel, C., Arrechi, A., Kit, K., McClements, D. J. & Weiss, J. Fabrication, functionalization, and application of electrospun biopolymer nanofibers. *Crit. Rev. Food Sci. Nutr.* **48**, 775–797 (2008).
 23. Zeleny, J. The electrical discharge from liquid points, and a hydrostatic method of measuring the electric intensity at their surfaces. *Phys. Rev.* **3**, 69–91 (1914).
 24. Burger, C., Hsiao, B. S. & Chu, B. Nanofibrous Materials and Their Applications. *Annu. Rev. Mater. Res.* **36**, 333–368 (2006).
 25. Agarwal, S., Wendorff, J. H. & Greiner, A. Use of electrospinning technique for biomedical applications. *Polymer (Guildf).* **49**, 5603–5621 (2008).

26. Sill, T. J. & von Recum, H. a. Electrospinning: Applications in drug delivery and tissue engineering. *Biomaterials* **29**, 1989–2006 (2008).
27. Macneil, S. Biomaterials for tissue. **11**, 26–35 (2008).
28. Chen, L., Remondetto, G. E. & Subirade, M. Food protein-based materials as nutraceutical delivery systems. *Trends Food Sci. Technol.* **17**, 272–283 (2006).
29. El-salam, M. H. A. & El-shibiny, S. *Natural Biopolymers As. Encapsulations* (Elsevier Inc., 2016). doi:10.1016/B978-0-12-804307-3/00019-3
30. Stijnman, A. C., Bodnar, I. & Hans Tromp, R. Electrospinning of food-grade polysaccharides. *Food Hydrocoll.* **25**, 1393–1398 (2011).
31. Rosalam, S. & England, R. Review of xanthan gum production from unmodified starches by *Xanthomonas compestris* sp. *Enzyme Microb. Technol.* **39**, 197–207 (2006).
32. Faria, S. *et al.* Characterization of xanthan gum produced from sugar cane broth. *Carbohydr. Polym.* **86**, 469–476 (2011).
33. Shekarforoush, E., Faralli, A., Ndoni, S., Mendes, A. C. & Chronakis, I. S. Electrospinning of Xanthan Polysaccharide. *Macromol. Mater. Eng.* **302**, 1–11 (2017).
34. Ungeheuer, S., Bewersdorff, H. & Singh, R. P. Turbulent Drag Effectiveness and Shear Stability of Xanthan-Gum-Based Graft Copolymers. **37**, 2933–2948 (1989).
35. Chimie, R. R. De, Bercea, M., Darie, R. N. & Morariu, S. Rheological Investigation of Xanthan / Pluronic F127 Hydrogels. **58**, 189–196 (2013).
36. Lachke, A. X a n t h a n -A V e r s a t i l e G u m. 25–33 (2004).

37. Zirnsak, M. a., Boger, D. V. & Tirtaatmadja, V. Steady shear and dynamic rheological properties of xanthan gum solutions in viscous solvents. *J. Rheol. (N. Y. N. Y)*. **43**, 627 (1999).
38. Mendes, A. C., Baran, E. T., Pereira, R. C., Azevedo, H. S. & Reis, R. L. Encapsulation and survival of a chondrocyte cell line within xanthan gum derivative. *Macromol. Biosci.* **12**, 350–9 (2012).
39. Alipour, S. M., Nouri, M., Mokhtari, J. & Bahrami, S. H. Electrospinning of poly(vinyl alcohol)-water-soluble quaternized chitosan derivative blend. *Carbohydr. Res.* **344**, 2496–2501 (2009).
40. Claesson, P. M. & Ninham, B. W. pH-Dependent Interactions between Adsorbed Chitosan Layers. *Langmuir* **8**, 1406–1412 (1992).
41. Sugimoto, M., Morimoto, M., Sashiwa, H., Saimoto, H. & Shigemasa, Y. Preparation and characterization of water-soluble chitin and chitosan derivatives. *Carbohydr. Polym.* **36**, 49–59 (1998).
42. Yao, K. D., Tu, H., Cheng, F., Zhang, J. W. & Liu, J. pH-sensitivity of the swelling of a chitosan-pectin polyelectrolyte complex. *Die Angew. Makromol. Chemie* **245**, 63–72 (1997).
43. Lee, K. Y., Jeong, L., Kang, Y. O., Lee, S. J. & Park, W. H. Electrospinning of polysaccharides for regenerative medicine. *Adv. Drug Deliv. Rev.* **61**, 1020–1032 (2009).
44. Gao, Y., Truong, Y. B., Zhu, Y. & Louis Kyratzis, I. Electrospun antibacterial nanofibers: Production, activity, and in vivo applications. *J. Appl. Polym. Sci.* **131**, 9041–9053 (2014).

45. Sencadas, V. *et al.* Determination of the parameters affecting electrospun chitosan fiber size distribution and morphology. *Carbohydr. Polym.* **87**, 1295–1301 (2012).
46. Homayoni, H., Ravandi, S. a H. & Valizadeh, M. Electrospinning of chitosan nanofibers: Processing optimization. *Carbohydr. Polym.* **77**, 656–661 (2009).
47. Geng, X., Kwon, O.-H. & Jang, J. Electrospinning of chitosan dissolved in concentrated acetic acid solution. *Biomaterials* **26**, 5427–5432 (2005).
48. Ohkawa, K., Cha, D., Kim, H., Nishida, A. & Yamamoto, H. Electrospinning of Chitosan. *Macromol. Rapid Commun.* **25**, 1600–1605 (2004).
49. Pakravan, M., Heuzey, M.-C. & Aiji, A. Core-shell structured PEO-chitosan nanofibers by coaxial electrospinning. *Biomacromolecules* **13**, 412–21 (2012).
50. Sun, K. & Li, Z. H. Preparations, properties and applications of chitosan based nanofibers fabricated by electrospinning. *Express Polym. Lett.* **5**, 342–361 (2011).
51. Sangsanoh, P. & Supaphol, P. Stability improvement of electrospun chitosan nanofibrous membranes in neutral or weak basic aqueous solutions. *Biomacromolecules* **7**, 2710–2714 (2006).
52. Schiffman, J. D. & Schauer, C. L. One-step electrospinning of cross-linked Chitosan fibers. *Biomacromolecules* **8**, 2665–2667 (2007).
53. Austero, M. S., Donius, A. E., Wegst, U. G. K. & Schauer, C. L. New crosslinkers for electrospun chitosan fibre mats. I. Chemical analysis. *J. R. Soc. Interface* **9**, 2551–62 (2012).

54. Aliabadi, M., Irani, M., Ismaeili, J., Piri, H. & Parnian, M. J. Electrospun nanofiber membrane of PEO/Chitosan for the adsorption of nickel, cadmium, lead and copper ions from aqueous solution. *Chem. Eng. J.* **220**, 237–243 (2013).
55. Bhattarai, N., Edmondson, D., Veiseh, O., Matsen, F. A. & Zhang, M. Electrospun chitosan-based nanofibers and their cellular compatibility. *Biomaterials* **26**, 6176–6184 (2005).
56. Duan, B., Dong, C., Yuan, X. & Yao, K. Electrospinning of chitosan solutions in acetic acid with poly(ethylene oxide). *J. Biomater. Sci. Polym. Ed.* **15**, 797–811 (2004).
57. Jia, Y. T. *et al.* Fabrication and characterization of poly (vinyl alcohol)/chitosan blend nanofibers produced by electrospinning method. *Carbohydr. Polym.* **67**, 403–409 (2007).
58. Zhou, Y., Yang, D. & Nie, J. Electrospinning of chitosan/poly(vinyl alcohol)/ acrylic acid aqueous solutions. *J. Appl. Polym. Sci.* **102**, 5692–5697 (2006).
59. Huang, X. J., Ge, D. & Xu, Z. K. Preparation and characterization of stable chitosan nanofibrous membrane for lipase immobilization. *Eur. Polym. J.* **43**, 3710–3718 (2007).
60. Li, L. & Hsieh, Y. Lo. Chitosan bicomponent nanofibers and nanoporous fibers. *Carbohydr. Res.* **341**, 374–381 (2006).
61. Lin, T., Fang, J., Wang, H., Cheng, T. & Wang, X. Using chitosan as a thickener for electrospinning dilute PVA solutions to improve fibre uniformity. *Nanotechnology* **17**, 3718–3723 (2006).
62. Park, W. H., Jeong, L., Yoo, D. Il & Hudson, S. Effect of chitosan on morphology and conformation of electrospun silk fibroin nanofibers. *Polymer (Guildf)*. **45**, 7151–7157

- (2004).
63. Lin, H. Y., Chen, H. H., Chang, S. H. & Ni, T. S. Pectin-chitosan-PVA nanofibrous scaffold made by electrospinning and its potential use as a skin tissue scaffold. *J. Biomater. Sci. Polym. Ed.* **24**, 470–484 (2013).
 64. Xu, F., Weng, B., Gilkerson, R., Materon, L. A. & Lozano, K. Development of tannic acid/chitosan/pullulan composite nanofibers from aqueous solution for potential applications as wound dressing. *Carbohydr. Polym.* **115**, 16–24 (2015).
 65. Torres-Giner, S., Ocio, M. J. & Lagaron, J. M. Novel antimicrobial ultrathin structures of zein/chitosan blends obtained by electrospinning. *Carbohydr. Polym.* **77**, 261–266 (2009).
 66. Wang, S. & Zhao, G. Quantitative characterization of the electrospun gelatin-chitosan nanofibers by coupling scanning electron microscopy and atomic force microscopy. *Mater. Lett.* **79**, 14–17 (2012).
 67. Chen, J. P., Chang, G. Y. & Chen, J. K. Electrospun collagen/chitosan nanofibrous membrane as wound dressing. *Colloids Surfaces A Physicochem. Eng. Asp.* **313–314**, 183–188 (2008).
 68. Chen, Z. G., Wang, P. W., Wei, B., Mo, X. M. & Cui, F. Z. Electrospun collagen-chitosan nanofiber: A biomimetic extracellular matrix for endothelial cell and smooth muscle cell. *Acta Biomater.* **6**, 372–382 (2010).
 69. Chen, Z., Mo, X. & Qing, F. Electrospinning of collagen-chitosan complex. *Mater. Lett.* **61**, 3490–3494 (2007).
 70. Gosangari, S. L. & Watkin, K. L. Effect of preparation techniques on the properties of

- curcumin liposomes: characterization of size, release and cytotoxicity on a squamous oral carcinoma cell line. *Pharm. Dev. Technol.* **17**, 103–9 (2012).
71. Maria, A., Maria, B., Sinico, C., Sapienza, L. & Moro, P. A. Phospholipid-detergent systems : effects of polysorbates on the release of liposomal caffeine. *Farmaco* **53**, 650–654 (1998).
 72. Shazly, G., Nawroth, T. & Langguth, P. Comparison of dialysis and dispersion methods for in vitro release determination of drugs from multilamellar liposomes. *Dissolution Technol.* **15**, 7–10 (2008).
 73. Hühn, E. *et al.* Predicting the in vivo release from a liposomal formulation by IVIVC and non-invasive positron emission tomography imaging. *Eur. J. Pharm. Sci.* **41**, 71–7 (2010).
 74. Huynh, N. T., Passirani, C., Saulnier, P. & Benoit, J. P. Lipid nanocapsules: a new platform for nanomedicine. *Int. J. Pharm.* **379**, 201–9 (2009).
 75. Mendes, A. C., Baran, E. T., Reis, R. L. & Azevedo, H. S. Fabrication of phospholipid-xanthan microcapsules by combining microfluidics with self-assembly. *Acta Biomater.* **9**, 6675–85 (2013).
 76. Taylor, T. M., Weiss, J., Davidson, P. M. & Bruce, B. D. Liposomal nanocapsules in food science and agriculture. *Crit. Rev. Food Sci. Nutr.* **45**, 587–605 (2005).
 77. Mouritsen, O. G. *LIFE – AS A MATTER OF FAT, The Emerging Science of Lipidomics.* (Springer, 2005).
 78. Mouritsen, O. G. Lipids, curvature, and nano-medicine. *Eur. J. Lipid Sci. Technol.* **113**, 1174–1187 (2011).

79. McKee, M. G., Layman, J. M., Cashion, M. P. & Long, T. E. Phospholipid nonwoven electrospun membranes. *Science* (80-.). **311**, 353–355 (2006).
80. Jørgensen, L., Qvortrup, K. & Chronakis, I. S. Phospholipid electrospun nanofibers: effect of solvents and co-axial processing on morphology and fiber diameter. *RSC Adv.* **5**, 53644–53652 (2015).
81. Mendes, A. C., Nikogeorgos, N., Lee, S. & Chronakis, I. S. Nanomechanics of electrospun phospholipid fiber. *Appl. Phys. Lett.* **106**, (2015).
82. Mendes, A. C., Gorzelanny, C., Halter, N., Schneider, S. W. & Chronakis, I. S. Hybrid electrospun chitosan-phospholipids nanofibers for transdermal drug delivery. *Int. J. Pharm.* **510**, 48–56 (2016).
83. Mendes, A. C. *et al.* Co-assembly of chitosan and phospholipids into hybrid hydrogels. *Pure Appl. Chem.* **88**, 905–916 (2016).
84. de Sousa, R. S., de Moraes Nogueira, A. O., Marques, V. G., Clementin, R. M. & de Lima, V. R. Effects of α -eleostearic acid on asolectin liposomes dynamics: relevance to its antioxidant activity. *Bioorg. Chem.* **51**, 8–15 (2013).
85. Pan, Y., Tikekar, R. V. & Nitin, N. Effect of antioxidant properties of lecithin emulsifier on oxidative stability of encapsulated bioactive compounds. *Int. J. Pharm.* **450**, 129–137 (2013).
86. Judde, A., Villeneuve, P., Rossignol-Castera, A. & Guillou, A. Antioxidant effect of soy lecithins on vegetable oil stability and their synergism with tocopherols. *J. Am. Oil Chem. Soc.* **80**, 1209–1215 (2003).

87. Cui, L. & Decker, E. A. Phospholipids in foods: prooxidants or antioxidants? (2015). doi:10.1002/jsfa.7320
88. Choe, E. & Min, D. B. Mechanisms of Antioxidants in the Oxidation of Foods. **8**, 345–358 (2015).
89. Yu, D.-G. *et al.* Self-assembled liposomes from amphiphilic electrospun nanofibers. *Soft Matter* **7**, 8239 (2011).
90. Zhang, J. *et al.* Atomic force microscopy of electrospun organic-inorganic lipid nanofibers. *Appl. Phys. Lett.* **99**, 103702–1037023 (2011).
91. Chronakis, I. S. *Micro- and Nano-fibers by Electrospinning Technology. Micromanufacturing Engineering and Technology* (Yi Qin, 2015). doi:10.1016/B978-0-323-31149-6.00022-0
92. Camerlo, A., Vebert-Nardin, C., Rossi, R. M. & Popa, A. M. Fragrance encapsulation in polymeric matrices by emulsion electrospinning. *Eur. Polym. J.* **49**, 3806–3813 (2013).
93. Dias, M. I., Ferreira, I. C. F. R. & Barreiro, M. F. Microencapsulation of bioactives for food applications. *Food Funct.* **6**, 1035–1052 (2015).
94. Jacobsen, C., Garcia-Moreno, P. J., Mendes, A. C., Mateiu, R. V & Chronakis, I. S. Use of Electrospinning for Encapsulation of Sensitive Bioactive Compounds and Applications in Food. *Annu. Rev. Food Sci. Technol.* **9**, 1–25 (2018).
95. Inoue, M. *et al.* Antioxidant, Gallic Acid, Induces Apoptosis in HL-60RG Cells. *Biochem. Biophys. Res. Commun.* **204**, 898–904 (1994).

96. Inoue, M. *et al.* Selective induction of cell death in cancer cells by gallic acid. *Biol. Pharm. Bull.* **18**, 1526–30 (1995).
97. Faridi Esfanjani, A. & Jafari, S. M. Biopolymer nano-particles and natural nano-carriers for nano-encapsulation of phenolic compounds. *Colloids Surfaces B Biointerfaces* **146**, 532–543 (2016).
98. Gali, H. U., Perchellet, E. M. & Perchellet, J. P. Inhibition of tumor promoter-induced ornithine decarboxylase activity by tannic acid and other polyphenols in mouse epidermis in vivo. *Cancer Res.* **51**, 2820–5 (1991).
99. Gali, H. U., Perchellet, E. M., Klish, D. S., Johnson, J. M. & Perchellet, J. P. Antitumor-promoting activities of hydrolyzable tannins in mouse skin. *Carcinogenesis* **13**, 715–8 (1992).
100. Rashidi, L. *et al.* A cellular uptake and cytotoxicity properties study of gallic acid-loaded mesoporous silica nanoparticles on Caco-2 cells. *J. Nanoparticle Res.* **16**, 2285 (2014).
101. Celebioglu, A., Kayaci-Senirmak, F., Kusku, S. İ., Durgun, E. & Uyar, T. Polymer-free nanofibers from vanillin/cyclodextrin inclusion complexes: high thermal stability, enhanced solubility and antioxidant property. *Food Funct.* (2016).
102. Hundre, S. Y., Karthik, P. & Anandharamakrishnan, C. Effect of whey protein isolate and β -cyclodextrin wall systems on stability of microencapsulated vanillin by spray-freeze drying method. *Food Chem.* **174**, 16–24 (2015).
103. Karathanos, V. T., Mourtzinou, I., Yannakopoulou, K. & Andrikopoulos, N. K. Study of the solubility, antioxidant activity and structure of inclusion complex of vanillin with β -

- cyclodextrin. *Food Chem.* **101**, 652–658 (2007).
104. Kayaci, F. & Uyar, T. Solid inclusion complexes of vanillin with cyclodextrins: Their formation, characterization, and high-temperature stability. *J. Agric. Food Chem.* **59**, 11772–11778 (2011).
 105. Tai, A., Sawano, T., Yazama, F. & Ito, H. Evaluation of antioxidant activity of vanillin by using multiple antioxidant assays. *Biochim. Biophys. Acta - Gen. Subj.* **1810**, 170–177 (2011).
 106. Kayaci, F. & Uyar, T. Encapsulation of vanillin/cyclodextrin inclusion complex in electrospun polyvinyl alcohol (PVA) nanowebs: prolonged shelf-life and high temperature stability of vanillin. *Food Chem.* **133**, 641–649 (2012).
 107. Lević, S. *et al.* Thermal, morphological, and mechanical properties of ethyl vanillin immobilized in polyvinyl alcohol by electrospinning process. *J. Therm. Anal. Calorim.* **118**, 661–668 (2014).
 108. Sun, X. Z., Williams, G. R., Hou, X. X. & Zhu, L. M. Electrospun curcumin-loaded fibers with potential biomedical applications. *Carbohydr. Polym.* **94**, 147–153 (2013).
 109. Kharat, M., Du, Z., Zhang, G. & McClements, D. J. Physical and chemical stability of curcumin in aqueous solutions and emulsions: Impact of pH, temperature, and molecular environment. *J. Agric. Food Chem.* [acs.jafc.6b04815](https://doi.org/10.1021/acs.jafc.6b04815) (2016).
doi:10.1021/acs.jafc.6b04815
 110. Price, L. C. & Buescher, R. W. Decomposition of turmeric curcuminoids as affected by light, solvent and oxygen. *J. Food Biochem.* **20**, 125–133 (1996).

111. Rüzgar, G., Birer, M., Tort, S. & Acartürk, F. Studies on improvement of water-solubility of curcumin with electrospun nanofibers. *Fabad J. Pharm. Sci.* **38**, 143–149 (2013).
112. Wang, C. *et al.* Enhanced Bioavailability and Anticancer Effect of Curcumin-Loaded Electrospun Nanofiber: In Vitro and In Vivo Study. *Nanoscale Res. Lett.* **10**, 439 (2015).
113. Aytac, Z. & Uyar, T. Core-shell nanofibers of curcumin/cyclodextrin inclusion complex and polylactic acid: Enhanced water solubility and slow release of curcumin. *Int. J. Pharm.* **518**, 177–184 (2017).
114. Ranjbar-Mohammadi, M., Kargozar, S., Bahrami, S. H. & Joghataei, M. T. Fabrication of curcumin-loaded gum tragacanth/poly(vinyl alcohol) nanofibers with optimized electrospinning parameters. *J. Ind. Text.* **46**, 1170–1192 (2017).
115. Blanco-Padilla, A., López-Rubio, A., Loarca-Piña, G., Gómez-Mascaraque, L. G. & Mendoza, S. Characterization, release and antioxidant activity of curcumin-loaded amaranth-pullulan electrospun fibers. *LWT - Food Sci. Technol.* 1–8 (2015). doi:10.1016/j.lwt.2015.03.081
116. Wang, H. *et al.* Release kinetics and antibacterial activity of curcumin loaded zein fibers. *Food Hydrocoll.* **63**, 437–446 (2017).
117. Li, H., Zhu, J., Chen, S., Jia, L. & Ma, Y. Fabrication of aqueous-based dual drug loaded silk fibroin electrospun nanofibers embedded with curcumin-loaded RSF nanospheres for drugs controlled release. *RSC Adv.* **7**, 56550–56558 (2017).
118. Rahma, A. *et al.* Intermolecular Interactions and the Release Pattern of Electrospun Curcumin-Polyvinylpyrrolidone) Fiber. *Biol. Pharm. Bull.* **39**, 163–173 (2016).

119. Fu, Y. & Koo, W. W. L. EGCG protects HT-22 cells against glutamate-induced oxidative stress. *Neurotox. Res.* **10**, 23–29 (2006).
120. Zeng, L., Ma, M., Li, C. & Luo, L. Stability of tea polyphenols solution with different pH at different temperatures. *Int. J. Food Prop.* **20**, 1–18 (2017).
121. Sang, S., Lee, M. J., Hou, Z., Ho, C. T. & Yang, C. S. Stability of tea polyphenol (-)-epigallocatechin-3-gallate and formation of dimers and epimers under common experimental conditions. *J. Agric. Food Chem.* **53**, 9478–9484 (2005).
122. Zhu, Q. Y., Zhang, A., Tsang, D., Huang, Y. & Chen, Z. Y. Stability of Green Tea Catechins. *J. Agric. Food Chem.* **45**, 4624–4628 (1997).
123. Song, Q. *et al.* Enhanced uptake and transport of (+)-catechin and (-)-epigallocatechin gallate in niosomal formulation by human intestinal Caco-2 cells. *Int. J. Nanomedicine* **9**, 2157 (2014).
124. Vaidyanathan, J. B. & Walle, T. Cellular Uptake and Efflux of the Tea Flavonoid (-)-Epicatechin-3-gallate in the Human Intestinal Cell Line Caco-2. *J. Pharmacol. Exp. Ther.* **307**, 745–752 (2003).
125. Chow, H. H. *et al.* Phase I pharmacokinetic study of tea polyphenols following single-dose administration of epigallocatechin gallate and polyphenon E. *Cancer Epidemiol. Biomarkers Prev.* **10**, 53–8 (2001).
126. Warden, B. A., Smith, L. S., Beecher, G. R., Balentine, D. A. & Clevidence, B. A. Catechins are bioavailable in men and women drinking black tea throughout the day. *J. Nutr.* **131**, 1731–7 (2001).

127. Shin, Y. C. *et al.* PLGA nanofiber membranes loaded with epigallocatechin-3-O-gallate are beneficial to prevention of postsurgical adhesions. *Int. J. Nanomedicine* **9**, 4067–4078 (2014).
128. Li, Y., Lim, L. T. & Kakuda, Y. Electrospun zein fibers as carriers to stabilize (-)-epigallocatechin gallate. *J. Food Sci.* **74**, 233–240 (2009).
129. Lee, E. J. *et al.* Hyaluronic acid/poly (lactic-co-glycolic acid) core/shell fiber meshes loaded with epigallocatechin-3-O-gallate as skin tissue engineering scaffolds. *J. Nanosci. Nanotechnol.* **12**, 8458–8463 (2014).
130. Lee, M. H. *et al.* Exovascular application of epigallocatechin-3-O-gallate-releasing electrospun poly (l-lactide glycolic acid) fiber sheets to reduce intimal hyperplasia in injured abdominal aorta. *Biomed. Mater.* **10**, 55010 (2015).
131. Lee, J. H. *et al.* Epigallocatechin-3-O-gallate-loaded poly (lactic-co-glycolic acid) fibrous sheets as anti-adhesion barriers. *J. Biomed. Nanotechnol.* **11**, 1461–1471 (2015).
132. Tian, J. *et al.* Antimicrobial application of nanofibrous mats self-assembled with chitosan and epigallocatechin gallate. *Colloids Surfaces B Biointerfaces* **145**, 643–652 (2016).
133. KONISHI, Y., KOBAYASHI, S. & SHIMIZU, M. Transepithelial Transport of *p* - Coumaric Acid and Gallic Acid in Caco-2 Cell Monolayers. *Biosci. Biotechnol. Biochem.* **67**, 2317–2324 (2003).
134. Krogh, R., Yunes, R. a & Andricopulo, a D. Structure-activity relationships for the analgesic activity of gallic acid derivatives. *Farmacologia* **55**, 730–5 (2000).
135. Shahrzad, S., Aoyagi, K., Winter, A., Koyama, A. & Bitsch, I. Pharmacokinetics of Gallic

- Acid and Its Relative Bioavailability from Tea in Healthy Humans. *J. Nutr.* **131**, 1207–1210 (2001).
136. Phiriyawirut, M. & Phaechamud, T. Gallic Acid-loaded Cellulose Acetate Electrospun Nanofibers : Thermal Properties , Mechanical Properties , and Drug Release Behavior. *Open J. Polym. Chem.* **2**, 21–29 (2012).
137. Aytac, Z., Kusku, S. I., Durgun, E. & Uyar, T. Encapsulation of gallic acid/cyclodextrin inclusion complex in electrospun polylactic acid nanofibers: Release behavior and antioxidant activity of gallic acid. *Mater. Sci. Eng. C* **63**, 231–239 (2016).
138. Hansen, C. M. & Just, L. Prediction of environmental stress cracking in plastics with Hansen solubility parameters. *Ind. Eng. Chem. Res.* **40**, 21–25 (2001).
139. Neo, Y. P. *et al.* Encapsulation of food grade antioxidant in natural biopolymer by electrospinning technique: A physicochemical study based on zein-gallic acid system. *Food Chem.* **136**, 1013–1021 (2013).
140. Chuysinuan, P., Chimnoi, N., Techasakul, S. & Supaphol, P. Gallic acid-loaded electrospun poly(L-lactic acid) fiber mats and their release characteristic. *Macromol. Chem. Phys.* **210**, 814–822 (2009).
141. Xu, L. *et al.* Semi-interpenetrating network (Sipn) co-electrospun gelatin/insulin fiber formulation for transbuccal insulin delivery. *Pharm. Res.* **32**, 275–285 (2015).
142. Sharma, A. *et al.* Electrospun composite nanofiber-based transmucosal patch for anti-diabetic drug delivery. *J. Mater. Chem. B* **1**, 3410 (2013).
143. Aduba, D. C. *et al.* Semi-interpenetrating network (sIPN) gelatin nanofiber scaffolds for

- oral mucosal drug delivery. *Acta Biomater.* **9**, 6576–6584 (2013).
144. Zeng, J. *et al.* Biodegradable electrospun fibers for drug delivery. *J. Control. Release* **92**, 227–231 (2003).
145. Verreck, G., Chun, I., Peeters, J., Rosenblatt, J. & Brewster, M. E. Preparation and characterization of nanofibers containing amorphous drug dispersions generated by electrostatic spinning. *Pharm. Res.* **20**, 810–817 (2003).
146. Ignatious, F., Sun, L., Lee, C.-P. & Baldoni, J. Electrospun Nanofibers in Oral Drug Delivery. *Pharm. Res.* **27**, 576–588 (2010).
147. Artursson, P., Palm, K. & Luthman, K. Caco-2 monolayers in experimental and theoretical predictions of drug transport. *Adv. Drug Deliv. Rev.* **46**, 27–43 (2001).
148. Pinto, M; Robineleon, S; Appay, MD; Kedinger, M; Triadou; Dussaulx, E; Lacroix, B; Simonassmann, P; Haffen, K; Fogh, J; Zweibaum, A. Enterocyte-like differentiation and polarization of the human colon carcinoma cell line Caco-2 in culture. *Biol. cell* **47**, 323–330 (1983).
149. Araújo, F. & Sarmiento, B. Towards the characterization of an in vitro triple co-culture intestine cell model for permeability studies. *Int. J. Pharm.* **458**, 128–134 (2013).
150. Antunes, F., Andrade, F., Araújo, F., Ferreira, D. & Sarmiento, B. Establishment of a triple co-culture in vitro cell models to study intestinal absorption of peptide drugs. *Eur. J. Pharm. Biopharm.* **83**, 427–435 (2013).
151. Tibolla, H., Pelissari, F. M., Martins, J. T., Vicente, A. A. & Menegalli, F. C. Cellulose nanofibers produced from banana peel by chemical and mechanical treatments:

- Characterization and cytotoxicity assessment. *Food Hydrocoll.* **75**, 192–201 (2017).
152. Stephansen, K., García-Díaz, M., Jessen, F., Chronakis, I. S. & Nielsen, H. M. Bioactive protein-based nanofibers interact with intestinal biological components resulting in transepithelial permeation of a therapeutic protein. *Int. J. Pharm.* **495**, 58–66 (2015).
153. Lin, T. C., Lin, F. H. & Lin, J. C. In vitro feasibility study of the use of a magnetic electrospun chitosan nanofiber composite for hyperthermia treatment of tumor cells. *Acta Biomater.* **8**, 2704–2711 (2012).

National Food Institute
Technical University of Denmark
Kemitorvet
2800 Lyngby

Tel. +45 35 88 70 00
Fax +45 35 88 70 01

www.food.dtu.dk